Spring 5-22-2020

Response of Large Diameter Offshore Wind Turbine Monopile Foundations to Extreme Event Loading Expected at U.S. Atlantic Coast Wind Energy Areas

Laura Hulliger
University of New Orleans, lhullige@uno.edu

Response of Large Diameter Offshore Wind Turbine Monopile Foundations to Extreme Event Loading Expected at U.S. Atlantic Coast Wind Energy Areas

A Thesis

Submitted to the Graduate Faculty of the
University of New Orleans fs
in partial fulfillment of the
requirements for the degree of

Master of Science
in
Engineering
Civil Engineering

By

Laura Emily Hulliger

B.S. University of New Orleans, 2013

May, 2020

ACKNOWLEDGEMENTS

Keystone Engineering Inc. and the many colleagues I had the pleasure of working besides have been pivotal in advancing my engineering career, with special thanks to Barry Reed and Gwen Accardo. I'd also like to thank Zachary Finucane and Rudy Hall for fostering my curiosity in the field of offshore wind technology. With an additional thanks to Keystone Engineering Inc. for offering the use of their SACS software to perform analyses for this research.

I'd also like to thank all of my colleagues at Orsted for being so understanding as I tried to balance a full-time job and a master's thesis. Your compassion was truly appreciated.

I'd also like to acknowledge my graduate professor, Dr. Malay Ghose Hajra, for guiding me not only during this thesis, but most of my academic career. I would also like to thank the remaining members of my committee, Dr. Mattei and Dr. Egeseli, your input and comments were greatly appreciated. With a special thanks to Dr. Egeseli for seeing talent in me as a structural engineer even as an undergraduate student in his Structural Analysis course.

Lastly, I'd like to thank my family and friends for supporting me during my research. I needed it, especially during the stressful times. With special thanks to my fiancé, Richard Ekstrom.

TABLE OF CONTENTS

List of Figures vi
List of Tables ix
List of Abbreviations x
List of Symbols xi
Definitions xii
Abstract xiii
1 Introduction 1
1.1 Objective and Scope 1
1.2 Report Organization 1
2 Background and Literature Review 2
2.1 Tropical Cyclones, Extra-Tropical Cyclones and Nor'easters 2
2.1.1 Definitions 2
2.1.2 Global Cyclone Regions 3
2.1.3 Proven Performance of OWTs in TC, ETC and Nor'easter Prone Regions 6
2.1.4 Failures in TC Regions 9
2.1.5 Additional Studies of OWTs in TC Prone Regions 10
2.2 US Offshore Experience 10
2.2.1 Gulf of Mexico Storms and Caisson Failures 11
2.3 Codes and Standards 12
2.4 Use of Finite Element Analyses in Place of P-Y Curves 13
2.4.1 P-Y Curves in Sand 13
2.4.2 Limitations and Differences in P-Y Method 15
2.4.3 Alternative Methods 17
2.4.4 Summary 18
2.5 Summary and Relevance of Research 19
3 U.S. Offshore Wind industry 20
3.1 U.S. Offshore Wind Industry Growth 20
3.2 U.S. Offshore Wind Energy Areas 22
3.2.1 WEAs Excluded from Research 22
4 U.S. Atlantic Coast Extreme Events 26
4.1 Tropical Cyclones 26
4.1.1 TC Event Frequency and Magnitude 27
4.2 Extra-Tropical Cyclones 29
4.3 Extreme Event Frequency and Magnitude 31
4.4 Design Extreme Events 33
5 Analysis Criteria 36
5.1 Metocean Criteria 36
5.1.1 Wind Speeds 36
5.1.2 Water Depths 36
5.1.3 Wave Height and Period 37
5.1.4 Surge and Tide 39
5.1.5 Current Speed 40
5.2 Turbines 43
5.2.1 Wind Turbines 43
5.2.2 Turbine Loading 43

5.3 Monopile Geometry 45
5.4 Soil Type 46
5.5 Design Soil Parameters 51
5.6 Design Load Case List 51
5.7 Mudline Loads as Calculated in Bentley SACS 51
6 Numerical Analysis 55
6.1 Model Description 55
6.1.1 Soil Properties 55
6.1.2 Pile and Interface Element Properties 56
6.1.3 Element Types 59
6.1.4 Mesh 60
6.1.5 Boundaries 61
6.1.6 Load Application 63
6.2 Model Validation 63
6.2.1 Mesh Quality Metrics 63
6.3 Methodology 64
6.4 Output 65
7 Results 67
7.1 Mudline Loads 67
7.2 Mudline Rotations 68
7.2.1 Effect of Mudline OTM and Pile Embedment Length on Mudline Rotations 68
7.2.2 Mudline Rotation as a Function of Wind Speed 69
7.2.3 Database 72
7.3 Expected Mudline Rotation at U.S. Atlantic Coast WEAs 72
8 Summary and Discussion 76
9 Recommendations and Future Research 78
10 References 79
Appendix A1 – U.S. Offshore Wind Current and Potential Projects 85
Appendix A2 – TC, ETC and Nor'easter Wind Speeds 88
Appendix A3 – Wave Height and Period Calculations 95
Appendix A4 – NOAA Tide Tables 104
Appendix A5 – Current Velocity Calculations 109
Appendix A6 – Surficial Sediments at WEAs 114
Appendix A7 – Design Load Case List 118
Appendix A8 – Mudline Loads 120
Appendix A9 – Database of Monopile Mudline Rotations 125
Appendix A10 –Monopile Mudline Rotations for U.S. Atlantic Coast WEAs 133
Appendix A11 – Numerical Analysis Input Parameters 136
Vita 138

LIST OF FIGURES

Figure 2-1: Global Cyclone Regions [8] 4
Figure 2-2: Cyclone Number of Occurrences Per Global Cyclone Regions Between 1842 and 2019 5
Figure 2-3: North Sea Wind Farms and 50-Year Design Wind Speeds [12] 6
Figure 2-4: Western North Pacific Category 5 TC Tracks during August 1842 – 2019 [1] 7
Figure 2-5: Western North Pacific Offshore Wind Farms and TC Tracks [11] 8
Figure 2-6: Example Damages to Wind Turbines from TCs [17] 9
Figure 2-7: Typical O&G Caisson Structure [22] 11
Figure 2-8: P-y nonlinear springs and p-y curves [33] 14
Figure 2-9: Deflected Shape of Rigid and Slender Piles to Lateral Load 16
Figure 2-10: (a) Soil Reaction Components Incorporated in the PISA design method. (b) 1D Finite Element Model employed in the PISA analysis model. [32] 18
Figure 3-1: U.S. OW Planned Commercial Operations – Cumulative by State 20
Figure 3-2: State Percentage of Total Commercial GW by 2027 21
Figure 3-3: State Call and Lease Area Potential GW 21
Figure 3-4: State Combined Lease and Call Area Potential GW 22
Figure 3-5: Projects, Lease Areas and Call Areas Along U.S. Atlantic Coast [50] 23
Figure 3-6: Wind Energy Call Areas Along U.S. Pacific Coast [54] 24
Figure 3-7: U.S. Atlantic Coast Regions [55] 25
Figure 4-1: U.S. Atlantic Coast TC Tracks and WEAs [55] 26
Figure 4-2: Historical Major TC Tracks Along the U.S. Atlantic Coast from 1842 to 2019 [1] 27
Figure 4-3: Historical TC Frequency and Magnitude per U.S. WEA from 1842 to 2019 28
Figure 4-4: Historical ETC Tracks Along the U.S. Atlantic Coast from 1842 to 2019 during October through April [1] 29
Figure 4-5: Historical ETC and Nor'easter Frequency and Magnitude per U.S. WEA from 1842 to 2019 30
Figure 4-6: Southern New England ETCs, TCs and Nor'easters 31
Figure 4-7: Delaware Bay ETCs, TCs and Nor'easters 32
Figure 4-8: Chesapeake Bay ETCs, TCs and Nor'easters 32
Figure 4-9: Long Bay ETCs, TCs and Nor'easters 33
Figure 4-10: Extreme Wind Speeds at WEAs along U.S. Atlantic Coast 34
Figure 5-1: Range of Water Depths for WEAs 37
Figure 5-2: Significant Wave Height Vs. Water Depth for H1 Category 38
Figure 5-3: Mean Higher High Water by Latitude 39

Figure 5-4: Saffir-Simpson Scale with Associated Surge [3] 40
Figure 5-5: Wind-Generated Surface Currents 41
Figure 5-6: Sub-Surface Current Speeds 41
Figure 5-7: Tower Base Fxy (kN) 44
Figure 5-8: Tower Base Mxy (kN-m) 44
Figure 5-9: Monopile Design Parameters 46
Figure 5-10: Surficial Sediments in Long Bay, SC WEAs [60] [55] 47
Figure 5-11: Surficial Sediments in Chesapeake Bay WEAs [60] [55] 48
Figure 5-12: Surficial Sediments in Delaware Bay WEAs [60] [55] 49
Figure 5-13: Surficial Sediments in Southern New England WEAs [60] [55] 50
Figure 5-14: 3D SACS Model 53
Figure 5-15: SACS Model Joint Fixities (Left) and Joint and Member Naming (Right) 53
Figure 5-16: Mudline Base Shear for Monopile Supporting 8 MW Turbine 54
Figure 5-17: Mudline OTM for Monopile Supporting 8 MW Turbine 54
Figure 6-1: Young's Modulus of Soil 56
Figure 6-2: Embedded Pile with Arbitrary Direction (Left) and Elastic Region Around Embedded Pile (Right) [62] 57
Figure 6-3: Results of Volume Pile Mudline Deflection against Embedded Pile Mudline Deflection from [62] 58
Figure 6-4: 10-node Tetrahedral Element Representing Soil [63] 59
Figure 6-5: Embedded Pile Represented as Beam Element (Dark Line) Paired to a 10-node Tetrahedral Element (Gray Lines) [63] 59
Figure 6-6: Full Mesh (Left) and Refined Mesh Area (Right) 60
Figure 6-7: Plaxis Mesh Relative Element Size Factor 60
Figure 6-8: Soil Volume Boundary Conditions [61] 61
Figure 6-9: Strain in the X-Direction 62
Figure 6-10: Size of Soil Volume 62
Figure 6-11: Lateral Load Application at Calculated Eccentricity 63
Figure 6-12: Mesh Quality 64
Figure 6-13: Deflection of 9.5 Meter Diameter Monopile Embedded 40 Meters in Medium Dense Sand (L/D = 4.21) Supporting an 8 MW Turbine in Case H1 66
Figure 7-1: Increase in Mudline OTM by Turbine Size and Water Depth 67
Figure 7-2: Mudline Rotation and Overturning Moment 68
Figure 7-3: Mudline Rotation and Pile Embedment Depth 69
Figure 7-4: Mudline Rotations in 20 meter Water Depth 70
Figure 7-5: Mudline Rotations in 40 meter Water Depth 70

Figure 7-6: Mudline Rotations in 50 meter Water Depth 71

Figure 7-7: Southern New England and Chesapeake Bay Robustness Case Mudline Rotations Corresponding to 64 m/s Wind Speed at El. (+) 10 meters 73

Figure 7-8: Delaware Bay Robustness Case Mudline Rotations Corresponding to 55 m/s Wind Speed at El. (+) 10 meters 74

Figure 7-9: Long Bay Robustness Case Mudline Rotations Corresponding to 64 m/s Wind Speed at El. (+) 10 meters 75

LIST OF TABLES

Table 2-1: Tropical Cyclone Categories by Wind Speed [3], [4] 2
Table 4-1: Locations for NHC Search Area 28
Table 5-1: Wind Speed for Each Saffir-Simpson Category and Turbine Size 36
Table 5-2: Tidal Variation at each WEA 39
Table 5-3: Design Water Level 40
Table 5-4: Total Current Velocity Per Depth 42
Table 5-5: Commercially Available Turbine Data 43
Table 5-6: Tower Base Loads 45
Table 5-7: Monopile Design Parameters 45
Table 5-8: Medium Dense Sand Design Parameters 51
Table 5-9: Simplified DLC List 51
Table 6-1: Pile Properties 58
Table 6-2: Number of Elements and Nodes in Soil Constitutive Model 61
Table 6-3: Mesh Quality Metrics 63
Table 8-1: Minimum and Maximum Mudline Rotations from DLCs 76
Table 8-2: Minimum and Maximum Mudline Rotations at U.S. Atlantic Coast WEAs 77

LIST OF ABBREVIATIONS

API	American Petroleum Institute
AWEA	American Wind Energy Association
BIWF	Block Island Wind Farm
BIWF	Block Island Wind Farm
BOEM	Bureau of Ocean Energy Management
BSEE	Bureau of Safety and Environmental Enforcement
CPT	cone penetration test
DD	decimal degrees
DLC	design load case
DNV	Det Norske Veritas
El.	elevation
ETC	extra-tropical cyclone
FEA	finite element analysis
FLS	fatigue limit state
GE	General Electric
GOM	Gulf of Mexico
GW	gigawatt
HH	hub height
IBTrACS	International Best Track Archive for Climate Stewardship
LC	load case
MW	megawatt
O&G	oil and gas
OCRP	offshore compliance recommended practices
OTM	overturning moment
OW	offshore wind
OWF	offshore wind farm
OWT	offshore wind turbine
PISA	Pile Soil Analysis project
RNA	rotor nacelle assembly
SACS	structural analysis computing software
TAP	technical assessment program
TC	tropical cyclone
TD	tropical depression
TS	tropical storm
U.S.	United States
ULS	ultimate limit state
WEA	wind energy area
WTG	wind turbine generator

LIST OF SYMBOLS

c	cohesion
d	water depth
E_{inc}	increase of stiffness
E_p	young's modulus of steel pile
E_s	young's modulus of soil
Fxy	base shear
g	acceleration due to gravity = 9.81 m/s^2
Hb	breaking wave height
Hmax	maximum wave height
Hs	significant wave height
L	pile embedment length
L/D	embedded pile length to diameter ratio
Mxy	overturning moment
OD_{intf}	monopile outer diameter at interface
OD_{mud}	monopile outer diameter at mudline
Thmax	period associated with maximum wave height
Tp	peak spectral period
$U_{T(z)}$	total current velocity
V_{hub}	wind speed at hub height
V_{ref}	wind speed and reference elevation
w.t.	wall thickness
z	depth below sea surface
$Z_{b.c.}$	bottom of cone elevation
Z_{hub}	hub height elevation
Z_{intf}	interface elevation
Z_{mud}	mudline elevation
Z_{ref}	reference elevation
$Z_{t.c.}$	top of cone elevation
α	wind shear factor
γ'	effective unit weight of soil
γ_{DRY}	dry unit weight of soil
γ_p	unit weight of steel pile
γ_{SAT}	saturated unit weight of soil
γ_{TOT}	total unit weight of soil
γ_w	unit weight of water
Δ	mudline deflection (also used to denote change in value)
ε_{xx}	soil strain in x-direction plane
Θ	mudline rotation
v	poisson's ratio
φ	friction angle
ψ	dilatancy angle

DEFINITIONS

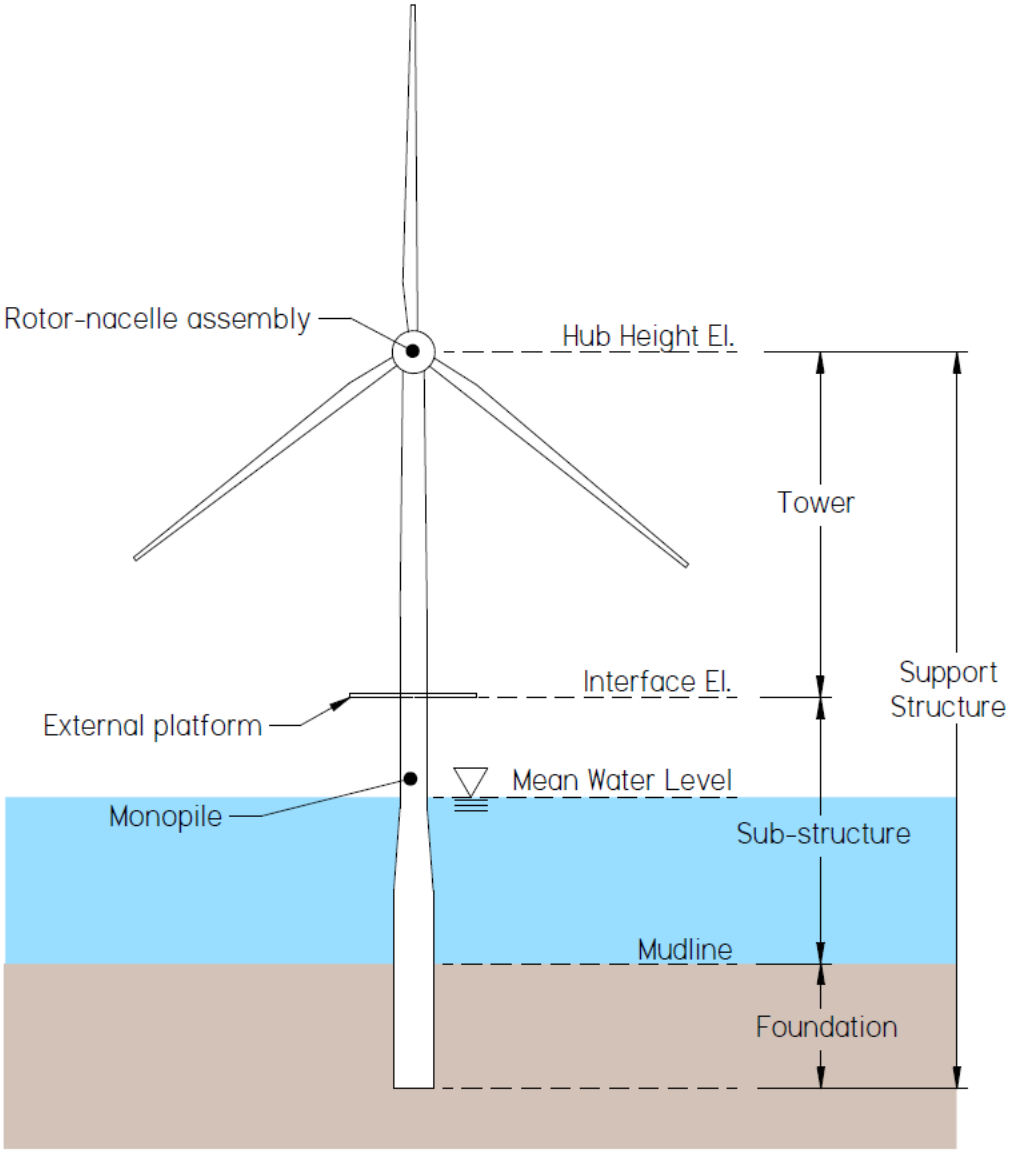

Figure i- 1: Offshore Wind Turbine Components

ABSTRACT

Extra-tropical (ETC) and tropical cyclones (TC) pose potential risks to offshore wind farms along the U.S. Atlantic coast, where the offshore wind energy industry is gaining momentum. This research aims to evaluate the stability of large diameter offshore wind turbine monopile foundations under these extreme conditions using the governing industry practice in IEC 61400-3-1. To quantify the risk at U.S. Atlantic coast wind energy areas (WEAs), the ETC and TC impact frequency and intensity are identified using the NHC Historical Hurricane Tracks Archive. Numerical simulations in Plaxis 3D are performed on foundations ranging from 8 to 12 meters in diameter embedded in medium dense sand. Storm conditions correspond to Saffir-Simpson category 1 through 4 wind speeds and associated metocean criteria. A database of foundation mudline rotation and deflection is presented for each storm intensity, turbine size and water depth. The anticipated monopile foundation stability is then predicted for each WEA.

Keywords: Offshore wind turbine; Plaxis 3D; monopile; hurricane; atlantic coast; mudline rotations

1 INTRODUCTION

Offshore wind turbines have been successfully supported by monopile type support structures since the nascent of the industry in the North Sea approximately 30 years ago. In the last ten years there has been increasing interest in pursuing offshore wind energy in the United States and the Pacific coast of Asia. These regions present a unique metocean condition from the North Sea, namely tropical cyclones, which affect the planned WEAs along the U.S. Atlantic coast as well as the Asian East China Sea and South China Sea. There have also been significant developments in offshore wind turbine technology in the last five years, which have allowed for larger capacity turbines in the range of 8 to 12 MW. This is a dramatic increase from the 3.6 MW turbines the early industry knowledge is based on. The current commercially available turbines require larger support structures with L/D ratios ranging from 3 to 5. Multiple studies have shown the typical industry practice of simulating soil-pile interaction with p-y curves does not accurately represent the behavior of rigid piles such as these. Therefore, finite element analyses are recommended to assess and validate the response of rigid OWT monopile foundations.

1.1 Objective and Scope

The objective of this research is to quantify the potentially unique extreme metocean conditions along the U.S. Atlantic coast and calculate the expected monopile mudline rotations from these extreme storms using 3D FEA in Plaxis.

1. Literature review.
2. Research U.S. Offshore Wind Industry including relevant WEAs.
3. Quantify extreme event frequency and magnitude at U.S. Atlantic coast WEAs using National Hurricane Center Historical Hurricane Tracks tool **[1]**.
4. Data gathering including metocean conditions, commercially available turbines and anticipated turbine loading, monopile designs, and geotechnical data.
5. Create a DLC list of simulations.
6. Perform seastate analyses using Bentley SACS to determine mudline overturning moment and lateral force from combined turbine and seastate loading.
7. Perform 3D FEA analyses in Plaxis 3D to determine mudline deflections and rotations to a static extreme event load for each load case.

1.2 Report Organization

This master's thesis is organized into the following chapters:

Chapter 1. Introduction
Chapter 2. Background and Literature Review
Chapter 3. U.S. Offshore Wind Industry
Chapter 4. U.S. Atlantic Coast Extreme Events
Chapter 5. Analysis Criteria
Chapter 6. Numerical Analysis
Chapter 7. Results
Chapter 8. Summary and Discussion
Chapter 9. Recommendations and Future Research

2 BACKGROUND AND LITERATURE REVIEW

The following sections describe ETCs, TCs and Nor'easters, provide an overview of offshore wind turbine performance in tropical cyclone regions thus far, a brief history of U.S. offshore experience with monopile type foundations in tropical cyclone regions, discuss relevant codes and standards for offshore wind turbine monopile foundation design as well as provide reference and summaries of relevant studies which determined that traditional p-y curves do not accurately represent rigid pile behavior.

2.1 Tropical Cyclones, Extra-Tropical Cyclones and Nor'easters

Several storm types including tropical cyclones, extra-tropical cyclones and nor'easters are prevalent along the U.S. Atlantic coast. It is of interest in this research to study the development, strength, and frequency of these systems to assess their potential impact to offshore wind farms. A discussion of global tropical cyclone regions is provided to draw from any existing experience with offshore wind farms subjected to extreme storms such as tropical cyclones as well as to establish the novelty of this industry in tropical cyclone regions from a global perspective.

2.1.1 Definitions

Tropical cyclones are low pressure, large scale weather systems which have warm air at their core, are not associated with fronts. These systems develop over tropical or subtropical waters and have a unique central "eye," about which winds rotate. Tropical cyclones derive energy from condensation of water vapor and typically range from 100 to 600 nautical miles diameter at maturity [2]. The hurricane season is defined as June 1 through November 30 in the North Atlantic. Though hurricanes have been observed outside of this range with the earliest recorded in March and the latest recorded in December [3].

Tropical cyclones are further classified depending upon 1-minute sustained wind speed at near surface (10 meter) elevation using the Saffir-Simpson Hurricane scale as shown below in Table 2-1 [3]. Tropical storms and tropical depressions are classified by the National Weather Association [4] as shown in Table 2-1.

Table 2-1: Tropical Cyclone Categories by Wind Speed [3], [4]

Scale Number (Category)	Wind Speed (m/s)
Tropical Depression	< 17
Tropical Storm	18 - 32
1	33 - 42
2	43 - 49
3	50 - 58
4	59 - 69
5	> 70

"Apart from wind, other destructive features of tropical cyclones include torrential rains over a large area and coastal storm tides of 4.5 to 9.0 meters above normal in extreme cases [3]." It should be noted that inconsistent terminology may be used to refer to these systems with the most common being "hurricane" in the North Atlantic and "typhoon" in Asia-Pacific.

Extra-tropical cyclones form outside of the tropics and have cold air at their core. These systems derive energy primarily from large-scale horizontal temperature contrasts when warm

and cold air masses meet. Extra-tropical cyclones are typically associated with cold and warm fronts [4]. “Extra-tropical cyclones occur in both the North Atlantic and North Pacific year-round. Their frequency typically beings to increase in October, peak in December and January, and tapers off sharply after March. They can range from less than 54 nautical miles in diameter to more than 2,100 nautical miles across [5].” Extra-tropical storms are not further classified by a wind speed criteria like tropical cyclones. However, these systems may in some cases achieve hurricane-force winds. Examples of extra-tropical cyclones include blizzards, Nor’easters and low-pressure systems that provide precipitation to continents at mid-latitudes.

“During the final stages of their life cycle, tropical cyclones are often classified as extratropical. This indicates that modification of the tropical circulation has started by movement of the system into a non-tropical environment. The transformation is a gradual process: the size of the circulation usually expands, the speed of the maximum wind usually decreases, and the distribution of winds, rainfall, and temperatures around the center becomes increasingly asymmetric. Some tropical features, such as a small area of strong, often hurricane force, winds near the center (the remnants of an eye) and extremely heavy rainfall may be retained for a considerable time. Usually, when storms move out of the tropics, wind speeds near the center of a storm gradually subside. In some cases, however, re-intensification of the system may occur when mechanisms conducive to extratropical development are present [2].

Nor’easters are a type of extra-tropical storm named for the prevailing wind direction over the coastal area, i.e. the northeast. These systems historically develop on the U.S. Atlantic coast between Georgia and New Jersey within approximately 100 miles east or west of the coast. Nor’easters generally progress northeastward and attain maximum intensity near the New England states. These systems may occur at any time of the year but are most frequent and violent between September and April. Nor’easters are generally associated with precipitation in the form of heavy rain or snow, as well as strong winds, rough seas, and occasionally coastal flooding [6].

In summary, TCs and ETCs have differing structures, energy type and appearance when viewed from weather satellites or radar [2]. TCs typically occur in the warmer months and develop closer to the equator whereas ETCs occur during the colder months and develop at the mid-latitudes. Though ETCs generally have a lower wind speed than TCs, they can produce hurricane-force winds for up to 24 hours. In addition, the increased diameter of ETCs when compared to TCs “allows for the development of large and energetic waves [7].”

2.1.2 Global Cyclone Regions

From a global perspective, there are seven tropical cyclone basins including the Atlantic, eastern North Pacific, western North Pacific, northern Indian Ocean, southwestern Indian Ocean, Australia/southeastern Indian Ocean and the Australia/southwestern Pacific [2]. These regions and their prevailing storm tracks are illustrated in Figure 2-1.

Of the seven tropical cyclone basins, only two have existing offshore wind farms and three additional regions have delineated offshore wind energy development areas as described below:

- **Eastern North Pacific:** No offshore wind farms are present within this region to date. There are however several development areas delineated. The Hawaiian offshore wind development areas may be subjected to TCs in this region; however, direct hits are uncommon and are generally concentrated just off the west coast of Mexico. Though it is not anticipated the Hawaiian wind energy areas may be subjected to hurricane force winds often, they can be

subjected to large seastates developed from TCs located nearby. This region predominantly affects Hawaii and the west coast of Mexico.

- **Western North Pacific:** Several offshore wind farms are present in this region along the coasts of Japan, South Korea, China, Taiwan and Vietnam. There is a significant number of planned offshore wind farms throughout this region anticipated to be installed between 2021 and 2023 as well as a significant number of development areas delineated. This region predominantly affects the coasts of China, Taiwan, South Korea, Japan, Philippines and Vietnam

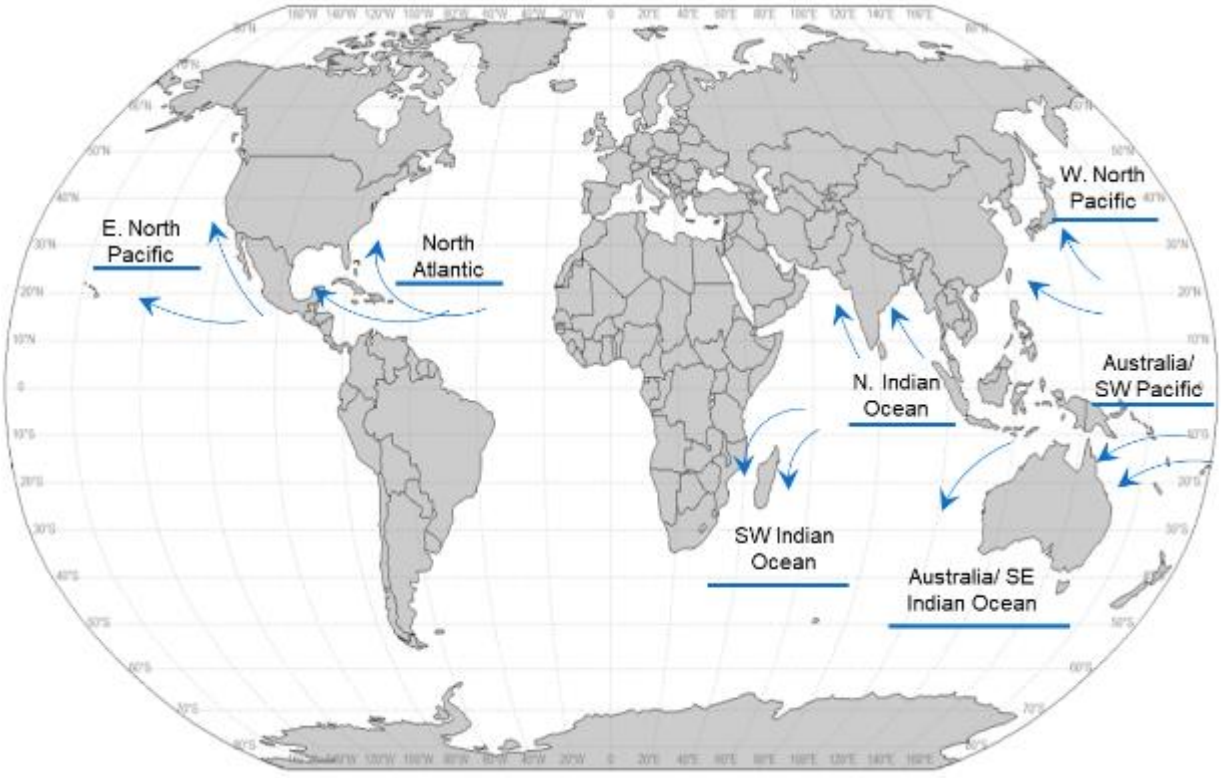

Figure 2-1: Global Cyclone Regions [8]

- **Northern Indian Ocean:** No offshore wind farms are present within this region to date. India has several development zones and projects in the conceptual /early planning phase located in the Gulf of Mannar, Palk Strait and the Arabian Sea. This region predominantly affects the Bay of Bengal and the Arabian sea including the coasts of Myanmar, Bangladesh, India, Sri Lanka, Pakistan, Oman, Yemen and Somalia.
- **Southwestern Indian Ocean:** No offshore wind farms are present within this region nor are there any projects in conceptual/ early planning phase or development areas delineated. This region predominantly effects the coasts of Madagascar and Mozambique.
- **Australia/southeastern Indian Ocean:** No offshore wind farms are present within this region nor are there any projects in conceptual/ early planning phase or development areas delineated. This region predominantly affects the west coast of Australia.
- **Australia/southwestern Pacific:** No offshore wind farms are present within this region to date. There is one project in conceptual /early planning phase located in the Bass Strait off the southeastern coast of Australia. This region predominantly effects the northern and eastern coasts of Australia, as well as the coasts of New Zealand.

- **North Atlantic:** This region is the topic of this research and will be discussed in detail in subsequent sections. One wind farm is in operation in this region located off the coast of Rhode Island. Several offshore wind farms are planned for installation in 2023 as well as many others in conceptual /early planning phase and development areas delineated throughout the Atlantic coast of the U.S. This region predominantly affects the U.S. East Coast, the Gulf of Mexico, and the Caribbean Sea.

Tropical cyclone and extra-tropical cyclone frequency and intensity within each region is shown in Figure 2-2. Number of occurrences for each basin was collected from the NHC Historical Hurricane Tracks – GIS Map Viewer [1] with dataset from IBTrACS [9] [10]. Whether an offshore wind farm exists or is planned within each region is also denoted in Figure 2-2, where data was gathered from 4c offshore [11].

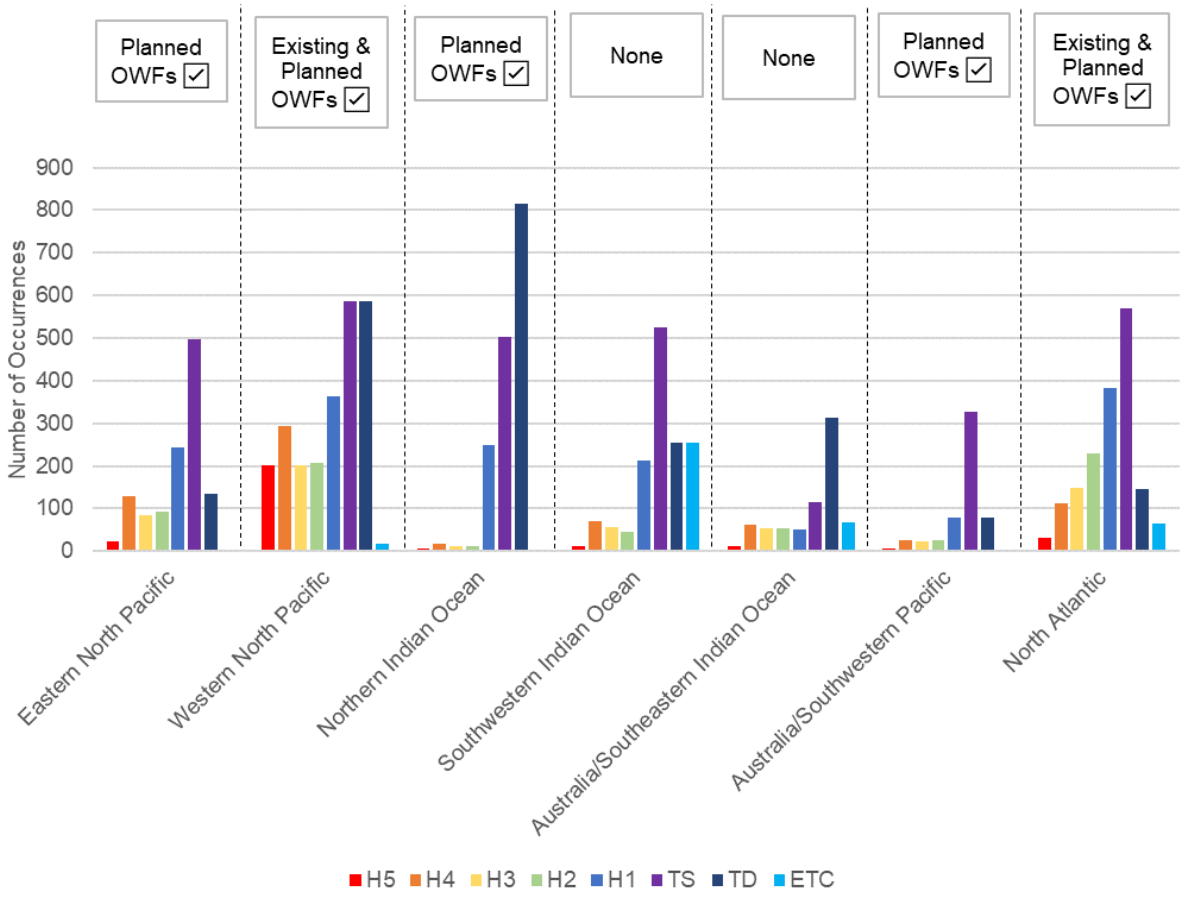

Figure 2-2: Cyclone Number of Occurrences Per Global Cyclone Regions Between 1842 and 2019

It can be seen from Figure 2-2, that the Western North Pacific region experiences the largest number of major hurricanes (greater than or equal to category 3). The North Atlantic region experiences the most category 1 and 2 storms of any region. Lastly, the North Atlantic region and the Eastern North Pacific region experienced approximately 110 category 4 storms in this 177-year time period. It should be noted modelling is typically used to determine the return period of storms for a specific area. The purpose of the data shown here is to demonstrate a holistic risk picture across regions and not to determine the return period storms.

From a global perspective, there is knowledge to be gained by studying the behavior of existing wind farms in the Western North Pacific and the North Atlantic under tropical cyclone conditions. However, as discussed in the following section, the wind farms in these regions have not been in place for significant enough time to assess their behavior over a typical offshore wind farm lifetime (25 years). In addition, these farms generally have used turbines in the range of 3 to 6 MW, much smaller than the turbines anticipated for use on the U.S. Atlantic Coast, ranging from 8 to 12 MW).

2.1.3 Proven Performance of OWTs in TC, ETC and Nor'easter Prone Regions

Northwest Europe

Much of the offshore wind farm industry experience stems from the southern portions of the North Sea along the coasts of the U.K., Denmark, Netherlands, Belgium, and Germany. This region is affected by extra-tropical storms, also known as windstorms. ETCs which affect Northern Europe historically originate in the North Atlantic region off the U.S. Atlantic coast and track across the Atlantic Ocean to Northern Europe as shown in Figure 2-3. Generally, the storms track north of Scotland into the Norwegian Sea but can track further south affecting the coasts of Ireland, the U.K., the Netherlands, Germany, Denmark and Norway.

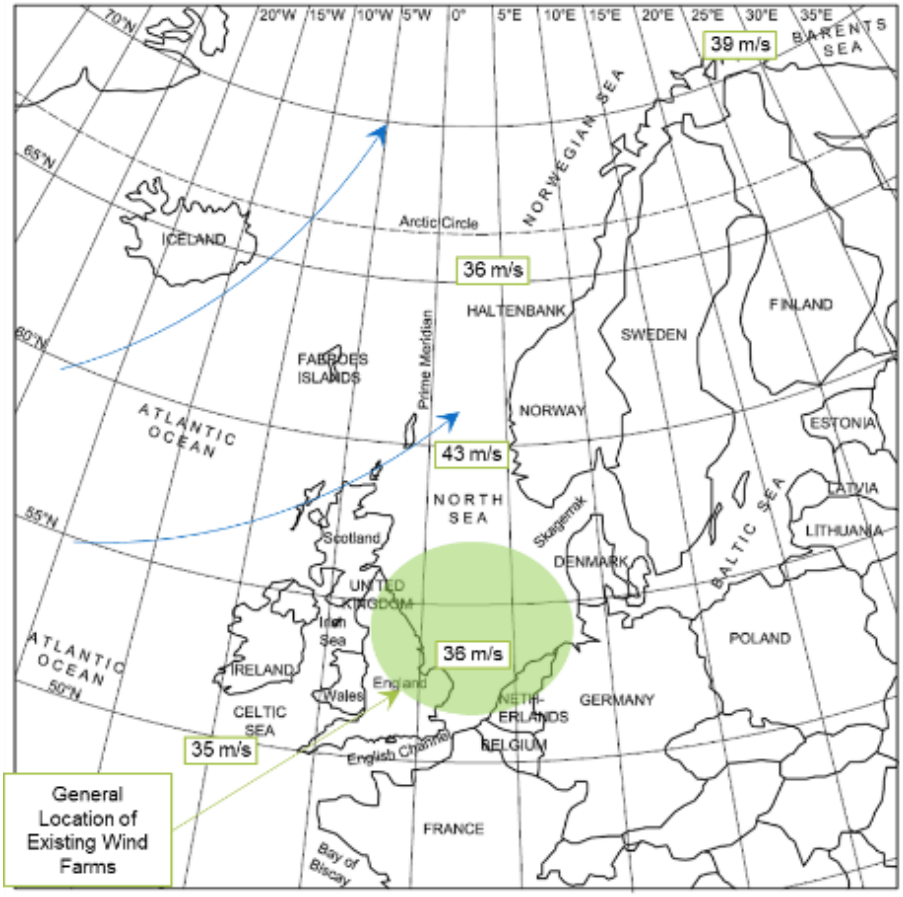

Figure 2-3: North Sea Wind Farms and 50-Year Design Wind Speeds [12]

The extra-tropical storms which affect Northern Europe can bring heavy precipitation, snowstorms, heavy winds and storm surge. However, only a small portion maintain hurricane-force winds [13]. For reference, the design 50-year return period extreme wind speed from API RP 2 MET [12] for northwestern Europe is shown in Figure 2-3 and ranges from 36 m/s to 43 m/s. These wind speeds are approximately 17% to 34% lower than the design 50-year return period extreme wind speeds expected at the U.S. Atlantic coast WEAs from South Carolina to Massachusetts. U.S. WEA wind speeds stated here were derived from BSEE TAP Studies [14] [15].

It should also be noted that the wind farms in this region are located within semi-enclosed seas where waves are fetch-restricted. Fetch-restricted waves will be shorter, steeper and lower than if they were in open ocean [12]. As will be shown in subsequent sections, the U.S. North Atlantic WEAs are located along the Atlantic coast where waves can build up in the open waters of the Atlantic Ocean.

Western North Pacific

The Western North Pacific region contains the most severe tropical cyclone activity of all global cyclone regions. This region is also prone to extra-tropical cyclone activity both in the form of winter storms and transformed TCs. A depiction of category 5 hurricane tracks during August 1842 to 2019 [1] is provided in Figure 2-4. A depiction of offshore wind farms within this region that are either in operation or in partial generation/partial construction [11] is also provided in Figure 2-5, along with the typical cyclone tracks.

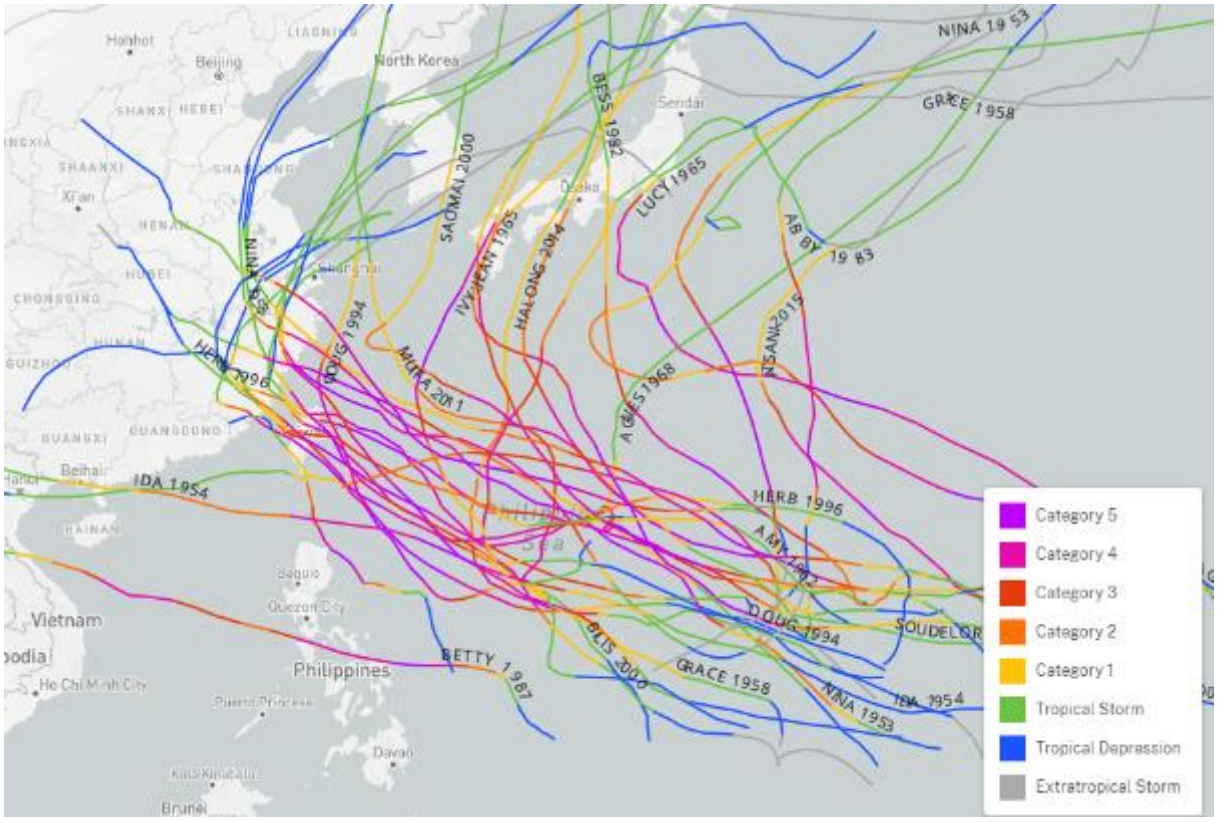

Figure 2-4: Western North Pacific Category 5 TC Tracks during August 1842 – 2019 [1]

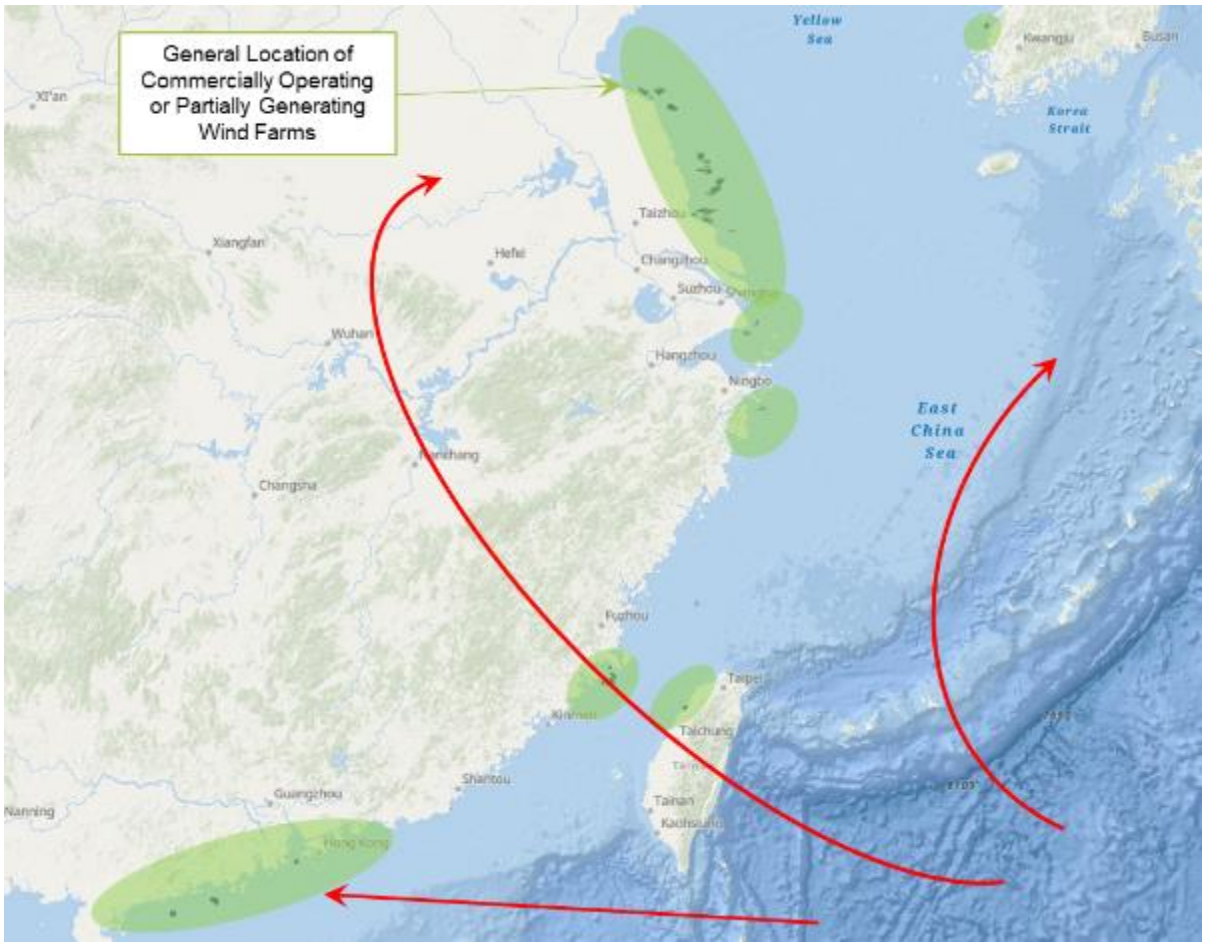

Figure 2-5: Western North Pacific Offshore Wind Farms and TC Tracks [11]

It can be seen from Figure 2-4 and Figure 2-5 that the Formosa Strait between Taiwan and Japan experiences the most severe tropical cyclone activity of any location with existing wind farms, including direct hits of category 5 storms. It is of interest to study the behavior of these wind farms under extreme environmental load as it could provide insight to the behaviors expected at U.S. WEAs as well.

However, offshore wind farms within this region have only been in operation for a maximum of five years. Therefore, it is a relatively new industry in this region as well and will take time for the wind farms to experience a full 25 years lifetime of extreme events. In addition, operating wind farms within this region support turbines in the range of 1.6 to 6 MW with the most frequent being 3 to 4 MW. These are significantly smaller than the 8 to 12 MW turbines commercially available at the time of performing this research.

Several foundation types are also utilized within this region in addition to monopile type, including fixed jackets, floating, suction bucket jackets and pile groups with pile caps. It should be noted that severe seismic activity occurs within this region along the Philippines, Taiwan and Japan and in many cases will have more of an effect on foundation type and design due to seismic vibration and soil liquefaction than cyclone activity.

North Atlantic

One offshore wind farm is in operation along the U.S. Atlantic coast. It is comprised of five, 4-pile jacket foundations installed in 2015, which support 6 MW turbines. However, due to the foundation type, it does not provide insight to behavior of offshore wind turbine monopile type foundations to extreme events anticipated along the U.S. Atlantic coast.

2.1.4 Failures in TC Regions

Offshore wind turbine generator, blade, tower, or sub-structure failures have not been recorded yet in cyclone regions. However, land-based failures of wind turbine generators, blades and towers from tropical cyclones have been reported [16]. For example, category 4 typhoon Usagi hit the southeastern coast of China in 2013 damaging all three components [17]. 35 out of 75 blades were fractured, 8 out of 25 towers collapsed, and 3 out of 25 wind turbine generators burned. A depiction of each failure from [17] is provided in Figure 2-6.

Figure 2-6: Example Damages to Wind Turbines from TCs [17]

Generator burn-up can be attributed to over-heating from excessively long braking times [17]. The mechanical brake stops the turbine from rotating during wind speeds in excess of the cutout speed, typically 25 m/s. If the turbine is not braked, the blades would reach over-speed, creating extreme loads that the blades and support structure are not designed to withstand [16].

Blade breakage can be attributed to experiencing wind speeds in excess of the design wind speeds. Failures including blade cracking and collapse of structural box beams.

The wind turbine generator also contains a yaw system which uses electrical motors to turn the nacelle and rotor into or out of the predominant wind direction. In the case of an extreme storm event such as a TC, the yaw system will rotate the nacelle and rotor out of the predominant wind direction, thus reducing the extreme loads on the turbine and support structure components [16]. It was found that unfavorable stop positions of the wind turbine generator played a large part in whether a tower buckled during typhoon Usagi. Towers were found to buckle approximately 8 to 10 meters above ground level in the location of smallest shell wall thickness [17].

2.1.5 Additional Studies of OWTs in TC Prone Regions

Several researchers have studied and attempted to identify gaps in industry knowledge when applying design methodology formulated for North Sea conditions to tropical cyclone regions. Multiple studies have recommended changes to design methodology with regards to probability of failure, turbine functionality, as well as risk and economic impact [18]. A few notable studies are mentioned below:

In [19] the risk to turbine tower failure from a category 1 through 5 hurricane in four regions along the U.S. coasts including TX, NC, NJ and MA was studied. A probabilistic model was employed which determined failure based on number of occurrences of a category storm and the intensity. Since this study looks purely at the probability of tower buckling and does not take into consideration foundation type or design, it is of interest in this thesis to study the expected foundation behavior taking into consideration sub-structure type and design.

In [20], a site in the Western North Pacific region along the Philippines was chosen in order to study if a change of load factor from 1.35, the industry accepted load factor from IEC 61400-1-1 [21], would achieve the same level of reliability for this region as intended for Europe. It was found that a load factor of 1.70 would be required to achieve the same level of reliability as intended for Europe due to the higher variability in the wind climate. It should be noted that the reference wind speed for a 50-year return period event used in this study was 67 m/s, correlating to a category 4 storm on the Saffir-Simpson scale. For comparison, wind speeds up to approximately 50 m/s are expected to reflect extreme 50-year return period events for U.S. Atlantic coast WEAs, correlating to a category 2 storm on the Saffir-Simpson scale.

Also noted in [20], is that “during direct passage of tropical cyclone over a wind farm, the wind direction will change 180 degrees within 0.5 to 1.5 hours.” The demand on the yaw control system to orient the nacelle out of the wind in these conditions was studied. It was determined that modern turbines can cope with the direction change if they are powered. Loss of grid connection is almost inevitable during a tropical cyclone and therefore a battery back-up system is required is required to maintain yaw control.

2.2 US Offshore Experience

Single element support structures such as monopiles have been effectively used in the Oil and Gas sector since the early 50s. Such structures are referred to as caissons as opposed to monopiles in the Oil and Gas sector and will be referred to as such for the remainder of this section. Caisson diameters installed in the Gulf of Mexico typically range from 0.6 meter (24 inch) to 3.70 meter (144 inch) and generally support smaller satellite production equipment decks as shown in Figure 2-7.


Figure E.2 - EC 222 D – Pre-Rita

Figure 2-7: Typical O&G Caisson Structure [22]

2.2.1 Gulf of Mexico Storms and Caisson Failures

As stated previously, the North Atlantic tropical cyclone region encompasses the Gulf of Mexico, Caribbean Sea and Atlantic coast of the U.S. Located within the Gulf of Mexico is a well-established oil and gas field, which has been subjected to numerous storms since its' inception in the early 50s. A few notable case studies with specific reference to caisson type structures are described in the following section.

Hurricane Andrew

Approximately 100 caisson type structures were observed to be leaning after the passage of Hurricane Andrew in 1992 as a category 5 storm. In order to determine the acceptable deflection criteria for caissons damaged by Hurricane Andrew, BSEE TAP Study 209 [23] was initiated. A database of minimum support structure failures including braced caissons, free-standing caissons and non-redundant tripod jackets were included. Lean angles for these structures ranged from 1 to 45 degrees with the mean range from 5 to 15 degrees. It should be noted that diameters of these structures ranged from 0.75 to 2 meters. Several platforms toppled and foundations sheared near mudline. Failures were attributed to straining of the steel, failure of the soil or both.

Total failure of a platform was defined as "the point at which the structure has been deflected so much that it can no longer support its vertical gravity loads, and collapses [23]." The second failure type was defined as a loss of serviceability. These platforms are designed for oil and gas production, and if the lean angle is such that manned operations cannot occur, then it has lost its serviceability. It was determined that an acceptable lean angle to maintain production without the need of repairs was three degrees. It was also noted that for small D/t ratios, such as those present for OWT monopiles, soil failure occurs before the caisson steel yields.

Approximately 40% of minimal support structures within 10 miles of Hurricane Andrew's path were damaged [23]. This underlines the fact that minimal support structures, including caissons, are non-redundant structures with typically only one load path as opposed to jacket type structures with multiple load paths.

Hurricanes Katrina and Rita

Additional notable platform failures followed category 5 Hurricanes Katrina and Rita in 2005. Approximately 159 structures including fixed jacket structures, caisson structures and rigs were damaged or destroyed. Approximately 24 caissons were destroyed and 2 were damaged. Diameters for these caisson structures ranged from 0.7 to 2.5 meters with L/D ratios ranging from 13 to 78. Caissons which were damaged were installed between 1968 and 2001 [22] [24].

Discussion and Lessons Learned

Following Hurricane Andrew, the industry determined a need "for a consistent and well tested process for assessing exiting platforms and ensure their fitness-for-purpose [25]. As a result, API introduced the exposure categories for structures including L-1, L-2 and L-3 based on environmental and economic risk in the event of a failure. L-1 is associated with high risk category, L-2 with medium and L-3 with low.

Since a significant amount of fixed jacket structures and minimal support structures were damaged during Hurricanes Katrina and Rita, some having been installed only 3 years prior, it was determined that a specific analysis case should be considered to ensure a platform would not fail in events greater than the design event, but within a reasonable chance of occurrence. In this analysis case, damage is acceptable, but it must be ensured the structure would not topple during nor immediately following the overload event until such time as repairs can be made. This analysis is titled the robustness case. It is required for all L-1 type structures and requires analysis with a 1,000-year return period event. The robustness case is also required for non-redundant, also called minimal support, structures within the L-2 category. The event return period for the non-redundant L-2 category case is 500-years [26] [27].

API has implemented design requirements for offshore structures based on the performance of structures in the GOM. OWT monopile foundations do have significant differences from the O&G caissons including larger moment arms, cyclic loading from the turbine, and in its current state, significantly lower L/D ratios. One item in common is the lack of redundancy in a single element design such as a caisson or monopile. Due to this lack of redundancy, a study of the applicable failure criterion is useful in assessing the risk of OWT monopile type foundations in tropical cyclone regions.

2.3 Codes and Standards

The following codes and standards are applied in the design of offshore turbines and support structures in the United States and are referenced for this research:

- **IEC 61400-1-1:** Wind energy generation systems – Part 1: Design requirement [21]
- **IEC 61400-3-1:** Wind energy generation systems – Part 3-1: Design requirements for fixed offshore wind turbines [28]
- **AWEA OCRP:** Recommended Practices for Design, Deployment and Operation of Offshore Wind Farms in the United States [29]
- **API RP 2A-LRFD:** Planning, Designing, and Constructing Fixed Offshore Platforms – Load and Resistance Factor Design [27]
- **DNV ST 0126:** Support structures for wind turbines [30]

As mentioned previously, structures in U.S. waters are categorized by L-1, L-2 and L-3 per API [27] [26]. This categorization has been adopted into the AWEA OCRP [29], with specific

reference to OWT's and their support structures categorized as L-2. Since monopile type foundations are non-redundant structures, the robustness case is required to be considered.

A form of the robustness case has also been adopted into IEC 61400-3-1 in informative Annex I, with reference to API for guidance on performing the analyses. This annex is recommended for use in tropical cyclone regions and includes two load cases, namely I.1 and I.2. Both load cases recommend 500-year return period environmental criteria and all load and resistance factors set to 1.0. In I.1, the turbine is able to maintain power to the yaw system to orient the nacelle out of the wind during the extreme event. In I.2, the yawing system has lost power and cannot orient the nacelle out of the direction of prevailing winds.

In the robustness case, the designer is required to ensure the OWT does not fail under loads greater than the design load but within a reasonable chance of occurring. However, there is no serviceability requirement set for the robustness check. OWT foundations are designed to support an offshore wind turbine and generate electricity. If they are not able to perform this function, then they have lost their serviceability. The industry standard serviceability requirement of total seabed rotation is 0.50 degrees as mentioned in DNV ST 0126 [30]. 0.25 degrees is reserved for installation tolerances and permanent accumulated rotation over the lifetime encompasses the remaining 0.25 degrees.

Since an allowable lean angle is not specified for the robustness case, insufficient pile embedment length to prevent excessive lateral deflections and rotations is a possibility after an extreme storm event. It is currently up to the developers to determine an allowable lean angle in the robustness case based on anticipated number of damages to all positions within a wind farm, economic losses from turbines out of production, possibility of monopile re-straightening, or cost to remove and replace damaged structures.

It is not anticipated the structures should be held to the 0.25 degree rotation in the robustness case. However, it is of interest to quantify the anticipated lean angle for monopiles installed along the U.S. Atlantic coast to aid designers, developers and code development committees in determining an acceptable lean angle.

2.4 Use of Finite Element Analyses in Place of P-Y Curves

Laterally loaded piles in the offshore industry are typically designed and analyzed using the lateral soil resistance – displacement curve methodology, also known as p-y curve method. The soil-pile interaction in this method is represented as a series of uncoupled nonlinear springs along the length of the pile. The original p-y curves were empirically derived by Reese et al. [31] from lateral load test results on two, 0.61 meter piles with L/D equal to 34.4 in a medium dense sand at Mustang Island, TX. For comparison, current monopile geometries range from 6 to 12 meters in diameter and L/D from 3 to 5. "These geometries fall significantly outside of the parameter space of the original p-y calibration field tests, so it is unclear whether extrapolating the p-y method to large diameter monopiles is justified." [32]

2.4.1 P-Y Curves in Sand

In the p-y method, the soil is considered to consist of uncoupled nonlinear springs with stiffness, E_{py}, acting on an elastic beam as shown in Figure 2-8. The spring stiffness, E_{py}, is calculated as the secant modulus of the p-y curve as shown in Figure 2-8 and is a function of both the lateral pile deflection, y, and depth, z.

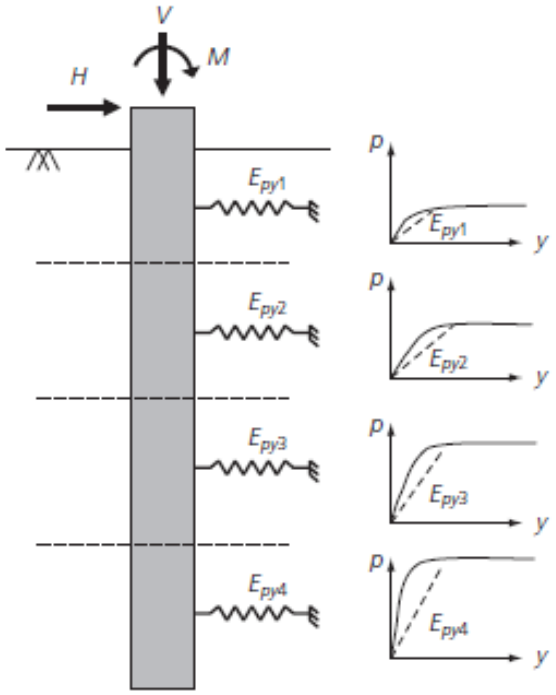

Figure 6. Winkler *p–y* model for lateral loading

Figure 2-8: P-y nonlinear springs and p-y curves [33]

The initial spring stiffness of the p-y curve at any depth is determined by a linear relationship between the initial modulus of subgrade reaction, k, and depth, z, as shown in Equation 2-1. The initial modulus of subgrade reaction, k, is dependent on soil properties alone, specifically the angle of internal friction, φ, or relative density, R_d [34].

$$E_{py} = k \times z \qquad \textbf{Equation 2-1}$$

The lateral soil resistance, p, for sand as described in API RP 2GEO [35] and DNV RP C212 [36] is provided below in Equation 2-2.

$$p = A \times p_u \tanh\left[\frac{k \times z}{A \times p_u} y\right] \qquad \textbf{Equation 2-2}$$

Where,

A is the factor to account for cyclic or static loading condition

p_u is the ultimate lateral resistance at depth z

k is the rate of increase with depth of initial modulus of subgrade reaction

y is the lateral deflection at depth z

z is the depth below original sea floor

Murchinson and O'Neill [37] recommended a hyperbolic model in place of the original p-y equation by Reese et al. [31] since it was found to better predict lateral deflections and maximum

moments than the original equation by Reese et al. This revision has been adapted into the recommended guidance [35] [36] and is shown in Equation 2-2.

The depth dependent empirical factor, A, shown in Equation 2-2 was derived in the original p-y formulation by Reese et al. [31]. The factor was determined in order to fit the field results from the flexible piles at Mustang Island with the theoretical results. Since the tests were performed on flexible piles, the use of curves still including the empirical factor, A, is uncertain [33].

2.4.2 Limitations and Differences in P-Y Method

Since "the experimental work to derive these curves were originally performed on small-diameter piles, many researchers have examined the discrepancy between predicted pile response from the p-y method for large diameter OWT monopiles and what is predicted via FEA [38]" laboratory and field testing. Several pertinent differences and limitations were discovered as described in this section.

Initial Modulus of Subgrade Reaction

As mentioned previously, the p-y method assumes a linear increase of initial modulus of subgrade reaction with depth by a factor of k. Lesny and Wiemann [39] [40] [41] determined that for large diameter monopiles, the initial modulus of subgrade reaction at deeper depths was overestimated when using a linearly increasing relationship. An overestimation of initial modulus of subgrade reaction results in an unrealistically high soil stiffness. Lesny and Wiemann [39] found that this may result in insufficient pile embedment length for large diameter piles to resist lateral loads.

In addition, Achmus and Abdel-Rahman et al. [42] [43] found based on a comparison of FEA to p-y in a dense sand for various loads and pile geometries up to approximately 7.5 meters, that the p-y curve method underestimated pile deflections and rotations due to unrealistically high soil stiffness at deeper depths.

Ultimate Soil Resistance

The ultimate lateral resistance of the soil, p_u, used in the formulation of the p-y curve for sand from API RP 2GEO [35] and DNV RP C212 [36] is shown in Equation 2-3 and Equation 2-4. The ultimate lateral resistance per unit length of the pile is taken as the minimum of the two equations, with Equation 2-3 valid for shallow depths and Equation 2-4 valid for greater depths.

$$p_{us} = (C_1\, z + C_2\, D)\, \gamma' z \qquad \textbf{Equation 2-3}$$

$$p_{ud} = C_3\, D\, \gamma'\, z \qquad \textbf{Equation 2-4}$$

Where,

D is the pile outside diameter

C_1 ,C_2, C_2 are coefficients determined as a function of the angle of internal friction of sand

These equations assume that "at shallow depths, an active Rankine-type wedge failure develops in front of the pile and a passive wedge behind the pile. At deeper levels, a block-type shear failure was assumed with the sand flowing around the pile. The transition depth between these modes of failure is determined where the soil resistances given by the two modes of failure

are equal." However, for piles with low slenderness ratios, which is the typical case for current monopile geometries, the shallow failure mechanism can act over the entire pile length. [33]

Since the original p-y curve formulation is based on fitting field lateral load test data of slender piles to theoretical formulations assuming these two failure mechanisms, it is uncertain whether the methodology can be extrapolated to larger pile diameters with a different failure mechanism.

Diameter Effect

As mentioned previously, the rate of increase of initial modulus of subgrade reaction, k, is dependent only on soil properties. Therefore, the initial stiffness of the p-y curve is assumed independent of the pile properties, including diameter. Many researchers have studied the effect of pile diameter on lateral soil stiffness by comparing results between FEA and p-y analysis. No clear consensus has been reached however as described in [34] and [33]. Additional studies of this phenomena need to be studied before the diameter effect can be considered negligible when applying p-y methodology to large diameter piles.

Deflection Behavior

Due to the relatively large stiffness compared to their length, non-slender piles move almost as rigid objects when subjected to lateral loading. Longer and more slender beams are more flexible and tend to bend, starting at the point of zero deflection, when subjected to lateral loading. A depiction of these two responses to lateral loading are shown in Figure 2-9.

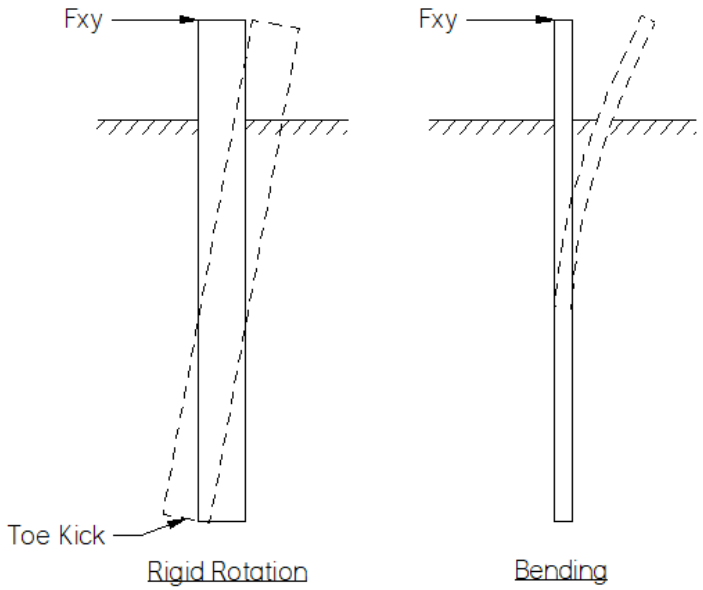

Figure 2-9: Deflected Shape of Rigid and Slender Piles to Lateral Load

Since the current p-y curve methodology was developed to match the response of flexible piles, there is considerable doubt in the validity of applying this methodology to piles with a rigid mode of failure. [33]

As shown in Figure 2-9, there is a deflection at the pile toe commonly referred to as the "toe kick." This deflection causes shearing stresses at the pile toe to occur, which increases the

total lateral resistance [34]. This increase shear resistance at the pile toe is discounted in the current p-y methodology.

2.4.3 Alternative Methods

Design guidance including DNV ST 0126 [30] and DNV RP C212 [36] have recently been updated to recognize the various shortcomings of extrapolating the nonlinear p-y method outside of the original method parameters. DNV ST 0126 specifically states that the use of nonlinear p-y curves for design of piles with diameters greater than 1.0 meter should be validated for such use, e.g. by means of FEA. However, numerous simulations are required in the design of an offshore wind farm and the use of purely FEA to represent soil-pile interaction is not feasible due to its computational intensity. Therefore, several researchers have proposed alternative or modified approaches to the p-y method.

Wiemann and Lesny [40] [39] suggested a modified p-y approach in which an adjustment factor is applied to the initial modulus of subgrade reaction to reflect a parabolic increase with depth as opposed to linear. These results, when compared with FEA, provide a better comparison than the traditional p-y method for rigid piles.

The PISA study proposes to extend the traditional p-y method to include additional components of lateral soil resistance found to be significant for large diameter piles. The intended goal is to represent a 3D finite element model of a rigid pile in a 1D spring model. The additional components of soil reaction components include “distributed moments due to vertical shaft shear stresses during pile rotation at a given depth, base shear during horizontal translation at the pile toe, and base moment during rotation of the pile toe” as shown in Figure 2-10. These components are added in addition to the lateral component of soil stiffness mobilized along the pile length in the traditional p-y curves.

“This approach benefits from the computational speed of the traditional p-y approach while retaining a comparable accuracy to the underlying finite element model.” A database and calibrated soil curve parameters were provided for the two field testing sites in the PISA project, namely Cowden clay and Dunkirk sand. Designers may use these soil reaction curves if their site conditions are similar. It should be noted that the Cowden and Dunkirk field tests were performed at land-based sites on soils which were not submerged. Further calibration of this method with submerged soils and different soil types is expected to occur over the next few years in order to further refine the provided database. A second application is also proposed where the designer may calculate soil reaction curves from FEA using their own soil properties. The second application is anticipated to be more the versatile and widely adopted approach. [32] [44]

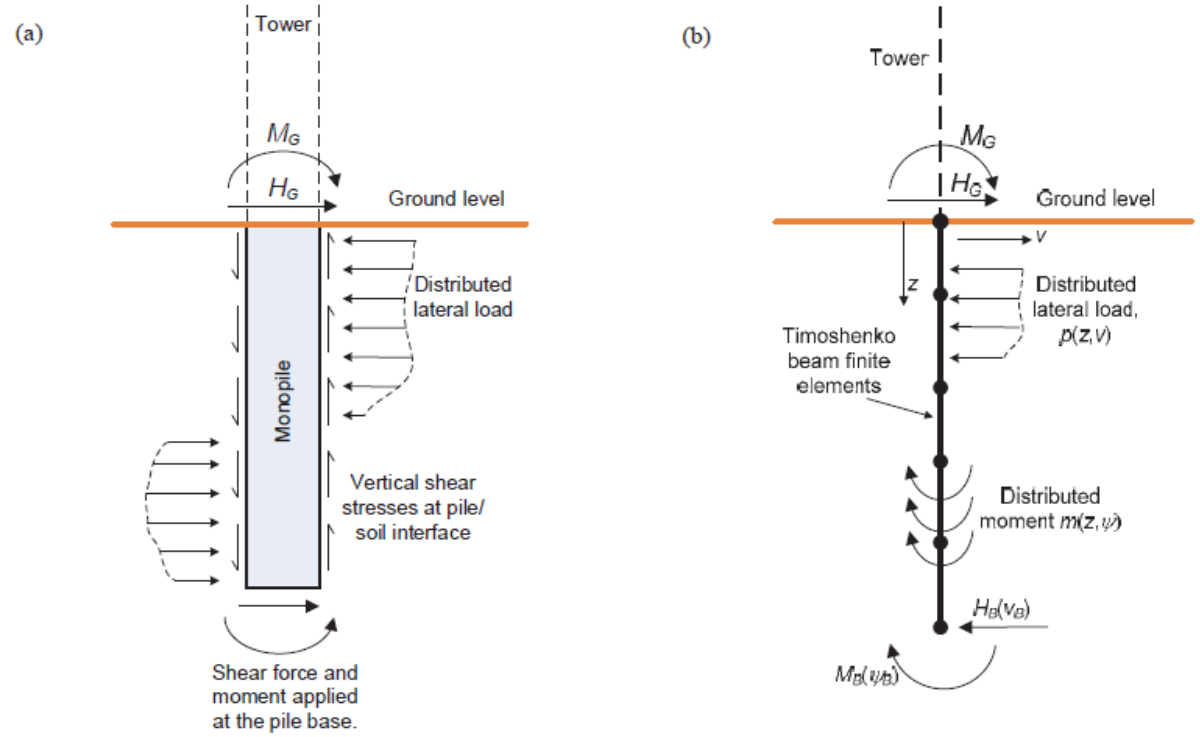

Figure 2-10: (a) Soil Reaction Components Incorporated in the PISA design method. (b) 1D Finite Element Model employed in the PISA analysis model. [32]

Cyclic Loading Effects

The studies mentioned in this section are primarily geared towards static monotonic loading. However, several researchers have assessed the effects of low and high amplitude cyclic loading on the near surface soil-pile interaction and the resulting permanent accumulated mudline rotation including [45] [38] [46] [47] . This is an area which is currently under further research in the offshore wind community.

2.4.4 Summary

Multiple researchers have studied the limitations, differences and proposed alternatives of the traditional p-y method due to the uncertainty in extrapolating p-y curve methodology outside of the original parameters. Recommended design practice such as DNV have recognized these uncertainties and recommended that in the event p-y methodology is applied for pile diameters greater than 1 meter, the validity of the approach must be validated. Finite element modelling provides the most accurate modelling technique; however, due to its computational intensity it is not a viable solution on its own. The PISA project proposes a method to accurately represent a finite element model in a 1D beam model. The method extends the traditional p-y approach to include additional components of soil resistance pertinent to large diameter piles. Based on these findings by previous researchers, it was determined that finite element modelling would provide the most realistic representation of mudline deflections and rotations of large diameter monopiles in this thesis.

2.5 Summary and Relevance of Research

A minimum rotation or deflection is not currently set for the robustness case and it is up to developers to pose a restriction. Quantifying the rotations and deflections to OWT monopile type foundations to the expected extreme storm events is hoped to aid in inspection and repair planning, predicting expected structural rotation/deflection when setting minimum deck elevation, aid in turbine manufacturer prediction of expected operability at expected foundation rotations, and aid developers and code committees in determining an acceptable lean angle for offshore wind turbine monopile foundations in post-storm conditions.

Additionally, due to the computational intensity of FEA, it cannot be utilized for all positions of an offshore wind farm during the design phase. Therefore, it is the hope that these results can help to predict expected foundation response to each category storm in the event a detailed FEA analysis cannot be performed.

Based on the many uncertainties outlined above, a regional snapshot of anticipated OWT monopile foundation stability under strong ETCs and TCs is necessary to understand the potential risks strong ETCs and TCs pose to offshore wind farms along the U.S. Atlantic Coast. As it is not economically feasible to “hurricane-proof” offshore wind farms, an accurate risk picture of foundation stability is assessed to inform developers and the public of the anticipated regional ETC and TC hazard.

3 U.S. OFFSHORE WIND INDUSTRY

3.1 U.S. Offshore Wind Industry Growth

At the time of conducting this research, the U.S. has only one offshore wind farm in operation. The 30 MW farm, which started operations in 2016, includes five, 6 MW GE turbines located approximately 3 miles southeast of Block Island, Rhode Island and is aptly named the Block Island Wind Farm. In the last two years, several state governments have enacted impressive climate plans, targeting up to 70% of its electricity sourced from renewable energy by 2030. To meet the demand, approximately 9 GW of offshore wind power is scheduled to be installed in U.S. waters along the Atlantic coast by 2027. This growth is depicted in Figure 3-1 and Figure 3-2.

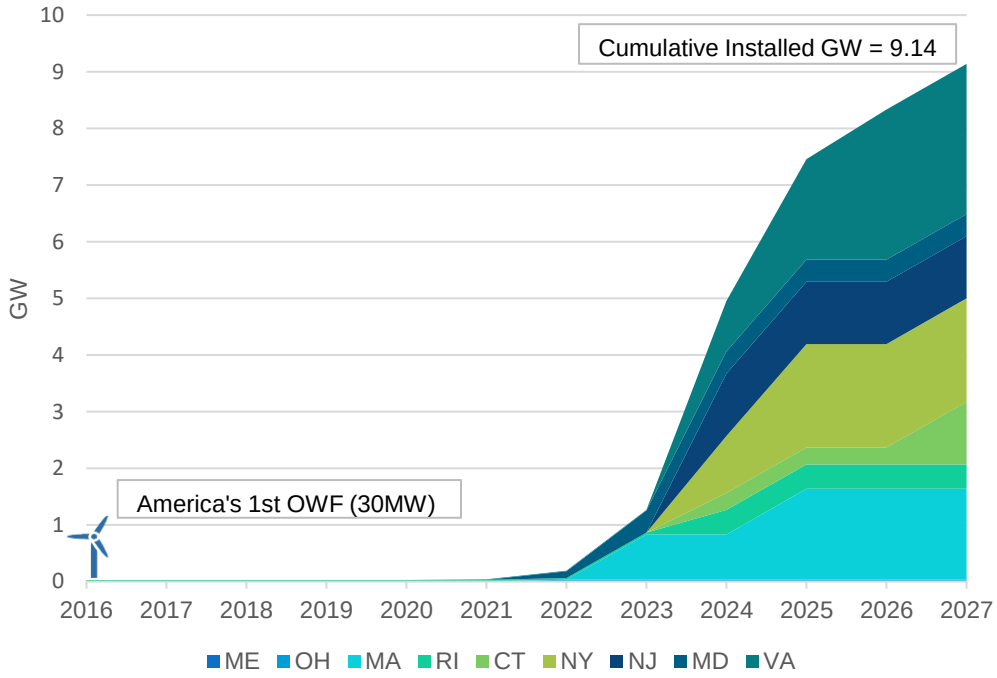

Figure 3-1: U.S. OW Planned Commercial Operations – Cumulative by State

The 9 GW projection includes projects which have been successfully awarded contracts to sell power to a neighboring state. However, there remains an additional 12.5 GW of potential capacity to be utilized from wind energy lease areas that have been purchased by developers but have not successfully secured power distribution contracts. This potential is titled “leased potential” and is shown in Figure 3-3.

BOEM has also designated several offshore wind energy call areas in U.S. waters including the Pacific Ocean along the Californian and Hawaiian coasts as well as along the U.S. Atlantic coast. BOEM seeks public input on the potential for wind energy development in these areas including site conditions, resources, and multiple uses near or within the call areas to determine whether to offer all or part of the call area for commercial wind leasing. Current call area potential capacity equals a total of 48 GW spread across U.S. waters as shown in Figure 3-3 and combined with the leased potential per state in Figure 3-4.

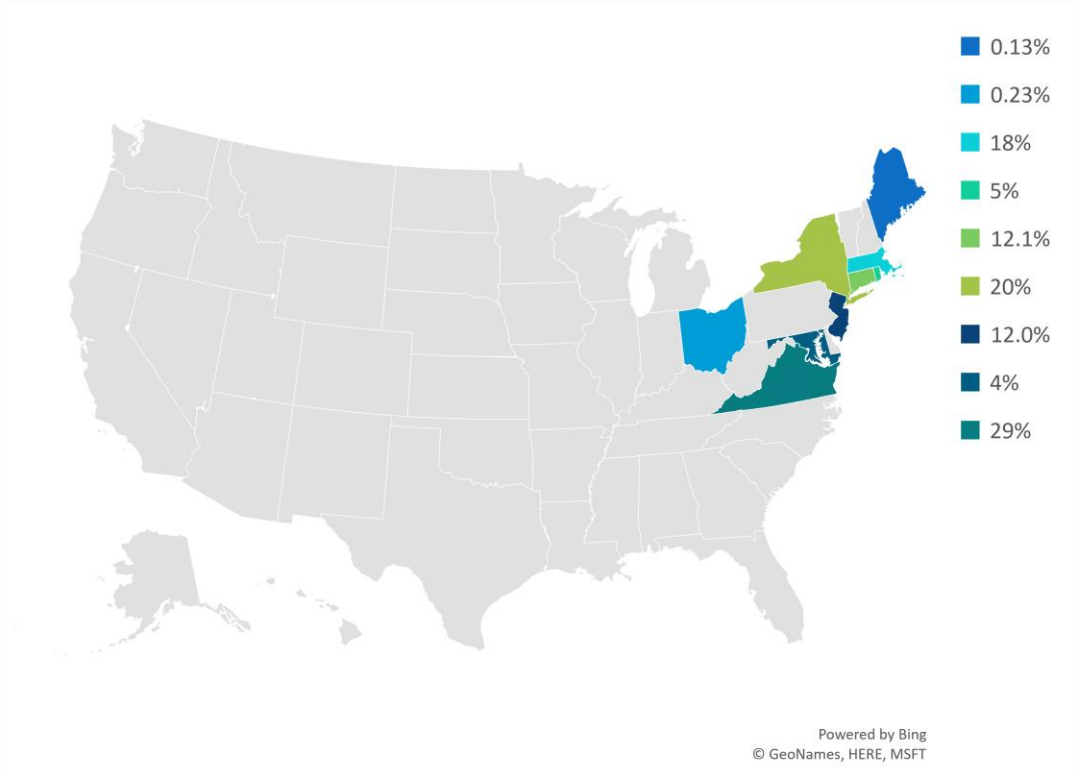

Figure 3-2: State Percentage of Total Commercial GW by 2027

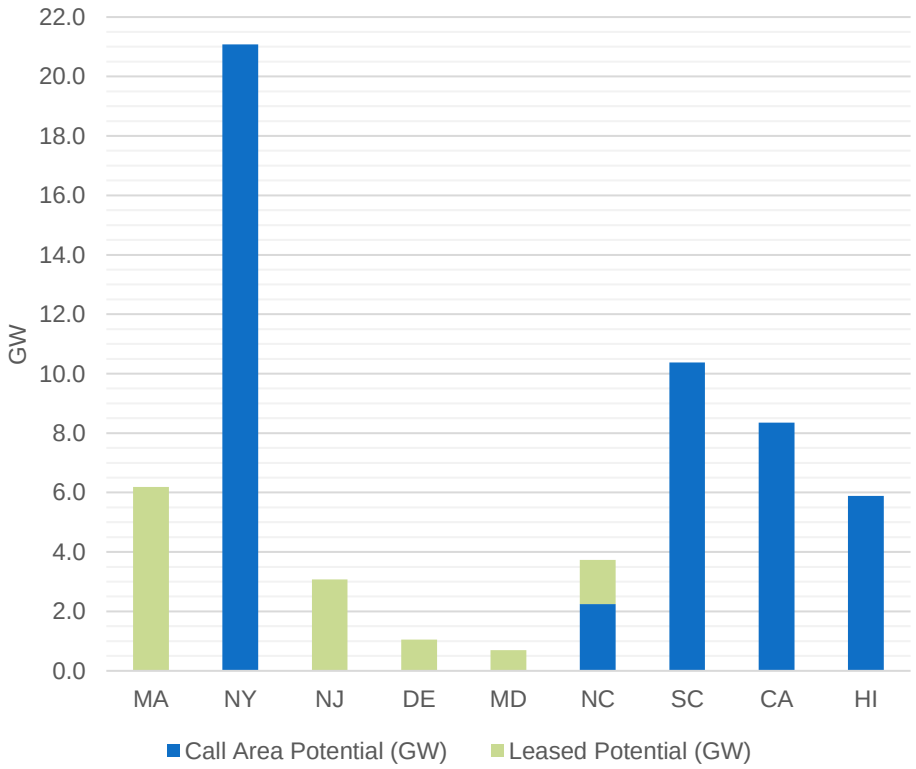

Figure 3-3: State Call and Lease Area Potential GW

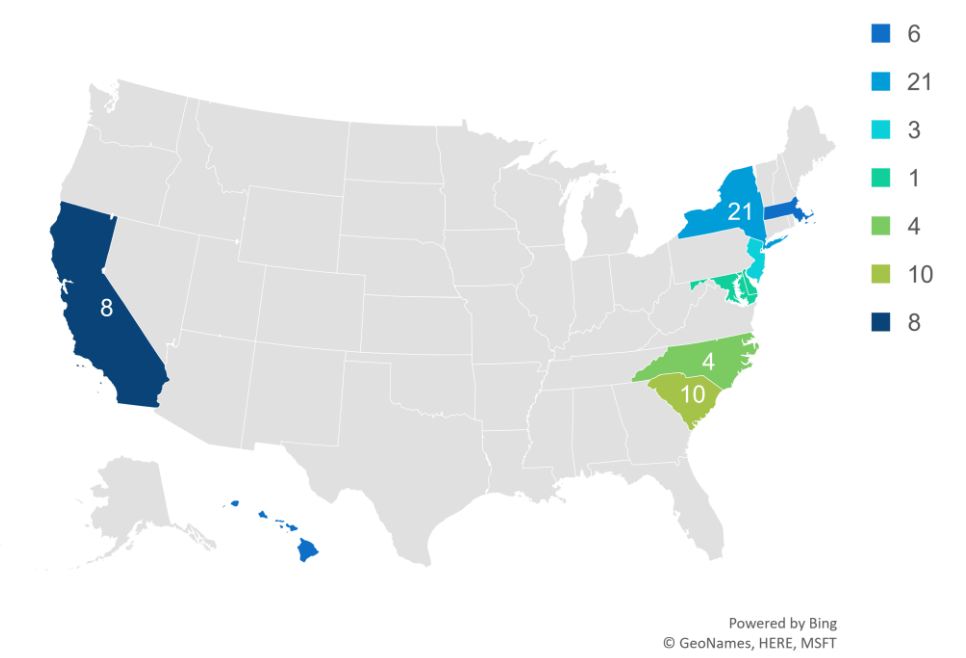

Figure 3-4: State Combined Lease and Call Area Potential GW

3.2 U.S. Offshore Wind Energy Areas

A depiction of U.S. wind energy lease and call areas is provided in Figure 3-6 for the Atlantic Ocean and Figure 3-6 for the Pacific Ocean. Since the Atlantic coast region of the U.S. currently has the most planned and projected GW, further refinement of the Atlantic coast into regions is required. Historically, the U.S. Atlantic Coast is broken into the South Atlantic, Mid-Atlantic, and Southern New England regions for coastal and environmental studies [48]. The traditional breakdown of the U.S. Atlantic coast was used for this research with a further refinement in the Mid-Atlantic region. A further refinement in the Mid-Atlantic region was needed to accurately depict the effect of tropical cyclones at lower latitudes. As such, the region was split by associated Bay, namely the Delaware Bay and Chesapeake Bay. A depiction of the regional delineation as well as coastal cities defining each region is provided in Figure 3-7.

In order to determine which energy areas were of potential interest for this research, data regarding expected turbine sizes for upcoming projects, expected range of water depths, as well as expected foundation type were required. Multiple sources including U.S. offshore wind market reports [49], [50], [51], 4c offshore renewable energy map [11] as well as the developer owned project websites were consulted to determine anticipated turbine size, number of turbine positions, farm capacity and commercial operations date. Call area and lease areas GIS files provided by BOEM [52] were overlaid by NOAA Raster Navigational Charts [53] to determine the minimum, mean, and maximum water depths at each site as well as the distance to nearest shore.

3.2.1 WEAs Excluded from Research

Several WEAs could be ruled out for this research based on water depth. The applicable water depth range for a monopile type support structure is approximately 0 – 60 meters, with the most common water depths ranging from 13 – 40 meters. Areas with water depths above 60 meters were therefore not included in this research. WEAs falling within this deep-water category include California, Hawaii and the Gulf of Maine, with water depths ranging from 400 – to 800

meters in California and Hawaii and 58 to 75 meters in the Gulf of Maine. Deep water depths such as these lend better to fixed jacket type structures or floating structures.

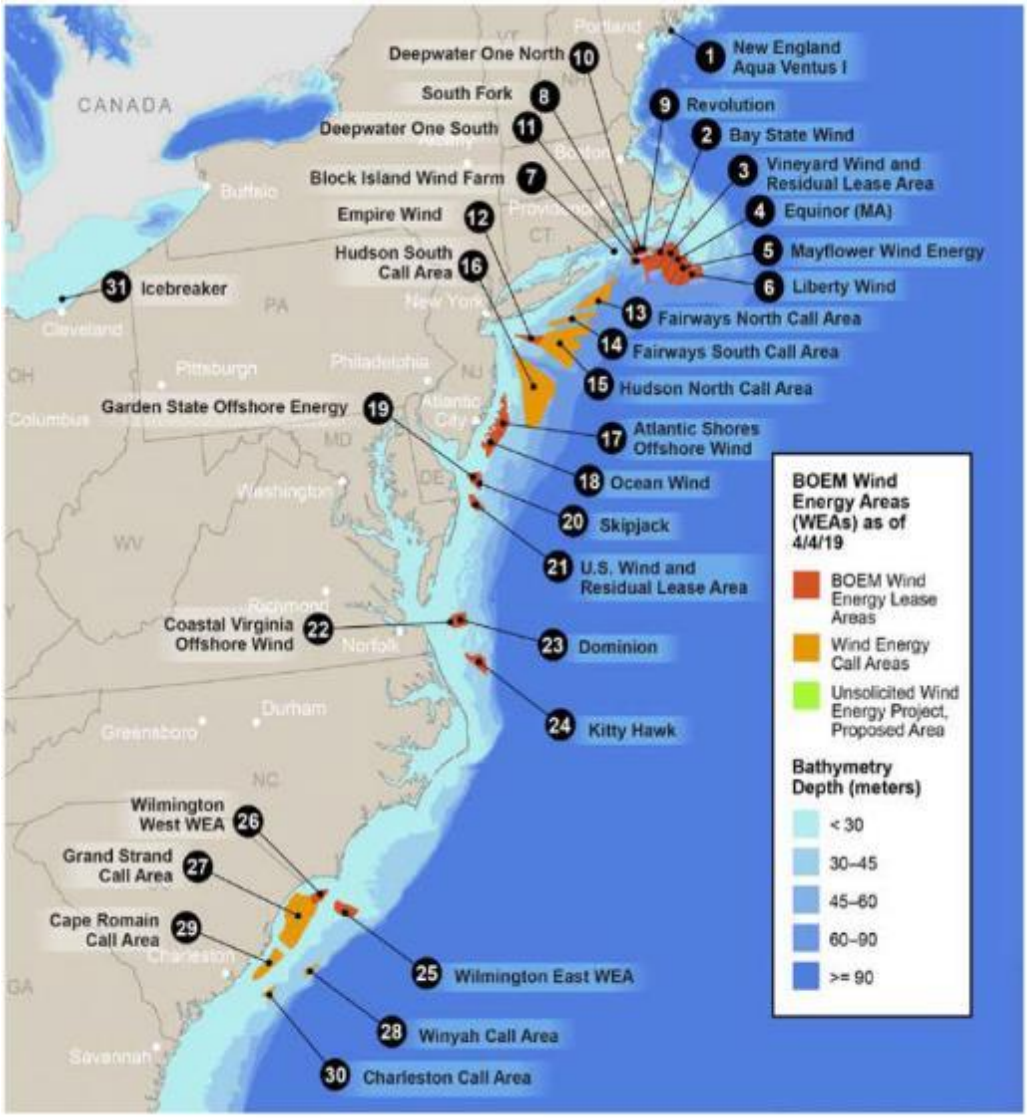

Figure 3-5: Projects, Lease Areas and Call Areas Along U.S. Atlantic Coast [50]

One additional wind farm was excluded from this study, namely, the Icebreaker wind farm located in Lake Eerie. The anticipated foundation type for this wind farm is a mono bucket structure due to the unique lake icing conditions experienced in this region. Since the design driving metocean criteria in the Great Lakes differs from the intention of this research to analyze the effect of design driving extra-tropical and tropical cyclones, the Great Lakes region was also excluded from this research.

Figure 3-6: Wind Energy Call Areas Along U.S. Pacific Coast [54]

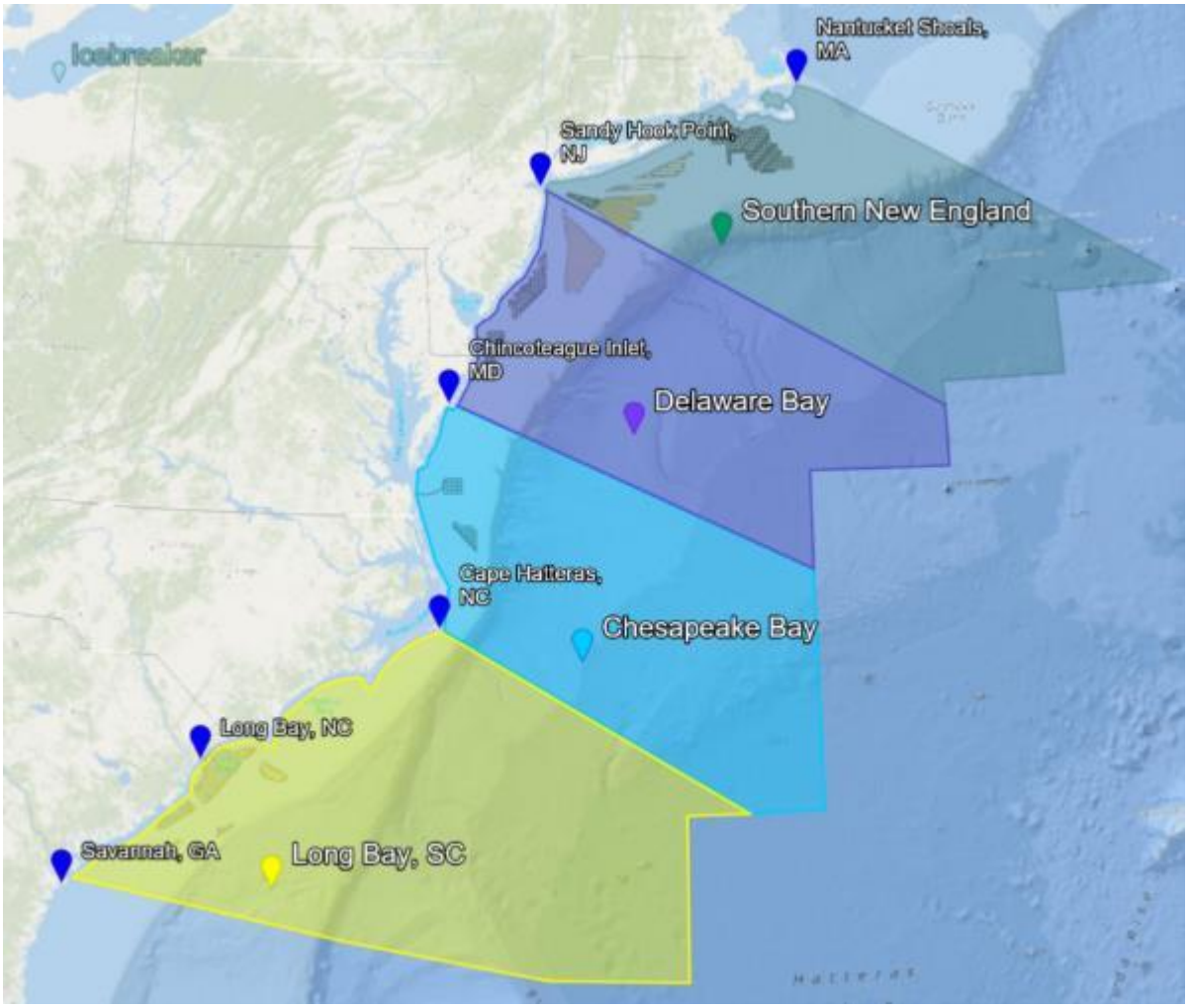

Figure 3-7: U.S. Atlantic Coast Regions [55]

A summary of planned commercial projects and the previously mentioned project information are included in Table A1- 1 of Appendix A1 along with the state purchasing power as well as BOEM lease area name.

A summary of lease areas without power distribution contracts as well as BOEM designated call for information areas are included in Table A1- 2 of Appendix A1. Provided information is similar to that of the commercial projects table excluding details such as turbine size, farm capacity and number of turbine positions as a project does not exist at these locations yet.

4 U.S. ATLANTIC COAST EXTREME EVENTS

As mentioned previously, the North Atlantic tropical cyclone basin includes the North Atlantic Ocean, the Caribbean Sea and the Gulf of Mexico. The focus of this study will be on the North Atlantic Ocean and specifically the U.S. coastline from SC to MA. The coastline is split into four regions as described in the previous section. In the South Atlantic region, WEAs are concentrated in Long Bay, SC; therefore, this sub-region will be referenced for the remainder of the report and encompasses projects in both SC and southern NC. The remaining Atlantic coast regions include Southern New England (NY/RI/MA) and the Mid-Atlantic region including both the Chesapeake Bay (NC/VA) and Delaware Bay (DE/MD/NJ) sub-regions.

4.1 Tropical Cyclones

Tropical cyclones in the North Atlantic region travel into the Gulf of Mexico, along the Atlantic coast of the U.S. or further offshore in the Atlantic Ocean proceeding northeast. Of interest for this research are tropical cyclones which travel along the U.S. Atlantic coast and could potentially affect U.S. offshore WEAs. The typical tropical cyclone tracks for systems which travel along the U.S. Atlantic coast are depicted in Figure 4-1 along with the WEAs and regional delineations.

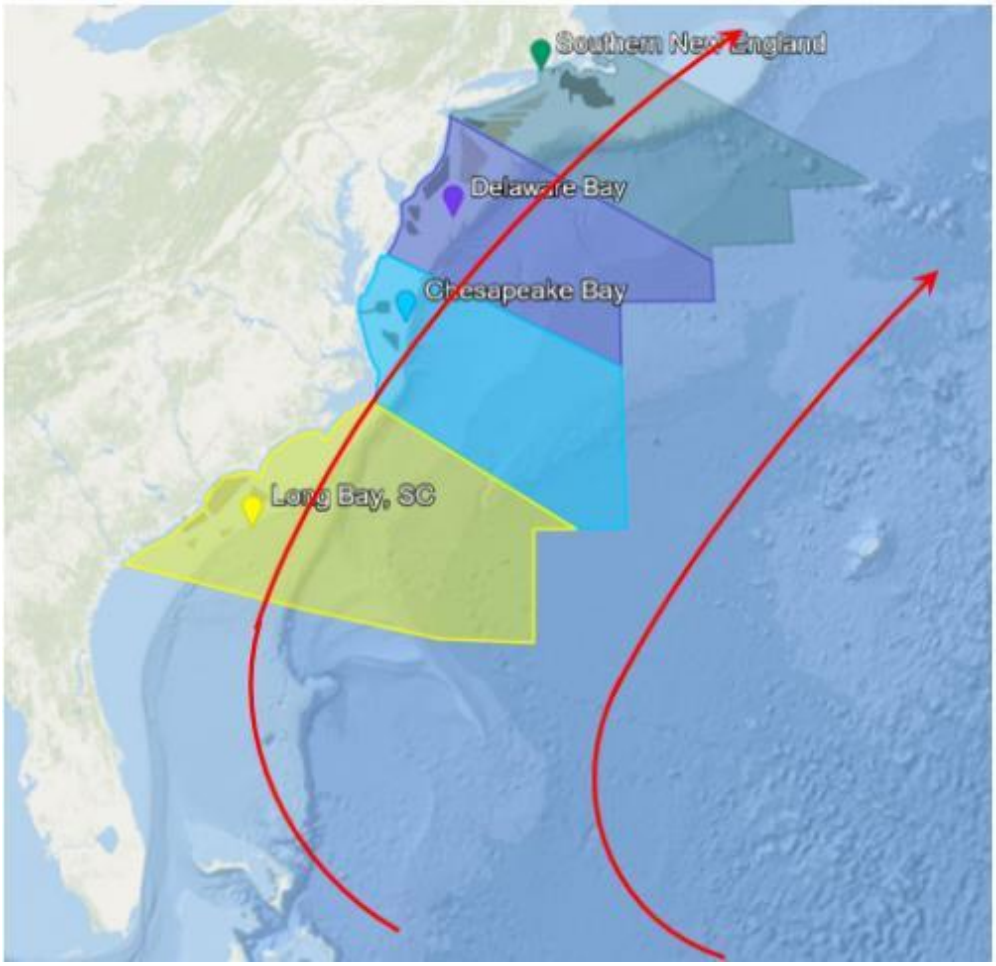

Figure 4-1: U.S. Atlantic Coast TC Tracks and WEAs [55]

A depiction of historical major hurricanes (greater than or equal to category 3) to travel along the U.S. Atlantic coast from 1842 to 2019 is provided in Figure 4-2. A search radius of 200 nautical miles with center located offshore of Long Bay, SC was used as the search criteria in the NHC Historical Hurricane Tracks – GIS Map Viewer [1] to generate Figure 4-2.

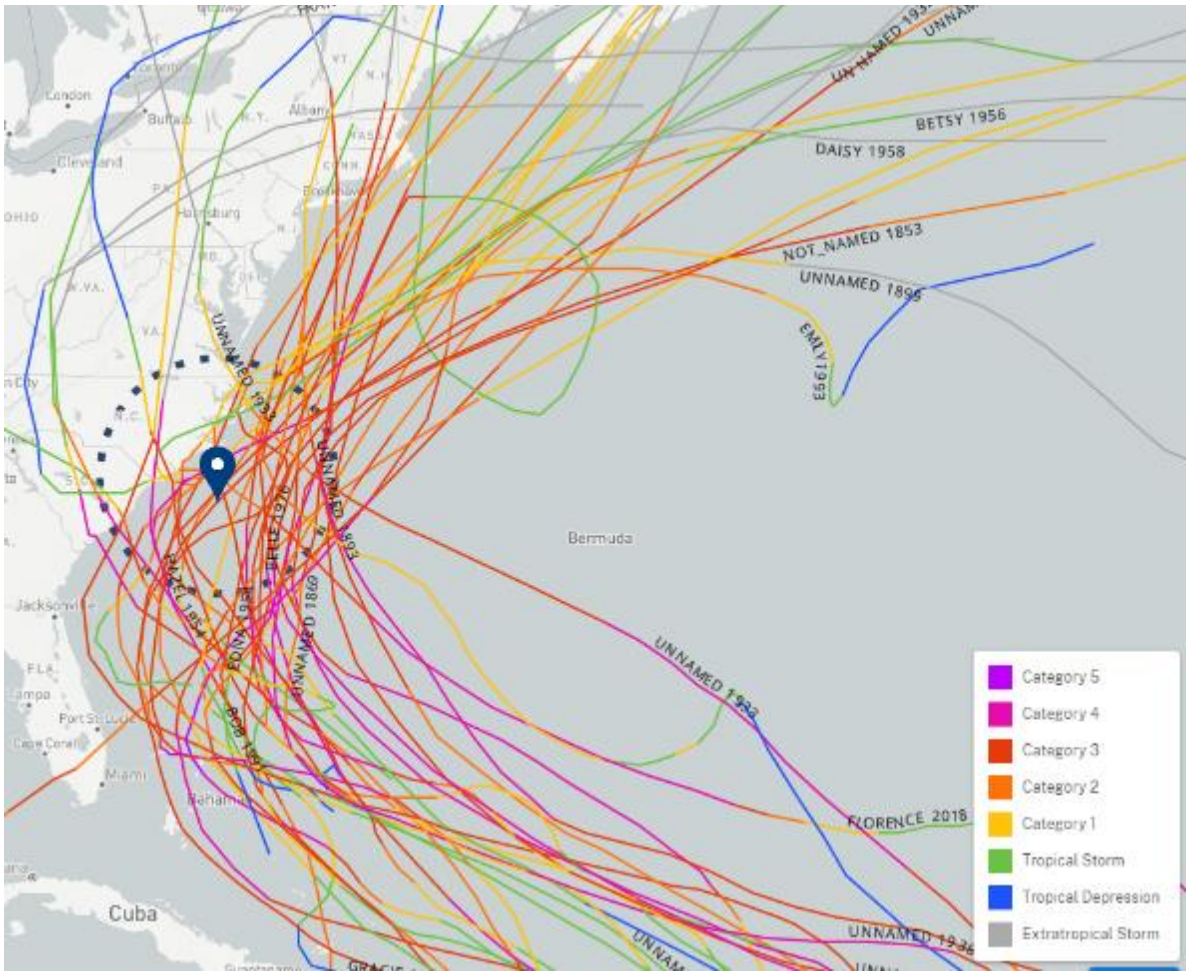

Figure 4-2: Historical Major TC Tracks Along the U.S. Atlantic Coast from 1842 to 2019 [1]

It can be seen from this figure that storms reaching a category 5 strength are located just offshore of southern Florida. Category 4 strength storms do not typically reach latitudes higher than Cape Hatteras, NC and therefore storms which reach the WEAs in Delaware Bay and Southern New England do not typically reach strengths greater than category 3.

4.1.1 TC Event Frequency and Magnitude

Historical TC number of occurrences and intensity for each WEA region was collected from the NHC Historical Hurricane Tracks – GIS Map Viewer [1] with dataset from IBTrACS [9] [10]. A search radius of 200 nautical miles was used to capture historical TCs within the four WEAs. The latitude and longitude used for the search area center is provided in Table 4-1. A bar chart illustrating TC number of occurrences by Saffir-Simpson category for each WEA region is provided in Figure 4-3.

Table 4-1: Locations for NHC Search Area

Sub-Region	State(s)	Latitude (deg)	Longitude (deg)
Long Bay	NC, SC	33.29	-78.47
Chesapeake Bay	NC, VA	36.63	-75.16
Delaware Bay	DE, MD, NJ	38.81	-74.23
Southern New England	NY, RI, MA	40.93	-70.60

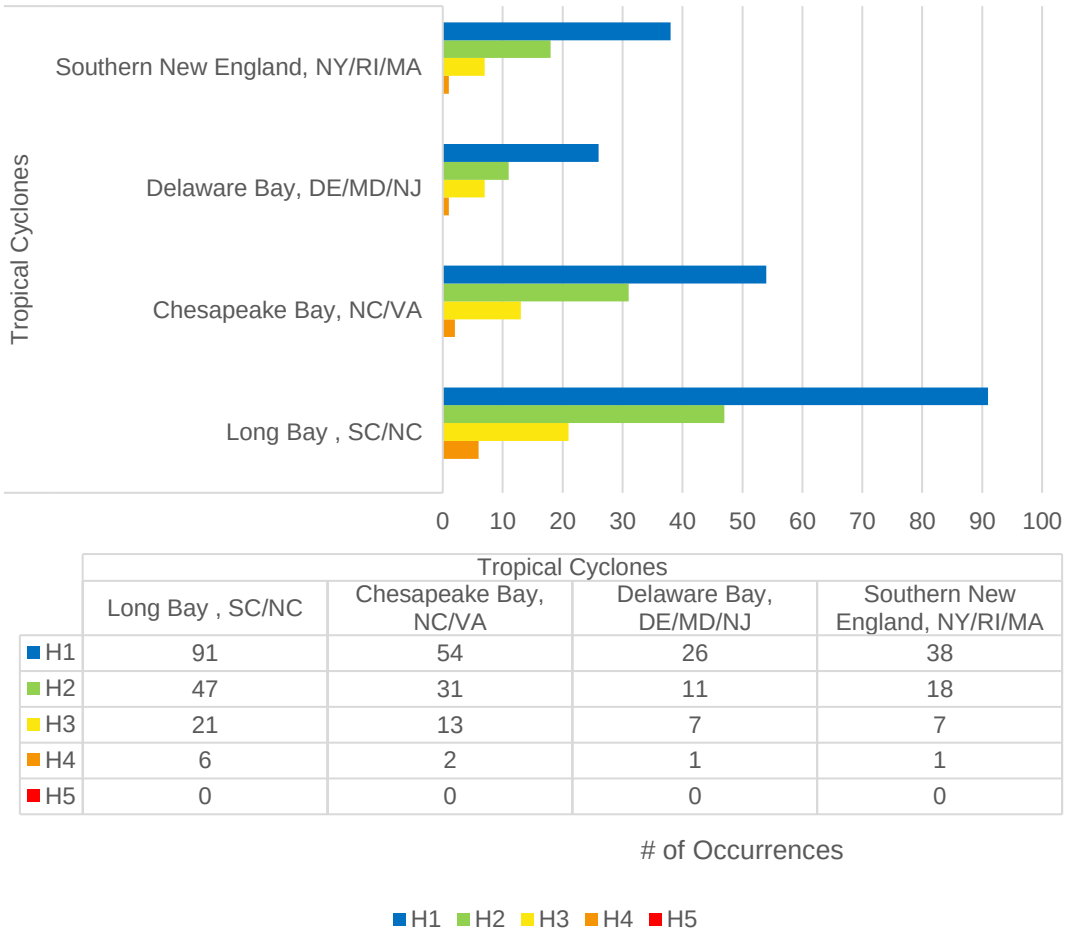

	Tropical Cyclones			
	Long Bay , SC/NC	Chesapeake Bay, NC/VA	Delaware Bay, DE/MD/NJ	Southern New England, NY/RI/MA
H1	91	54	26	38
H2	47	31	11	18
H3	21	13	7	7
H4	6	2	1	1
H5	0	0	0	0

Figure 4-3: Historical TC Frequency and Magnitude per U.S. WEA from 1842 to 2019

No region experiences greater than a category 4 storm, with category 1 storms as the most prevalent. The risk generally decreases by increasing latitude with the one exception being the Southern New England region. This region is located the farther offshore than the Delaware bay region and could explain the higher number of occurrences when compared with the Delaware Bay region.

It should be noted that the NHC dataset [1] does not include all possible sources of historical hurricanes. For a more accurate number of occurrences, this dataset could be supplemented by additional sources such as those stated in [2]. However, for the purposes of this research the dataset is adequate to demonstrate a holistic risk picture across the WEAs.

4.2 Extra-Tropical Cyclones

Since extra-tropical cyclones form near the mid-latitudes, the Delaware Bay and Southern New England WEAs are the most susceptible to extreme event loading caused by ETCs. ETCs affecting these WEAs are typically modified TCs that transformed from a warm core system to a cold core system as it moved out of the tropics.

The U.S. Atlantic coast also provides ideal conditions for formation of Nor'easter type ETCs. During the winter, cold air from the Arctic is transported further southeast towards Canada and the U.S. by the polar jet stream. Warm water from the Gulf Stream helps to keep the coastal waters of the Atlantic relatively warm during the winter, which in turn warms the air directly above the sea surface. The temperature contrast when these two air masses meet generate ideal conditions for formation of Nor'easters [6].

A depiction of historical extra-tropical cyclones affecting the Chesapeake Bay, Delaware Bay and Southern New England regions from 1842 to 2019 during October through April is provided in Figure 4-4. It can be seen from this figure that ETC activity is concentrated north of Cape Hatteras, NC.

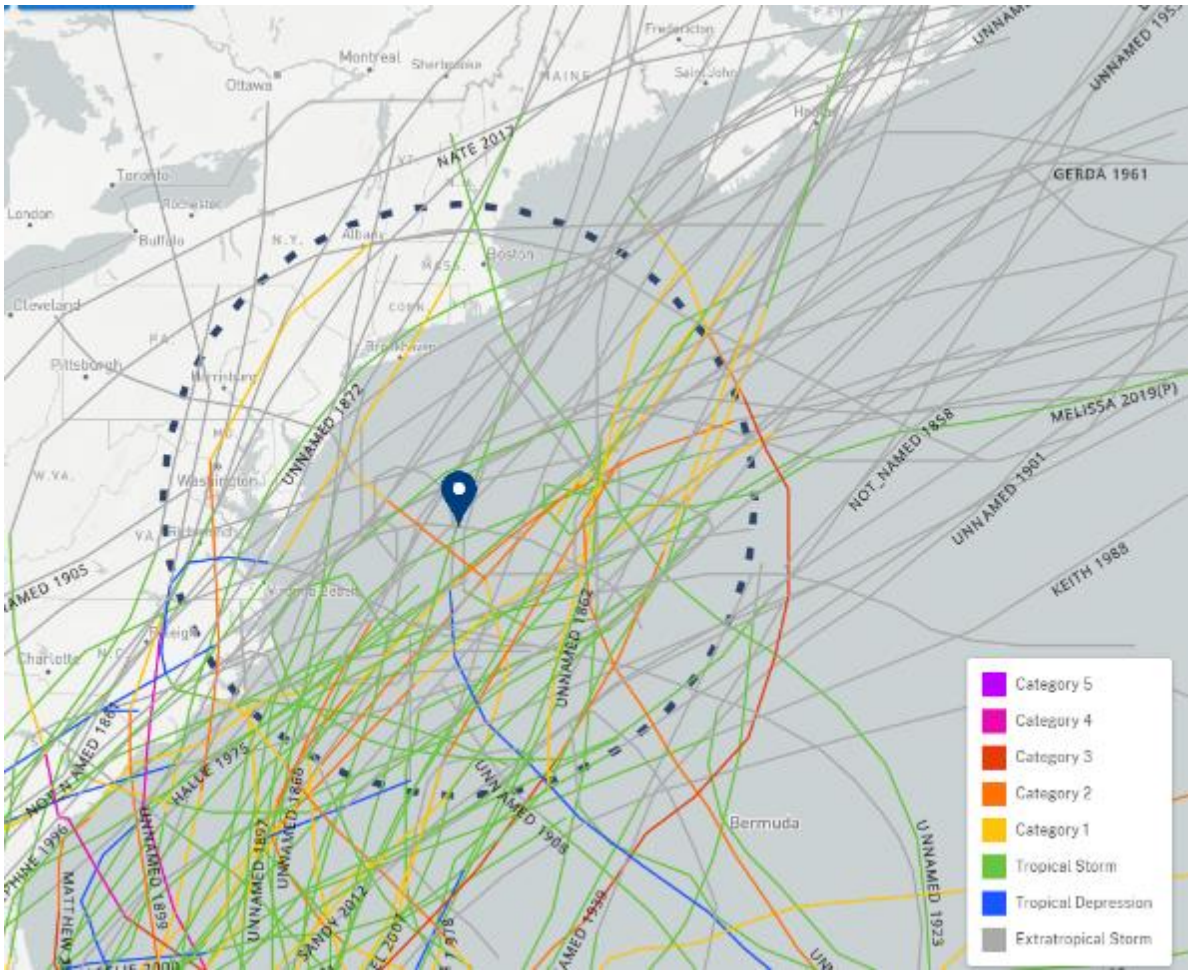

Figure 4-4: Historical ETC Tracks Along the U.S. Atlantic Coast from 1842 to 2019 during October through April [1]

Historical ETC number of occurrences and intensity for each WEA region was collected from the NHC Historical Hurricane Tracks – GIS Map Viewer [1] with dataset from IBTrACS [9] [10]. A search radius of 200 nautical miles was used to capture historical ETCs within the four WEAs. Though the diameter of ETCs are generally larger than 400 nautical miles, this search diameter was chosen in order to capture ETCs directly within the WEA regions. If a larger search radius was chosen, the ETC number of occurrences would have been generally the same for Mid-Atlantic and Southern New England regions. The latitude and longitude used for the search area center is the same as was used for TCs and shown in Table 4-1.

Though ETC's are not categorized by magnitude like TCs, an equivalent Saffir-Simpson scale category was assigned to ETCs to illustrate ETC intensity. Nor'easters were separated from typical ETC's based on the months in which they occur. Nor'easters were taken from October through and April and ETCs taken from May through September.

A bar chart illustrating ETC and Nor'easter number of occurrences by equivalent Saffir-Simpson category for each WEA region is provided in Figure 4-5.

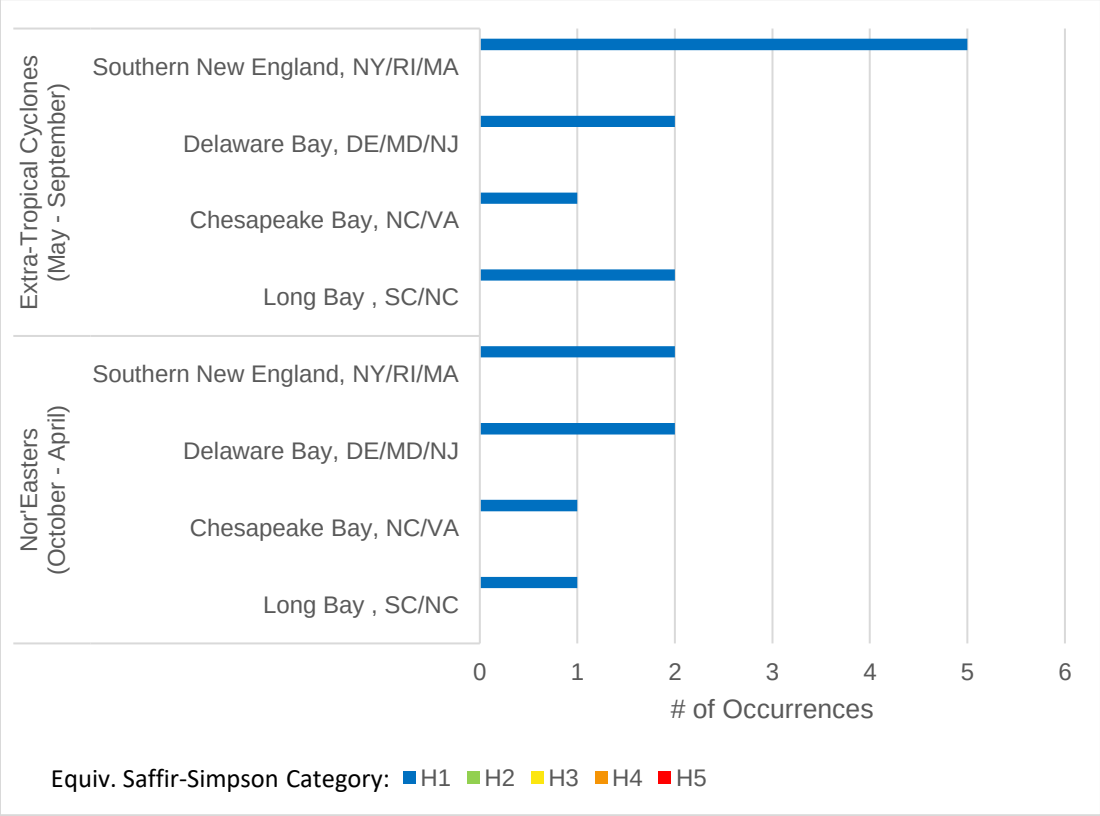

Figure 4-5: Historical ETC and Nor'easter Frequency and Magnitude per U.S. WEA from 1842 to 2019

The largest number of ETCs is experienced at the northernmost WEA, Southern New England. Both ETCs and Nor'easters affecting the WEAs do not reach wind speeds higher than a category 1 on the Saffir-Simpson scale. It should be noted that the risk picture illustrated here is purely based on wind speed; however due to the geographic size of ETCs and Nor'easters, large and energetic waves can build up over the open waters of the North Atlantic and affect the WEAs. These waves may be larger than those generally associated with category 1 TCs.

It is anticipated that the number of occurrences for ETCs and Nor'easters is underestimated when solely using the NHC historical archive [1]. The NHC dataset is not comprehensive for Nor'easters or ETC. In order to reflect a more accurate number of occurrences for these events a supplemental data set such as the NOAA Storm Events Database [56] is recommended. However, for the purposes of this research the dataset is adequate to demonstrate a holistic risk picture across the WEAs.

4.3 Extreme Event Frequency and Magnitude

The gathered TC, ETC and Nor'easter number of occurrences and magnitude were graphed by region to illustrate the total risk picture for each WEA. These charts are provided in Figure 4-6 through Figure 4-9.

Storm Class	Wind Speed m/s	Wind Speed m/s
H5	70	
H4	59	69
H3	50	58
H2	43	49
H1	32	43

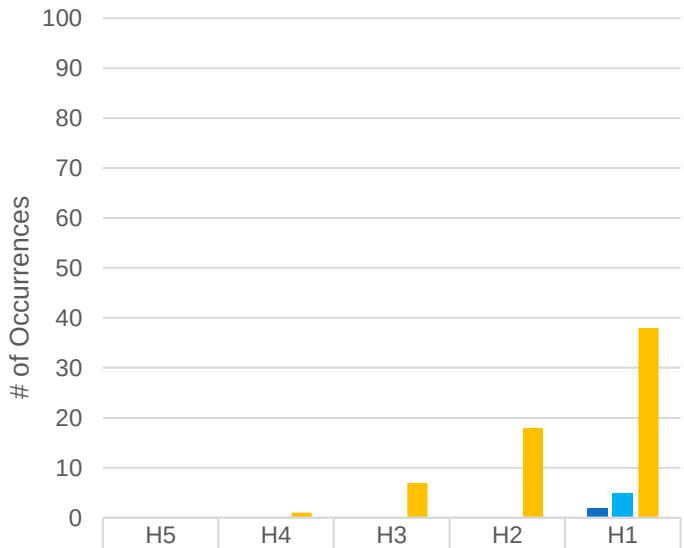

	H5	H4	H3	H2	H1
Nor'Easters (October - April)	0	0	0	0	2
Extra-Tropical Cyclones (May - September)	0	0	0	0	5
Tropical Cyclones	0	1	7	18	38

Saffir-Simpson Storm Category

Figure 4-6: Southern New England ETCs, TCs and Nor'easters

Storm Class	Wind Speed m/s	Wind Speed m/s
H5	70	
H4	59	69
H3	50	58
H2	43	49
H1	32	43

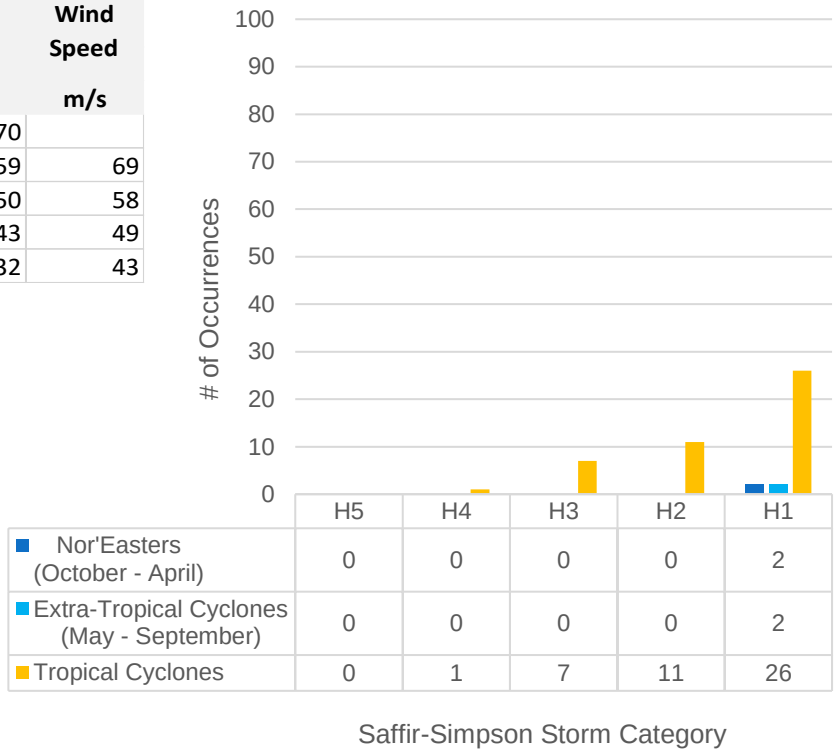

Figure 4-7: Delaware Bay ETCs, TCs and Nor'easters

Storm Class	Wind Speed m/s	Wind Speed m/s
H5	70	
H4	59	69
H3	50	58
H2	43	49
H1	32	43

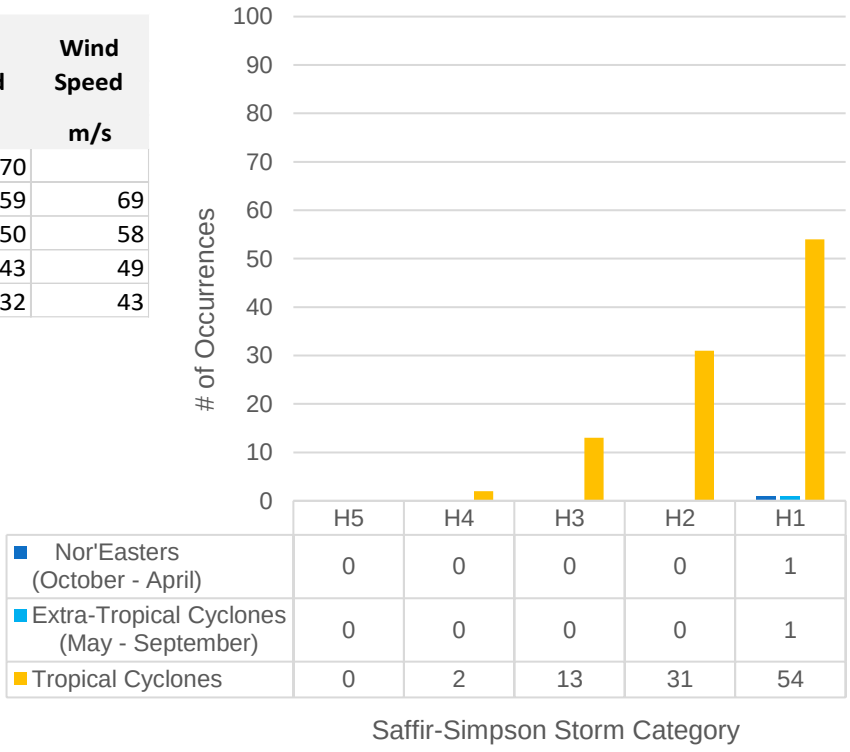

Figure 4-8: Chesapeake Bay ETCs, TCs and Nor'easters

Storm Class	Wind Speed m/s	Wind Speed m/s
H5	70	
H4	59	69
H3	50	58
H2	43	49
H1	32	43

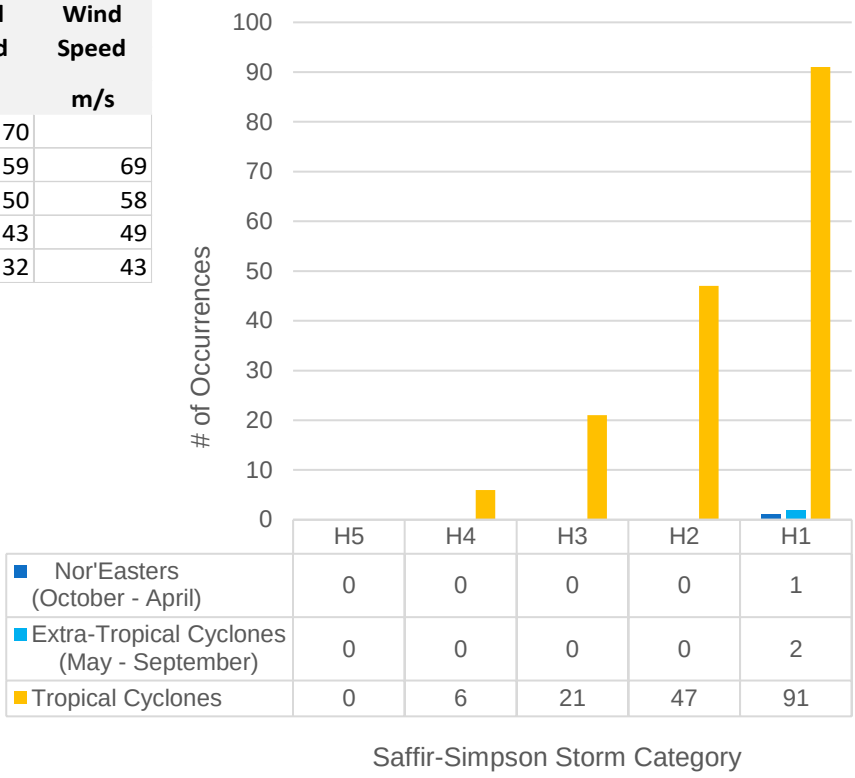

Figure 4-9: Long Bay ETCs, TCs and Nor'easters

Based on these figures it can be anticipated that major TCs with wind speeds greater than 50 m/s will dominate the higher return period design wind speeds since these events have a lower historical number of occurrences. Category 1 and 2 TCs with wind speeds lower than 50 m/s are expected to influence lower return period event wind speeds. Nor'easters and ETCs will have an influence on the lower return period events in both the Delaware Bay and the Southern New England regions and minimal influence on the Chesapeake Bay and Long Bay region design wind speeds.

4.4 Design Extreme Events

In order to illustrate the predominant wind speed for each storm type and region, the mean and standard deviation of 1-minute sustained surface wind speeds gathered from the NHC historical database [1] were calculated. These values are plotted in Figure 4-10. The full dataset for each storm type and region is included as a part of this report in Appendix A2.

Historical data such as the IBTrACS [10] [9] does not provide sufficient enough data to establish exceedance curves for each WEA. In design, hindcast, forecast and reanalysis models are calibrated against historical measurements and utilized to establish exceedance curves. Theoretical storm criteria is then extracted for each required return period event and applied in design. The exceedance curves and theoretical storm criteria included as a part of two publically available studies [45] [14] funded by BOEM were used for this research to determine the 50-year and 500-year return period wind speeds in each WEA. These values are plotted in Figure 4-10 for each region by latitude.

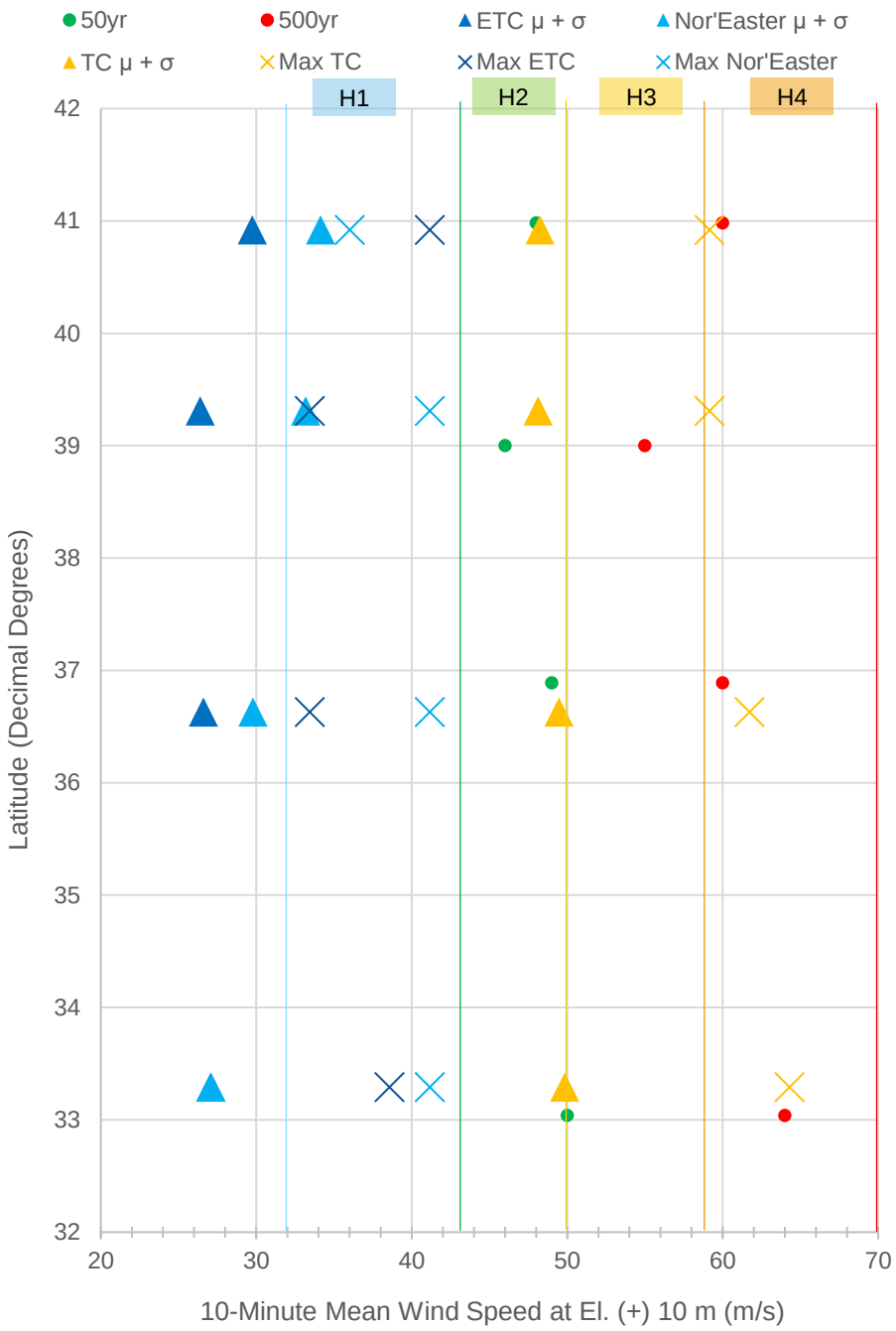

Figure 4-10: Extreme Wind Speeds at WEAs along U.S. Atlantic Coast

Based on this chart it can be seen that a category 4 storm wind speed ranging from 60 to 64 m/s and associated metocean criteria would be used in the robustness case analysis in the Southern New England, Chesapeake Bay and Long Bay regions. A category 3 storm wind speed of 55 m/s and associated metocean critera would be used in the robustness case analysis of the Delaware Bay region.

All regions correspond to a category 2 storm for the 50-year return period design criteria, with wind speeds ranging from 46 to 50 m/s. 50 m/s corresponds to a Class I turbine in IEC 61400-

1-1 [21] and therefore fits within the criteria originally determined for North Sea turbines. Therefore, it is only the robustness case wind speeds and metocean criteria that are significantly different from North sea design values. As mentioned previously, the robustness case analysis is included as a part of the design process due to the steep hazard curve in tropical cyclone regions to ensure the structures do not fail during events within a reasonable chance of ocurring. It should be mentioned, the robustness case analysis applies only to the support structure including nacelle to tower flange, tower, sub-structure and foundation and does not apply to the RNA.

It can be seen from this study of North Atlantic TC and ETC hazard that the wind speeds expected at the WEAs for the robustnes case are larger than those included in the typical North Sea design methodology and therefore require additional study as to the affects to design and behavior of offshore wind turbine sub-structures

5 ANALYSIS CRITERIA

The following sections describe all analysis criteria required to determine monopile mudline loads to be applied in the subsequent Plaxis 3D analyses.

5.1 Metocean Criteria

5.1.1 Wind Speeds

The 1-minute sustained surface wind speed associated with the lower bound criteria for each Saffir-Simpson category was used as the reference wind speed, Vref, for each analysis. Extreme wind speed variation with height above sea level was calculated using Equation 5-1 from IEC 61400-3-1 [28].

$$V_{hub} = V_{ref}\left(\frac{z_{hub}}{z_{ref}}\right)^{0.11} \qquad \textbf{Equation 5-1}$$

Using Equation 5-1, the wind speed at hub height for each turbine was calculated. Surface and hub height wind speeds for each turbine size are provided in Table 5-1.

Table 5-1: Wind Speed for Each Saffir-Simpson Category and Turbine Size

Turbine Size (MW)	z_{ref} (m)	H1 V_{ref} (m/s)	H2 V_{ref} (m/s)	H3 V_{ref} (m/s)	H4 V_{ref} (m/s)	HH El. (m)	α, Shear Factor	H1 V_{hub} (m/s)	H2 V_{hub} (m/s)	H3 V_{hub} (m/s)	H4 V_{hub} (m/s)
6	10	32.00	43.00	50.00	59.00	105	0.11	41.50	55.70	64.80	76.50
8	10	32.00	43.00	50.00	59.00	115	0.11	41.90	56.30	65.50	77.20
10	10	32.00	43.00	50.00	59.00	125	0.11	42.30	56.80	66.10	77.90
12	10	32.00	43.00	50.00	59.00	135	0.11	42.70	57.30	66.60	78.60

5.1.2 Water Depths

Water depths at each site were gathered using NOAA Raster Navigational Charts [53]. A depiction of minimum, mean and maximum water depths at each Atlantic coast Region is provided in Figure 5-1. In addition, a shaded range is shown, highlighting the optimal range of water depths for a monopile type support structures. It can be seen from Figure 5-1, that the Southern New England Region includes the deepest water depths up to 62 meters, with an average water depth of 46 meters. The Long Bay, SC call areas include the shallowest water depth at 7meters and an average of 22 meters. Based on these observed water depth ranges, it was concluded that depths of 20, 40 and 50 meters would be representative of the future commercial offshore wind farms.

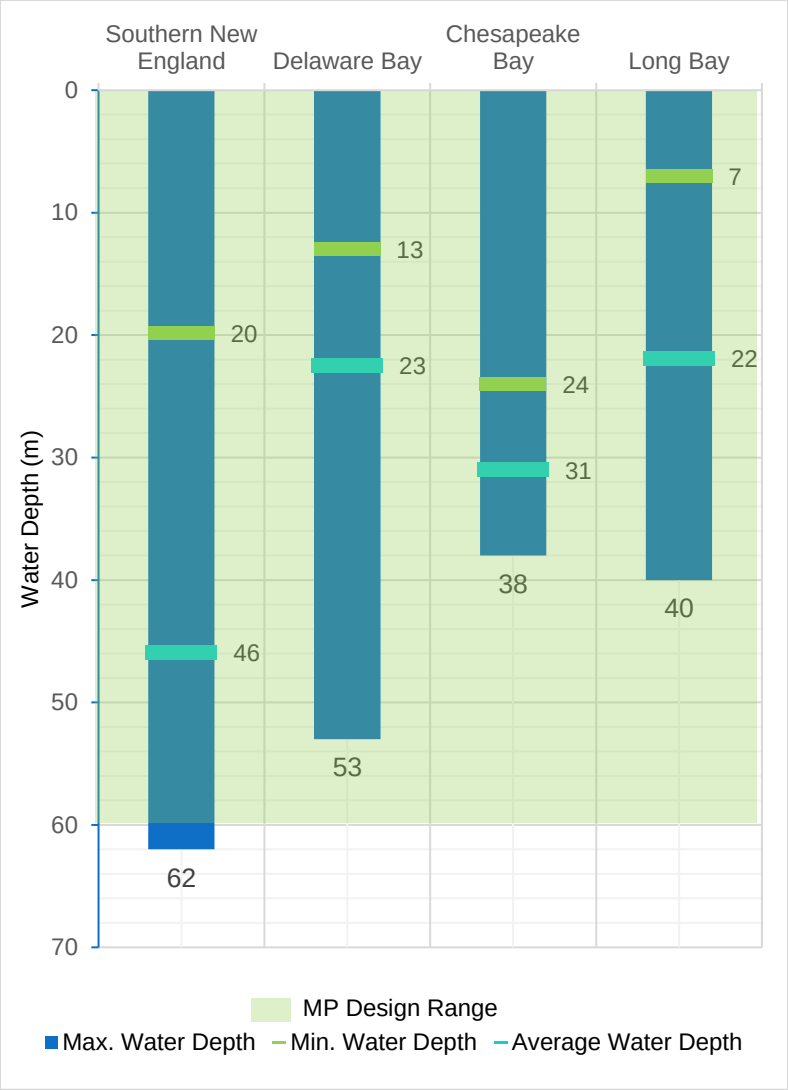

Figure 5-1: Range of Water Depths for WEAs

5.1.3 Wave Height and Period

The Bureau of Ocean and Energy Management funded two studies [15] [14] be performed to characterize metocean conditions at U.S. Atlantic coast WEAs. These studies used NOAA buoy data as well as hindcast and forecast modelling to determine 50, 100 and 500 year design return period values at specific points in each WEA. The studies each generated a database of 10-minute mean wind speed at (+) 10 meter elevation and associated significant wave height and water depth for both ETCs and TCs.

Wind speed values from these databases were binned by Saffir-Simpson category for use in this research. The associated significant wave heights for each Saffir-Simpson category were plotted by water depth. A trendline was fit to each dataset to determine the associated significant wave height for each water depth as shown in Figure 5-2.

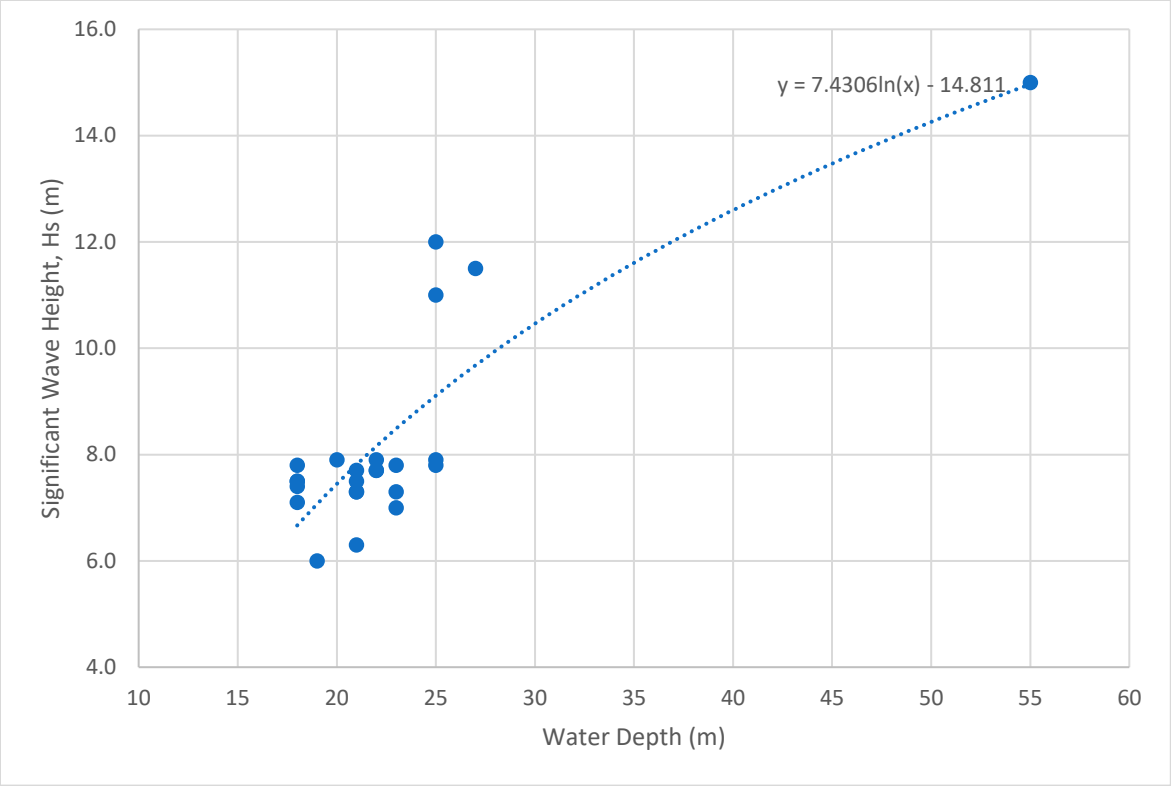

Figure 5-2: Significant Wave Height Vs. Water Depth for H1 Category

Maximum wave height was calculated from the significant wave height for each water depth as shown in Equation 5-2 [28].

$$H_{max} = 1.86\, H_s \qquad \textbf{Equation 5-2}$$

Associated wave period was calculated from the significant wave height using Equation 5-3 [28]. In design, both the min and max period would be analyzed to determine which produces the largest force on the structure. For this research however the mean value was used for each load case.

$$11.1\sqrt{\frac{H_s}{g}} \leq T \leq 14.3\sqrt{\frac{H_s}{g}} \qquad \textbf{Equation 5-3}$$

For the higher wind speed cases corresponding to Saffir-Simpson category 3 through 5, waves were breaking depth limited. Breaking wave heights were calculated using Equation 5-4 [28] .

$$H_b = 0.78\, d \qquad \textbf{Equation 5-4}$$

Database of parameters used from [15] [14] as well as the calculations to determine maximum wave height and associated period are included as a part of this report in Appendix A3.

As Bentley SACS does not offer a breaking wave theory option, higher order stream function wave theory was used to model expected hydrodynamic events. Wave theory was determined via Figure B.1 in [28] using the breaking wave height from Equation 5-4. Calculations are included as a part of this report in Appendix A3. In design or future research, breaking wave theory should

be utilized to determine expected hydrodynamic loading for category 3 to 5 storms, especially in shallow water depths such as 20 – 30 meters.

5.1.4 Surge and Tide

NOAA tide tables [57] were used to determine maximum tidal variation at each site. Station reports are included as a part of this report in Appendix A4.

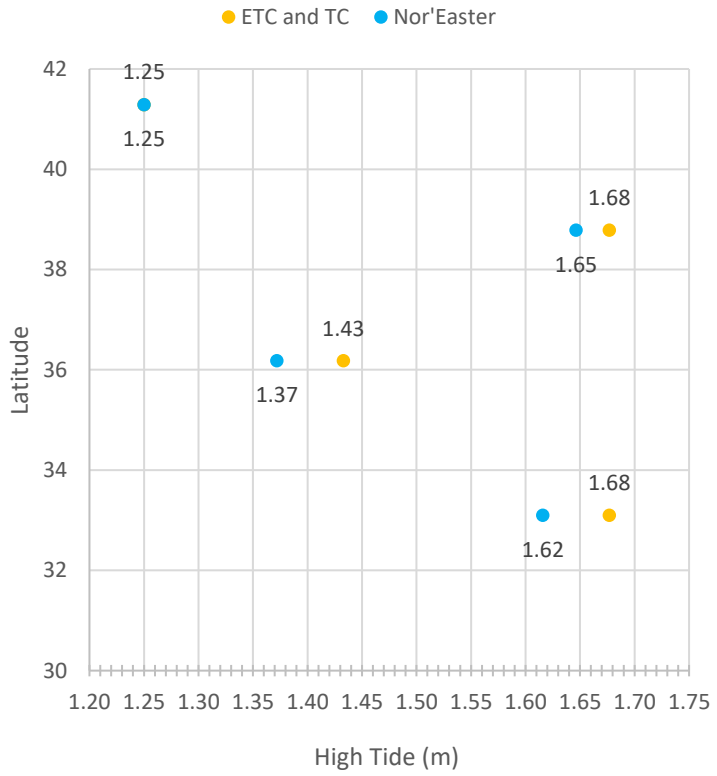

Figure 5-3: Mean Higher High Water by Latitude

Table 5-2: Tidal Variation at each WEA

NOAA Station Name	Latitude (Decimal Degrees)	Tidal Range (m)	High Tide (m MLLW)	Storm Type
TEC3011	33.1	1.79832	1.68	ETC and TC
8651370	36.18	1.55448	1.43	ETC and TC
8557380	38.783	1.85928	1.68	ETC and TC
8449130	41.29	1.40208	1.25	ETC and TC
TEC3011	33.1	1.73736	1.62	Nor'easter
8651370	36.18	1.49352	1.37	Nor'easter
8557380	38.783	1.8288	1.65	Nor'easter
8449130	41.29	1.40208	1.25	Nor'easter

MEAN (μ): 1.49

Strongest tides are found to be typical during the warmer months and would be applied in conjunction with a TC analysis or ETC analysis. However, since the cases analyzed for this

research are for a combined maximum from ETCs, TCs and Nor'easters, the mean value was used to represent the high tide water level.

The surge associated with each Saffir-Simpson category storm from [3] as shown in Figure 5-4 was used for this study. The minimum surge was used as this is assumed to correspond to the minimum wind speed for each category.

Scale Number (Category)	Winds (Mph)	Typical characteristics of hurricanes by category			
		(Millibars)	(Inches)	Surge (Feet)	Damage
1	74-95	> 979	> 28.91	4 to 5	Minimal
2	96-110	965-979	28.50-28.91	6 to 8	Moderate
3	111-130	945-964	27.91-28.47	9 to 12	Extensive
4	131-155	920-944	27.17-27.88	13 to 18	Extreme
5	> 155	< 920	< 27.17	> 18	Catastrophic

Figure 5-4: Saffir-Simpson Scale with Associated Surge [3]

The minimum surge was combined with the mean tide to determine the total water level for each category storm. The design water later levels are provided in Table 5-3.

Table 5-3: Design Water Level

Saffir-Simpson Category	Min Surge (m)	Median Surge (m)	Max Surge (m)	Min Surge + Tide (m)	Median Surge + Tide (m)	Max Surge + Tide (m)	Design Surge + Tide (m)
H1	1.22	1.37	1.52	2.71	2.86	3.01	2.70
H2	1.83	2.13	2.44	3.32	3.62	3.93	3.30
H3	2.74	3.20	3.66	4.23	4.69	5.15	4.25
H4	3.96	4.73	5.49	5.45	6.22	6.98	5.50

5.1.5 Current Speed

Wind-generated surface current velocities were calculated as specified in IEC 61400-3-1 Section 6.3.3.3 [28]. As stated in IEC 61400-3-1 [28], the depth of influence for wind generated currents is 20 meters. Therefore, the wind-generated current speed increases from zero m/s at a 20 meter depth for each category storm as shown in Figure 5-5.

The 500-year return period sea surface current velocity was taken as 1.25 m/s. The subsequent sub-surface current velocities were then calculated using as specified in IEC 61400-3-1 Section 6.3.3.3.2 [28] and shown in Figure 5-6.

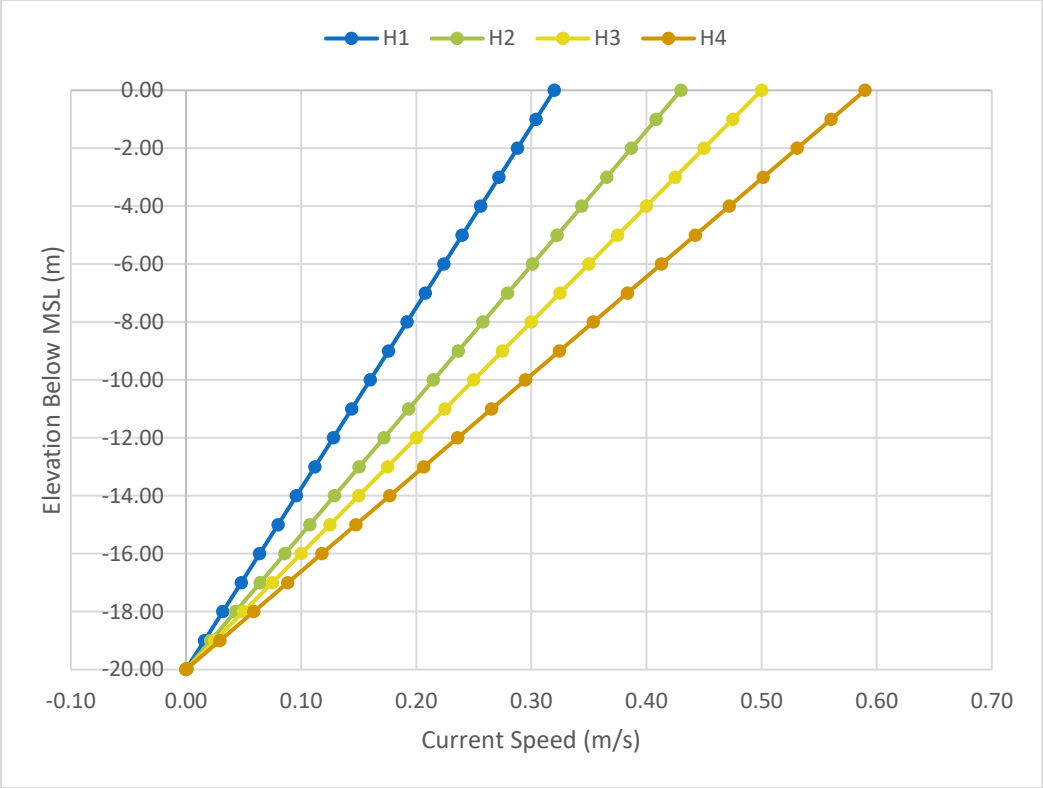

Figure 5-5: Wind-Generated Surface Currents

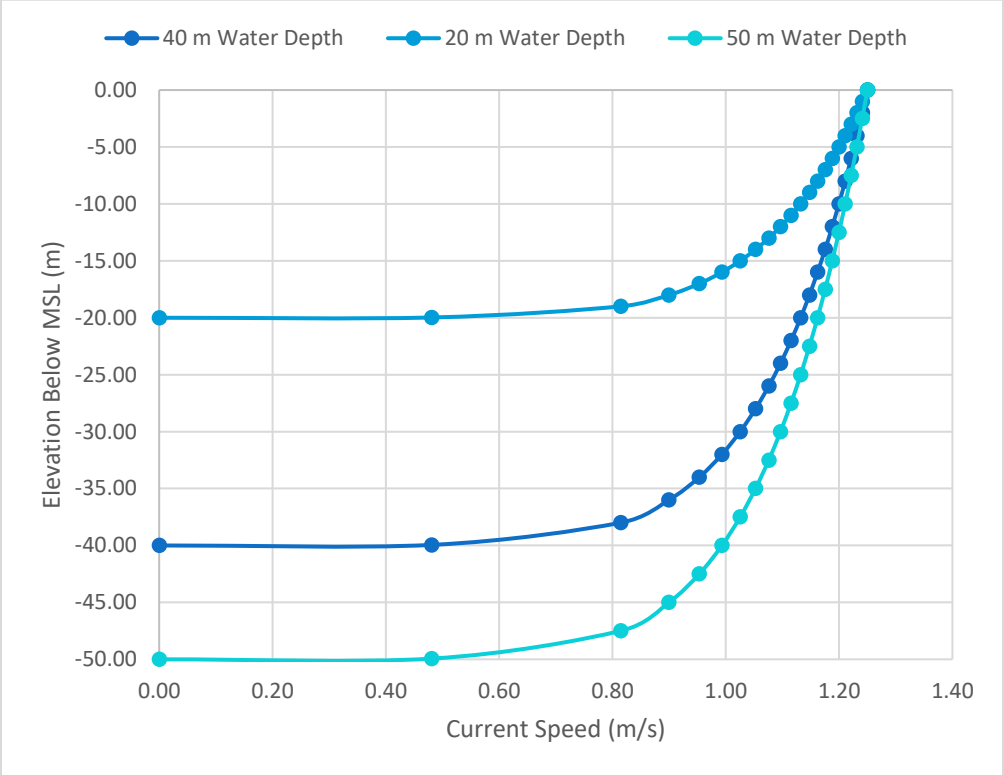

Figure 5-6: Sub-Surface Current Speeds

The total current profile for each water depth is provided in Appendix A5. Since the sub-surface current velocity is independent of storm category, the velocity converges at a 20 meter depth below sea surface for each storm category.

The total current values applied in the SACS metocean analysis are shown in Table 5-4. Calculations of wind-generated and sub-surface velocity are provided as a part of this report in Appendix A5.

Table 5-4: Total Current Velocity Per Depth

Sub-surface and Wind-Generated Currents

Water Depth (m) =	20			
Saffir-Simpson Cat =	**H1**	**H2**	**H3**	**H4**
z (%)	**$U_{T(z)}$ (m/s)**	**$U_{T(z)}$ (m/s)**	**$U_{T(z)}$ (m/s)**	**$U_{T(z)}$ (m/s)**
0.05	0.48	0.48	0.48	0.48
25.00	1.11	1.21	1.34	1.49
50.00	1.29	1.51	1.76	2.05
75.00	1.44	1.76	2.14	2.58
100.00	1.57	2.00	2.50	3.09

Sub-surface and Wind-Generated Currents

Water Depth (m) =	40			
Saffir-Simpson Cat =	**H1**	**H2**	**H3**	**H4**
z (%)	**$U_{T(z)}$ (m/s)**	**$U_{T(z)}$ (m/s)**	**$U_{T(z)}$ (m/s)**	**$U_{T(z)}$ (m/s)**
0.05	0.48	0.48	0.48	0.48
25.00	1.03	1.03	1.03	1.03
50.00	1.13	1.13	1.13	1.13
75.00	1.36	1.57	1.82	2.12
100.00	1.57	2.00	2.50	3.09

Sub-surface and Wind-Generated Currents

Water Depth (m) =	50			
Saffir-Simpson Cat =	**H1**	**H2**	**H3**	**H4**
z (%)	**$U_{T(z)}$ (m/s)**	**$U_{T(z)}$ (m/s)**	**$U_{T(z)}$ (m/s)**	**$U_{T(z)}$ (m/s)**
0.05	0.48	0.48	0.48	0.48
25.00	1.03	1.03	1.03	1.03
50.00	1.13	1.13	1.13	1.13
75.00	1.32	1.48	1.67	1.89
100.00	1.57	2.00	2.50	3.09

5.2 Turbines

5.2.1 Wind Turbines

Commercially available turbines are in the range of 8 to 12 MW. The BIWF in Rhode Island is currently operating with 6 MW turbines and the Coastal Virginia Offshore Wind Project in Virginia includes two, 6 MW turbines scheduled for installation in summer of 2020. Therefore, it was decided to also include 6 MW turbines in this research, even though they are no longer commercially available for offshore use. The turbines capacities included within this research are 6, 8, 10 and 12 MW.

Turbines used in this study are theoretical and based on the commercially available turbines shown in Table 5-5 . Other size turbines are commercially available including 7, 9.5 and 11 MW, but it is anticipated that the mudline rotations for monopiles supporting these turbines can be interpolated from the results of this research. Values shown in Table 5-5 may be found from the turbine manufacturer websites. Interface height and tower length changes by project specifics and values noted here are only typical preliminary design values. The reference hub height wind speed, Vhub, is typically 50 m/s, as this corresponds to an IEC 61400-1-1 [21] Class I turbine.

Table 5-5: Commercially Available Turbine Data

Manufacturer	Model	Rotor Diameter (m)	Power (MW)	Vhub (m/s)	HH (m)	Interface Height (m)	Tower Length (m)
GE	HAL 150-6MW	150	6	50	106	24	82
SG	SG-8.0-167	167	8	50	119	34	83
MHI Vestas	V164-8.0 MW	164	8	50	116	21	87
SG	SG-10.0-193	193	10	50	128		96
MHI Vestas	V164-10.0 MW	164	10	50	121	32	96
GE	HAL-X 12MW	220	12	50	139	26	111

5.2.2 Turbine Loading

Tower base lateral shear force and overturning moment for 6, 8, 10 and 12 MW turbines for a 50 m/s reference wind speed at hub height were derived in communication with offshore wind farm designers. Turbine loads provided are for either DLC 6.2 or I.2 [28], meaning that the nacelle is unable to orient out of the wind during extreme events due to a loss of grid connection or failure of the yaw power battery back-up system. Loads were scaled to hub height wind speed expected in each Saffir-Simpson category using Equation 5-5 below:

$$Load(V_{hub}) = \frac{V_{hub}^2}{50^2} \cdot Load(50\ m/s) \qquad \textbf{Equation 5-5}$$

Resulting tower base loads at interface elevation are provided in Table 5-6 and depicted in Figure 5-7 and Figure 5-8. It can be seen from these figures that tower base loads increase by corresponding turbine size and Saffir-Simpson category storm.

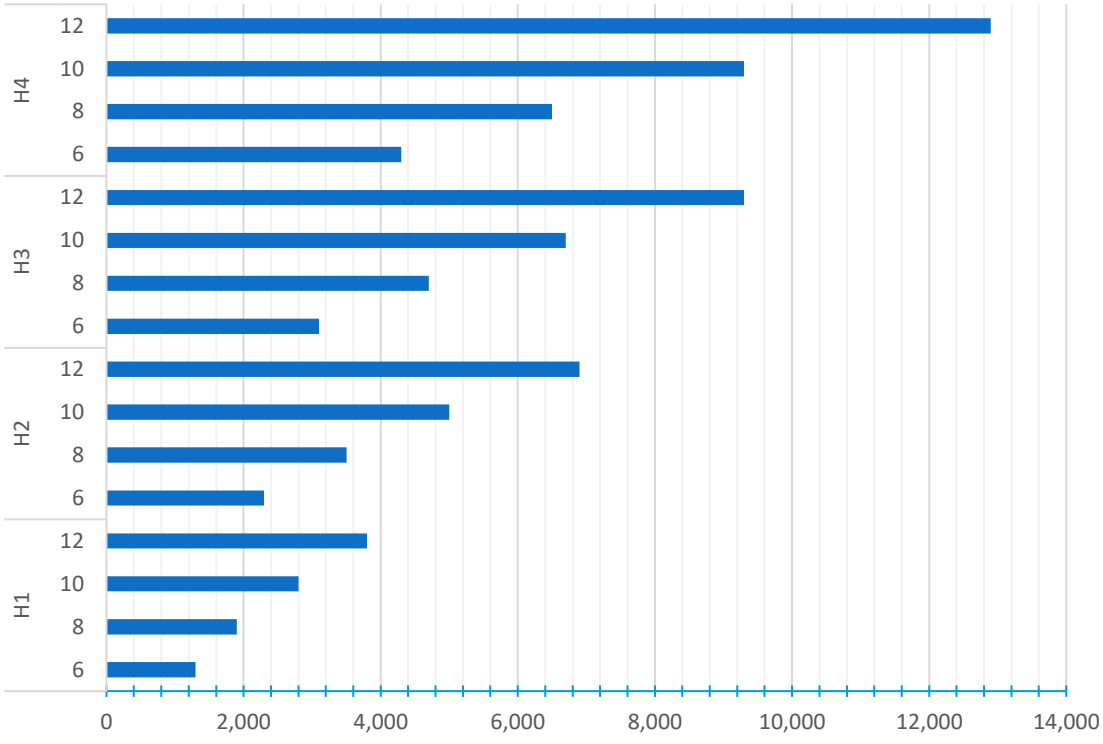

Figure 5-7: Tower Base Fxy (kN)

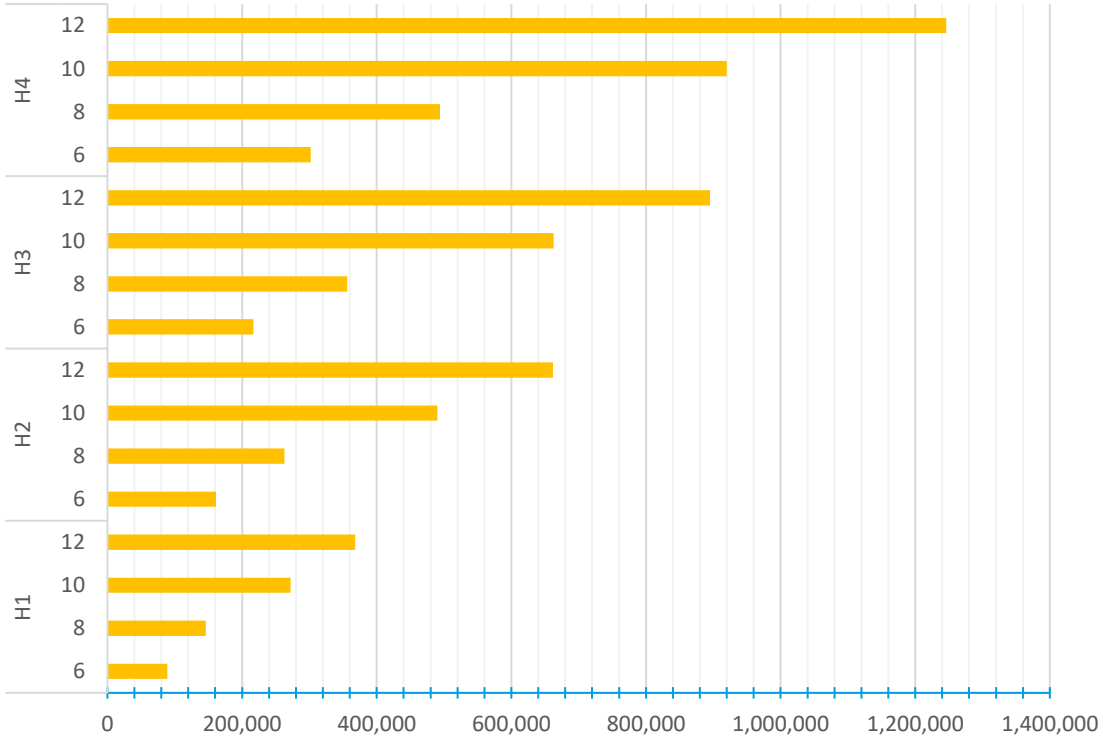

Figure 5-8: Tower Base Mxy (kN-m)

Table 5-6: Tower Base Loads

Turbine Size (MW)	Z hub (m)	Saffir-Simpson Category	Vhub (m/s)	Tower Base Fxy (kN)	Tower Base Mxy (kN-m)
6	105	H1	41.50	1,300	89,000
6	105	H2	55.70	2,300	161,000
6	105	H3	64.80	3,100	217,000
6	105	H4	76.50	4,300	302,000
8	115	H1	41.90	1,900	146,000
8	115	H2	56.30	3,500	263,000
8	115	H3	65.50	4,700	356,000
8	115	H4	77.20	6,500	494,000
10	125	H1	42.30	2,800	272,000
10	125	H2	56.80	5,000	490,000
10	125	H3	66.10	6,700	663,000
10	125	H4	77.90	9,300	920,000
12	135	H1	42.70	3,800	368,000
12	135	H2	57.30	6,900	662,000
12	135	H3	66.60	9,300	895,000
12	135	H4	78.60	12,900	1,246,000

5.3 Monopile Geometry

A different monopile design was used for each turbine size and water depth. The same design was used for each Saffir-Simpson storm category wind speed. The monopile designs chosen are assumed capable of withstanding a 50-year design extreme return period event for each WEA. This methodology follows the typical industry standard, where support structures are designed based on IEC 61400-3-1 [28] DLCs and then the design is checked using robustness case loading to ensure the support structure can withstand events within a reasonable chance of occurring.

Monopile design parameters are provided in Table 5-7 with parameters shown for reference in Figure 5-9.

Table 5-7: Monopile Design Parameters

Water Depth (m)	Turbine Size (MW)	Z_{INTF} (m)	Pile Pen. (m)	OD_{INTF} (m)	OD_{MUD} (m)	$Z_{T.C.}$ (m)	Cone Length (m)	W.T. (mm)	L/D
20	6	23	29	6	8	-1.2	10	75	3.63
40	6	23	39	6	8	-1.2	20	80	4.88
20	8	24	30	6.5	9	-2.5	15	70	3.33
40	8	24	40	6.5	9.5	-2.5	20	75	4.21
50	8	24	43	6.5	9.5	-2.5	25	80	4.53
20	10	24	35	7	10	-3	25	80	3.50
40	10	24	43	7	10	-3	25	80	4.30
50	10	24	46	7	10.5	-3	25	85	4.38
20	12	24	38	8	10	-3	15	75	3.80
40	12	24	45	8	11.5	-1.2	20	85	3.91
50	12	24	47	8	12	-1.2	25	95	3.92

Pile embedment length was calculated to ensure a maximum of 0.20 degree mudline rotation in the H1 case, as described in Section 6 Numerical Analysis. A simplified monopile design was used where wall thickness remained constant. For detailed monopile design each steel can may have a different wall thickness, optimized for expected ULS and FLS loading. Wall thickness was shown to have a negligible effect on the lateral capacity and mudline deflection of the embedded portion of monopile foundation in the PISA project [58]; therefore it is considered a reasonable simplification.

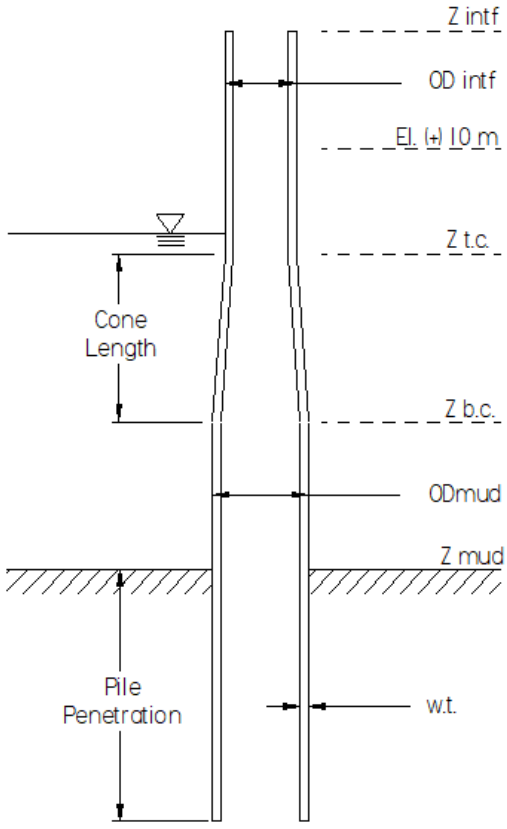

Figure 5-9: Monopile Design Parameters

5.4 Soil Type

The Continental Margin Mapping database from Woods Hole Coastal and Marine Science Center [59] [60] for the United States East Coast Continental Margin was used to determine expected soil type at each WEA. Sediment sample locations are included in the database by latitude and longitude coordinates. The database was sorted by a bounding box of latitude and longitude coordinates for the four WEAs. The resulting percentage of surficial sediments types was then charted as shown in Figure 5-10 through Figure 5-13. Percentage of each soil type at each sample location is also charted and provided as a part of this report in Appendix A6. A GIS layer provided by Woods Hole Coastal and Marine Science Center [60] [59] was added to the BOEM Wind Energy Areas GIS layer [55] for a geographical view of surficial soil type expected at each offshore wind farm project site. These geographical snapshots are also provided in Figure 5-10 through Figure 5-13.

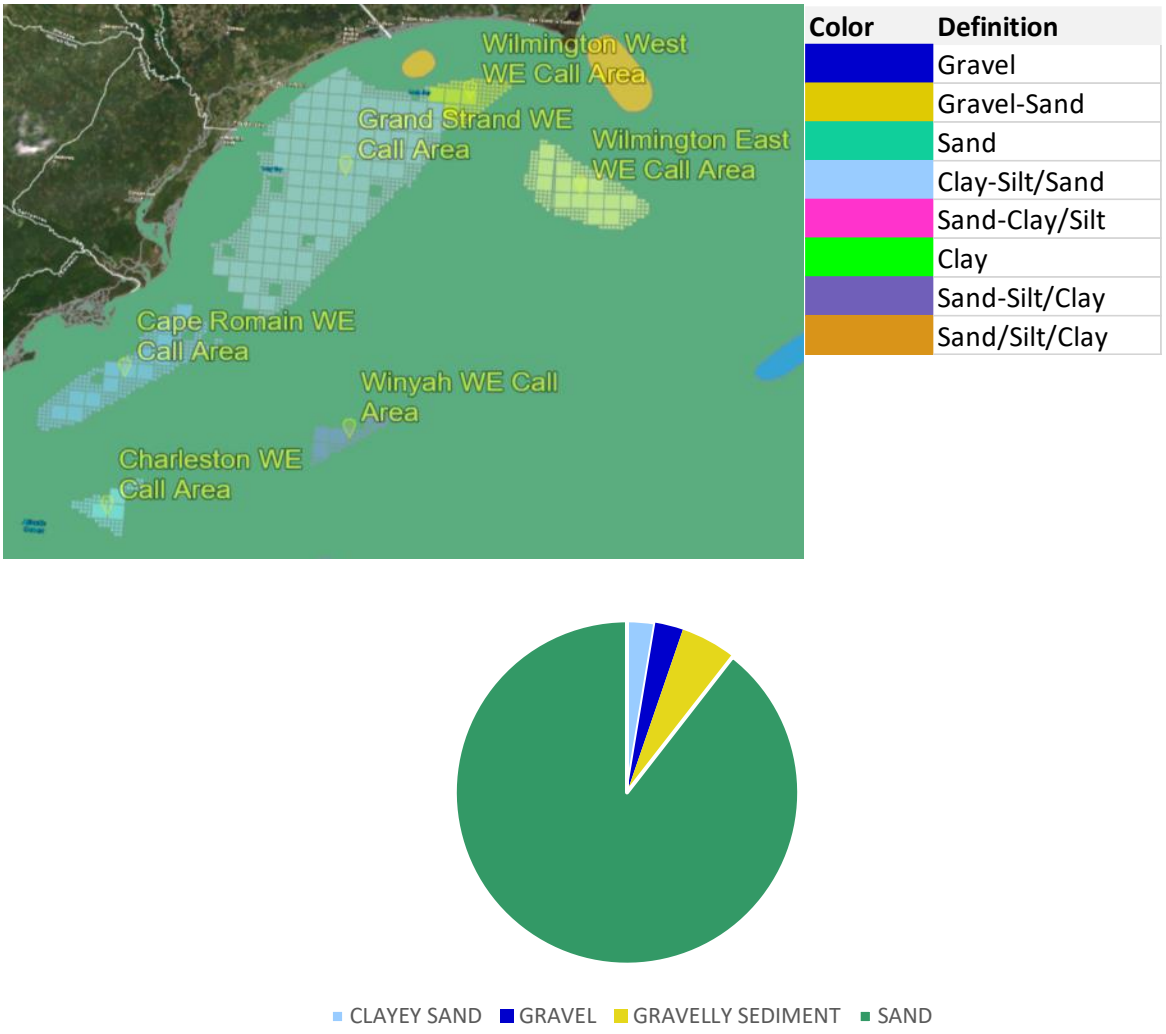

Figure 5-10: Surficial Sediments in Long Bay, SC WEAs [60] [55]

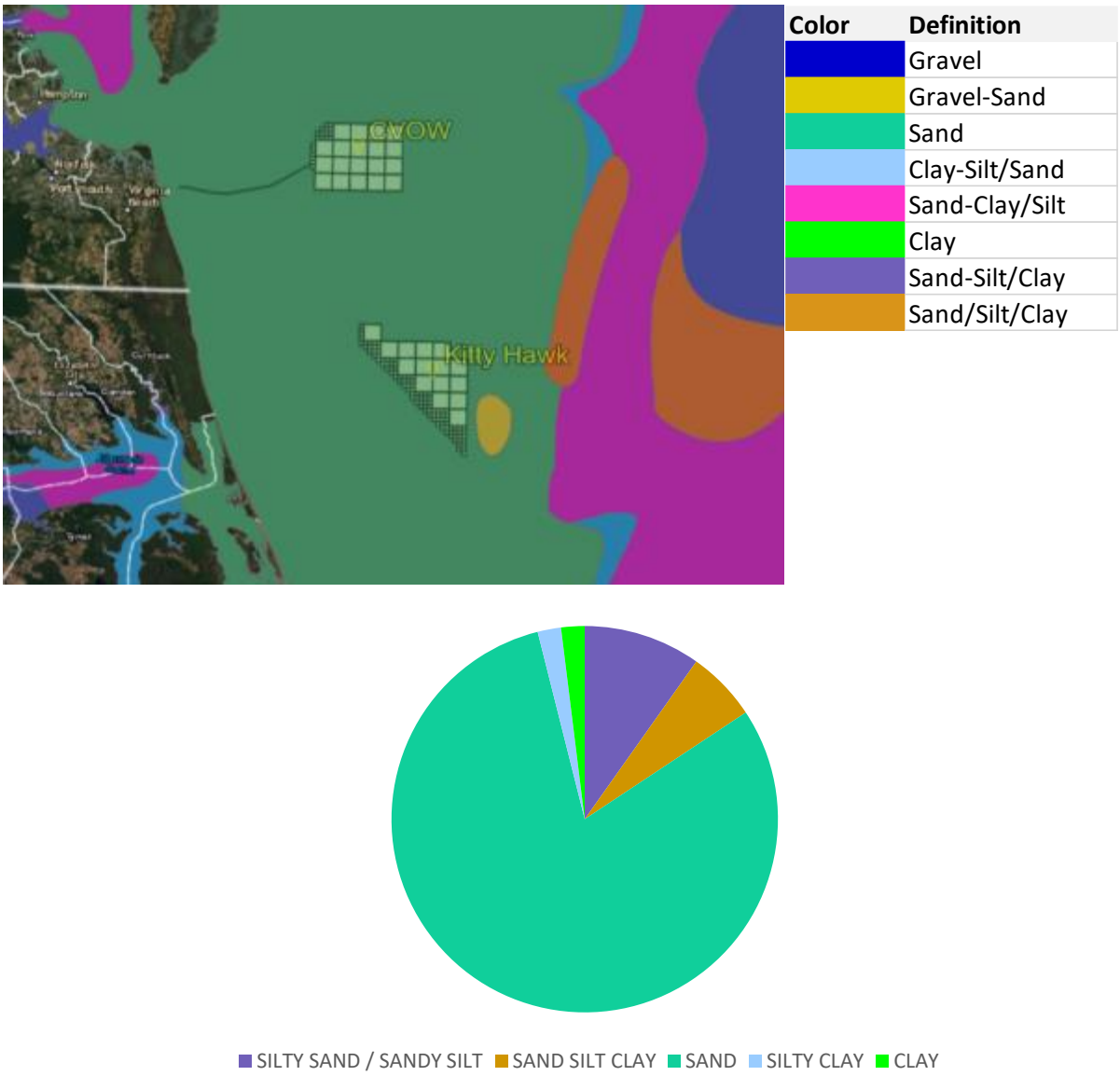

Figure 5-11: Surficial Sediments in Chesapeake Bay WEAs [60] [55]

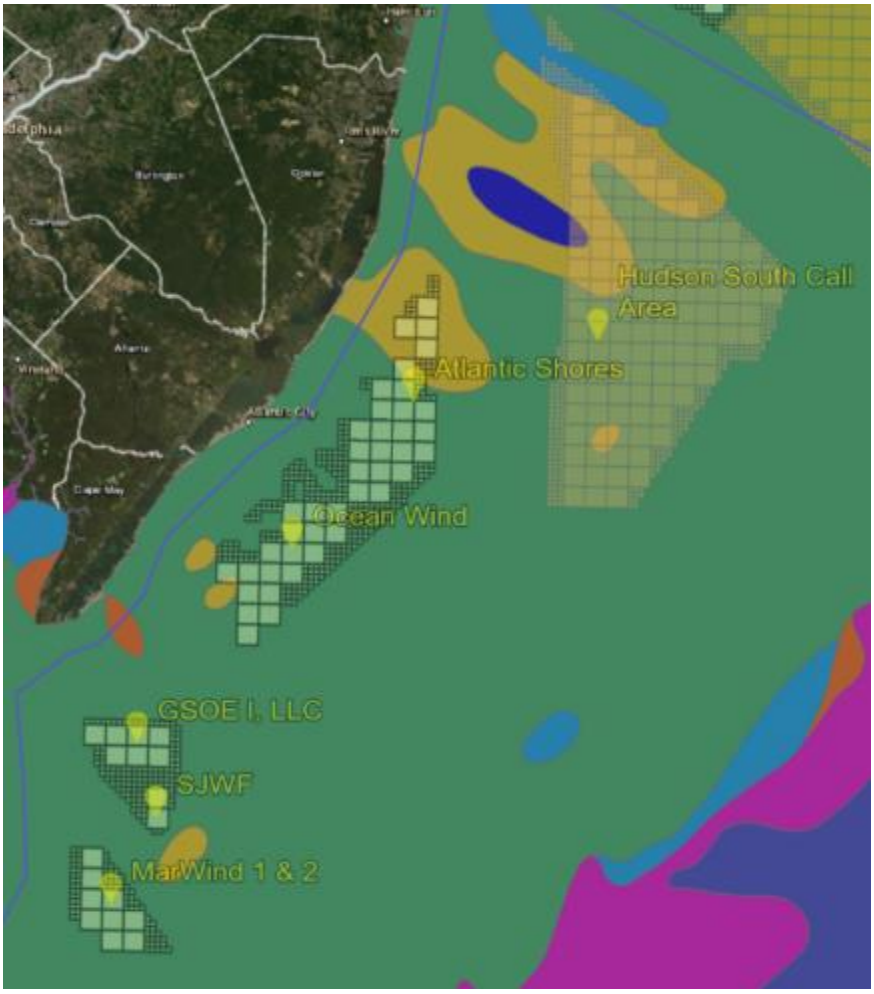

Color	Definition
	Gravel
	Gravel-Sand
	Sand
	Clay-Silt/Sand
	Sand-Clay/Silt
	Clay
	Sand-Silt/Clay
	Sand/Silt/Clay

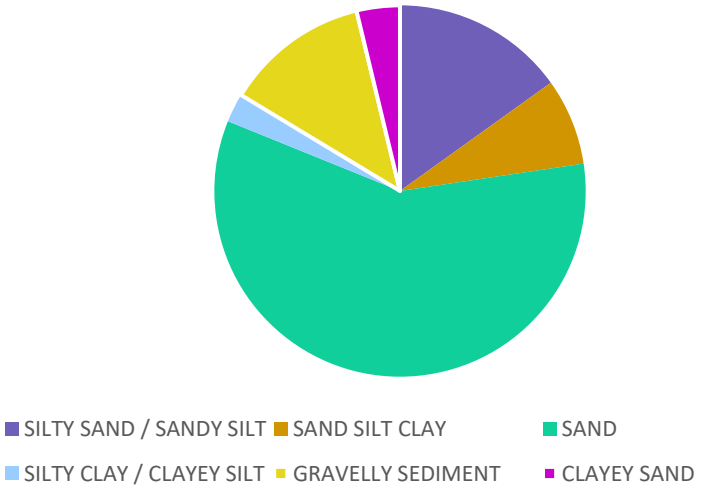

Figure 5-12: Surficial Sediments in Delaware Bay WEAs [60] [55]

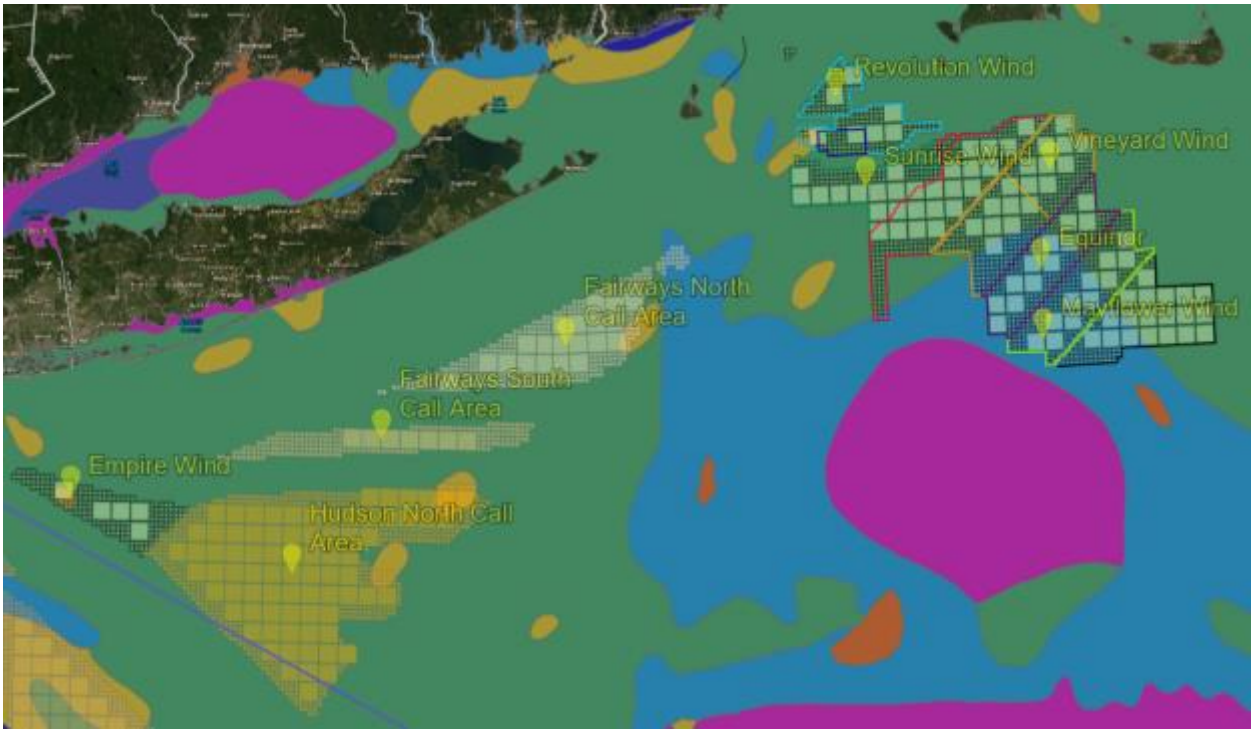

Color	Definition
	Gravel
	Gravel-Sand
	Sand
	Clay-Silt/Sand
	Sand-Clay/Silt
	Clay
	Sand-Silt/Clay
	Sand/Silt/Clay

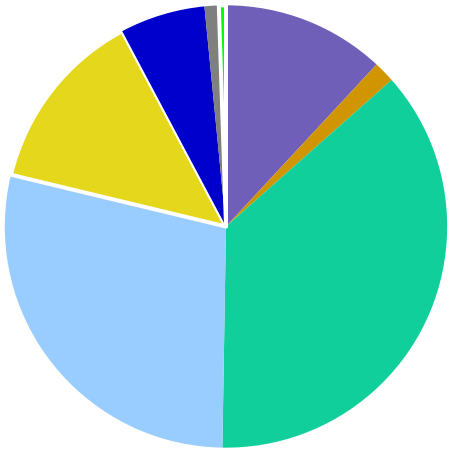

Figure 5-13: Surficial Sediments in Southern New England WEAs [60] [55]

As can be seen from Figure 5-10 through Figure 5-13, medium sand is the most common surficial sediment in all four regions. It should be noted that only surficial sediments up to a 2 meter depth below seabed were publicly available. For detailed design of these projects, borings and CPTs will be performed during site investigation to determine the expected subsurface soil type and parameters up to approximately 100 meters in depth below seabed.

5.5 Design Soil Parameters

A homogenous layer of well-graded medium dense sand was chosen for this study based on the surficial soil type results from Woods Hole Coastal and Marine Science Center [59] [60]. Soil parameters are provided in Table 5-8. The medium dense sand is considered to be fully saturated due its location below the sea surface; therefore, the saturated unit weight is equal to the total unit weight of the soil.

Table 5-8: Medium Dense Sand Design Parameters

$\gamma_{TOT} = \gamma_{SAT}$ [1] (kN/m^3)	γ_{DRY} (kN/m^3)	γ_w (kN/m^3)	γ' (kN/m^3)	Ø' [2] (deg)	Soil Type	v [3]	Min E_s [4] (MN/m^2)	Mean E_s [5] (MN/m^2)	Max E_s [6] (MN/m^2)	c [7] (kN/m^2)	ψ [8] (deg)
19.5	16.5	9.81	9.69	34	Sand; well-graded, medium	0.3	25	50	120	0.2	4

5.6 Design Load Case List

Forty-four load cases were analyzed in SACS and Plaxis to determine the anticipated mudline rotations for large diameter offshore wind turbine monopile foundations. The design load case list is included as a part of this report in Appendix A7. A simplified table of load case parameters is provided in Table 5-9.

Table 5-9: Simplified DLC List

Soil Type	Turbine (MW)	Water Depth (m)	Saffir-Simpson Wind Category
Sand; well-graded, medium	6, 8, 10, 12	20, 40, 50	H1, H2, H3, H4

All turbines are analyzed for the minimum wind speed from each Saffir-Simpson category as described in Section 5.1.1. Foundations supporting each turbine are analyzed for each water depth, excluding the 6 MW turbine in a 50 meter depth. As 6 MW turbines are included to represent the existing farms, it was unnecessary to analyze as existing 6MW turbine farms on U.S. East Coast are located in waters only up to 30 meters in depth.

5.7 Mudline Loads as Calculated in Bentley SACS

Each monopile design was modelled using Bentley SACS. A depiction of one of the SACS input models is shown in Figure 5-14. Monopiles were modelled with fixed boundary conditions at the mudline to determine pile head lateral force and overturning moment as shown in Figure

[1] Bowles Table 3-4, for Medium Dense Sand [59]
[2] Bowles Table 2-6, Max Value for a Loose Saturated Sand [59]
[3] Bowles Table 2-7, Cohesionless Medium Dense Soil Type [59]
[4] Bowles Table 2-8, Maximum Value for Loose Sand [59]
[5] Bowles Table 2-8, Minimum Value for Dense Sand [59]
[6] Using a Similar Extrapolation from Mean to Max Value as shown in [38]
[7] As Recommended in Plaxis Manual for Cohesionless Soil [64]
[8] As Recommended in Plaxis Manual for Sands [64]

5-15. In design, a superelement representing the pile-soil stiffness would be utilized. It is assumed for this research that a fixed condition is a reasonably conservative assumption.

Tower base loads were applied at the interface node, depicted in Figure 5-15. Using the SACS seastate module, non-linear higher-order stream function theory was used to model the extreme wave for each DLC. A static analysis was performed in Bentley SACS to determine the peak loading. As shown in [38], “only the largest load cycles during extreme storms have significant impact on the accumulated permanent rotation.” Therefore, for this research, only the extreme wave height, period, surge and tide are included in lieu of a dynamic analysis.

Input data for the seastate analysis is as described earlier in this section including current profile, extreme wave height, extreme wave period, water depth and water level. For simplicity, these analyses did not account for increased drag area due to marine growth or spray ice. Before extracting the resultant peak loads, it was ensured that the full wavelength was stepped through the structure to achieve the maximum load on the monopile surface.

It is current design practice to “perform separate analyses that consider (i) axial loading only to determine bearing capacity and settlement response, and (ii) lateral loading only to determine flexural behavior through cantilever action.” “The pile size and embedment length necessary to satisfy the lateral load requirements are generally greater compared with those necessary to satisfy the axial loading requirements.” [47] In lieu of this, only lateral loading is extracted from the SACS analysis for application in the subsequent Plaxis 3D numerical analyses and for sizing of the monopile embedment lengths. In addition, previous research has “indicated that for sandy soils, the presence of vertical loads increases the pile’s lateral load-carrying capacity by as much as 40 % (depending on the magnitude of the axial loading).” [47] It is therefore considered conservative to exclude vertical loading for the determination of pile lateral capacity and response.

For reference, the resultant mudline lateral force and moment for a monopile supporting an 8 MW turbine in 20, 40 and 50 meters of water depth are provided in Figure 5-16 and Figure 5-17. The full list of resultant mudline loads are provided as a part of this report in Appendix A8.

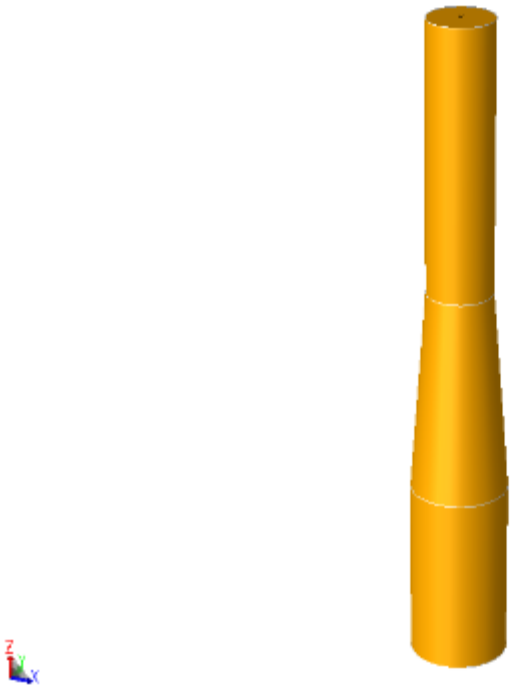

Figure 5-14: 3D SACS Model

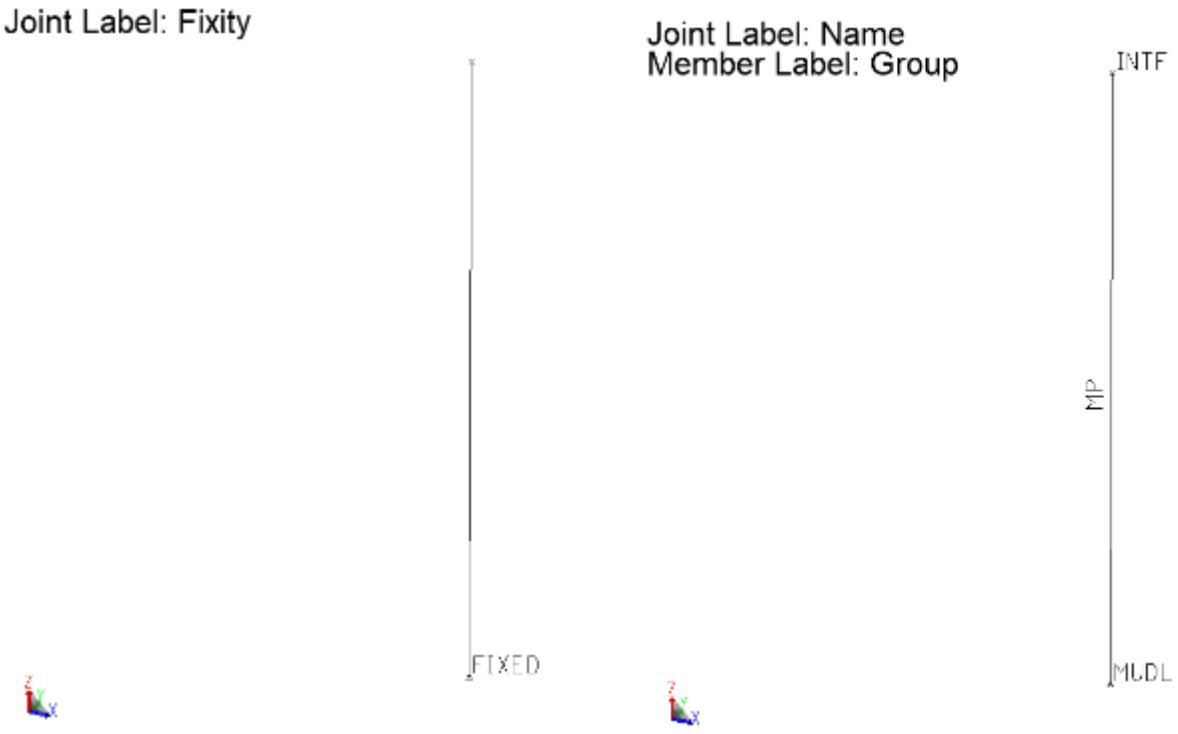

Figure 5-15: SACS Model Joint Fixities (Left) and Joint and Member Naming (Right)

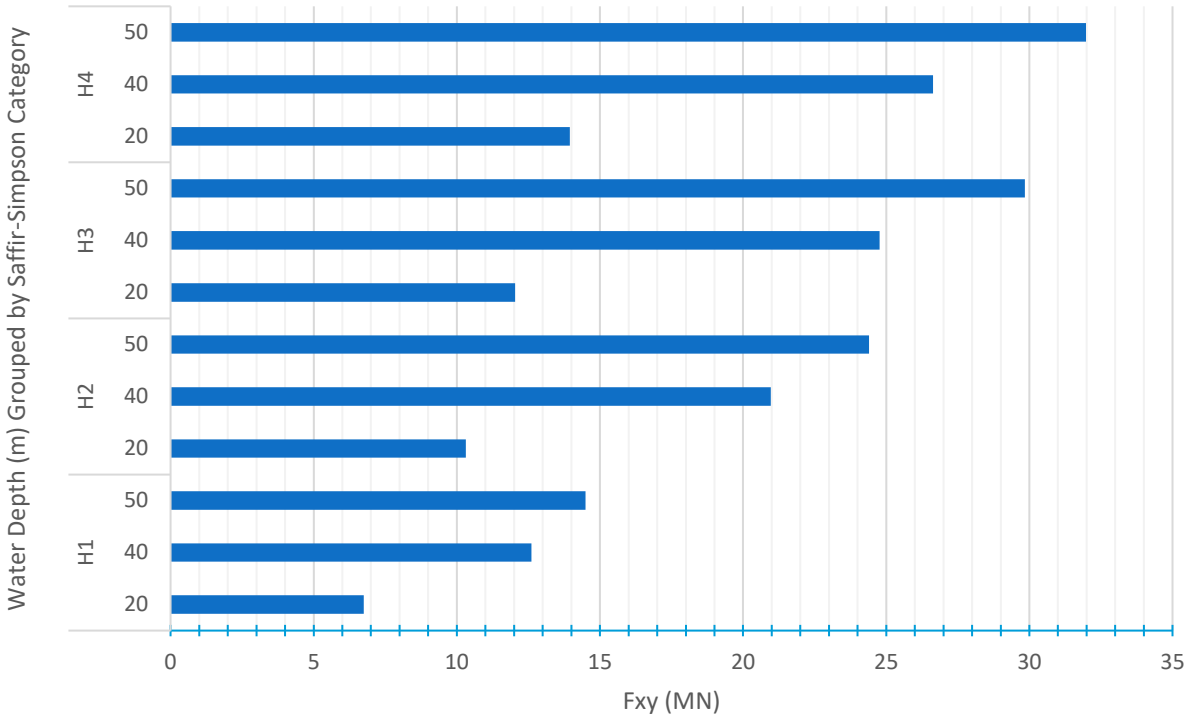

Figure 5-16: Mudline Base Shear for Monopile Supporting 8 MW Turbine

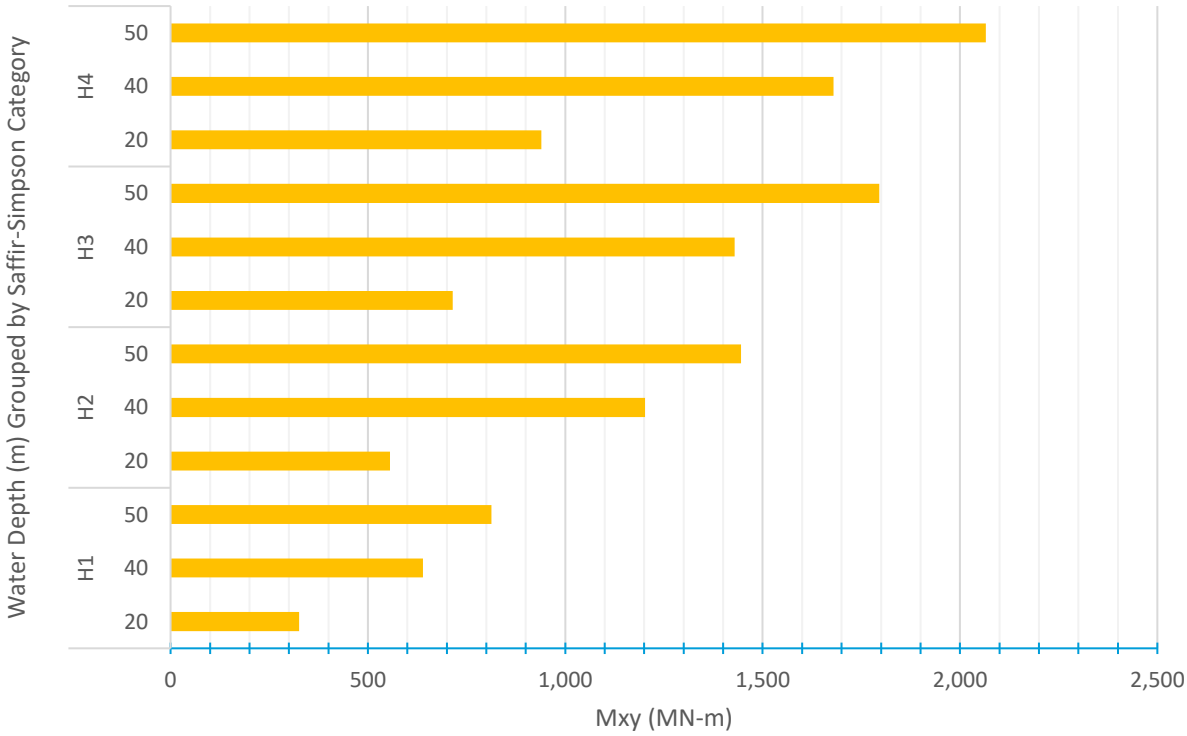

Figure 5-17: Mudline OTM for Monopile Supporting 8 MW Turbine

6 NUMERICAL ANALYSIS

6.1 Model Description

A three-dimensional model of a homogenous medium dense sand was constructed in introductory academic version of Bentley Plaxis 3D 2018. The software is based on the finite element method and developed to provide geotechnical solutions.

6.1.1 Soil Properties

Material Properties

Soil material properties applied in the constitutive model are as described in Section 5.5. The Plaxis 3D parameter E_{inc} was utilized to model linearly increasing soil stiffness with depth. As mentioned in Section 2.4.2, a linearly increasing soil stiffness with depth over-estimates the soil stiffness at greater depths for large diameter piles. In lieu of this, the relationship of increasing soil stiffness with depth was calculated based on a parabolic relationship as described in [40] and shown in Equation 6-1.

$$E_s(z) = E_{s,ref} \times \left(\frac{z}{z_{ref}}\right)^a \qquad \textbf{Equation 6-1}$$

Where,

$E_{s,ref}$ is the maximum soil stiffness equal to 120 MN/m2

z_{ref} is the depth at which maximum soil stiffness is attained equal to 65 meters

a chosen as 0.6 for medium dense cohesionless soil per [40]

Stiffness was restricted to a maximum of 120 MN/m^2 as stated in Table 5-8. It should be noted the maximum pile embedment for this study is 47 meters. The Plaxis equation [61] for calculating increasing soil stiffness with depth using the parameter E_{inc} is provided in Equation 6-2.

$$E_s(z) = E_{s,ref} + (z_{ref} - z)E_{inc} \qquad \textbf{Equation 6-2}$$

A value of E_{inc} was then calculated to best fit a line calculated using Equation 6-2 to the parabolically increasing soil stiffness with depth in Equation 6-1. The required value of E_{inc} was calculated to be 1.55 MN/m^2 and the relationship of soil stiffness with depth is plotted along with the parabolic relationship in Figure 6-1.

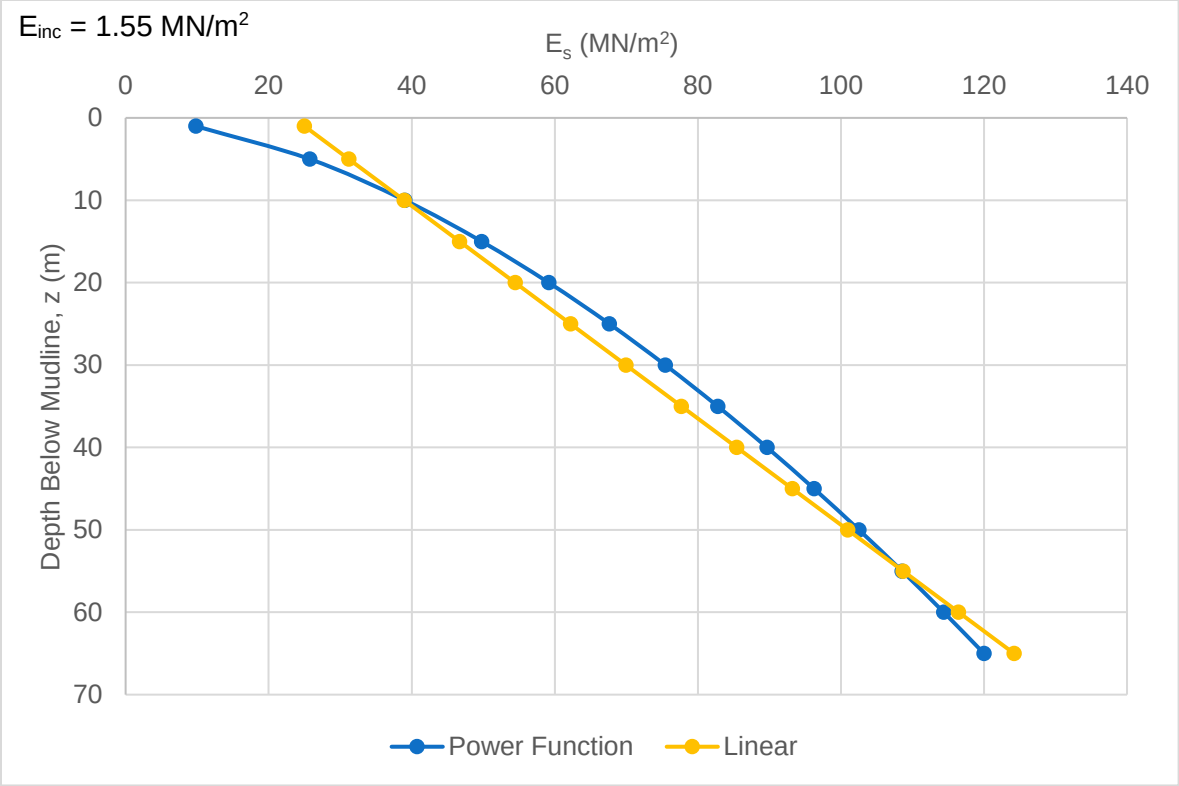

Figure 6-1: Young's Modulus of Soil

It can be seen from Figure 6-1 that this value of E_{inc} provides a reasonable fit to the parabolic relationship. The value of E_{inc} also ensures that the linear relationship is on the conservative side of the parabolic relationship and restricts soil stiffness with depth so it is not over-estimated at larger depths.

Material Model

The elasto-plastic Mohr-coulomb theory was employed in the soil constitutive model. Hooke's law is used to represent the linear elastic portion of the stress-strain curve. Mohr coulomb failure criterion is used to establish the plastic portion of the stress strain curve. It should be noted that soil stiffness is not stress-dependent in the Mohr-Coulomb model. More advanced modelling techniques such as the Hardening Soil Model in Plaxis 3D may be utilized to compare with the results of this research in medium dense sand.

A drained condition is simulated in the constitutive model, where all soil parameters are effective stiffness properties. Additional pore water pressure is therefore not included. Though the rate of loading for the peak event is instantaneous, a drained condition was still utilized since the soil is a highly permeable medium dense sand.

6.1.2 Pile and Interface Element Properties

Embedded Pile Element Description

An embedded beam type element was used to represent the embedded portion of the monopile. An embedded beam is a structural object in Plaxis 3D which interacts with the surrounding soil by means of special interface elements. An embedded beam does not occupy

volume within the model. Instead, an elastic region of soil volume is maintained around the pile. This region is titled the elastic zone and is equal to one pile diameter as shown in Figure 6-2. Plastic soil behavior is excluded within this zone. “This makes the pile behave almost like a volume pile.” [61]

The pile soil interaction is modelled at the center as opposed to the circumference. The interaction involves skin resistance as well as toe resistance. The skin friction and tip force are determined by the relative displacement between the soil and the pile. The element allows for beam deflections due to shearing as well as bending. [61]

In general, the embedded pile composed of line elements is considered a simplified model of the volume pile. This element type was chosen in place of the volume pile since embedded pile elements do not generate additional nodes within the model. The embedded pile elements do not affect the mesh generation and therefore results in fewer nodes and elements than the volume pile [62]. This simplification of the model was necessary due to the 50,000 node restriction in Plaxis Introductory.

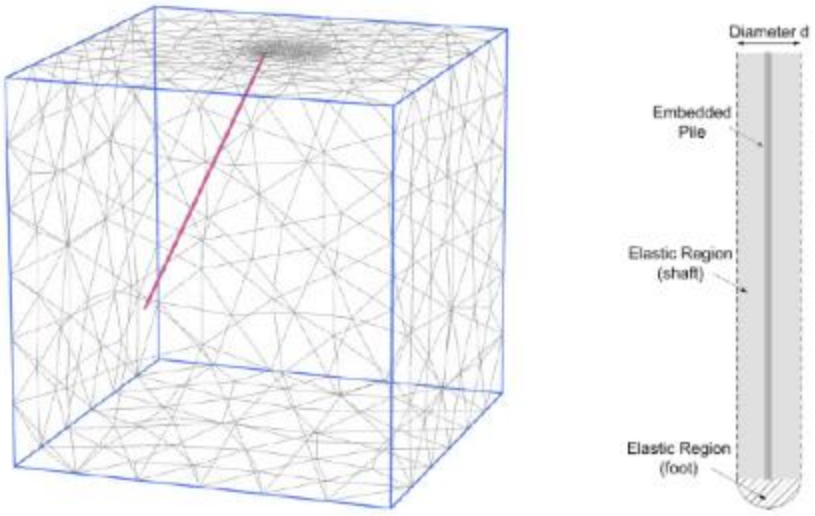

Figure 6-2: Embedded Pile with Arbitrary Direction (Left) and Elastic Region Around Embedded Pile (Right) [62]

In order to ensure the embedded pile elements will accurately represent the lateral monopile behavior, a study performed by TU Delft University and Plaxis [62] was consulted. Results of the study showed that the embedded pile model provides a reasonable representation of lateral pile behavior for rough interfaces between pile and soil. The recommended interface coefficient for sand-steel is 0.67φ [61]. Results of a comparison of mudline deflection between embedded pile, volume pile with interface coefficient equal to 1.0 (without interface) and volume pile with interface coefficient equal to 0.67 (with interface) performed in [62] is replicated in Figure 6-3 for reference.

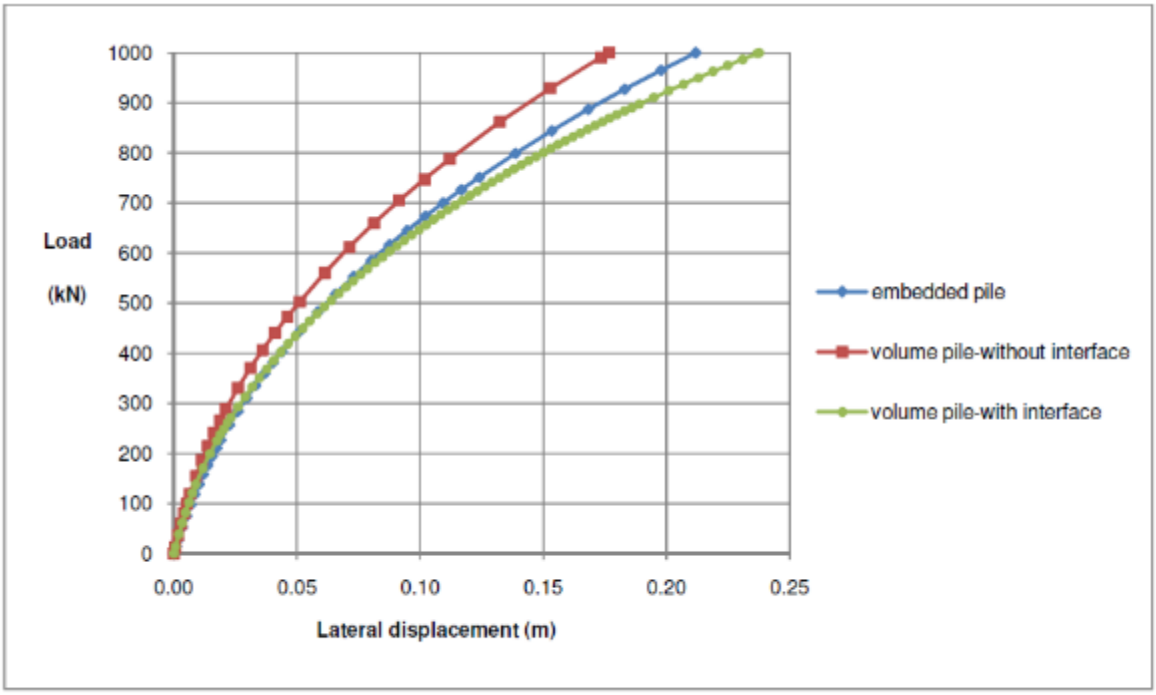

Figure 4.9 Load-displacement curves

Figure 6-3: Results of Volume Pile Mudline Deflection against Embedded Pile Mudline Deflection from [62]

It can be seen from Figure 6-3 that the embedded beam element provides a reasonable representation of the volume pile with interface coefficient equal to 0.67. However, the mudline displacement is slightly under predicted at larger lateral loads. It is recommended as a topic of further study to validate the results of this research with embedded pile properties against a volume pile model with appropriate interface coefficients.

Material Properties

The steel pile properties assigned to the embedded beam element are provided in Table 6-1. Additional pile properties including OD, wall thickness, and embedment length are provided in Appendix 11.

Table 6-1: Pile Properties

γ_p (kN/m^3)	E_p (MPa)
77.98	210,000

A beam element above mudline was modelled for application of lateral load as described later in Section 6.1.6. The element was assigned the same material properties including moment of inertia, cross-sectional area, and young's modulus as the embedded portion of pile. Material unit weight was set to 0.0001 kN/m^3.

Material Model

Embedded beam elements and beam above mudline were modelled as linear elastic elements.

An elasto-plastic model is used to describe the behavior of the interface elements. For both skin resistance and tip resistance, a failure criteria is applied to distinguish between the interface elastic behavior and interface plastic behavior. However, this criteria is for determination of axial pile capacity; whereas, the topic of this study is lateral pile capacity. For this reason the TU Delft and Plaxis study [62], as previously mentioned, was consulted to ensure embedded pile elements could accurately represent lateral pile behavior. The values of shaft resistance, T_{max}, and tip resistance, F_{max}, input to Plaxis are provided Appendix A11 for reference, however they were shown to have no effect on lateral pile capacity. Lateral pile capacity is shown to be dependent on soil stiffness.

6.1.3 Element Types

User-defined element types are not a functionality of Plaxis 3D. The element types the software uses are as follows:

- Soil Elements: The soil volume is discretized into 10-node tetrahedral elements as shown in Figure 6-4. These elements have three degrees of freedom per node.

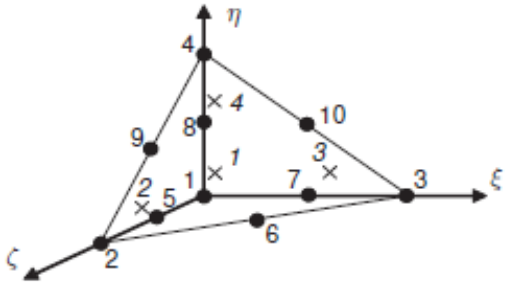

Figure 6-4: 10-node Tetrahedral Element Representing Soil [63]

- Embedded Piles: The pile is considered as a beam which can cross a 10-node tetrahedral element at any place with any arbitrary orientation. Due to the existence of the beam element, three extra nodes are introduced inside the 10-node tetrahedral element as shown in Figure 6-5.

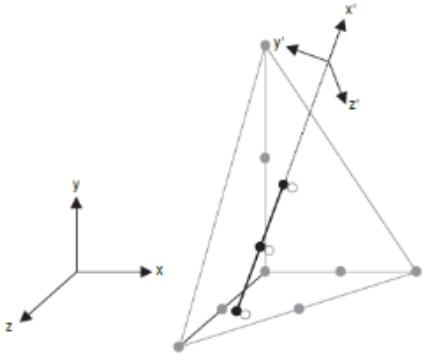

Figure 6-5: Embedded Pile Represented as Beam Element (Dark Line) Paired to a 10-node Tetrahedral Element (Gray Lines) [63]

- Interface Elements: The interaction of the pile skin and at the pile foot are described by means of embedded interface elements. These interface elements are based on 3-node line elements with pairs of nodes instead of single nodes. One node of each pair belongs to the beam element and the other (virtual) node is appoint in the 10-node tetrahedral soil element.

6.1.4 Mesh

The mesh was generated using the inbuilt Plaxis meshing procedure and was refined until a satisfactory mesh quality index was achieved. A finer mesh in the area directly surrounding the pile was added as recommended in [62] and as shown in Figure 6-6. The width of this area was chosen as 2D, where D is the pile diameter.

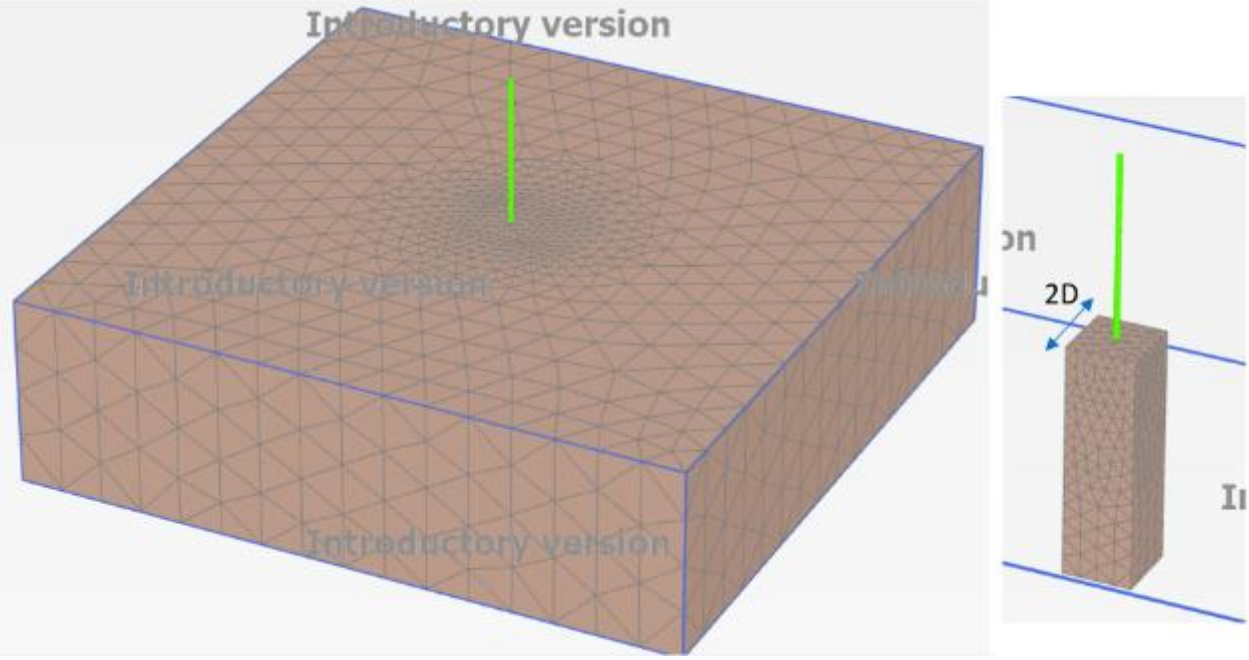

Figure 6-6: Full Mesh (Left) and Refined Mesh Area (Right)

Plaxis uses a relative element size factor to adjust mesh fineness of model geometry. The fineness factor is defined in the Plaxis references manual [61] and reproduced in Figure 6-7 for reference.

Very coarse	:	$r_e = 2.0$
Coarse	:	$r_e = 1.5$
Medium	:	$r_e = 1.0$
Fine	:	$r_e = 0.7$
Very fine	:	$r_e = 0.5$

Figure 6-7: Plaxis Mesh Relative Element Size Factor

For the soil volume mesh, a factor of 0.85 was used, corresponding to a fine to medium mesh size. For the refined mesh area, a factor of 0.30 was used, corresponding to a very fine

mesh. The surface element, representing the top surface of the refined mesh area, used a factor of 0.20. These values were varied slightly as necessary to achieve a sufficient quality mesh as discussed in Section 6.2.1. The resulting number of nodes and elements in the model of an 8 MW turbine in a 40 meter water depth is provided in Table 6-2 for reference.

Table 6-2: Number of Elements and Nodes in Soil Constitutive Model

Number of Soil Elements	21,114
Number of Nodes	30,785

6.1.5 Boundaries

Plaxis automatically imposes a set of general fixities to the boundaries of the geometry in the model. [61] These conditions are generated according the following rules:

Soil volume:

- Vertical model boundaries with their normal in x-direction (i.e. parallel to the yz-plane), are fixed in x-direction ($u_x = 0$) and free in y- and z-direction.
- Vertical model boundaries with their normal in y-direction (i.e. parallel to the xz-plane), are fixed in y-direction ($u_y = 0$) and free in x- and z-direction.
- Vertical model boundaries with their normal neither in x- nor in y-direction, are fixed in x- and y-direction ($u_x = u_y = 0$) and free in z-direction.
- The model bottom boundary is fixed in all directions ($u_x = u_y = u_z = 0$).
- The 'ground surface' is free in all directions.

Figure 6-8: Soil Volume Boundary Conditions [61]

In order to avoid the outer boundaries providing artificial soil resistance, a plane strain state was ensured at the boundaries of the model in each analysis. In this case, the ratio of undeformed length to deformed length in the x direction was ensured to be less than 0.2%. It can be assumed that if strain in the x-directional plane is less than or equal to 0.2%, the boundaries of the model are sufficient to have no effect on the deformations of the model. A depiction of the strain in x-direction, ε_{xx}, for the case of an 8MW turbine in a 40 meter water undergoing H4 case loading is shown in Figure 6-9 for reference. It can be seen that the strain at the outer boundaries is approximately 0.05%.

Adequate dimensions of the soil volume were determined to be 12D in the lateral directions and 1.6L in depth, where D is pile diameter and L is embedded pile length. These boundaries are depicted in Figure 6-10. The lateral and vertical boundaries used in each simulation is listed in Appendix A11.

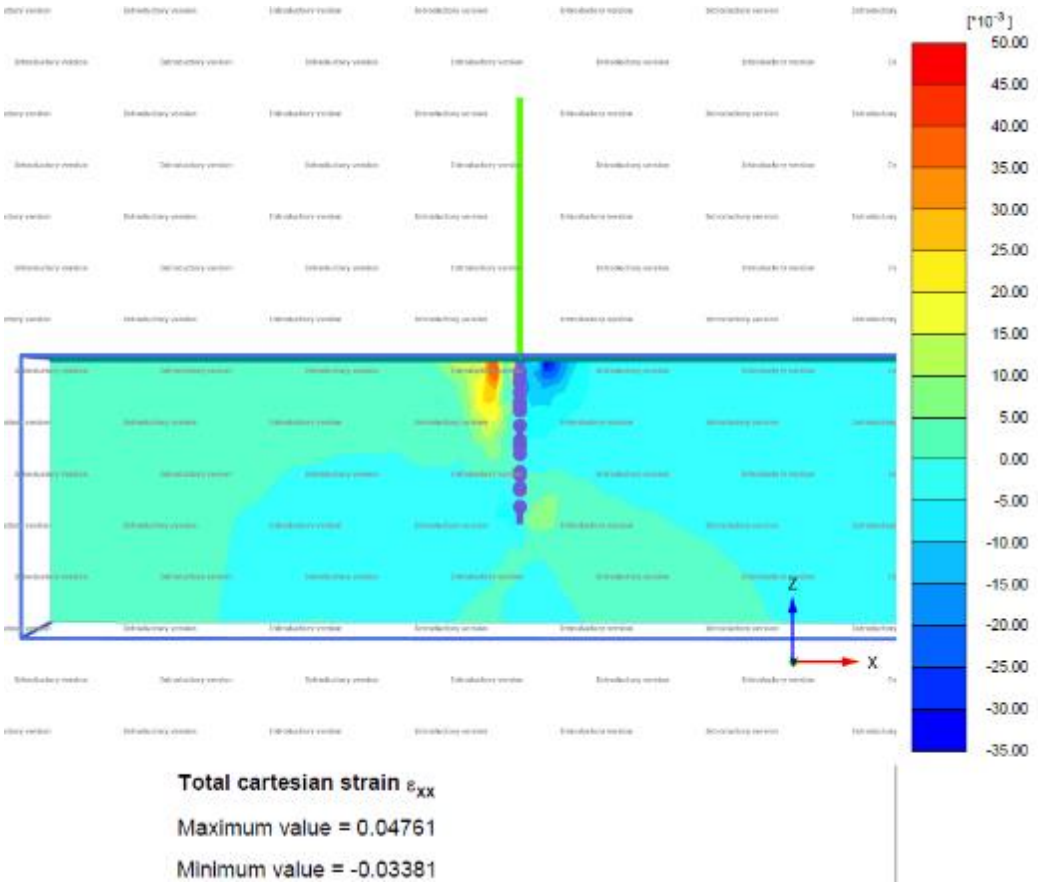

Figure 6-9: Strain in the X-Direction

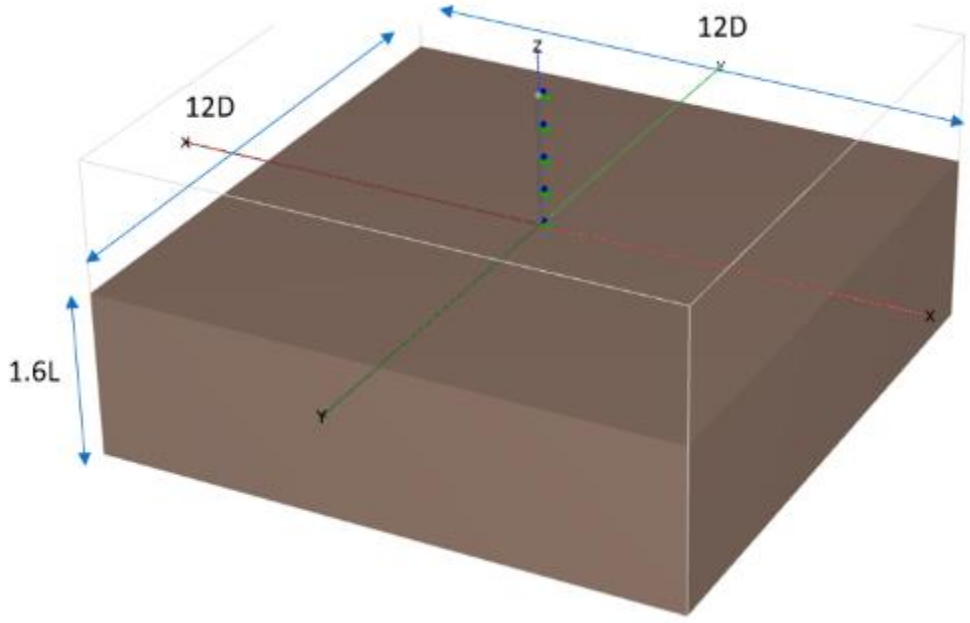

Figure 6-10: Size of Soil Volume

6.1.6 Load Application

The introductory version of Plaxis 3D does not allow for the application of a moment directly to a node. A rigid beam was therefore modelled above the mudline and rigidly connected to the top of the monopile. A lateral force was applied at a calculated eccentricity, e, as shown in Figure 6-11 to generate the required moment at mudline for each simulation. The eccentricity and lateral force applied in each simulation is listed in Appendix A11. Results of each model were checked to ensure the required mudline lateral force and mudline overturning moment were generated.

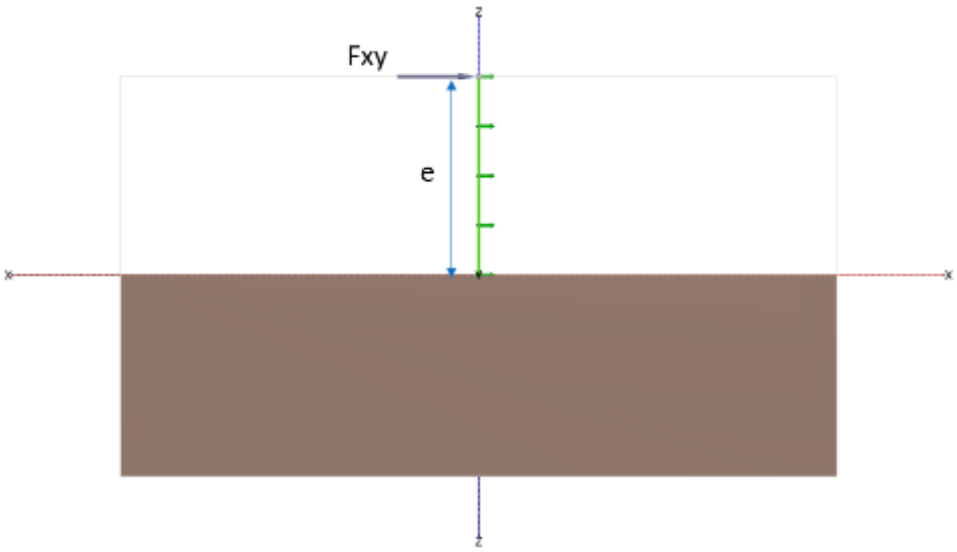

Figure 6-11: Lateral Load Application at Calculated Eccentricity

6.2 Model Validation

6.2.1 Mesh Quality Metrics

The mesh quality for each simulation was checked to ensure the value is within the acceptable limits. An example of the mesh quality from the model of a monopile supporting an 8 MW turbine in 40 meter water depth with load from case H4 is shown in Figure 6-12 and tabulated in Table 6-3. The minimum value for mesh quality achieved in any load simulation was 0.34, greater than the acceptable limit of 0.30.

Table 6-3: Mesh Quality Metrics

Mesh Quality Criteria	Max Value	Min Value	Acceptable Limit	Acceptable?
Element Quality	0.9994	0.5091	>0.30	Yes

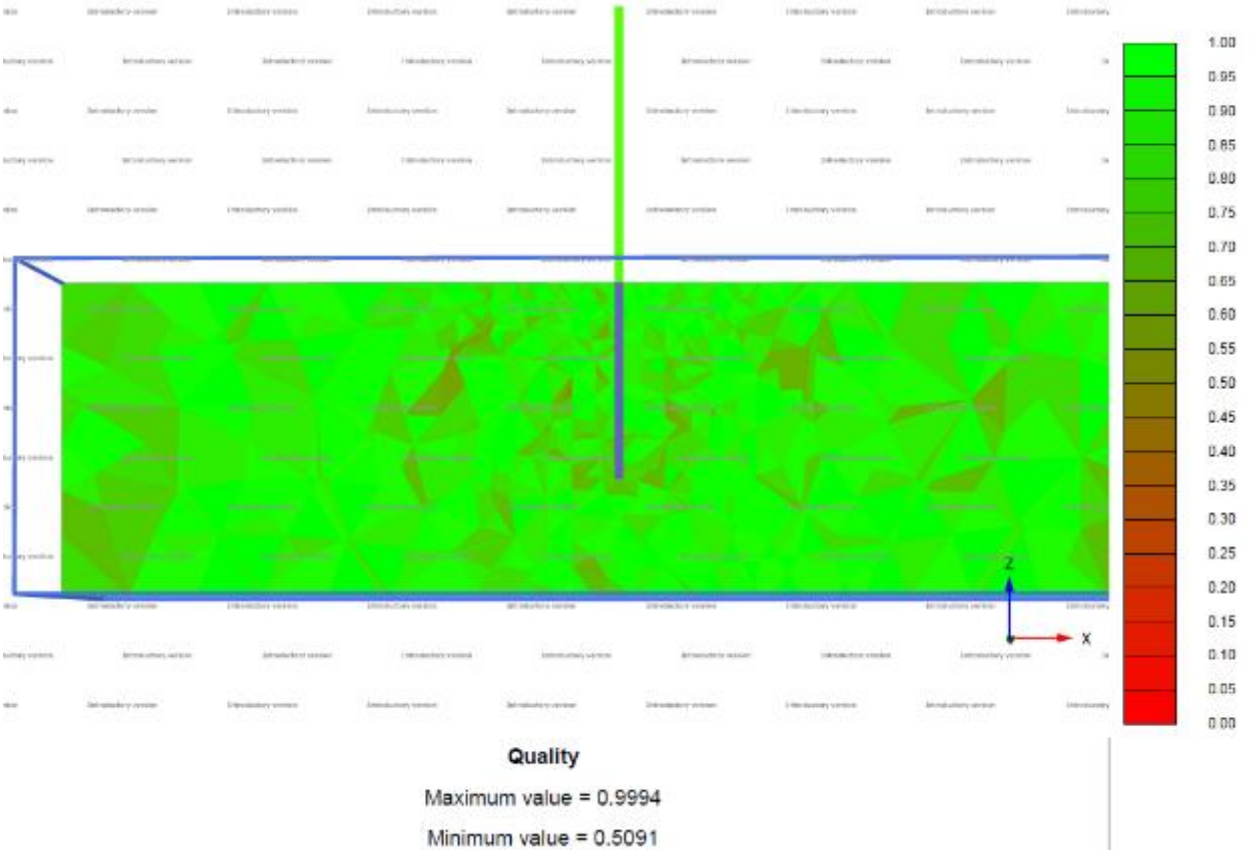

Figure 6-12: Mesh Quality

6.3 Methodology

A staged construction approach was used to establish the initial stress state of soil, installed pile and application of load. The first phase included the soil only with hydrostatic pressure from associated water depth, this is titled the K0 procedure in Plaxis [61] and establishes the at rest stress state of the soil. Before the next phase all displacements are set back to zero. In the second phase, the structural elements including embedded beam in soil volume and beam above soil were added. It should be noted that this analysis does not include any soil disturbance from installation of the pile. Before the next phase all displacements are set back to zero. In the final phase, the lateral force at calculated eccentricity are applied to the beam above soil.

The following steps were used in the Plaxis analysis for each analysis case:

1. Adjust top of beam elevation to required eccentricity
2. Input lateral force value
3. Adjust bottom of embedded pile element elevation to required pile penetration depth
4. Adjust width of soil contour to 12D
5. Update bottom of borehole elevation to 1.6L
6. Update head in boring to required water depth

7. Input embedded pile properties including diameter, thickness, T_{max}, F_{max}
8. Update beam properties to match embedded beam properties
9. Draw polygon and soil volume for refined mesh area to 2D wide by 1.6L deep.
10. Assign fineness factors for mesh to each geometry component
11. Check mesh quality
12. Check boundary effects
13. Extract mudline deflection and pile toe deflection
14. Update pile embedment depth and repeat as needed in Case H1 for each turbine size and water depth combination to ensure a 0.20 degree rotation

As stated in Step 14 above, pile embedment depth for each monopile design was optimized to achieve a 0.20 degree mudline rotation in load case H1. Case H1 includes the minimum wind speed, 32 m/s, in Saffir-Simpson storm category 1.

This may lead to somewhat conservative predictions of mudline rotation for the Atlantic Coast WEAs presented later in this report. The 50-year return period design case for U.S. Atlantic Coast WEAs as discussed in Section 4.4 is approximately 46 to 50 m/s corresponding to a category 2 storm.

It should also be mentioned that in detailed design 50-year return period loads will be increased by a factor of 1.35 or 1.10, with lower load factor corresponding to failure of the yaw system. The increased load factor may result in a mudline OTM corresponding to a Saffir-Simpson category higher than 2 in the 50-year design case.

However, the restriction of rotation to 0.20 degrees for case H1 was considered relevant for this research to show change in mudline rotation when embedment depth is optimized in design for a lower wind speed and then subjected to loads higher than the design loading, but within a reasonable probability of occurring during the lifetime of the structure. The 0.20 degree rotation in H1 cases is assumed to result in the max allowable mudline rotation of 0.25 degrees from [30] in category 1 storms with wind speed near 35 to 40 m/s.

6.4 Output

Mudline deflection and pile toe deflection were extracted from each analysis to determine the mudline rotation. Values for each of these parameters are provided in Appendix A9. A depiction of the lateral pile response for an 8 MW turbine in 40 meters water depth with load from case H1 is provided in Figure 6-13 for reference. The deflection behavior of the large diameter monopile in Figure 6-13 is rigid with a small toe kick realized at the base of the pile.

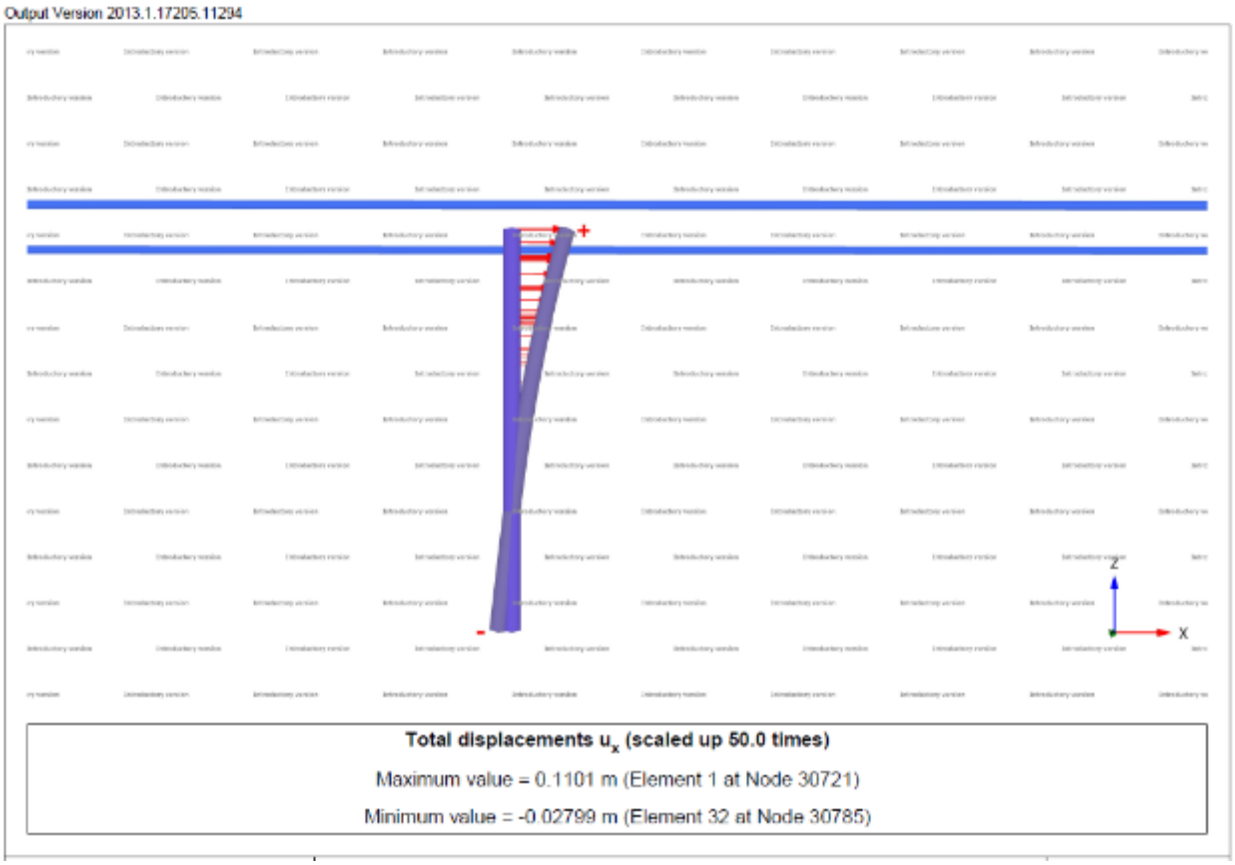

Figure 6-13: Deflection of 9.5 Meter Diameter Monopile Embedded 40 Meters in Medium Dense Sand (L/D = 4.21) Supporting an 8 MW Turbine in Case H1

7 RESULTS

Mudline load, soil stiffness, and monopile embedment depth were found to have the greatest effect on expected monopile rotation during extreme storm events. The relationship between these values and mudline rotation are discussed in the subsequent sections. The resulting mudline rotation for all DLCs is also provided along with the expected rotation at each U.S. Atlantic Coast WEA.

7.1 Mudline Loads

As shown in Figure 7-1, monopile mudline OTM has the greatest increase between a category 1 and category 2 storm. This can most likely be attributed to the fact that the category 1 wind speed range is largest, ranging from 32 m/s to 42 m/s for a total of 11 m/s whereas category 2 to 3 range totals 6 m/s and category 3 to 4 range totals 8 m/s. However, the OTM for a category 1 storm is quite low when compared with a category 4.

In addition, mudline OTM is seen to increase by turbine size as well as water depth. This can largely be attributed to the increasing distance between hub height and mudline for larger turbines as well as larger water depths. Hub heights increase by approximately 10 meters for each turbine size starting from 105 m elevation for 6 MW to 135 meter elevation for 12 MW. The moment arm is then increased by increasing water depth. Additionally, drag area plays a part in increasing mudline OTM both from wind drag area on larger turbines as well as wave drag area on larger diameter sub-structures.

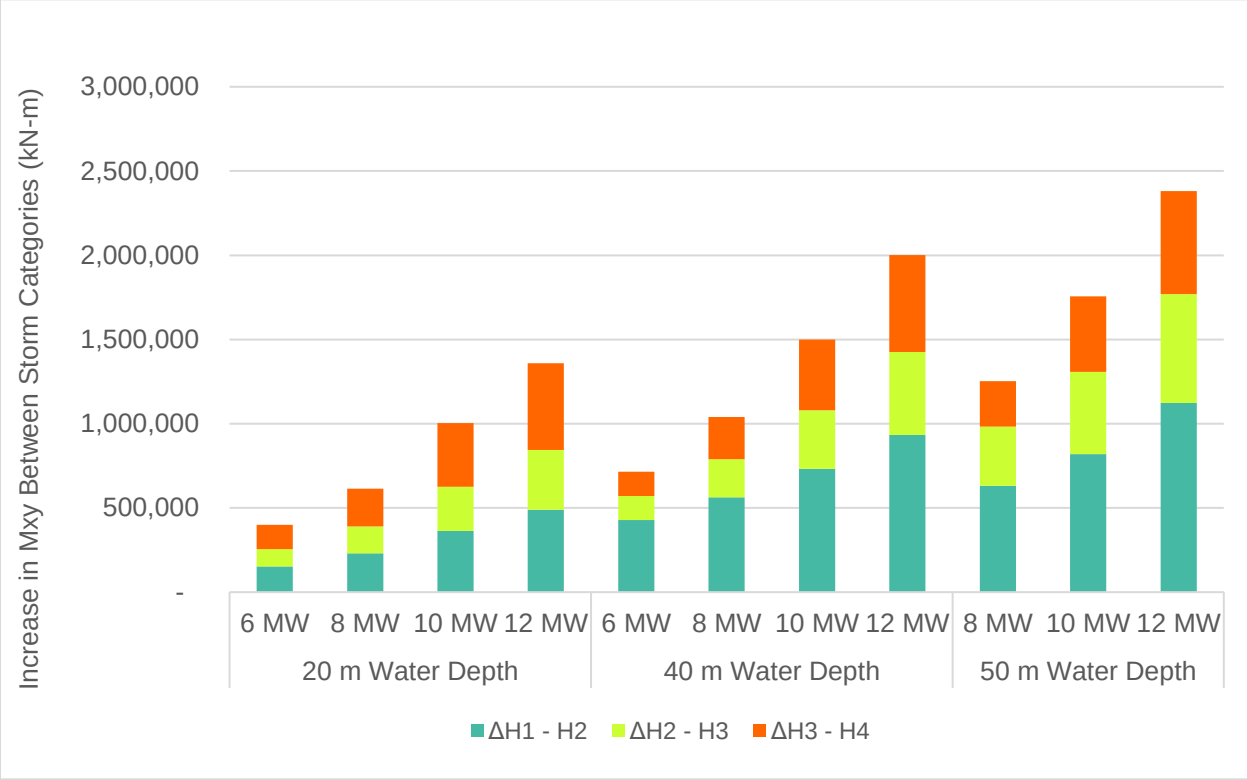

Figure 7-1: Increase in Mudline OTM by Turbine Size and Water Depth

7.2 Mudline Rotations

7.2.1 Effect of Mudline OTM and Pile Embedment Length on Mudline Rotations

The resulting mudline rotation for all load cases analyzed are provided in Figure 7-2 along with the corresponding mudline OTM. Load cases are named as listed in the DLC list in Appendix A7 with the nomenclature in the format of “Turbine Size_Water Depth_Saffir-Simpson Storm Category.”

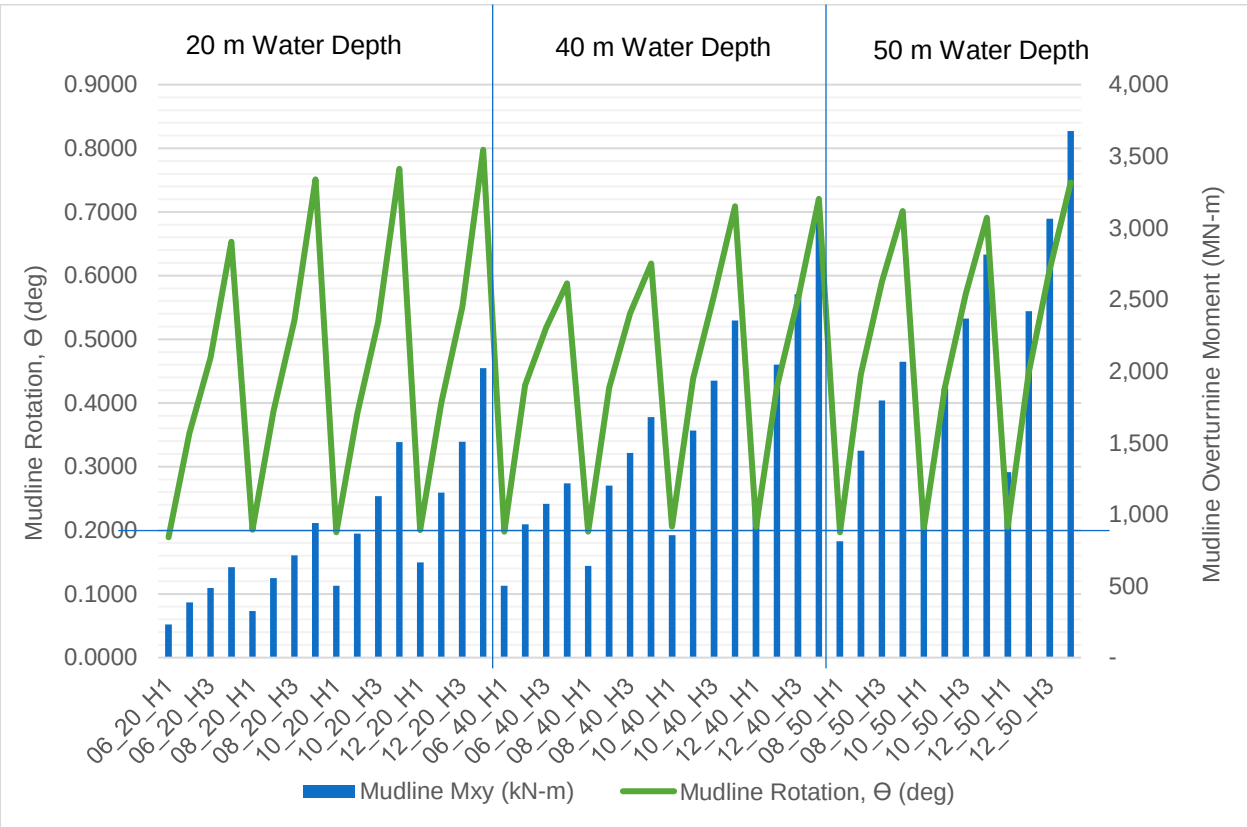

Figure 7-2: Mudline Rotation and Overturning Moment

It can be seen from Figure 7-2 that the largest mudline rotations, approximately 0.80 degrees, are experienced in the shallowest water depth, i.e. 20 meters. This can be attributed to the fact that pile embedment depths are optimized to reach a 0.20 degree rotation in Saffir-Simpson category H1 as marked with a horizontal line in Figure 7-2. For reference, mudline rotation is plotted along with pile embedment depth in

As discussed previously, mudline OTM is at its minimum for shallow water depths and lower wind speeds. As a result, the design pile embedment length is shorter for the shallow water depths. It is suspected that the reduced embedment length for piles in shallow water depths is more sensitive to increased loading from higher wind speed storm events. Since soil stiffness increases with depth, a short pile embedment length has less resistance to larger OTMs.

In the deeper water depths, mudline rotation generally increases with turbine size as well as water depth.

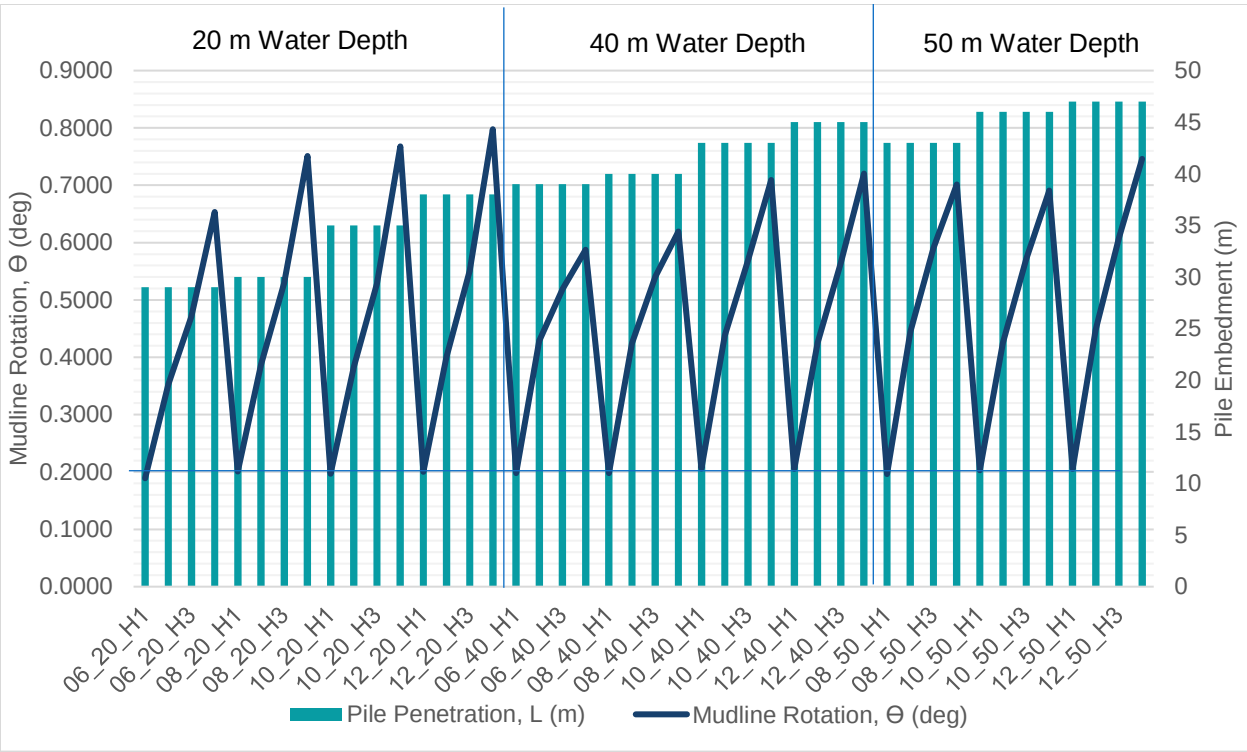

Figure 7-3: Mudline Rotation and Pile Embedment Depth

7.2.2 Mudline Rotation as a Function of Wind Speed

The mudline rotation was plotted as a function of wind speed for each turbine. A chart for each water depth, i.e. 20, 40 and 50 meters is provided in Figure 7-4 through Figure 7-6.

A 2nd order polynomial trendline was fit and extrapolated to a wind speed of 70 m/s in order to extend the results to a Saffir-Simpson Category 5 storm since insufficient metocean data was available to include a category 5 storm as an analysis case for this research.

The 20 meter water depth results in Figure 7-4 show that the shallow water depths have a steeper rotation curve. As mentioned previously, this is expected to be a result of shorter pile embedment lengths required in the design case. Mudline rotations for wind speeds higher than design values, such as those for the robustness case, have the greatest effect on designs with shorter embedment lengths. In deeper water depths, the piles are designed for a larger moment arm in the design case and therefore have larger pile embedment lengths to resist higher lateral loads.

The effects of this can be seen in Figure 7-5 for a 40 meter depth. The 6 and 8 MW turbine support structures have sufficient embedment length to withstand higher lateral loads associated with more extreme Saffir-Simpson storm categories. However, as the loads increase due to larger moment, such as the case for the 10 and 12MW turbine support structures, the increased load beings to produce a larger mudline rotation than what is seen for the smaller turbines.

The mudline rotations for 8, 10 and 12 MW turbine support structures are generally similar in 50 meters water depth. Most likely due to the largest moment arm and therefore larger embedment length required even in the design case. It can be seen that with increasing turbine size, mudline rotations also increase.

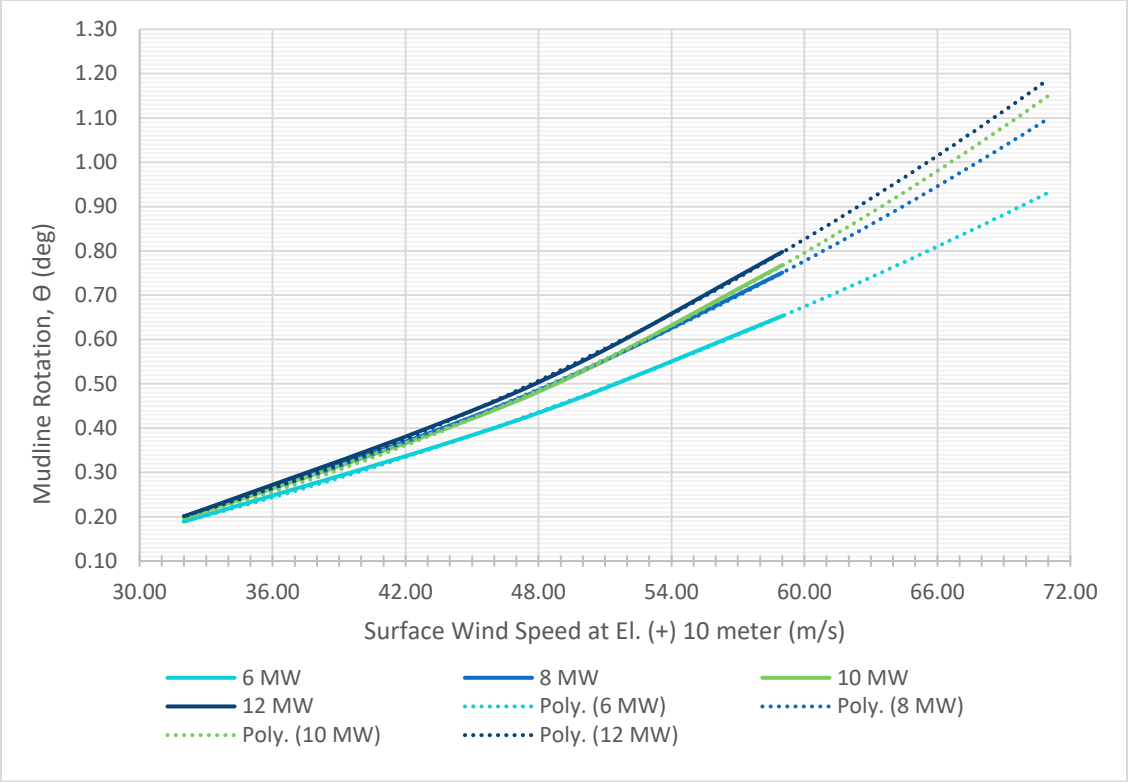

Figure 7-4: Mudline Rotations in 20 meter Water Depth

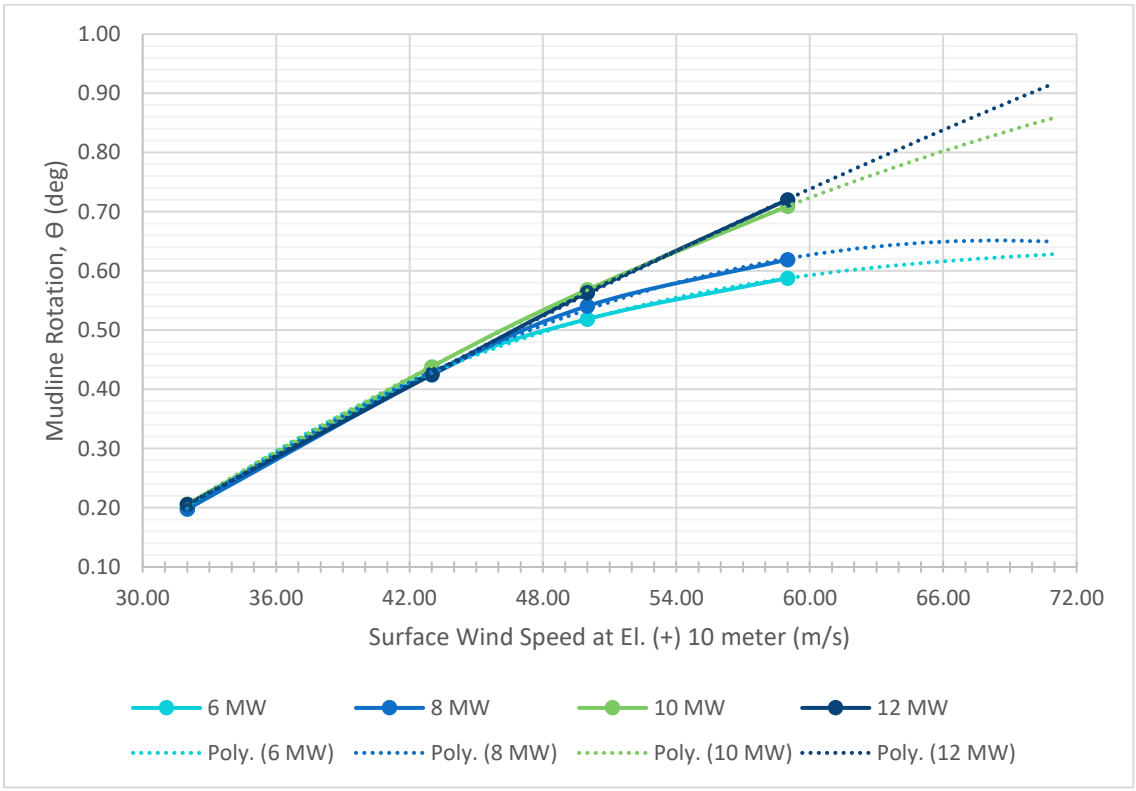

Figure 7-5: Mudline Rotations in 40 meter Water Depth

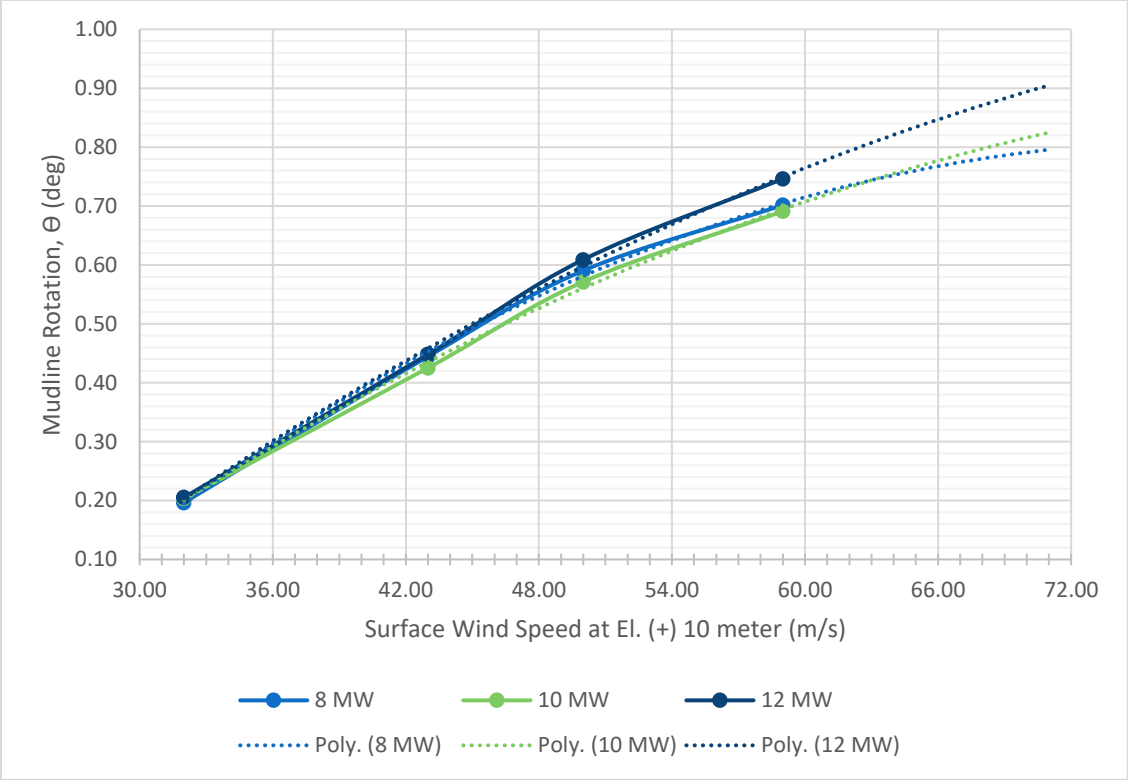

Figure 7-6: Mudline Rotations in 50 meter Water Depth

7.2.3 Database

Mudline rotations for intermediate turbine sizes, including 7, 9.5 and 10 MW were interpolated based on the results of this study and are included in the database in Appendix A9. In addition, the mudline rotations for all turbine sizes including 6, 7, 8, 9.5, 10 and 12 MW were interpolated for a 30 meter water depth and are included as a part of the database in Appendix A9. The database includes charts for each water depth, i.e. 20, 30, 40 and 50 meters, with a line plotted for each turbine size as a function of wind speed up to a category 5 storm. In addition, tables of values used to generate charts are also included in Appendix A9. For intermediate water depths, designers may interpolate between charts for a specific turbine size and wind speed to determine a preliminary mudline rotation for the robustness case.

It should be noted that turbine loads used for this study correspond to DLC I.2, where the yaw system has failed, and the turbine is unable to orient out of the wind during extreme events. It should not be considered conservative to use these results for DLC I.1, since the pile embedment length for the 50-year design case may be lower when yaw power back up is assumed. This will result in a shorter design pile embedment length and possibly increased rotation of the foundation during robustness case loading.

Similarities of soil properties, especially expected soil stiffness with depth, should be compared between design site and the database. If values are significantly lower, mudline rotations in the database will be unconservative.

7.3 Expected Mudline Rotation at U.S. Atlantic Coast WEAs

To determine the expected robustness case mudline rotations at the U.S. Atlantic Coast WEAs. The database in Appendix A9 was utilized to calculate the expected mudline rotation at the 500-year return period wind speed for a range of water depths and turbines sizes. Charts are provided in Figure 7-7 through Figure 7-9. A table of these values for each WEA is also provided in Appendix A10.

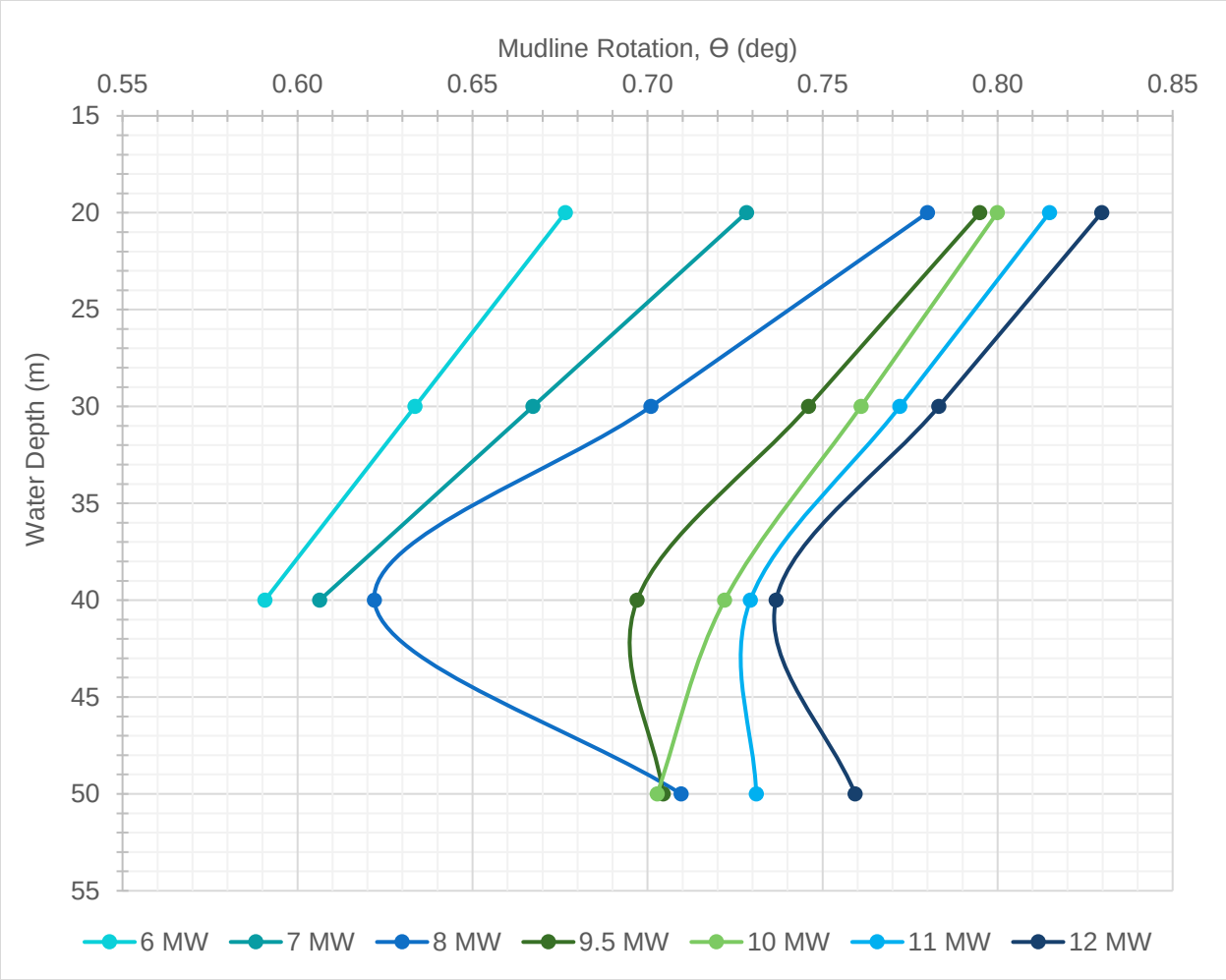

Figure 7-7: Southern New England and Chesapeake Bay Robustness Case Mudline Rotations Corresponding to 64 m/s Wind Speed at El. (+) 10 meters

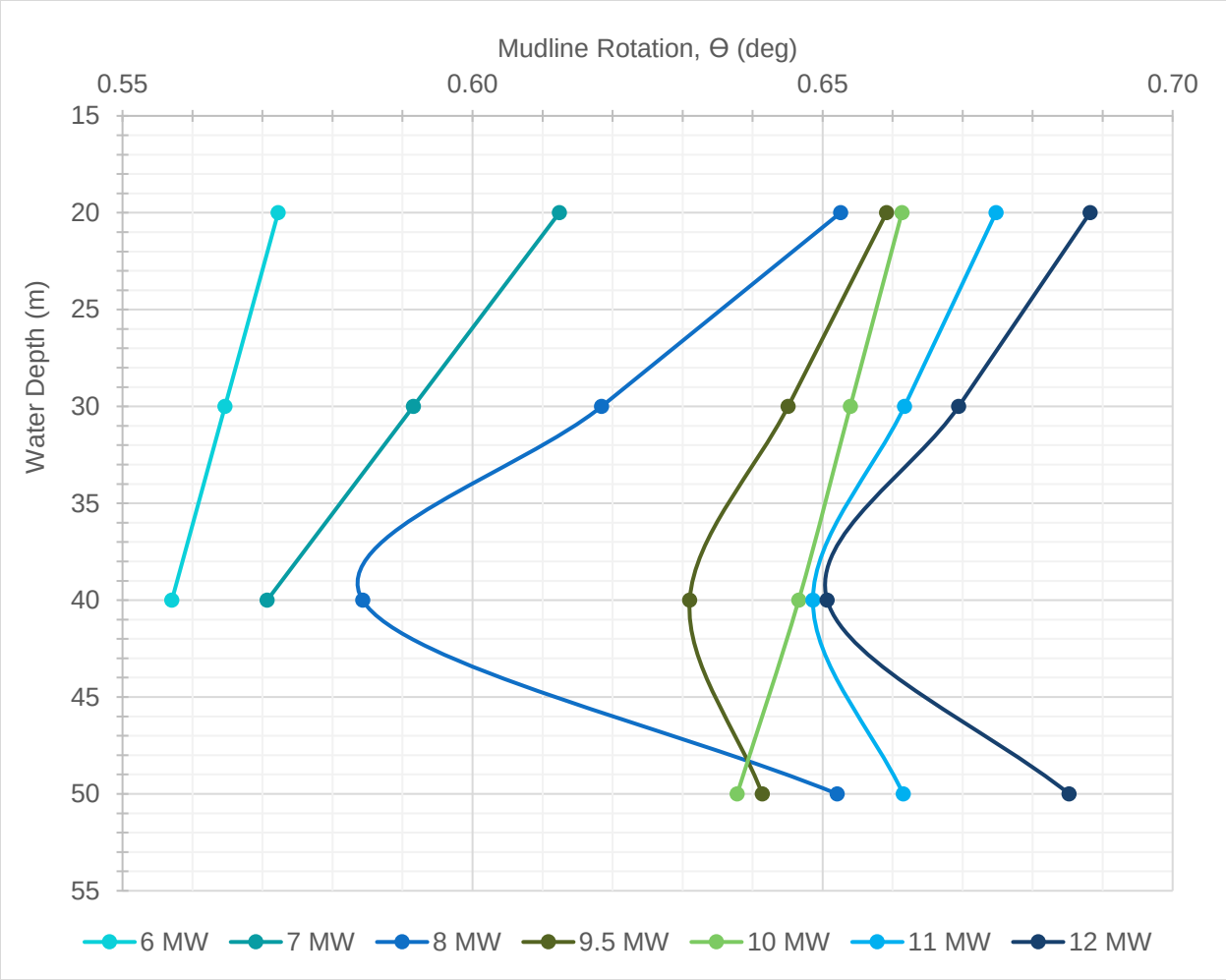

Figure 7-8: Delaware Bay Robustness Case Mudline Rotations Corresponding to 55 m/s Wind Speed at El. (+) 10 meters

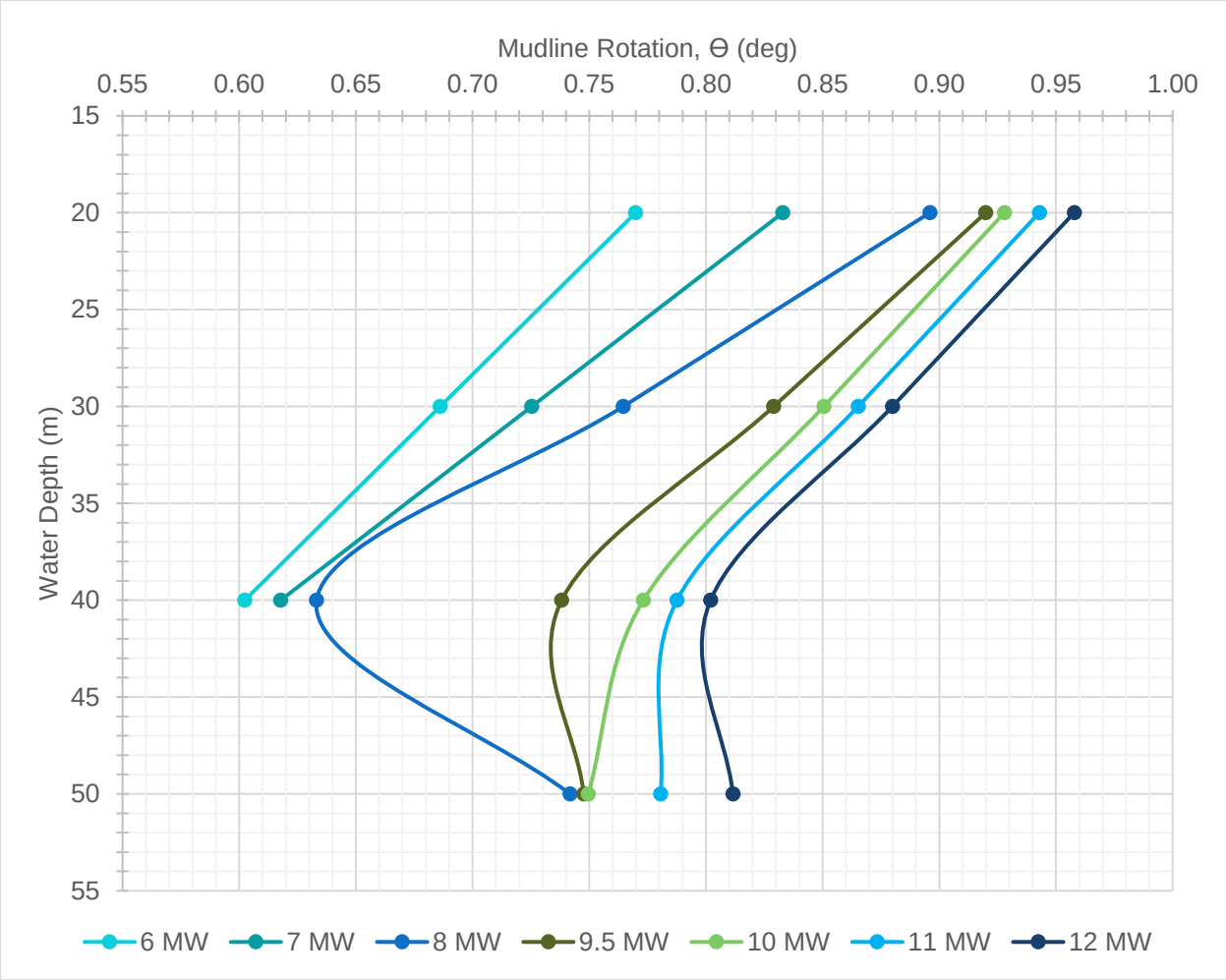

Figure 7-9: Long Bay Robustness Case Mudline Rotations Corresponding to 64 m/s Wind Speed at El. (+) 10 meters

As shown previously in Figure 4-10, the 500-year return period extreme wind speed for Southern New England, Chesapeake Bay and Long Bay correspond to a Saffir-Simpson category 4 storm. Delaware Bay 500-year return period extreme wind speed corresponds to a Saffir-Simpson category 3 storm. Based on the results shown here for each WEA, the mudline rotation is greater than the industry standard allowable of 0.25 degrees but is not near the point of failure.

8 SUMMARY AND DISCUSSION

In order to determine the extreme event risk picture as U.S. Atlantic Coast WEAs, the NHC historical hurricane database [1] was used to calculate the historical number of occurrences and intensity of TCs, ETCs and Nor'easter type storm events in four WEA regions. These storm intensities were compared with the 50-year and 500-year return period wind speeds as determined in BSEE [14] [45]. It can be seen from the results of this study that extreme event wind speeds corresponding to a 500-year return period event will range from a category 3 to a category 4 storm at the four U.S. Atlantic Coast WEAs and are dominated by tropical cyclone events.

Commercially available turbine loading was applied along with corresponding sea states in Bentley SACS to determine mudline loading. Cases analyzed correspond to the minimum wind speed in each Saffir-Simpson category 1 through 4. Monopile embedment depth was then optimized in Plaxis 3D to achieve a 0.20 degree mudline rotation in load case H1. The remaining cases, H2 through H4 were then analyzed on the same monopile geometry to assess mudline rotation when the design was subjected to lateral loads greater than the design load but within a reasonable chance of occurring. The larger lateral loads were applied to mimic the required robustness analysis for offshore wind turbine support structures.

Results of this study show that if the monopiles are design to meet the 50-year return period load cases as specified in IEC 61400-3-1, it can be assumed that the same design will be sufficient for the robustness return period case with respect to adequate pile embedment length to prevent failure under these lateral loads. Resulting mudline rotations ranged from 0.35 to 0.75 degrees as shown in Table 8-1.

Table 8-1: Minimum and Maximum Mudline Rotations from DLCs

	Min Mudline Rotation (deg)	Case	Max Mudline Rotation (deg)	Case
H2	0.35	06_20	0.45	12_50
H3	0.47	06_20	0.61	12_50
H4	0.65	06_20	0.75	12_50

Moment arm from hub height to mudline plays a significant role in mudline overturning moments and subsequent mudline rotations. Required pile embedment lengths increase for larger turbines and deeper water depths. In addition, mudline rotations increase with increasing turbine size. However, the largest mudline rotations were experiences in the shallow water depth sites, due to the initially shallow pile embedment length in design.

The mudline rotations at each U.S. Atlantic Coast WEA region was then predicted based on the anticipated robustness case wind speed. Maximum and minimum values of rotation are summarized for each WEA region in Table 8-2. The maximum values are experience in the Long Bay region as the hazard curve for this region is steeper due to the more frequent occurrence of tropical cyclone events. Delaware Bay experiences the smallest rotations of all regions due to its more sheltered location than the Southern New England, Chesapeake Bay and Long Bay regions from extreme storm events.

Table 8-2: Minimum and Maximum Mudline Rotations at U.S. Atlantic Coast WEAs

Region	Ws (m/s)	Min Mudline Rotation (deg)	Case	Max Mudline Rotation (deg)	Case
SNE & CB	60.00	0.59	06_40	0.83	12_20
DB	55.00	0.56	06_40	0.69	12_20
LB	64.00	0.60	06_40	0.96	12_20

Results from the cases analyzed as a part of this research were extrapolated to a Saffir-Simpson category 5 storm for reference. In addition, mudline rotations for intermediate turbine sizes including 7, 9.5 and 11 MW were also calculated. Mudline rotations for all turbines in all storm cases were also calculated for a 30 meter depth site. A database of mudline rotation with these turbine sizes, water depths and wind speeds was then created. Designers may use these charts and tables for sizing of monopiles in preliminary design phases.

It is recommended that designers review the assumptions made as a part of this research before directly applying mudline rotations. Parameters expected to have the most affect on mudline rotations if different from those included in this study are soil type, soil stiffness and embedment length.

In addition, turbine loads applied in this research assume a failure of the yaw system during extreme events. Pile penetrations optimized for a design case where the yaw system has grid connection or battery back up will result in shorter pile embedment lengths than those in this study. This should be kept in mind when using embedment lengths in this research for preliminary sizing of monopiles.

Lastly, it should be noted that the maximum mudline rotation realized as a part of this study was 1.15 degrees for a 12MW turbine in 50 meters water depth and exposed to the minimum wind speed in a Saffir-Simpson category 5 event. This value is greater than the industry accepted allowable degree of rotation from design loads, equal to 0.25 degrees, but does not indicate a geotechnical failure which would result in collapse of the wind turbine support structure. Additional studies should be performed as outlined in the following section to validate these results; however, from these findings it can be speculated that the monopile sizing determined from the design case is adequate to prevent collapse of the monopile type support structure due to geotechnical failure in higher return period events.

9 RECOMMENDATIONS AND FUTURE RESEARCH

Several areas which would benefit from refinement in this research were identified and noted previously including:

- A different material model for representing the soil behavior in the numerical analysis which takes into consideration variation of soil stiffness with applied stress including the Hardening Soil Model in Plaxis 3D.
- Modelling of monopile in the numerical analysis in Plaxis 3D as a surface element with interface nodes as opposed to the embedded pile type element used in this research.
- Including additional datasets for ETCs and Nor'easters at U.S. Atlantic Coast WEAs to refine the risk picture presented in this research.
- Modelling breaking waves using breaking wave theory as opposed to breaking depth limited waves modelled with higher order stream function theory.

In addition, several additional items were realized as a part of this research would could benefit from additional study including:

- Expanding this research to encompass different soil types expected in the WEAs including silty sand, stiff clay, and layered strata.
- Expand the study to larger turbine sizes including 15 to 20 MW.
- Repeat the study using turbine loads which assume a powered yaw system during the extreme events to assess the change in design pile penetration and effect on subsequent robustness case mudline rotations.
- Compare the percentage of peak mudline overturning moment and base shear between turbine loading from wind or hydrodynamic loading to determine the controlling variable, i.e. wind speed or wave height for pile embedment length in extreme storm events.
- Use aeroelastic software such as NREL's FAST to calculate turbine loads as opposed to using scaled values.
- Include permanent deformations from operational cases to mimic the effect of cyclic degradation on the soil prior to extreme load event.
- Validate mudline deflections and rotations against field and model testing.
- Comparison of these results with field data after the passage of an extreme event at the U.S. Atlantic Coast WEAs as well as Asia-Pacific WEAs to validate the findings.

10 REFERENCES

[1] Office for Coastal Management, "Historical Hurricane Tracks," 28 06 2018. [Online]. Available: https://www.coast.noaa.gov/hurricanes/.

[2] National Climate Data Center, "Historical Climatology Series 6-2; Tropical Cyclones of the North Atlantic Ocean, 1851 - 2006," U.S. Department of Commerce; National Oceanic and Atmospheric Administration, Asheville, 2009.

[3] National Oceanic and Atmospheric Administration, "NOAA Technical Memorandum NWS TPC-5; The Deadliest, Costliest, and Most Intense United States Tropical Cyclones from 1851 to 2006 (And Other Frequently Requested Hurricane Facts)," National Weather Service & National Hurricane Center, Miami, 2007.

[4] National Weather Service, "Tropical Definitions," US Department of Commerce; National Oceanic and Atmospheric Administration, [Online]. Available: https://www.weather.gov/mob/tropical_definitions.

[5] NASA Jet Propulsion Laboratory; California Institute of Technology, "QuikScat Finds Tempests Brewing in "Ordinary" Storms," NASA, 25 06 2009. [Online]. Available: https://www.jpl.nasa.gov/news/news.php?feature=2196.

[6] National Weather Service, "What is a Nor'easter," U.S. Department of Commerce; National Oceanic and Atmospheric Administration, [Online]. Available: https://www.weather.gov/safety/winter-noreaster.

[7] Tarp-Johansen et al., "Application of Design Standards to the Design of Offshore Wind Turbines in the U.S.," in *OTC 18359*, Houston, 2006.

[8] "R: simple world map (Robinson, ggplot)," [Online]. Available: https://seethedatablog.wordpress.com/2016/12/23/r-simple-world-map-robinson-ggplot/.

[9] Knapp et al., "The International Best Track Archive for Climate Stewardship (IBTrACS): Unifying tropical cyclone best track data.," *Bulletin of the American Metorological Society,* vol. 91, pp. 363-376, 2010.

[10] H. D. J. K. M. K. C. S. K.R. Knapp, "International Best Track Archive for Climate Stewardship (IBTrACS) Project, Version 4," NOAA National Centers for Environmental Information, 2018. [Online]. Available: https://doi.org/10.25921/82ty-9e16.

[11] 4c Offshore, "Global Offshore Renewable Map," 2019. [Online]. Available: https://www.4coffshore.com/offshorewind/.

[12] American Petroleum Institute, *ANSI/API Recommended Practice 2 MET; Derivation of Metocan Design and Operating Conditions, 1st Edition,* 2014.

[13] Dekker et al., *Characteristics and development of European cyclones with tropical origin in reanalysis data,* Springer; http://creativecommons.org/licenses/by/4.0/, 2017.

[14] P. Gayes, "TAP-724-Development of Hazard Curves for WEAs off the Atlantic Seaboard," Bureau of Safety and Environmental Enforcement (BSEE), VA, 2016.

[15] G. Hagerman, "TAP-672-Development of an Integrated Extreme Wind, Wave, Current, and Water Level Climatology to Support Standards-Based Design of Offshore Wind Projects," Bureau of Safety and Environmental Enforcement (BSEE), VA, 2014.

[16] L. H. a. B. Moller, "Risks of tropical cyclones on offshore wind farms in China," in *6th Dubrovnik Conference on Sustainable Development of Energy, Water Environment Systems*, Dubrovnik, 2011.

[17] Chen et al., "Failure investigation on a coastal wind farm damaged by super typhoon: A forensic engineering study," *Journal of Wind Engineering and Industrial Aerodynamics,* vol. 147, pp. 132-142, 2015.

[18] Beiter et al., "A Spatial-Economic Coast-Reduction Pathway Analysis for U.S. Offshore Wind Energy Development from 2015-2030," National Renewable Energy Laboratory, Golden, CO, 2016.

[19] Rose et al., "Quantifying the hurricane risk to offshore wind turbines," *PNAS,* vol. 109, no. 9, pp. 3247-3252, 2012.

[20] S. H. Niels-Erik Clausen, "Wind Farms in Regions Exposed to Tropical Cyclones," in *European Wind Energy Conference*, Milan, 2007.

[21] International Electrotechnical Commission, *IEC 61400-1-1: Wind Energy Generation Systems - Part 1: Design Requirements,* 2019.

[22] Energo Engineering Inc., "TAP 578 - Assessment of Fixed Offshore Platform Performance in Hurricanes Katrina and Rita," U.S. Department of the Interior Mineral Management Service, Engineering and Research Branch, Herndon, 2007.

[23] Barnett and Basbarian, Inc., "TAP 209 - Development of Acceptance Criteria for Caisson Structures Damaged During Hurricane Andrew," U.S. Department of the Interior, Minerals Management Service, Herndon, 1995.

[24] Det Norske Veritas, "TAP 581 - Pipeline Damage Assessment from Hurricanes Katrina and Rita in the Gulf of Mexico," U.S. Department of the Interior, Minerals Management Service, Herndon, 2007.

[25] Mangiavacchi et al., "API Offshore Structure Standards: RP 2A and Much More," in *OTC 17697*, Houston, 2005.

[26] American Petroleum Institute, *API Recommended Practice 2A-WSD: Planning, Designing, and Constructing Fixed Offshore Platforms - Working Stress Design, 22nd Edition,* 2014.

[27] American Petroleum Institute, *API Recommended Practice 2A-LRFD; Planning, Designing, and Constructing Fixed Offshore Platforms - Load and Resistance Factor Design, 2nd Edition,* 2019.

[28] International Electrotechnical Commission, *IEC 61400-3-1: Design requirements for fixed offshore wind turbines,* 2019.

[29] American Wind Energy Association, *AWEA OCRP: Recommended Practices for Design, Deployment, and Operation of Offshore Wind Turbines in the United States,* 2020.

[30] DNV GL, *DNVGL-ST-0126: Support structures for wind turbines,* 2018.

[31] Cox et al., "Field Testing of Laterally Loaded Piles in Sand," in *OTC 2079*, Houston, 1974.

[32] Byrne et al., "PISA: New Design Methods for Offshore Wind Turbine Monopiles," in *Offshore Site Investigation and Geotechnics; Smarter Solutions for Future Offshore Developments*, London, 2017.

[33] K. G. Paul Doherty, "Laterally loaded monopile design for offshore wind farms," in *Proceedings of the ICE - Energy, 165 (1):7-17*, 2011.

[34] Sorensen et al., "Evaluation of Load-Displacement Relationships for Large-Diameter Piles," Aalborg University, Aalborg, 2009.

[35] American Petroleum Institute, *ANSI/API Recommended Practice 2GEO; Geotechnical and foundation design consideration, 1st edition,* 2014.

[36] DNVGL, *DNVGL-RP-C212; Offshore soil mechanics and geotechnical engineering,* 2019.

[37] M. O. J.M. Murchinson, "Evaluation of p-y relationships in cohesionless soil: analysis and design of pile foundations," in *Proceedings of Symposium in Conjunction with the ASCE National Convention; ASCE Technical Council on Codes and Standards, pp. 174-191*, San Francisco, 1984.

[38] Carswell et al., "Natural frequency degradation and permanent accumulated rotation for offshore wind turbine monopiles in clay," *Renewable Energy,* vol. 97, pp. 319-330, 2016.

[39] K. L. a. J. Wiemann, "Finite-Element-Modelling of Large Diameter Monopiles for Offshore Wind Energy Converters," in *DOI: 10.1061/40803(187)212*, Atlanta, 2006.

[40] Wiemann et al., "Evaluation of Pile Diameter Effects on Soil-Pile Stiffness," gigawind.de, 2004.

[41] Lesny et al., "Scale Effects in Lateral Load Response of Large Diameter Monopiles," in *DOI/10.1061/40902(221)40*, Denver, 2007.

[42] M. A. Khalid Abdel-Rahman, "Finite Element Modelling of Horizontally Loaded Monopile Foundations for Offshore Wind Energy Converters in Germany," 10.1201/NOE0415390637.ch38., 2005.

[43] K. A.-R. Martin Achmus, "Design of Monopile Foundations for Offshore Wind Energy Plants," in *11th International Colloquium on Structural and Geotechnical Engineering*, Cairo, 2005.

[44] Murphy et al., "3D FEM approach for laterally loaded monopile design," *Computers and Geotechnics,* vol. 100, pp. 76-83, 2017.

[45] D. R. Gilbert, "BSEE TAP 769; Laboratory Testing of Lateral Load Response for Monopiles in Sand," 2018.

[46] LeBlanc et al., "Response of stiff piles in sand to long-term cyclic lateral loading," *Geotechnique,* vol. 60, no. 2, pp. 79-90, 2010.

[47] M. A. a. B. C. O'Kelly, "Analysis and Design of Monopile Foundations for Offshore Wind-Turbine Structures," *Marine Georesources & Geotechnology,* vol. 34, pp. 503-525, 2016.

[48] Fugro Marine GeoServices, Inc., "Geophysical and Geotechnical Investigation Methodology Assessment for Siting Renewable Energy Facilities on the Atlantic OCS," BOEM Office of Renewable Energy Programs, Norfolk, 2017.

[49] The Business Network for Offshore Wind, "U.S. Offshore Wind Market Report & Insights," 2020.

[50] Musial et al., "2018 Offshore Wind Technologies Market Report," U.S. Department of Energy; Office of Energy Efficiency & Renewable Energy, 2018.

[51] Bureau of Ocean Energy Management, "Renewable Energy Leases Map Book," March 2019. [Online]. Available:

https://www.boem.gov/sites/default/files/renewable-energy-program/Mapping-and-Data/Renewable_Energy_Leases_Map_Book_March_2019.pdf.

[52] Bureau of Ocean Energy Management;, "Renewable Energy GIS Data," U.S. Department of the Interior, [Online]. Available: https://www.boem.gov/renewable-energy/mapping-and-data/renewable-energy-gis-data.

[53] Office of Coast Survey, "NOAA RNC Viewer," National Oceanic and Atmospheric Administration, U.S. Department of Commerce, [Online]. Available: https://www.nauticalcharts.noaa.gov/RNCOnline/rnconline.html.

[54] Bureau of Ocean Energy Management, "Outer Continental Shelf Renewable Energy Map," U.S. Department of the Interior, Bureau of Ocean Energy Management, Office of Renewable Energy Programs, 2019.

[55] BOEM, "Renewable Energy GIS Data," [Online]. Available: https://www.boem.gov/renewable-energy/mapping-and-data/renewable-energy-gis-data.

[56] National Centers for Environmental Information (NCEI), "Storm Events Database," [Online]. Available: https://www.ncdc.noaa.gov/stormevents/.

[57] NOAA, "Tides & Currents," [Online]. Available: https://tidesandcurrents.noaa.gov/.

[58] Potts et al., "Numerical modelling of large diameter piles under loateral loading for offshore wind applications," in *ISFOG*, Oslo, 2015.

[59] Woods Hole Coastal and Marine Science Center, Woods Hole, MA, "U.S. Geological Survey, 2014, ECSTDB2014.SHP: U.S. Geological Survey East Coast Sediment Texture Database; Open File Report 2005-1001," U.S. Geologic Survey, 2005.

[60] Coastal and Marine Geology Program, Woods Hole Science Center, "U.S. Geological Survey, 200506 CONMAPSG: Continental Margin Mapping (CONMAP) Sediments Grainsize Distribution for the United States East Coast Continental Margin: Open-File Report 2005-1001," U.S. Geologic Survey, Woods Hole, MA, 2005.

[61] Plaxis, "Plaxis 3D Reference Manual," 2018.

[62] T. Dao, "Validation of PLAXIS Embedded Piles for Lateral Loading," Delft University of Technology, Delft, 2011.

[63] Plaxis, "Plaxis Scientific Manual," 2018.

[64] H. Matlock, "Correlations for design of laterally loaded piles in soft clay," in *Offshore Technology Conference*, Houston, 1970.

[65] J. E. Bowles, in *Foundation Analysis and Design, 5th Ed.*, Peoria, The McGraw-Hill Companies, Inc., 1997.

[66] Department of the Army; Waterways Experiment Station, "Shore Protection Manual Volume II," US Army Corps of Engineers, Washington D.C., 1984.

APPENDIX A1 – U.S. OFFSHORE WIND CURRENT AND POTENTIAL PROJECTS

Table A1- 1 – U.S. Offshore Wind Projects in Development or Installed

Lease Area	Project Name	State[1]	Project Capacity (MW)	Commercial Operation Date[2]	Developer	Distance from Shore (km)	Latitude (DD)	Longitude (DD)	Foundation Type	# of Positions	Turbine Size (MW)	Min Water Depth (m)	Average Water Depth (m)	Max Water Depth (m)
State	AquaVentus	ME	12	2022	UMaine	19	43.73	-69.32	Floating (Volturn US)	2	6	58	67	75
State	Icebreaker	OH	20.7	2022	LEEDCO & Fred Olsen Renewables	13	41.67	-81.89	Mono Bucket	6	3.45	29	33	37
OCS-A-0486	Revolution	CT	300	2024	Orsted/Eversource	24	41.19	-71.14	Monopile	37.5	8	30	36	43
OCS-A-0486	Revolution	RI	400	2024	Orsted/Eversource	24	41.19	-71.14	Monopile	50	8	30	36	43
State	Block Island	RI	30	2016	Orsted	4.85	41.12	-71.52	4-Pile Jacket	5	6	23	26	28
OCS-A-0486	South Fork	NY	130	2024	Orsted/Eversource	24	41.09	-71.12	Monopile	16	8	33	35	38
OCS-A-0501	Vineyard Wind	MA	800	2023	Vineyard Wind, LLC	45	41.02	-70.50	Monopile	84	9.5	34	44	49
OCS-A-0487	Sunrise	NY	880	2024	Orsted/Eversource	50	40.99	-71.06	Monopile	110	8	38	47	57
OCS-A-0501	Park City	CT	804	2027	Vineyard Wind, LLC	58	40.89	-70.66	Monopile	53 - 80	10 - 15	49	53	57
OCS-A-0521	Mayflower Wind	MA	804	2025	Shell New Energies & EDPR	72	40.74	-70.41	Floating (WindFloat)	53 - 80	10-15	47	53	57
OCS-A-0512	Empire Wind	NY	816	2025	Equinor	22	40.30	-73.32	Gravity	54 - 82	10-15	20	33	40
OCS-A-0498	Ocean Wind	NJ	1100	2024	Orsted	13	39.10	-74.31	Monopile	92	12	16	26	38
OCS-A-0519	Skipjack	MD	120	2022	Orsted	28	38.61	-74.64	Monopile	10	12	19	26	32
OCS-A-0490	MarWin	MD	270	2023	US Wind, Inc.	27	38.35	-74.76	-	32	8.5	16	13	35
OCS-A-0483	CVOW	VA	880	2024	Dominion Energy	40	36.91	-75.35	Monopile	-	-	27	32	38
OCS-A-0483	CVOW	VA	880	2025	Dominion Energy	40	36.91	-75.35	Monopile	-	-	27	32	38
OCS-A-0483	CVOW	VA	880	2026	Dominion Energy	40	36.91	-75.35	Monopile	-	-	27	32	38
OCS-A-0497	CVOW	VA	12	2021	Dominion Energy	40	36.89	75.35	Monopile	12	6	24	24	24[12]

[1] State refers to the state which power is delivered to and not the physical location.
[2] Future commercial operations dates may change.

Table A1- 2 – U.S. Offshore Wind Potential Project Areas

Lease Area	Area Name [2,4]	Call Area Size (km^2)	State [1]	Lease Area Potential[3] (MW)	Developer	Distance from Shore (km)	Latitude (DD)	Longitude (DD)	Foundation Type	Minimum Water Depth (m)	Average Water Depth (m)	Max Water Depth (m)
OCS-A-0500	Bay State	759	MA	2278	Orsted/Eversource	45	40.98	-70.78	-	35	49	60
Call Area	Humboldt	536	CA	1608	-	32	40.98	-124.67	Floating	470	700	986
OCS-A-0520	Equinor MA	522	MA	1565	Equinor	60	40.80	-70.54	-	47	51	57
OCS-A-0521	MayFlower Wind +	-	MA	743	Shell New Energies & EDPR	72	40.74	-70.41	-	47	53	57
OCS-A-0522	Liberty Wind	536	MA	1608	Vineyard Wind, LLC	80	40.69	-70.20	-	47	55	62
Call Area	Fairways North	858	NY	2574	-	27	40.65	-71.96	-	40	53	60
Call Area	Fairways South	434	NY	1301	-	27	40.45	-72.51	-	38	48	60
Call Area	Hudson North	2391	NY	7174	-	38	40.15	-72.77	-	40	50	60
Call Area	Hudson South	3342	NY	10026	-	27	39.63	-73.38	-	27	40	53
OCS-A-0499	Atlantic Shores	742	NJ	2227	EDF-RE & Shell New Energies US	15	39.41	-74.00	-	15	22	32
OCS-A-0498	Ocean Wind +	-	NJ	847	Orsted	13	39.10	-74.31	-	16	26	38
OCS-A-0482	Garden State Offshore Energy	284	DE	851	GSOE I, LLC	20	38.69	-74.70	-	15	22	31
OCS-A-0519	Skipjack +	-	DE	200	Orsted	20	38.55	-74.67	-	13	18	26
OCS-A-0490	MarWin +	-	MD	698	US Wind, Inc.	27	38.35	-74.76	-	16	13	35
OCS-A-0508	Kitty Hawk	496	NC	1487	Avangrid Renewables, LLC	44	36.34	-75.11	-	24	35	32
Call Area	Morro Bay	807	CA	2420	-	37	35.59	-121.81	Floating	874	967	1033
Call Area	Diablo Canyon	1442	CA	4326	-	30	35.10	-121.40	Floating	413	662	1064
Call Area	Wilmington West	209	NC	627	-	18	33.69	-78.28	-	14	16	20
Call Area	Grand Strand	2543	SC	7628	-	6	33.47	-78.65	-	7	14	22
Call Area	Wilmington East	541	NC	1623	-	24	33.45	-77.91	-	16	26	30
Call Area	Cape Romain	630	SC	1889	-	9	32.88	-72.29	-	7	12	22
Call Area	Winyah	141	SC	423	-	37	32.75	-78.58	-	33	33	40
Call Area	Charleston	144	SC	432	-	30	32.49	-79.32	-	27	31	33
Call Area	Oahu North	982	HI	2945	-	24	21.70	-158.51	Floating	497	872	1018
Call Area	Oahu South	982	HI	2945	-	24	20.97	-157.81	Floating	388	475	722[1234]

[1] State refers to the physical location of the project as stipulated by BOEM in Federal Leasing and Call for Information Areas.
[2] Some area names may change based on successful bids to state procurement solicitations.
[3] Lease area potential describes the potential capacity that could be installed in an area using a 3MW/km^2 density.
[4] Lease areas can often accommodate multiple project phases build incrementally. The “+” refers to remaining space in a lease area that may be utilized in the future.

APPENDIX A2 – TC, ETC AND NOR'EASTER WIND SPEEDS

Table A2- 1: ETC 1-Minute Average Surface Wind Speeds

Oct - April

	Wind Speed (m/s)	Wind Speed (m/s)	Wind Speed (m/s)	Wind Speed (m/s)
Latitude	**33.292**	**36.632**	**39.312**	**40.923**
	15.43	23.15	23.15	20.58
	20.58	18.52	30.87	25.72
	20.58	20.58	36.01	30.87
	18.01	20.58	20.58	28.29
	18.01	28.29	30.87	18.01
	12.86	18.01	30.87	23.15
	20.58	18.01	23.15	18.01
	23.15	18.01	28.29	25.72
	15.43	20.58	18.01	28.29
	23.15	20.58	18.01	38.58
	30.87	18.01	23.15	41.16
	18.01	23.15	23.15	28.29
	36.01	41.16	41.16	
		30.87	25.72	
		30.87	28.29	
			30.87	
MEAN (μ):	20.97	23.36	27.01	27.22
STD DEV (σ1):	6.12	6.44	6.17	6.92
μ + σ1	27.10	29.80	33.18	34.15
MAX:	36.01	41.16	41.16	41.16

Table A2- 2: ETC 1-Minute Average Surface Wind Speeds

May - September

	Wind Speed (m/s)	Wind Speed (m/s)	Wind Speed (m/s)	Wind Speed (m/s)
Latitude	**33.292**	**36.632**	**39.312**	**40.923**
	25.72	12.86	23.15	25.72
	18.01	18.01	23.15	23.15
	20.58	20.58	20.58	23.15
	20.58	20.58	20.58	15.43
	20.58	21.61	20.58	20.58
	23.15	20.58	20.58	20.58
	25.72	20.58	20.58	18.01
	18.01	25.72	12.86	18.01
	15.43	23.15	18.01	18.01
	18.01	20.58	10.29	20.58
	15.43	23.15	12.86	33.44
	20.58	20.58	15.43	15.43
	20.58	12.86	23.15	23.15
	25.72	18.01	15.43	16.46
	20.58	19.03	28.29	10.29
	25.72	12.86	23.15	10.29
	12.86	20.58	12.86	23.15
	12.86	18.01	20.58	15.43
	18.01	20.58	18.01	20.58
	15.43	18.01	18.01	28.29
	15.43	23.15	18.01	28.29
	23.15	25.72	33.44	38.58
	20.58	20.58	33.44	28.29
	30.87	25.72	30.87	18.01
	33.44	12.86	15.43	15.43
	23.15	30.87		23.15
	20.58	18.01		20.58
	41.16	18.01		18.01
	20.58	12.86		25.72
	23.15	18.01		38.58
	15.43	23.15		33.44
	7.72	23.15		23.15
	18.01	30.87		38.58
	25.72	29.32		30.87
	18.01	26.75		20.58
	25.72	20.58		12.86
		18.01		30.87
		33.44		23.15
		30.87		20.58
		28.29		18.01
		20.58		23.15
MEAN (μ):	21.01	21.43	20.37	22.67
STD DEV (σ_1):	6.08	5.17	6.04	7.08
$\mu + \sigma_1$	27.08	26.60	26.41	29.75
Max:	41.16	33.44	33.44	38.58

Table A2- 3: TC 1-Minute Average Surface Wind Speeds

	Wind Speed (m/s)	Wind Speed (m/s)	Wind Speed (m/s)	Wind Speed (m/s)
Latitude	**33.29**	**36.63**	**39.31**	**40.9**
[redacted]	59.16	61.73	59.16	59.16
	59.16	59.16	51.44	51.44
	59.16	54.02	51.44	49.90
	64.31	51.44	51.44	56.59
	61.73	51.44	51.44	56.59
	61.73	54.02	54.02	51.44
	56.59	51.44	51.44	49.90
	51.44	56.59	48.87	54.02
	56.59	56.59	47.84	46.30
	51.44	51.44	43.73	43.73
	56.59	51.44	43.73	46.30
	51.44	56.59	42.18	46.30
	51.44	54.02	43.73	43.73
	56.59	54.02	48.87	43.73
	56.59	55.05	42.18	48.87
	51.44	52.99	44.76	48.87
	51.44	43.73	46.30	46.30
	51.44	43.73	36.01	46.30
	56.59	47.33	38.58	46.30
	54.02	51.44	41.16	46.30
	51.44	51.44	33.44	47.84
	54.02	43.73	36.01	43.73
	43.73	48.87	30.87	43.73
	54.02	43.73	38.58	47.84
	51.44	43.73	33.44	46.30
	54.02	41.16	39.61	46.30
	57.62	43.73	41.16	38.58
	43.73	46.30	41.16	41.16
	43.73	46.30	38.58	33.44
	43.73	48.87	36.01	37.55
	46.30	43.73	36.01	36.01
	46.30	46.30	34.47	38.58
	48.87	46.30	33.44	38.58
	48.87	46.30	39.61	41.16
	43.73	46.30	36.01	33.44
	46.30	46.30	38.58	36.01
	48.87	46.30	36.01	38.58
	44.76	43.73	34.47	33.44
	46.30	46.30	41.16	41.16
	46.30	46.30	34.47	38.58
	46.30	43.73	36.01	36.01
	43.73	46.30	39.61	38.58
	44.76	43.73	33.44	41.16
	46.30	46.30	[redacted]	41.16
	51.44	43.73		41.16
	43.73	48.87		41.16
	43.73	46.30		36.01
	46.30	38.58		38.58
	43.73	41.16		36.01

	Wind Speed (m/s)	Wind Speed (m/s)	Wind Speed (m/s)	Wind Speed (m/s)
Latitude	**33.29**	**36.63**	**39.31**	**40.9**
	46.30	36.01		36.01
	46.30	38.58		41.16
	43.73	41.16		36.01
	46.30	33.44		33.44
	46.30	36.01		38.58
	46.30	33.44		38.58
	46.30	38.58		36.01
	46.30	34.47		34.47
	46.30	33.44		41.16
	46.30	41.16		38.07
	46.30	36.01		33.44
	46.30	41.16		38.58
	46.30	38.58		38.58
	46.30	36.01		33.44
	43.73	38.58		33.44
	46.30	36.01		
	43.73	41.16		
	48.87	36.01		
	43.73	41.16		
	48.87	33.44		
	46.30	36.01		
	44.76	33.44		
	43.73	34.47		
	46.30	33.44		
	47.84	36.01		
	37.55	41.16		
	38.58	36.01		
	34.47	41.16		
	41.16	36.01		
	37.55	36.01		
	36.01	36.01		
	33.44	36.01		
	39.61	36.01		
	38.58	38.58		
	41.16	36.01		
	33.44	36.01		
	36.01	33.44		
	33.44	36.01		
	41.16	33.44		
	36.01	36.01		
	38.58	36.01		
	36.01	38.58		
	41.16	33.44		
	33.44	36.01		
	41.16	33.44		
	37.55	41.16		
	33.44	36.01		
	33.44	41.16		
	34.47	37.04		
	38.58	33.44		

	Wind Speed (m/s)	Wind Speed (m/s)	Wind Speed (m/s)	Wind Speed (m/s)
Latitude	**33.29**	**36.63**	**39.31**	**40.9**
	36.01	41.16		
	38.58	33.44		
	41.16			
	37.55			
	33.44			
	38.58			
	36.01			
	41.16			
	38.58			
	36.01			
	33.44			
	36.01			
	33.44			
	36.01			
	41.16			
	38.58			
	38.58			
	41.16			
	36.01			
	36.01			
	36.01			
	41.16			
	36.01			
	41.16			
	38.58			
	38.58			
	41.16			
	41.16			
	41.16			
	36.01			
	36.01			
	41.16			
	36.01			
	36.01			
	38.58			
	36.01			
	36.01			
	36.01			
	36.01			
	41.16			
	36.01			
	33.44			
	36.01			
	36.01			
	38.58			
	38.58			
	36.01			
	41.16			
	38.58			
	33.44			

	Wind Speed (m/s)	Wind Speed (m/s)	Wind Speed (m/s)	Wind Speed (m/s)
Latitude	**33.29**	**36.63**	**39.31**	**40.9**
	36.01			
	41.16			
	39.61			
	38.58			
	33.44			
	38.58			
	33.44			
	38.58			
	38.58			
	41.16			
	41.16			
	38.58			
	39.61			
	36.01			
	33.44			
	38.58			
MEAN (μ):	42.75	42.37	41.41	41.95
STD DEV (σ_1):	7.09	7.11	6.71	6.30
$\mu + \sigma_1$	49.85	49.48	48.12	48.25
MAX :	64.31	61.73	59.16	59.16

APPENDIX A3 – WAVE HEIGHT AND PERIOD CALCULATIONS

H1 Case Metocean Data

Table A3- 1: H1 Wave Heights and Periods from BSEE TAP Studies

Source	Storm Type	Latitude (DD)	Longitude (DD)	State	Return Period	Vref (m/s)	Zref (m)	Water Depth (m)	Hs (m)	Notes
63124	TC	40.420	-73.670	NY	100	30.00	10	23	7.0	BSEE TAP 672
Site 3	ETC	38.370	-74.750	MD	100	30.00	10	25	11.0	BSEE TAP 724
Site 4	ETC	36.430	-75.300	NC	500	30.00	10	27	11.5	BSEE TAP 724
Site 1	ETC	40.760	-70.550	MA	500	31.00	10	55	15.0	BSEE TAP 724
63155	TC	38.670	-74.830	DE	100	32.20	10	21	6.3	BSEE TAP 672
63157	TC	38.580	-74.830	DE	100	32.30	10	23	7.3	BSEE TAP 672
63194	TC	37.000	-75.500	VA	50	32.30	10	25	7.9	BSEE TAP 672
63136	TC	39.670	-73.920	NJ	100	32.40	10	25	7.8	BSEE TAP 672
63137	TC	39.580	-74.000	NJ	100	32.40	10	23	7.8	BSEE TAP 672
63140	TC	39.330	-74.170	NJ	100	32.50	10	18	7.8	BSEE TAP 672
63196	TC	36.920	-75.500	VA	50	32.60	10	20	7.9	BSEE TAP 672
63153	TC	38.750	-74.750	DE	100	32.70	10	19	6.0	BSEE TAP 672
63141	TC	39.250	-74.250	NJ	100	32.80	10	21	7.3	BSEE TAP 672
63144	TC	39.080	-74.420	NJ	100	32.80	10	18	7.5	BSEE TAP 672
63161	TC	38.420	-74.830	MD	100	32.90	10	21	7.3	BSEE TAP 672
63138	TC	39.500	-74.000	NJ	100	32.90	10	22	7.9	BSEE TAP 672
63139	TC	39.420	-74.080	NJ	100	33.00	10	21	7.5	BSEE TAP 672
63142	TC	39.170	-74.330	NJ	100	33.10	10	18	7.4	BSEE TAP 672
63163	TC	38.330	-74.830	MD	100	33.40	10	18	7.1	BSEE TAP 672
Site 3	ETC	38.370	-74.750	MD	500	33.50	10	25	12.0	BSEE TAP 724
63148	TC	38.920	-74.500	NJ	100	33.60	10	22	7.7	BSEE TAP 672
63165	TC	38.250	-74.830	MD	100	33.60	10	21	7.7	BSEE TAP 672
63146	TC	39.000	-74.420	NJ	100	33.70	10	18	7.5	BSEE TAP 672
63198	TC	36.830	-75.500	VA	50	33.90	10	22	7.7	BSEE TAP 672

Table A3- 2: H1 Case Design Maximum Wave Height and Period

Saffir-Simpson Category	Water Depth (m)	Vref (m/s)	Hs (m)	Hmax (m)	Thmax (s)
H1	20	32	7.45	13.80	11.07
H1	40	32	12.60	23.40	14.39
H1	50	32	14.26	26.50	15.31

Table A3- 3: Calculation of Maximum Wave Height and Period for H1 Case

Water Depth (m)	Hs (m)	Hmax (m)	Hb (m)	Min Tp (s)	Max Tp (s)	Mean Tp (s)
20	7.45	13.86	15.60	9.67	12.46	11.07
40	12.60	23.44	31.20	12.58	16.21	14.39
50	14.26	26.52	39.00	13.38	17.24	15.31

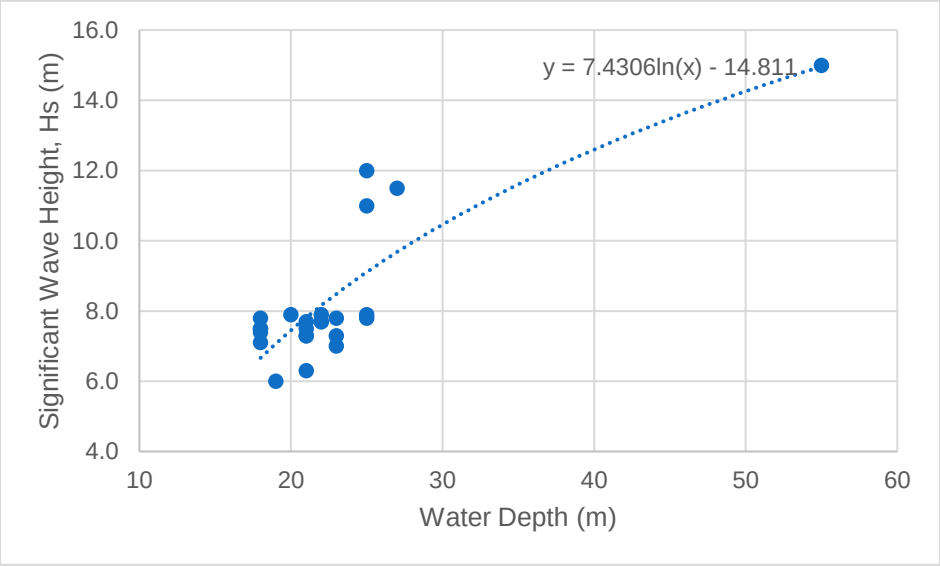

Figure A3- 1: Significant Wave Height Vs. Water Depth for H1 Case

H2 Case Metocean Data

Table A3- 4: H2 Wave Heights and Periods from BSEE TAP Studies

Source	Storm Type	Latitude (DD)	Longitude (DD)	State	Return Period	Vref (m/s)	Zref (m)	Water Depth (m)	Hs (m)	Notes
Site 3	TC	38.370	-74.750	MD	50	41.0	10	25	17	BSEE TAP 724
Site 1	TC	40.760	-70.550	MA	50	42.0	10	55	17	BSEE TAP 724
Site 4	TC	36.430	-75.300	NC	50	42.0	10	27	17	BSEE TAP 724
Site 1	TC	40.760	-70.550	MA	100	44.0	10	55	18	BSEE TAP 724
Site 3	TC	38.370	-74.750	MD	100	44.1	10	25	18	BSEE TAP 724
Site 2	TC	38.980	-74.017	NJ	50	45.0	10	37	21	BSEE TAP 724

Table A3- 5: H2 Case Design Maximum Wave Height and Period

Saffir-Simpson Category	Water Depth (m)	Vref (m/s)	Hs (m)	Hmax (m)	Thmax (s)
H2	20	43	18	15.60	15.04
H2	40	43	18	31.20	17.20
H2	50	43	18	33.48	19.37

Table A3- 6: Calculation of Maximum Wave Height and Period for H2 Case

Water Depth (m)	Hs (m)	Hmax (m)	Hb (m)	Min Tp (s)	Max Tp (s)	Mean Tp (s)
20	18.00	15.60	15.60	15.04	19.37	17.20
40	18.00	31.20	31.20	15.04	19.37	17.20
50	18.00	33.48	39.00	15.04	19.37	17.20

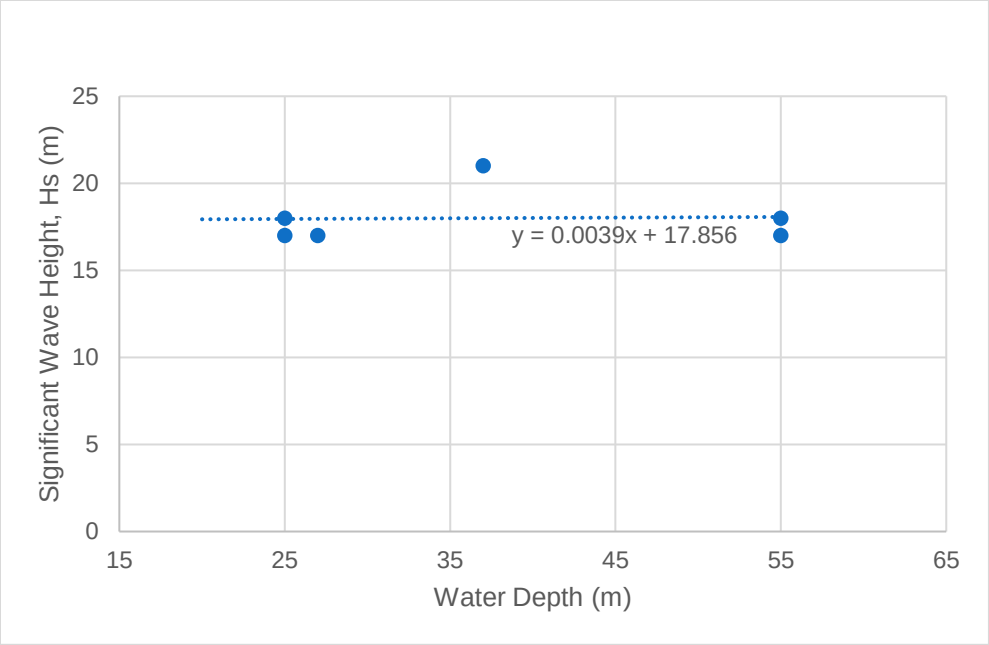

Figure A3- 2: Significant Wave Height Vs. Water Depth for H2 Case

H3 Case Metocean Data

Table A3- 7: H3 Wave Heights and Periods from BSEE TAP Studies

Source	Storm Type	Latitude (DD)	Longitude (DD)	State	Return Period	Vref (m/s)	Zref (m)	Water Depth (m)	Hs (m)	Notes
Site 3	TC	38.370	-74.750	MD	500	48	10	25	23.0	BSEE TAP 724
Site 4	TC	36.430	-75.300	NC	100	48	10	27	20.5	BSEE TAP 724
Site 4	TC	36.430	-75.300	NC	500	48	10	27	25.3	BSEE TAP 724
Site 5	TC	33.040	-78.600	SC	50	48	10	31	24.0	BSEE TAP 724
Site 5	TC	33.040	-78.600	SC	100	51	10	31	26.0	BSEE TAP 724
Site 2	TC	38.980	-74.017	NJ	100	48	10	37	23.5	BSEE TAP 724

Table A3- 8: H3 Case Design Maximum Wave Height and Period

Saffir-Simpson Category	Water Depth (m)	Vref (m/s)	Hs (m)	Hmax (m)	Thmax (s)
H3	20	50	22.70	15.60	16.89
H3	40	50	24.70	31.20	20.15
H3	50	50	25.70	39.00	23.15

Table A3- 9: Calculation of Maximum Wave Height and Period for H3 Case

Water Depth (m)	Hs (m)	Hmax (m)	Hb (m)	Min Tp (s)	Max Tp (s)	Mean Tp (s)
20	22.70	15.60	15.60	16.89	21.75	
40	24.70	31.20	31.20	17.61	22.69	
50	25.70	39.00	39.00	17.97	23.15	

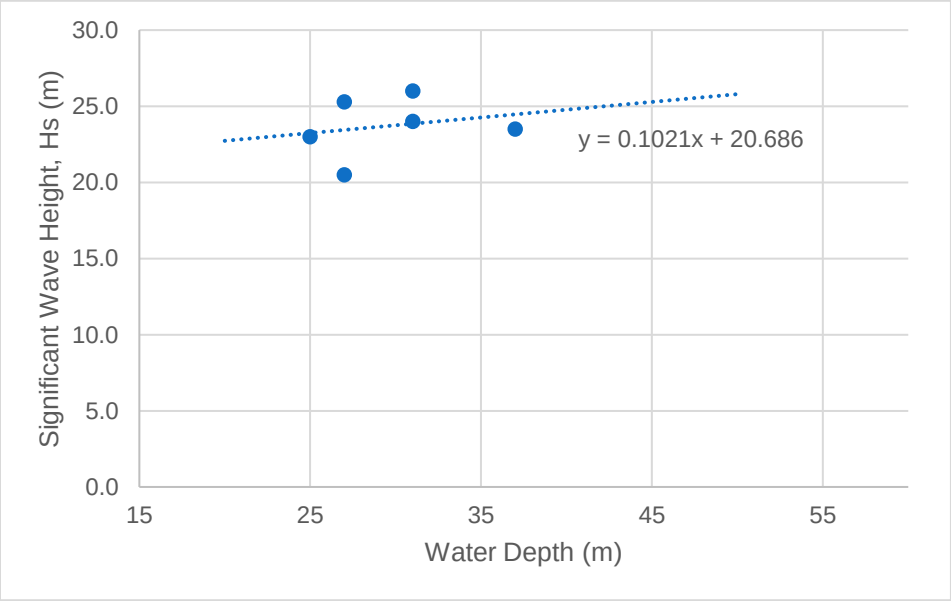

Figure A3- 3: Significant Wave Height Vs. Water Depth for H3 Case

H4 Case Metocean Data

Table A3- 10: H4 Wave Heights and Periods from BSEE TAP Studies

Source	Storm Type	Latitude (DD)	Longitude (DD)	State	Return Period	Vref (m/s)	Zref (m)	Water Depth (m)	Hs (m)	Notes
Site 2	TC	38.980	-74.017	NJ	500	54	10	37	30	BSEE TAP 724
Site 5	TC	33.040	-78.600	SC	500	56	10	31	34	BSEE TAP 724

Table A3- 11: H4 Case Design Maximum Wave Height and Period

Saffir-Simpson Category	Water Depth (m)	Vref (m/s)	Hs (m)	Hmax (m)	Thmax (s)
H4	20	59	26.00	15.60	17.07
H4	40	59	26.00	31.20	20.68
H4	50	59	28.00	39.00	24.16

Table A3- 12: Calculation of Maximum Wave Height and Period for H4 Case

Water Depth (m)	Hs (m)	Hmax (m)	Hb (m)	Min Tp (s)	Max Tp (s)	Mean Tp (s)
20	26.00	15.60	15.60	18.07	23.28	20.68
40	26.00	31.20	31.20	18.07	23.28	20.68
50	28.00	39.00	39.00	18.75	24.16	21.46

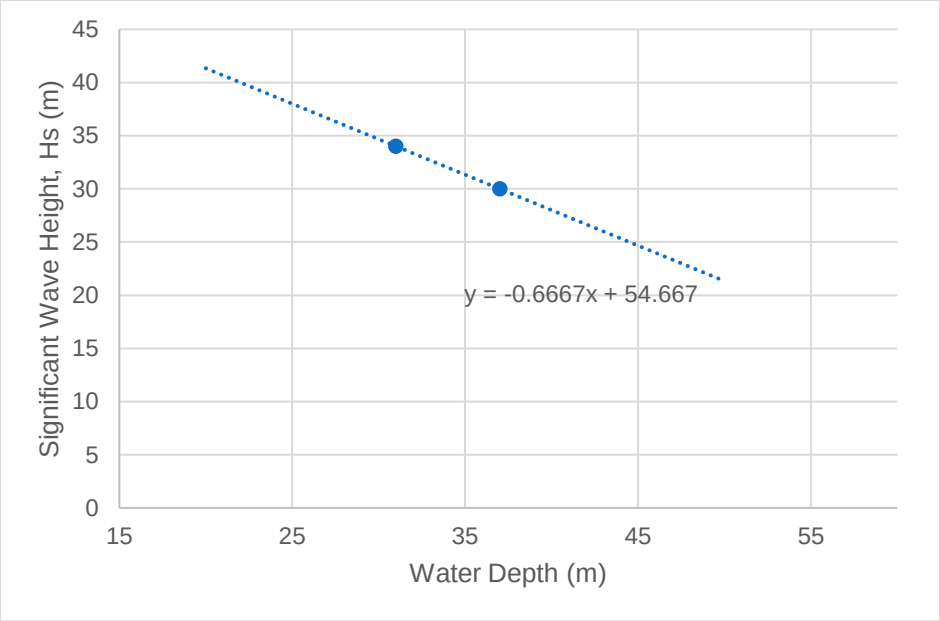

Figure A3- 4: Significant Wave Height Vs. Water Depth for H4 Case

Table A3- : Wave Theory Calculation

WAVE THEORY FOR ALL ENVIRONMENTAL CASES																
LC	**d, Water Level (m)**	**Surge + Tide (m)**	**H, Wave Height (m)**	**T, Wave Period (m)**	**$d/(gT^2)$, Non-Dimensional Depth**	**$H/(gT^2)$, Non-Dimensional Wave Height**	**L_0, Deepwater Wavelength from Linear Wave Theory (m)**	**U_r, Ursell Number [1] L^2H/d^3**	**Shallow, Intermediate, Deep [(2)]**	**Linear, Non-Linear, Breaking [2]**	**Wave Theory [3]**	**d/L_0**	**d/L [4]**	**L, Wavelength (m)**	**H/d = 0.78, Breaking Limit (Solitary Wave)**	**$H/L_0 > 0.14$, Breaking Limit (Deepwater Waves)**
XX_20_H1	20	2.7	13.80	11.07	0.0166	0.0115	191.24	32.83	Intermediate	Non-Linear	Stream 11	0.1046	0.1450	137.95	0.69	0.07
XX_40_H1	40	2.7	23.40	14.39	0.0197	0.0115	323.44	22.50	Intermediate	Non-Linear	Stream 11	0.1237	0.1613	248.05	0.59	0.07
XX_50_H1	50	2.7	26.50	15.31	0.0217	0.0115	366.06	17.90	Intermediate	Non-Linear	Stream 7	0.1366	0.1721	290.56	0.53	0.07
XX_20_H2	20	3.3	15.60	15.04	0.0090	0.0070	352.97	76.46	Intermediate	Non-Linear	Stream 11	0.0567	0.1010	198.02	0.78	0.04
XX_40_H2	40	3.3	31.20	17.20	0.0138	0.0107	462.06	46.77	Intermediate	Non-Linear	Stream 11	0.0866	0.1291	309.74	0.78	0.07
XX_50_H2	50	3.3	33.48	19.37	0.0136	0.0091	585.82	40.83	Intermediate	Non-Linear	Stream 11	0.0854	0.1281	390.44	0.67	0.06
XX_20_H3	20	4.25	15.60	16.89	0.0072	0.0056	445.14	99.09	Intermediate	Non-Linear	Stream 11	0.0449	0.0887	225.43	0.78	0.04
XX_40_H3	40	4.25	31.20	20.15	0.0100	0.0078	634.05	67.63	Intermediate	Non-Linear	Stream 11	0.0631	0.1074	372.47	0.78	0.05
XX_50_H3	50	4.25	39.00	23.15	0.0095	0.0074	836.42	71.98	Intermediate	Non-Linear	Stream 11	0.0598	0.1041	480.31	0.78	0.05
XX_20_H4	20	5.5	15.60	17.07	0.0070	0.0055	454.94	101.32	Intermediate	Non-Linear	Stream 11	0.0440	0.0877	227.95	0.78	0.03
XX_40_H4	40	5.5	31.20	20.68	0.0095	0.0074	667.42	71.84	Intermediate	Non-Linear	Stream 11	0.0599	0.1042	383.88	0.78	0.05
XX_50_H4	50	5.5	39.00	24.16	0.0087	0.0068	911.28	79.26	Intermediate	Non-Linear	Stream 11	0.0549	0.0992	504.04	0.78	0.04

[1] Ur > 26 Stokes Theory Does Not Apply
[2] Determined from Figure B.1 [28]
[3] Determined from Figure B.1 [28]
[4] Determined from Table C-1 [65]

APPENDIX A4 – NOAA TIDE TABLES

StationId: 8449130
Source: NOAA/NOS/CO-OPS
Station Type: Primary
Time Zone: LST_LDT
Datum: MLLW

NOAA Tide Predictions

Nantucket Island, MA,2019

Times and Heights of High and Low Waters

October

	Time	Height		Time	Height
	h m	ft cm		h m	ft cm
1 Tu	02:39 AM	3.7 113	16 W	02:29 AM	3.0 91
	08:14 AM	-0.1 -3		07:59 AM	0.6 18
	02:54 PM	4.1 125		02:31 PM	3.5 107
	08:54 PM	-0.4 -12		08:37 PM	0.2 6
2 W	03:36 AM	3.5 107	17 Th	03:12 AM	2.9 88
	09:06 AM	0.1 3		08:38 AM	0.7 21
	03:48 PM	4.1 125		03:12 PM	3.5 107
	09:50 PM	-0.3 -9		09:21 PM	0.2 6
3 Th	04:33 AM	3.3 101	18 F	03:57 AM	2.8 85
	09:59 AM	0.3 9		09:19 AM	0.7 21
	04:42 PM	4.0 122		03:56 PM	3.5 107
	10:48 PM	-0.1 -3		10:07 PM	0.1 3
4 F	05:32 AM	3.1 94	19 Sa	04:45 AM	2.8 85
	10:54 AM	0.5 15		10:05 AM	0.7 21
	05:38 PM	3.8 116		04:44 PM	3.6 110
	11:48 PM	0.0 0		10:58 PM	0.1 3
5 Sa	06:31 AM	3.0 91	20 Su	05:36 AM	2.8 85
	11:52 AM	0.6 18		10:57 AM	0.7 21
	06:36 PM	3.7 113		05:37 PM	3.6 110
				11:52 PM	0.1 3
6 Su	12:49 AM	0.2 6	21 M	06:29 AM	2.8 85
	07:31 AM	2.9 88		11:54 AM	0.6 18
	12:52 PM	0.7 21		06:34 PM	3.6 110
	07:35 PM	3.5 107			
7 M	01:49 AM	0.3 9	22 Tu	12:49 AM	0.1 3
	08:30 AM	2.9 88		07:25 AM	2.9 88
	01:53 PM	0.8 24		12:55 PM	0.5 15
	08:33 PM	3.4 104		07:34 PM	3.6 110
8 Tu	02:45 AM	0.4 12	23 W	01:46 AM	0.1 3
	09:24 AM	2.9 88		08:21 AM	3.0 91
	02:51 PM	0.8 24		01:58 PM	0.4 12
	09:28 PM	3.3 101		08:35 PM	3.7 113
9 W	03:35 AM	0.4 12	24 Th	02:42 AM	0.0 0
	10:12 AM	2.9 88		09:17 AM	3.2 98
	03:44 PM	0.7 21		03:00 PM	0.2 6
	10:19 PM	3.3 101		09:36 PM	3.7 113
10 Th	04:20 AM	0.5 15	25 F	03:36 AM	-0.1 -3
	10:54 AM	3.0 91		10:11 AM	3.5 107
	04:32 PM	0.6 18		04:00 PM	0.0 0
	11:05 PM	3.2 98		10:37 PM	3.7 113
11 F	05:00 AM	0.5 15	26 Sa	04:29 AM	-0.1 -3
	11:30 AM	3.1 94		11:04 AM	3.7 113
	05:16 PM	0.5 15		04:58 PM	-0.3 -9
	11:47 PM	3.2 98		11:36 PM	3.6 110
12 Sa	05:37 AM	0.5 15	27 Su	05:19 AM	-0.1 -3
	12:05 PM	3.2 98		11:56 AM	3.9 119
	05:57 PM	0.5 15		05:54 PM	-0.4 -12
13 Su	12:28 AM	3.1 94	28 M	12:33 AM	3.6 110
	06:13 AM	0.6 18		06:09 AM	-0.1 -3
	12:40 PM	3.2 98		12:47 PM	4.1 125
○	06:37 PM	0.4 12	●	06:49 PM	-0.5 -15
14 M	01:07 AM	3.1 94	29 Tu	01:29 AM	3.5 107
	06:48 AM	0.6 18		06:58 AM	0.0 0
	01:16 PM	3.3 101		01:38 PM	4.2 128
	07:17 PM	0.3 9		07:42 PM	-0.5 -15
15 Tu	01:48 AM	3.0 91	30 W	02:24 AM	3.3 101
	07:23 AM	0.6 18		07:48 AM	0.1 3
	01:53 PM	3.4 104		02:29 PM	4.1 125
	07:56 PM	0.2 6		08:36 PM	-0.5 -15
			31 Th	03:19 AM	3.2 98
				08:39 AM	0.2 6
				03:20 PM	4.0 122
				09:29 PM	-0.3 -9

November

	Time	Height		Time	Height
	h m	ft cm		h m	ft cm
1 F	04:13 AM	3.1 94	16 Sa	02:36 AM	2.8 85
	09:31 AM	0.4 12		07:52 AM	0.6 18
	04:12 PM	3.9 119		02:31 PM	3.7 113
	10:23 PM	-0.2 -6		08:45 PM	-0.1 -3
2 Sa	05:08 AM	3.0 91	17 Su	03:25 AM	2.8 85
	10:25 AM	0.6 18		08:41 AM	0.6 18
	05:06 PM	3.7 113		03:22 PM	3.7 113
	11:19 PM	0.0 0		09:36 PM	-0.1 -3
3 Su	05:02 AM	2.9 88	18 M	04:16 AM	2.8 85
	10:22 AM	0.7 21		09:36 AM	0.5 15
	05:00 PM	3.5 107		04:17 PM	3.6 110
	11:15 PM	0.2 6		10:29 PM	-0.1 -3
4 M	05:57 AM	2.9 88	19 Tu	05:10 AM	2.9 88
	11:21 AM	0.8 24		10:36 AM	0.5 15
	05:56 PM	3.3 101		05:15 PM	3.6 110
◐			◑	11:25 PM	0.0 0
5 Tu	12:11 AM	0.3 9	20 W	06:06 AM	3.0 91
	06:50 AM	2.9 88		11:40 AM	0.4 12
	12:22 PM	0.8 24		06:17 PM	3.5 107
	06:52 PM	3.2 98			
6 W	01:04 AM	0.4 12	21 Th	12:22 AM	0.0 0
	07:40 AM	2.9 88		07:02 AM	3.2 98
	01:20 PM	0.8 24		12:45 PM	0.3 9
	07:47 PM	3.1 94		07:19 PM	3.4 104
7 Th	01:53 AM	0.5 15	22 F	01:17 AM	0.0 0
	08:26 AM	3.0 91		07:58 AM	3.5 107
	02:15 PM	0.7 21		01:49 PM	0.1 3
	08:39 PM	3.0 91		08:22 PM	3.4 104
8 F	02:37 AM	0.5 15	23 Sa	02:12 AM	0.0 0
	09:08 AM	3.1 94		08:53 AM	3.7 113
	03:04 PM	0.6 18		02:50 PM	-0.1 -3
	09:27 PM	3.0 91		09:24 PM	3.3 101
9 Sa	03:18 AM	0.6 18	24 Su	03:04 AM	0.0 0
	09:47 AM	3.2 98		09:46 AM	3.9 119
	03:49 PM	0.5 15		03:48 PM	-0.3 -9
	10:13 PM	2.9 88		10:24 PM	3.2 98
10 Su	03:56 AM	0.6 18	25 M	03:55 AM	0.0 0
	10:25 AM	3.3 101		10:38 AM	4.0 122
	04:31 PM	0.3 9		04:43 PM	-0.4 -12
	10:57 PM	2.9 88		11:22 PM	3.2 98
11 M	04:33 AM	0.6 18	26 Tu	04:45 AM	0.0 0
	11:03 AM	3.4 104		11:28 AM	4.1 125
	05:11 PM	0.2 6		05:36 PM	-0.5 -15
	11:39 PM	2.9 88	●		
12 Tu	05:09 AM	0.6 18	27 W	12:17 AM	3.1 94
	11:41 AM	3.5 107		05:35 AM	0.1 3
	05:51 PM	0.1 3		12:17 PM	4.1 125
○				06:27 PM	-0.5 -15
13 W	12:22 AM	2.8 85	28 Th	01:09 AM	3.0 91
	05:47 AM	0.6 18		06:24 AM	0.2 6
	12:20 PM	3.6 110		01:06 PM	4.0 122
	06:31 PM	0.0 0		07:17 PM	-0.4 -12
14 Th	01:05 AM	2.8 85	29 F	02:00 AM	3.0 91
	06:25 AM	0.6 18		07:13 AM	0.3 9
	01:00 PM	3.6 110		01:54 PM	3.9 119
	07:13 PM	0.0 0		08:06 PM	-0.3 -9
15 F	01:49 AM	2.8 85	30 Sa	02:49 AM	2.9 88
	07:07 AM	0.6 18		08:04 AM	0.5 15
	01:44 PM	3.7 113		02:43 PM	3.7 113
	07:58 PM	-0.1 -3		08:56 PM	-0.1 -3

December

	Time	Height		Time	Height
	h m	ft cm		h m	ft cm
1 Su	03:38 AM	2.8 85	16 M	03:03 AM	2.9 88
	08:56 AM	0.6 18		08:23 AM	0.3 9
	03:32 PM	3.5 107		03:05 PM	3.8 116
	09:46 PM	0.0 0		09:15 PM	-0.3 -9
2 M	04:27 AM	2.8 85	17 Tu	03:56 AM	3.0 91
	09:50 AM	0.7 21		09:20 AM	0.3 9
	04:23 PM	3.3 101		04:01 PM	3.7 113
	10:37 PM	0.2 6		10:07 PM	-0.2 -6
3 Tu	05:15 AM	2.8 85	18 W	04:50 AM	3.1 94
	10:46 AM	0.7 21		10:22 AM	0.3 9
	05:14 PM	3.2 98		05:00 PM	3.5 107
	11:27 PM	0.3 9		11:02 PM	-0.2 -6
4 W	06:04 AM	2.8 85	19 Th	05:46 AM	3.3 101
	11:45 AM	0.8 24		11:27 AM	0.2 6
	06:07 PM	3.0 91		06:02 PM	3.3 101
◐			◑	11:57 PM	-0.1 -3
5 Th	12:17 AM	0.4 12	20 F	06:43 AM	3.4 104
	06:51 AM	2.9 88		12:33 PM	0.1 3
	12:43 PM	0.7 21		07:06 PM	3.2 98
	07:00 PM	2.9 88			
6 F	01:05 AM	0.5 15	21 Sa	12:53 AM	0.0 0
	07:36 AM	3.0 91		07:39 AM	3.6 110
	01:38 PM	0.6 18		01:38 PM	0.0 0
	07:54 PM	2.8 85		08:11 PM	3.1 94
7 Sa	01:50 AM	0.5 15	22 Su	01:48 AM	0.0 0
	08:21 AM	3.1 94		08:35 AM	3.8 116
	02:30 PM	0.5 15		02:40 PM	-0.1 -3
	08:45 PM	2.7 82		09:14 PM	3.0 91
8 Su	02:32 AM	0.6 18	23 M	02:42 AM	0.1 3
	09:03 AM	3.2 98		09:30 AM	3.9 119
	03:17 PM	0.4 12		03:38 PM	-0.3 -9
	09:35 PM	2.7 82		10:15 PM	2.9 88
9 M	03:13 AM	0.6 18	24 Tu	03:35 AM	0.1 3
	09:45 AM	3.4 104		10:22 AM	4.0 122
	04:01 PM	0.3 9		04:32 PM	-0.3 -9
	10:23 PM	2.7 82		11:12 PM	2.9 88
10 Tu	03:53 AM	0.6 18	25 W	04:25 AM	0.2 6
	10:26 AM	3.5 107		11:12 AM	4.0 122
	04:43 PM	0.1 3		05:22 PM	-0.4 -12
	11:09 PM	2.7 82			
11 W	04:33 AM	0.5 15	26 Th	12:05 AM	2.8 85
	11:08 AM	3.6 110		05:15 AM	0.2 6
	05:24 PM	0.0 0		12:00 PM	3.9 119
	11:54 PM	2.7 82	●	06:10 PM	-0.3 -9
12 Th	05:13 AM	0.5 15	27 F	12:53 AM	2.8 85
	11:51 AM	3.7 113		06:03 AM	0.3 9
	06:06 PM	-0.1 -3		12:46 PM	3.8 116
○				06:57 PM	-0.3 -9
13 F	12:39 AM	2.7 82	28 Sa	01:39 AM	2.8 85
	05:56 AM	0.4 12		06:50 AM	0.4 12
	12:35 PM	3.8 116		01:31 PM	3.7 113
	06:50 PM	-0.2 -6		07:42 PM	-0.2 -6
14 Sa	01:25 AM	2.7 82	29 Su	02:22 AM	2.8 85
	06:42 AM	0.4 12		07:38 AM	0.4 12
	01:22 PM	3.8 116		02:16 PM	3.6 110
	07:36 PM	-0.3 -9		08:27 PM	-0.1 -3
15 Su	02:13 AM	2.8 85	30 M	03:04 AM	2.8 85
	07:30 AM	0.3 9		08:27 AM	0.5 15
	02:12 PM	3.8 116		03:00 PM	3.4 104
	08:24 PM	-0.3 -9		09:11 PM	0.0 0
			31 Tu	03:47 AM	2.8 85
				09:17 AM	0.6 18
				03:46 PM	3.2 98
				09:57 PM	0.2 6

StationId: 8557380
Source: NOAA/NOS/CO-OPS
Station Type: Primary
Time Zone: LST_LDT
Datum: MLLW

NOAA Tide Predictions

Lewes, DE,2019

Times and Heights of High and Low Waters

October

	Time	Height (ft)	Height (cm)	Time	Height (ft)	Height (cm)
1 Tu	04:49 AM	-0.4	-12	16 W	04:23 AM	0.3	9
	11:16 AM	5.5	168		10:49 AM	4.8	146
	05:26 PM	-0.4	-12		05:00 PM	0.3	9
	11:40 PM	4.7	143		11:10 PM	4.0	122
2 W	05:37 AM	-0.2	-6	17 Th	05:00 AM	0.3	9
	12:07 PM	5.3	162		11:28 AM	4.8	146
	06:20 PM	-0.1	-3		05:42 PM	0.4	12
					11:51 PM	3.9	119
3 Th	12:32 AM	4.3	131	18 F	05:40 AM	0.4	12
	06:27 AM	0.1	3		12:12 PM	4.8	146
	01:00 PM	5.1	155		06:30 PM	0.5	15
	07:18 PM	0.2	6				
4 F	01:28 AM	4.0	122	19 Sa	12:38 AM	3.7	113
	07:21 AM	0.4	12		06:26 AM	0.5	15
	01:56 PM	4.8	146		01:01 PM	4.7	143
	08:19 PM	0.5	15		07:23 PM	0.5	15
5 Sa ◐	02:28 AM	3.7	113	20 Su	01:31 AM	3.6	110
	08:19 AM	0.7	21		07:20 AM	0.6	18
	02:57 PM	4.6	140		01:56 PM	4.7	143
	09:24 PM	0.7	21		08:22 PM	0.6	18
6 Su	03:34 AM	3.6	110	21 M ◑	02:32 AM	3.6	110
	09:23 AM	0.9	27		08:21 AM	0.6	18
	04:01 PM	4.5	137		02:56 PM	4.7	143
	10:29 PM	0.7	21		09:25 PM	0.5	15
7 M	04:40 AM	3.5	107	22 Tu	03:38 AM	3.6	110
	10:28 AM	0.9	27		09:26 AM	0.5	15
	05:03 PM	4.4	134		04:04 PM	4.7	143
	11:28 PM	0.7	21		10:29 PM	0.4	12
8 Tu	05:39 AM	3.6	110	23 W	04:45 AM	3.9	119
	11:29 AM	0.9	27		10:36 AM	0.4	12
	05:59 PM	4.4	134		05:09 PM	4.8	146
					11:28 PM	0.1	3
9 W	12:18 AM	0.7	21	24 Th	05:47 AM	4.2	128
	06:29 AM	3.8	116		11:41 AM	0.1	3
	12:21 PM	0.7	21		06:10 PM	4.9	149
	06:47 PM	4.4	134				
10 Th	01:01 AM	0.6	18	25 F	12:23 AM	-0.1	-3
	07:12 AM	4.0	122		06:45 AM	4.6	140
	01:08 PM	0.6	18		12:42 PM	-0.2	-6
	07:29 PM	4.5	137		07:07 PM	5.0	152
11 F	01:39 AM	0.5	15	26 Sa	01:14 AM	-0.4	-12
	07:51 AM	4.2	128		07:36 AM	5.0	152
	01:49 PM	0.5	15		01:39 PM	-0.4	-12
	08:08 PM	4.5	137		08:00 PM	5.0	152
12 Sa	02:13 AM	0.4	12	27 Su	02:02 AM	-0.5	-15
	08:27 AM	4.4	134		08:26 AM	5.3	162
	02:28 PM	0.4	12		02:33 PM	-0.6	-18
	08:44 PM	4.5	137		08:50 PM	5.0	152
13 Su ○	02:45 AM	0.3	9	28 M ●	02:49 AM	-0.6	-18
	09:02 AM	4.5	137		09:17 AM	5.5	168
	03:05 PM	0.3	9		03:25 PM	-0.6	-18
	09:20 PM	4.4	134		09:40 PM	4.8	146
14 M	03:17 AM	0.3	9	29 Tu	03:35 AM	-0.5	-15
	09:36 AM	4.7	143		10:04 AM	5.6	171
	03:42 PM	0.3	9		04:16 PM	-0.5	-15
	09:55 PM	4.3	131		10:28 PM	4.6	140
15 Tu	03:49 AM	0.2	6	30 W	04:21 AM	-0.4	-12
	10:12 AM	4.8	146		10:52 AM	5.5	168
	04:20 PM	0.3	9		05:07 PM	-0.4	-12
	10:32 PM	4.2	128		11:17 PM	4.3	131
				31 Th	05:08 AM	-0.1	-3
					11:40 AM	5.3	162
					05:59 PM	-0.1	-3

November

	Time	Height (ft)	Height (cm)	Time	Height (ft)	Height (cm)
1 F	12:07 AM	4.0	122	16 Sa	04:18 AM	0.1	3
	05:56 AM	0.2	6		10:52 AM	4.9	149
	12:30 PM	5.0	152		05:14 PM	0.1	3
	06:53 PM	0.2	6		11:22 PM	3.6	110
2 Sa	01:00 AM	3.7	113	17 Su	05:07 AM	0.2	6
	06:48 AM	0.5	15		11:43 AM	4.8	146
	01:22 PM	4.7	143		06:06 PM	0.2	6
	07:49 PM	0.4	12				
3 Su	01:57 AM	3.5	107	18 M	12:17 AM	3.5	107
	06:44 AM	0.7	21		06:03 AM	0.3	9
	01:18 PM	4.4	134		12:38 PM	4.7	143
	07:49 PM	0.6	18		07:04 PM	0.2	6
4 M ◐	01:58 AM	3.4	104	19 Tu ◑	01:18 AM	3.6	110
	07:46 AM	0.9	27		07:05 AM	0.4	12
	02:18 PM	4.2	128		01:39 PM	4.6	140
	08:49 PM	0.7	21		08:05 PM	0.2	6
5 Tu	03:00 AM	3.4	104	20 W	02:23 AM	3.7	113
	08:51 AM	0.9	27		08:13 AM	0.3	9
	03:18 PM	4.1	125		02:43 PM	4.5	137
	09:46 PM	0.7	21		09:05 PM	0.0	0
6 W	03:58 AM	3.5	107	21 Th	03:29 AM	4.0	122
	09:52 AM	0.9	27		09:22 AM	0.2	6
	04:14 PM	4.1	125		03:48 PM	4.5	137
	10:35 PM	0.6	18		10:04 PM	-0.1	-3
7 Th	04:49 AM	3.7	113	22 F	04:31 AM	4.3	131
	10:48 AM	0.8	24		10:29 AM	0.0	0
	05:04 PM	4.1	125		04:50 PM	4.5	137
	11:18 PM	0.5	15		10:58 PM	-0.3	-9
8 F	05:34 AM	3.9	119	23 Sa	05:28 AM	4.7	143
	11:37 AM	0.6	18		11:31 AM	-0.2	-6
	05:49 PM	4.1	125		05:47 PM	4.4	134
	11:56 PM	0.4	12		11:49 PM	-0.5	-15
9 Sa	06:15 AM	4.2	128	24 Su	06:21 AM	5.0	152
	12:20 PM	0.5	15		12:28 PM	-0.4	-12
	06:31 PM	4.1	125		06:41 PM	4.4	134
10 Su	12:31 AM	0.3	9	25 M	12:38 AM	-0.6	-18
	06:53 AM	4.4	134		07:11 AM	5.3	162
	01:01 PM	0.3	9		01:21 PM	-0.5	-15
	07:10 PM	4.1	125		07:32 PM	4.3	131
11 M	01:05 AM	0.2	6	26 Tu ●	01:25 AM	-0.6	-18
	07:30 AM	4.6	140		07:59 AM	5.4	165
	01:40 PM	0.2	6		02:12 PM	-0.6	-18
	07:49 PM	4.0	122		08:21 PM	4.2	128
12 Tu ○	01:40 AM	0.1	3	27 W	02:11 AM	-0.5	-15
	06:07 AM	4.8	146		08:45 AM	5.4	165
	02:19 PM	0.1	3		03:01 PM	-0.5	-15
	08:27 PM	4.0	122		09:09 PM	4.1	125
13 W	02:15 AM	0.0	0	28 Th	02:56 AM	-0.4	-12
	06:45 AM	4.9	149		09:30 AM	5.3	162
	02:59 PM	0.1	3		03:49 PM	-0.4	-12
	09:07 PM	3.9	119		09:55 PM	3.9	119
14 Th	02:53 AM	0.0	0	29 F	03:42 AM	-0.2	-6
	09:25 AM	5.0	152		10:15 AM	5.1	155
	03:41 PM	0.0	0		04:37 PM	-0.2	-6
	09:48 PM	3.8	116		10:42 PM	3.7	113
15 F	03:33 AM	0.0	0	30 Sa	04:28 AM	0.1	3
	10:07 AM	5.0	152		11:01 AM	4.8	146
	04:25 PM	0.1	3		05:25 PM	0.0	0
	10:33 PM	3.7	113		11:30 PM	3.5	107

December

	Time	Height (ft)	Height (cm)	Time	Height (ft)	Height (cm)
1 Su	05:16 AM	0.3	9	16 M	04:53 AM	-0.2	-6
	11:48 AM	4.5	137		11:28 AM	4.9	149
	06:15 PM	0.2	6		05:49 PM	-0.3	-9
2 M	12:20 AM	3.4	104	17 Tu	12:03 AM	3.7	113
	06:06 AM	0.5	15		05:50 AM	-0.1	-3
	12:36 PM	4.3	131		12:22 PM	4.7	143
	07:07 PM	0.4	12		06:44 PM	-0.2	-6
3 Tu	01:13 AM	3.3	101	18 W	01:02 AM	3.7	113
	07:03 AM	0.7	21		06:52 AM	0.0	0
	01:30 PM	4.0	122		01:21 PM	4.5	137
	07:59 PM	0.5	15		07:41 PM	-0.2	-6
4 W ◐	02:09 AM	3.3	101	19 Th ◑	02:05 AM	3.9	119
	08:03 AM	0.8	24		07:59 AM	0.1	3
	02:25 PM	3.8	116		02:22 PM	4.2	128
	08:51 PM	0.5	15		08:40 PM	-0.2	-6
5 Th	03:06 AM	3.4	104	20 F	03:10 AM	4.1	125
	09:05 AM	0.8	24		09:08 AM	0.1	3
	03:19 PM	3.7	113		03:27 PM	4.1	125
	09:40 PM	0.5	15		09:38 PM	-0.3	-9
6 F	03:59 AM	3.6	110	21 Sa	04:13 AM	4.3	131
	10:04 AM	0.8	24		10:16 AM	0.0	0
	04:13 PM	3.6	110		04:30 PM	3.9	119
	10:25 PM	0.4	12		10:34 PM	-0.4	-12
7 Sa	04:49 AM	3.8	116	22 Su	05:12 AM	4.6	140
	10:56 AM	0.6	18		11:20 AM	-0.1	-3
	05:03 PM	3.6	110		05:31 PM	3.9	119
	11:07 PM	0.3	9		11:27 PM	-0.4	-12
8 Su	05:35 AM	4.1	125	23 M	06:06 AM	4.8	146
	11:47 AM	0.4	12		12:18 PM	-0.3	-9
	05:50 PM	3.6	110		06:27 PM	3.8	116
	11:47 PM	0.1	3				
9 M	06:18 AM	4.3	131	24 Tu	12:18 AM	-0.5	-15
	12:32 PM	0.3	9		06:57 AM	5.0	152
	06:35 PM	3.6	110		01:11 PM	-0.4	-12
					07:19 PM	3.8	116
10 Tu	12:26 AM	0.0	0	25 W	01:06 AM	-0.5	-15
	06:59 AM	4.6	140		07:44 AM	5.1	155
	01:15 PM	0.1	3		02:00 PM	-0.5	-15
	07:18 PM	3.7	113		08:07 PM	3.8	116
11 W	01:06 AM	-0.1	-3	26 Th ●	01:52 AM	-0.5	-15
	07:41 AM	4.8	146		08:29 AM	5.1	155
	01:57 PM	-0.1	-3		02:46 PM	-0.5	-15
	08:02 PM	3.7	113		08:51 PM	3.7	113
12 Th ○	01:47 AM	-0.2	-6	27 F	02:37 AM	-0.4	-12
	08:22 AM	5.0	152		09:12 AM	5.0	152
	02:39 PM	-0.2	-6		03:30 PM	-0.4	-12
	08:45 PM	3.7	113		09:34 PM	3.6	110
13 F	02:29 AM	-0.3	-9	28 Sa	03:20 AM	-0.3	-9
	09:05 AM	5.1	155		09:53 AM	4.8	146
	03:23 PM	-0.3	-9		04:13 PM	-0.3	-9
	09:30 PM	3.7	113		10:16 PM	3.5	107
14 Sa	03:14 AM	-0.3	-9	29 Su	04:04 AM	-0.1	-3
	09:50 AM	5.1	155		10:34 AM	4.6	140
	04:09 PM	-0.3	-9		04:55 PM	-0.1	-3
	10:17 PM	3.7	113		10:58 PM	3.4	104
15 Su	04:02 AM	-0.3	-9	30 M	04:47 AM	0.1	3
	10:37 AM	5.0	152		11:16 AM	4.4	134
	04:58 PM	-0.3	-9		05:38 PM	0.0	0
	11:06 PM	3.6	110		11:41 PM	3.4	104
				31 Tu	05:32 AM	0.3	9
					11:59 AM	4.1	125
					06:21 PM	0.2	6

StationId: 8651370
Source: NOAA/NOS/CO-OPS
Station Type: Primary
Time Zone: LST_LDT
Datum: MLLW

NOAA Tide Predictions

Duck, NC,2019

Times and Heights of High and Low Waters

October

	Time	Height			Time	Height
	h m	ft	cm		h m	ft	cm
1	03:42 AM	-0.3	-9	16	03:13 AM	0.3	9
	10:01 AM	4.7	143		09:33 AM	4.0	122
Tu	04:25 PM	-0.1	-3	W	03:56 PM	0.5	15
	10:21 PM	3.8	116		09:51 PM	3.3	101
2	04:30 AM	-0.1	-3	17	03:51 AM	0.4	12
	10:52 AM	4.5	137		10:11 AM	4.0	122
W	05:20 PM	0.1	3	Th	04:36 PM	0.5	15
	11:13 PM	3.5	107		10:33 PM	3.2	98
3	05:21 AM	0.2	6	18	04:32 AM	0.5	15
	11:45 AM	4.3	131		10:54 AM	3.9	119
Th	06:19 PM	0.4	12	F	05:25 PM	0.6	18
					11:19 PM	3.1	94
4	12:08 AM	3.3	101	19	05:19 AM	0.6	18
	06:15 AM	0.5	15		11:42 AM	3.9	119
F	12:42 PM	4.0	122	Sa	06:17 PM	0.6	18
	07:21 PM	0.6	18				
5	01:10 AM	3.0	91	20	12:11 AM	3.0	91
	07:16 AM	0.7	21		06:12 AM	0.6	18
Sa	01:45 PM	3.8	116	Su	12:37 PM	3.8	116
◐	08:28 PM	0.7	21		07:15 PM	0.6	18
6	02:20 AM	2.9	88	21	01:11 AM	3.0	91
	08:23 AM	0.9	27		07:13 AM	0.6	18
Su	02:51 PM	3.6	110	M	01:36 PM	3.8	116
	09:32 PM	0.8	24	◑	08:18 PM	0.6	18
7	03:31 AM	2.9	88	22	02:17 AM	3.1	94
	09:32 AM	0.9	27		08:21 AM	0.6	18
M	03:54 PM	3.5	107	Tu	02:43 PM	3.8	116
	10:29 PM	0.8	24		09:20 PM	0.4	12
8	04:33 AM	3.0	91	23	03:24 AM	3.3	101
	10:34 AM	0.9	27		09:30 AM	0.4	12
Tu	04:49 PM	3.5	107	W	03:48 PM	3.9	119
	11:17 PM	0.7	21		10:20 PM	0.2	6
9	05:22 AM	3.2	98	24	04:28 AM	3.6	110
	11:27 AM	0.8	24		10:37 AM	0.2	6
W	05:36 PM	3.5	107	Th	04:49 PM	4.0	122
	11:56 PM	0.6	18		11:14 PM	0.0	0
10	06:04 AM	3.3	101	25	05:26 AM	4.0	122
	12:11 PM	0.7	21		11:39 AM	0.0	0
Th	06:16 PM	3.6	110	F	05:46 PM	4.0	122
11	12:30 AM	0.5	15	26	12:05 AM	-0.2	-6
	06:40 AM	3.5	107		06:20 AM	4.3	131
F	12:51 PM	0.6	18	Sa	12:37 PM	-0.2	-6
	06:52 PM	3.6	110		06:40 PM	4.0	122
12	01:02 AM	0.4	12	27	12:54 AM	-0.4	-12
	07:15 AM	3.7	113		07:11 AM	4.6	140
Sa	01:27 PM	0.5	15	Su	01:32 PM	-0.3	-9
	07:27 PM	3.6	110		07:31 PM	4.0	122
13	01:33 AM	0.3	9	28	01:41 AM	-0.4	-12
	07:48 AM	3.8	116		08:00 AM	4.7	143
Su	02:03 PM	0.5	15	M	02:24 PM	-0.4	-12
○	08:01 PM	3.6	110	●	08:20 PM	3.9	119
14	02:05 AM	0.3	9	29	02:26 AM	-0.4	-12
	08:22 AM	3.9	119		08:48 AM	4.7	143
M	02:39 PM	0.4	12	Tu	03:15 PM	-0.3	-9
	08:37 PM	3.5	107		09:09 PM	3.7	113
15	02:38 AM	0.3	9	30	03:14 AM	-0.2	-6
	08:56 AM	4.0	122		09:36 AM	4.6	140
Tu	03:16 PM	0.4	12	W	04:06 PM	-0.1	-3
	09:13 PM	3.4	104		09:58 PM	3.5	107
				31	04:02 AM	0.0	0
					10:25 AM	4.4	134
				Th	04:58 PM	0.1	3
					10:48 PM	3.3	101

November

	Time	Height			Time	Height
	h m	ft	cm		h m	ft	cm
1	04:51 AM	0.2	6	16	03:11 AM	0.2	6
	11:15 AM	4.1	125		09:34 AM	4.0	122
F	05:52 PM	0.3	9	Sa	04:08 PM	0.2	6
	11:42 PM	3.1	94		10:02 PM	3.0	91
2	05:44 AM	0.5	15	17	04:01 AM	0.3	9
	12:08 PM	3.8	116		10:23 AM	3.9	119
Sa	06:49 PM	0.5	15	Su	05:01 PM	0.3	9
					10:57 PM	3.0	91
3	12:40 AM	2.9	88	18	04:57 AM	0.4	12
	05:42 AM	0.7	21		11:18 AM	3.8	116
Su	12:05 PM	3.5	107	M	05:57 PM	0.3	9
	06:48 PM	0.7	21		11:57 PM	3.0	91
4	12:45 AM	2.8	85	19	06:00 AM	0.4	12
	06:47 AM	0.9	27		12:18 PM	3.7	113
M	01:06 PM	3.3	101	Tu	06:56 PM	0.2	6
◐	07:48 PM	0.7	21	◑			
5	01:53 AM	2.8	85	20	01:03 AM	3.1	94
	07:56 AM	1.0	30		07:09 AM	0.4	12
Tu	02:07 PM	3.2	98	W	01:22 PM	3.6	110
	08:42 PM	0.7	21		07:56 PM	0.1	3
6	02:54 AM	2.9	88	21	02:09 AM	3.4	104
	09:00 AM	0.9	27		08:19 AM	0.3	9
W	03:03 PM	3.2	98	Th	02:26 PM	3.5	107
	09:28 PM	0.6	18		08:54 PM	0.0	0
7	03:44 AM	3.1	94	22	03:13 AM	3.7	113
	09:54 AM	0.8	24		09:27 AM	0.1	3
Th	03:51 PM	3.2	98	F	03:29 PM	3.5	107
	10:07 PM	0.5	15		09:49 PM	-0.2	-6
8	04:27 AM	3.3	101	23	04:11 AM	4.0	122
	10:40 AM	0.7	21		10:30 AM	-0.1	-3
F	04:34 PM	3.2	98	Sa	04:27 PM	3.5	107
	10:43 PM	0.4	12		10:40 PM	-0.3	-9
9	05:04 AM	3.5	107	24	05:04 AM	4.3	131
	11:21 AM	0.6	18		11:27 AM	-0.2	-6
Sa	05:14 PM	3.2	98	Su	05:21 PM	3.5	107
	11:17 PM	0.3	9		11:30 PM	-0.4	-12
10	05:40 AM	3.7	113	25	05:54 AM	4.4	134
	12:00 PM	0.4	12		12:21 PM	-0.3	-9
Su	05:52 PM	3.3	101	M	06:12 PM	3.5	107
	11:52 PM	0.2	6				
11	06:15 AM	3.9	119	26	12:18 AM	-0.4	-12
	12:37 PM	0.3	9		06:42 AM	4.5	137
M	06:30 PM	3.3	101	Tu	01:11 PM	-0.4	-12
				●	07:02 PM	3.4	104
12	12:28 AM	0.1	3	27	01:05 AM	-0.4	-12
	06:51 AM	4.0	122		07:29 AM	4.5	137
Tu	01:15 PM	0.2	6	W	02:00 PM	-0.3	-9
○	07:08 PM	3.2	98		07:49 PM	3.3	101
13	01:05 AM	0.1	3	28	01:51 AM	-0.3	-9
	07:28 AM	4.1	125		08:15 AM	4.3	131
W	01:55 PM	0.2	6	Th	02:48 PM	-0.2	-6
	07:48 PM	3.2	98		08:37 PM	3.1	94
14	01:44 AM	0.1	3	29	02:37 AM	-0.1	-3
	08:07 AM	4.1	125		09:01 AM	4.1	125
Th	02:36 PM	0.2	6	F	03:35 PM	0.0	0
	08:29 PM	3.1	94		09:24 PM	3.0	91
15	02:26 AM	0.2	6	30	03:24 AM	0.2	6
	08:48 AM	4.1	125		09:47 AM	3.8	116
F	03:20 PM	0.2	6	Sa	04:22 PM	0.1	3
	09:14 PM	3.0	91		10:13 PM	2.9	88

December

	Time	Height			Time	Height
	h m	ft	cm		h m	ft	cm
1	04:13 AM	0.4	12	16	03:48 AM	-0.1	-3
	10:34 AM	3.6	110		10:08 AM	3.9	119
Su	05:11 PM	0.3	9	M	04:43 PM	-0.2	-6
	11:05 PM	2.7	82		10:43 PM	3.0	91
2	05:05 AM	0.6	18	17	04:46 AM	0.0	0
	11:23 AM	3.3	101		11:01 AM	3.7	113
M	06:00 PM	0.4	12	Tu	05:36 PM	-0.2	-6
					11:43 PM	3.1	94
3	12:01 AM	2.7	82	18	05:48 AM	0.1	3
	06:02 AM	0.7	21		11:59 AM	3.5	107
Tu	12:15 PM	3.1	94	W	06:32 PM	-0.2	-6
	06:50 PM	0.5	15				
4	01:00 AM	2.7	82	19	12:46 AM	3.2	98
	07:05 AM	0.8	24		06:57 AM	0.2	6
W	01:09 PM	2.9	88	Th	01:00 PM	3.3	101
◐	07:39 PM	0.5	15	◑	07:30 PM	-0.2	-6
5	01:59 AM	2.8	85	20	01:52 AM	3.4	104
	08:06 AM	0.8	24		08:08 AM	0.1	3
Th	02:03 PM	2.8	85	F	02:05 PM	3.1	94
	08:26 PM	0.4	12		08:28 PM	-0.2	-6
6	02:53 AM	2.9	88	21	02:56 AM	3.6	110
	09:08 AM	0.8	24		09:17 AM	0.1	3
F	02:56 PM	2.8	85	Sa	03:09 PM	3.0	91
	09:10 PM	0.4	12		09:25 PM	-0.3	-9
7	03:40 AM	3.1	94	22	03:55 AM	3.8	116
	10:00 AM	0.6	18		10:21 AM	-0.1	-3
Sa	03:46 PM	2.8	85	Su	04:10 PM	3.0	91
	09:52 PM	0.2	6		10:20 PM	-0.4	-12
8	04:23 AM	3.3	101	23	04:50 AM	4.0	122
	10:46 AM	0.5	15		11:19 AM	-0.2	-6
Su	04:32 PM	2.8	85	M	05:07 PM	3.0	91
	10:33 PM	0.1	3		11:11 PM	-0.4	-12
9	05:03 AM	3.6	110	24	05:41 AM	4.1	125
	11:29 AM	0.3	9		12:12 PM	-0.3	-9
M	05:16 PM	2.9	88	Tu	05:59 PM	3.0	91
	11:14 PM	0.0	0				
10	05:43 AM	3.7	113	25	12:00 AM	-0.4	-12
	12:10 PM	0.1	3		06:28 AM	4.1	125
Tu	05:59 PM	2.9	88	W	01:00 PM	-0.3	-9
	11:55 PM	-0.1	-3		06:47 PM	3.0	91
11	06:23 AM	3.9	119	26	12:47 AM	-0.4	-12
	12:52 PM	0.0	0		07:13 AM	4.1	125
W	06:42 PM	3.0	91	Th	01:45 PM	-0.3	-9
				●	07:33 PM	2.9	88
12	12:38 AM	-0.2	-6	27	01:33 AM	-0.3	-9
	07:04 AM	4.0	122		07:57 AM	4.0	122
Th	01:34 PM	-0.1	-3	F	02:29 PM	-0.3	-9
○	07:26 PM	3.0	91		08:17 PM	2.9	88
13	01:22 AM	-0.2	-6	28	02:17 AM	-0.2	-6
	07:46 AM	4.1	125		08:38 AM	3.8	116
F	02:18 PM	-0.2	-6	Sa	03:10 PM	-0.2	-6
	08:11 PM	3.0	91		09:00 PM	2.8	85
14	02:07 AM	-0.2	-6	29	03:00 AM	0.0	0
	08:31 AM	4.1	125		09:20 AM	3.6	110
Sa	03:04 PM	-0.2	-6	Su	03:50 PM	0.0	0
	08:58 PM	3.0	91		09:43 PM	2.8	85
15	02:56 AM	-0.2	-6	30	03:44 AM	0.2	6
	09:18 AM	4.0	122		10:01 AM	3.4	104
Su	03:52 PM	-0.2	-6	M	04:30 PM	0.1	3
	09:49 PM	3.0	91		10:28 PM	2.7	82
				31	04:29 AM	0.4	12
					10:43 AM	3.1	94
				Tu	05:10 PM	0.2	6
					11:17 PM	2.6	79

StationId: TEC3011
Source: NOAA/NOS/CO-OPS
Station Type: Subordinate
Time Zone: LST_LDT
Datum: MLLW

NOAA Tide Predictions

Cape Romain, 46 miles east of, ,2019

Times and Heights of High and Low Waters

October

	Time	Height		Time	Height
	h m	ft	cm	h m	ft	cm
1	03:10 AM	-0.3	-9	16 02:39 AM	0.4	12
	09:41 AM	5.4	165	08:54 AM	4.7	143
Tu	03:47 PM	-0.1	-3	W 03:12 PM	0.7	21
	09:54 PM	4.8	146	09:17 PM	4.1	125
2	03:59 AM	-0.1	-3	17 03:17 AM	0.4	12
	10:34 AM	5.2	158	09:30 AM	4.7	143
W	04:40 PM	0.1	3	Th 03:54 PM	0.7	21
	10:45 PM	4.5	137	09:53 PM	4.0	122
3	04:49 AM	0.2	6	18 03:58 AM	0.5	15
	11:29 AM	5.0	152	10:11 AM	4.7	143
Th	05:36 PM	0.4	12	F 04:40 PM	0.8	24
	11:39 PM	4.2	128	10:36 PM	3.9	119
4	05:41 AM	0.4	12	19 04:44 AM	0.5	15
	12:25 PM	4.8	146	11:00 AM	4.7	143
F	06:33 PM	0.7	21	Sa 05:32 PM	0.9	27
				11:28 PM	3.9	119
5	12:34 AM	4.0	122	20 05:38 AM	0.6	18
	06:38 AM	0.7	21	11:58 AM	4.7	143
Sa	01:24 PM	4.6	140	Su 06:31 PM	0.9	27
◐	07:31 PM	0.9	27			
6	01:32 AM	3.9	119	21 12:30 AM	3.9	119
	07:37 AM	0.8	24	06:39 AM	0.6	18
Su	02:21 PM	4.5	137	M 01:03 PM	4.7	143
	08:29 PM	0.9	27	◑ 07:35 PM	0.8	24
7	02:30 AM	3.9	119	22 01:40 AM	3.9	119
	08:37 AM	0.9	27	07:46 AM	0.5	15
M	03:17 PM	4.5	137	Tu 02:11 PM	4.7	143
	09:24 PM	0.9	27	08:39 PM	0.7	21
8	03:25 AM	3.9	119	23 02:49 AM	4.2	128
	09:34 AM	0.9	27	08:55 AM	0.3	9
Tu	04:08 PM	4.5	137	W 03:17 PM	4.8	146
	10:13 PM	0.8	24	09:40 PM	0.4	12
9	04:17 AM	4.1	125	24 03:54 AM	4.5	137
	10:26 AM	0.8	24	10:00 AM	0.1	3
W	04:55 PM	4.5	137	Th 04:19 PM	5.0	152
	10:58 PM	0.7	21	10:37 PM	0.1	3
10	05:05 AM	4.2	128	25 04:55 AM	4.8	146
	11:14 AM	0.7	21	11:01 AM	-0.1	-3
Th	05:38 PM	4.6	140	F 05:16 PM	5.1	155
	11:39 PM	0.6	18	11:29 PM	-0.2	-6
11	05:49 AM	4.4	134	26 05:51 AM	5.1	155
	11:57 AM	0.6	18	11:58 AM	-0.3	-9
F	06:19 PM	4.6	140	Sa 06:09 PM	5.1	155
12	12:18 AM	0.4	12	27 12:20 AM	-0.4	-12
	06:31 AM	4.5	137	06:45 AM	5.4	165
Sa	12:38 PM	0.6	18	Su 12:52 PM	-0.4	-12
	06:58 PM	4.6	140	07:01 PM	5.1	155
13	12:54 AM	0.4	12	28 01:08 AM	-0.5	-15
	07:09 AM	4.6	140	07:36 AM	5.5	168
Su	01:17 PM	0.5	15	M 01:44 PM	-0.4	-12
○	07:34 PM	4.5	137	● 07:50 PM	4.9	149
14	01:29 AM	0.3	9	29 01:56 AM	-0.4	-12
	07:46 AM	4.7	143	08:27 AM	5.5	168
M	01:55 PM	0.5	15	Tu 02:35 PM	-0.3	-9
	08:09 PM	4.4	134	08:39 PM	4.7	143
15	02:04 AM	0.3	9	30 02:43 AM	-0.3	-9
	08:20 AM	4.7	143	09:16 AM	5.4	165
Tu	02:33 PM	0.6	18	W 03:26 PM	-0.1	-3
	08:43 PM	4.3	131	09:28 PM	4.5	137
				31 03:30 AM	0.0	0
				10:07 AM	5.2	158
				Th 04:17 PM	0.2	6
				10:17 PM	4.3	131

November

	Time	Height		Time	Height
	h m	ft	cm	h m	ft	cm
1	04:18 AM	0.3	9	16 02:38 AM	0.2	6
	10:58 AM	4.9	149	08:56 AM	4.8	146
F	05:08 PM	0.5	15	Sa 03:25 PM	0.5	15
	11:08 PM	4.0	122	09:22 PM	3.8	116
2	05:09 AM	0.5	15	17 03:27 AM	0.2	6
	11:51 AM	4.6	140	09:46 AM	4.7	143
Sa	06:01 PM	0.7	21	Su 04:17 PM	0.5	15
				10:17 PM	3.8	116
3	12:02 AM	3.9	119	18 04:23 AM	0.3	9
	05:02 AM	0.8	24	10:44 AM	4.6	140
Su	11:46 AM	4.4	134	M 05:14 PM	0.5	15
	05:56 PM	0.9	27	11:21 PM	3.8	116
	11:58 PM	3.8	116			
4	06:00 AM	1.0	30	19 05:25 AM	0.4	12
	12:41 PM	4.3	131	11:47 AM	4.6	140
M	06:50 PM	0.9	27	Tu 06:15 PM	0.5	15
◐				◑		
5	12:55 AM	3.8	116	20 12:30 AM	4.0	122
	07:00 AM	1.0	30	06:32 AM	0.3	9
Tu	01:35 PM	4.2	128	W 12:53 PM	4.6	140
	07:43 PM	0.9	27	07:17 PM	0.3	9
6	01:51 AM	3.8	116	21 01:38 AM	4.2	128
	07:59 AM	1.0	30	07:40 AM	0.2	6
W	02:27 PM	4.2	128	Th 01:57 PM	4.6	140
	08:32 PM	0.8	24	08:17 PM	0.1	3
7	02:44 AM	4.0	122	22 02:42 AM	4.5	137
	08:53 AM	0.9	27	08:46 AM	0.1	3
Th	03:15 PM	4.2	128	F 02:57 PM	4.6	140
	09:18 PM	0.6	18	09:13 PM	-0.1	-3
8	03:32 AM	4.2	128	23 03:41 AM	4.8	146
	09:42 AM	0.8	24	09:47 AM	-0.1	-3
F	04:00 PM	4.3	131	Sa 03:54 PM	4.6	140
	10:00 PM	0.5	15	10:06 PM	-0.3	-9
9	04:18 AM	4.4	134	24 04:36 AM	5.1	155
	10:28 AM	0.7	21	10:43 AM	-0.3	-9
Sa	04:43 PM	4.3	131	Su 04:48 PM	4.6	140
	10:39 PM	0.3	9	10:56 PM	-0.5	-15
10	05:00 AM	4.6	140	25 05:29 AM	5.2	158
	11:11 AM	0.5	15	11:37 AM	-0.4	-12
Su	05:24 PM	4.3	131	M 05:39 PM	4.6	140
	11:18 PM	0.2	6	11:45 PM	-0.5	-15
11	05:40 AM	4.7	143	26 06:19 AM	5.3	162
	11:52 AM	0.4	12	12:28 PM	-0.4	-12
M	06:03 PM	4.2	128	Tu 06:28 PM	4.5	137
	11:55 PM	0.1	3	●		
12	06:18 AM	4.8	146	27 12:32 AM	-0.5	-15
	12:32 PM	0.4	12	07:07 AM	5.3	162
Tu	06:40 PM	4.2	128	W 01:17 PM	-0.3	-9
○				07:16 PM	4.3	131
13	12:33 AM	0.1	3	28 01:18 AM	-0.3	-9
	06:54 AM	4.9	149	07:54 AM	5.1	155
W	01:13 PM	0.4	12	Th 02:04 PM	-0.1	-3
	07:17 PM	4.1	125	08:02 PM	4.2	128
14	01:12 AM	0.1	3	29 02:04 AM	-0.1	-3
	07:32 AM	4.9	149	08:40 AM	4.9	149
Th	01:54 PM	0.4	12	F 02:51 PM	0.1	3
	07:55 PM	4.0	122	08:49 PM	4.0	122
15	01:53 AM	0.1	3	30 02:49 AM	0.2	6
	08:11 AM	4.8	146	09:27 AM	4.7	143
F	02:38 PM	0.4	12	Sa 03:38 PM	0.3	9
	08:35 PM	3.9	119	09:36 PM	3.8	116

December

	Time	Height		Time	Height
	h m	ft	cm	h m	ft	cm
1	03:36 AM	0.4	12	16 03:15 AM	-0.2	-6
	10:14 AM	4.4	134	09:37 AM	4.7	143
Su	04:26 PM	0.5	15	M 04:02 PM	0.0	0
	10:25 PM	3.7	113	10:10 PM	3.8	116
2	04:24 AM	0.7	21	17 04:11 AM	-0.1	-3
	11:03 AM	4.2	128	10:32 AM	4.5	137
M	05:14 PM	0.6	18	Tu 04:56 PM	0.0	0
	11:17 PM	3.6	110	11:12 PM	3.9	119
3	05:16 AM	0.8	24	18 05:13 AM	0.0	0
	11:54 AM	4.0	122	11:32 AM	4.4	134
Tu	06:03 PM	0.7	21	W 05:53 PM	0.0	0
4	12:12 AM	3.6	110	19 12:17 AM	4.0	122
	06:13 AM	0.9	27	06:18 AM	0.1	3
W	12:46 PM	3.9	119	Th 12:33 PM	4.3	131
◐	06:53 PM	0.7	21	◑ 06:53 PM	-0.1	-3
5	01:07 AM	3.6	110	20 01:23 AM	4.2	128
	07:12 AM	1.0	30	07:26 AM	0.1	3
Th	01:37 PM	3.8	116	F 01:36 PM	4.2	128
	07:42 PM	0.6	18	07:52 PM	-0.2	-6
6	02:01 AM	3.8	116	21 02:27 AM	4.4	134
	08:10 AM	0.9	27	08:31 AM	0.0	0
F	02:28 PM	3.8	116	Sa 02:36 PM	4.1	125
	08:30 PM	0.5	15	08:49 PM	-0.3	-9
7	02:53 AM	4.0	122	22 03:26 AM	4.6	140
	09:05 AM	0.8	24	09:32 AM	-0.1	-3
Sa	03:17 PM	3.8	116	Su 03:34 PM	4.1	125
	09:15 PM	0.3	9	09:44 PM	-0.4	-12
8	03:41 AM	4.2	128	23 04:22 AM	4.8	146
	09:54 AM	0.6	18	10:29 AM	-0.2	-6
Su	04:04 PM	3.8	116	M 04:29 PM	4.1	125
	09:59 PM	0.2	6	10:36 PM	-0.5	-15
9	04:26 AM	4.4	134	24 05:14 AM	4.9	149
	10:41 AM	0.4	12	11:21 AM	-0.3	-9
M	04:48 PM	3.9	119	Tu 05:21 PM	4.1	125
	10:42 PM	0.0	0	11:25 PM	-0.5	-15
10	05:09 AM	4.6	140	25 06:03 AM	4.9	149
	11:26 AM	0.3	9	12:10 PM	-0.4	-12
Tu	05:32 PM	3.9	119	W 06:09 PM	4.0	122
	11:24 PM	-0.1	-3			
11	05:51 AM	4.7	143	26 12:12 AM	-0.5	-15
	12:09 PM	0.1	3	06:49 AM	4.9	149
W	06:13 PM	3.9	119	Th 12:57 PM	-0.3	-9
				● 06:55 PM	4.0	122
12	12:07 AM	-0.2	-6	27 12:57 AM	-0.4	-12
	06:33 AM	4.8	146	07:34 AM	4.8	146
Th	12:53 PM	0.0	0	F 01:42 PM	-0.2	-6
○	06:55 PM	3.9	119	07:39 PM	3.9	119
13	12:51 AM	-0.3	-9	28 01:41 AM	-0.2	-6
	07:15 AM	4.9	149	08:16 AM	4.6	140
F	01:37 PM	0.0	0	Sa 02:25 PM	-0.1	-3
	07:38 PM	3.9	119	08:22 PM	3.8	116
14	01:36 AM	-0.3	-9	29 02:23 AM	0.0	0
	07:59 AM	4.9	149	08:57 AM	4.4	134
Sa	02:22 PM	0.0	0	Su 03:06 PM	0.1	3
	08:23 PM	3.9	119	09:04 PM	3.6	110
15	02:24 AM	-0.3	-9	30 03:04 AM	0.2	6
	08:46 AM	4.8	146	09:39 AM	4.2	128
Su	03:10 PM	0.0	0	M 03:47 PM	0.2	6
	09:14 PM	3.8	116	09:48 PM	3.5	107
				31 03:47 AM	0.4	12
				10:21 AM	4.0	122
				Tu 04:29 PM	0.4	12
				10:36 PM	3.4	104

APPENDIX A5 – CURRENT VELOCITY CALCULATIONS

Table A5- 1: 20 Meter Water Depth Current Velocities

Water Depth (m) =			20							
Saffir-Simpson Cat =			H1		H2		H3		H4	
$V_{1\text{-hour, z=10m}}$ (m/s) =			32		43		50		59	
$U_{w(0)}$ (m/s) =			0.32		0.43		0.50		0.59	
$U_{ss(0)}$ (m/s) =		1.25	**$U_{w(z)}$ (m/s)**	**$U_{T(z)}$ (m/s)**	**$U_{w(z)}$ (m/s)**	**$U_{T(z)}$ (m/s)**	**$U_{w(z)}$ (m/s)**	**$U_{T(z)}$ (m/s)**	**$U_{w(z)}$ (m/s)**	**$U_{T(z)}$ (m/s)**
z (%)	**z (m)**	**$U_{ss(z)}$ (m/s)**								
1.00	0.00	1.25	0.32	1.57	0.43	2.00	0.50	2.50	0.59	3.09
0.95	-1.00	1.24	0.30	1.54	0.41	1.95	0.48	2.43	0.56	2.99
0.90	-2.00	1.23	0.29	1.52	0.39	1.91	0.45	2.36	0.53	2.89
0.85	-3.00	1.22	0.27	1.49	0.37	1.86	0.43	2.28	0.50	2.79
0.80	-4.00	1.21	0.26	1.47	0.34	1.81	0.40	2.21	0.47	2.68
0.75	-5.00	1.20	0.24	1.44	0.32	1.76	0.38	2.14	0.44	2.58
0.70	-6.00	1.19	0.22	1.41	0.30	1.71	0.35	2.06	0.41	2.48
0.65	-7.00	1.18	0.21	1.38	0.28	1.66	0.33	1.99	0.38	2.37
0.60	-8.00	1.16	0.19	1.35	0.26	1.61	0.30	1.91	0.35	2.27
0.55	-9.00	1.15	0.18	1.32	0.24	1.56	0.28	1.84	0.32	2.16
0.50	-10.00	1.13	0.16	1.29	0.22	1.51	0.25	1.76	0.30	2.05
0.45	-11.00	1.12	0.14	1.26	0.19	1.45	0.23	1.68	0.27	1.94
0.40	-12.00	1.10	0.13	1.22	0.17	1.40	0.20	1.60	0.24	1.83
0.35	-13.00	1.08	0.11	1.19	0.15	1.34	0.18	1.51	0.21	1.72
0.30	-14.00	1.05	0.10	1.15	0.13	1.28	0.15	1.43	0.18	1.60
0.25	-15.00	1.03	0.08	1.11	0.11	1.21	0.13	1.34	0.15	1.49
0.20	-16.00	0.99	0.06	1.06	0.09	1.14	0.10	1.24	0.12	1.36
0.15	-17.00	0.95	0.05	1.00	0.06	1.07	0.08	1.14	0.09	1.23
0.10	-18.00	0.90	0.03	0.93	0.04	0.97	0.05	1.02	0.06	1.08
0.05	-19.00	0.81	0.02	0.83	0.02	0.85	0.03	0.88	0.03	0.91
0.00125	-19.98	0.48	0.00	0.48	0.00	0.48	0.00	0.48	0.00	0.48
0.00	-20.00	0.00	0.00	0.00	0.00	0.00	0.00	0.00	0.00	0.00

Table A5- 2: 40 Meter Water Depth Current Velocities

Water Depth (m) =			40							
Saffir-Simpson Cat =			H1		H2		H3		H4	
$V_{1\text{-hour, z=10m}}$ (m/s) =			32		43		50		59	
$U_{w(0)}$ (m/s) =			0.32		0.43		0.50		0.59	
$U_{ss(0)}$ (m/s) =		1.25	**$U_{w(z)}$ (m/s)**	**$U_{T(z)}$ (m/s)**	**$U_{w(z)}$ (m/s)**	**$U_{T(z)}$ (m/s)**	**$U_{w(z)}$ (m/s)**	**$U_{T(z)}$ (m/s)**	**$U_{w(z)}$ (m/s)**	**$U_{T(z)}$ (m/s)**
z (%)	**z (m)**	**$U_{ss(z)}$ (m/s)**								
1.00	0.00	1.25	0.32	1.57	0.43	2.00	0.50	2.50	0.59	3.09
0.95	-2.00	1.24	0.29	1.53	0.39	1.92	0.45	2.37	0.53	2.90
0.90	-4.00	1.23	0.26	1.49	0.34	1.83	0.40	2.23	0.47	2.70
0.85	-6.00	1.22	0.22	1.45	0.30	1.75	0.35	2.10	0.41	2.51
0.80	-8.00	1.21	0.19	1.40	0.26	1.66	0.30	1.96	0.35	2.31
0.75	-10.00	1.20	0.16	1.36	0.22	1.57	0.25	1.82	0.30	2.12
0.70	-12.00	1.19	0.13	1.32	0.17	1.49	0.20	1.69	0.24	1.92
0.65	-14.00	1.18	0.10	1.27	0.13	1.40	0.15	1.55	0.18	1.73
0.60	-16.00	1.16	0.06	1.23	0.09	1.31	0.10	1.41	0.12	1.53
0.55	-18.00	1.15	0.03	1.18	0.04	1.22	0.05	1.27	0.06	1.33
0.50	-20.00	1.13	0.00	1.13	0.00	1.13	0.00	1.13	0.00	1.13
0.45	-22.00	1.12		1.12		1.12		1.12		1.12
0.40	-24.00	1.10		1.10		1.10		1.10		1.10
0.35	-26.00	1.08		1.08		1.08		1.08		1.08
0.30	-28.00	1.05		1.05		1.05		1.05		1.05
0.25	-30.00	1.03		1.03		1.03		1.03		1.03
0.20	-32.00	0.99		0.99		0.99		0.99		0.99
0.15	-34.00	0.95		0.95		0.95		0.95		0.95
0.10	-36.00	0.90		0.90		0.90		0.90		0.90
0.05	-38.00	0.81		0.81		0.81		0.81		0.81
0.00125	-39.95	0.48		0.48		0.48		0.48		0.48
0.00	-40.00	0.00		0.00		0.00		0.00		0.00

Table A5- 3: 50 Meter Water Depth Current Velocities

Water Depth (m) =			50							
Saffir-Simpson Cat =			H1		H2		H3		H4	
$V_{1\text{-hour, z=10m}}$ (m/s) =			32		43		50		59	
$U_{w(0)}$ (m/s) =			0.32		0.43		0.50		0.59	
$U_{ss(0)}$ (m/s) =		1.25	$U_{w(z)}$ (m/s)	$U_{T(z)}$ (m/s)	$U_{w(z)}$ (m/s)	$U_{T(z)}$ (m/s)	$U_{w(z)}$ (m/s)	$U_{T(z)}$ (m/s)	$U_{w(z)}$ (m/s)	$U_{T(z)}$ (m/s)
z (%)	z (m)	$U_{ss(z)}$ (m/s)								
1.00	0.00	1.25	0.32	1.57	0.43	2.00	0.50	2.50	0.59	3.09
0.95	-2.50	1.24	0.28	1.52	0.38	1.90	0.44	2.33	0.52	2.85
0.90	-5.00	1.23	0.24	1.47	0.32	1.79	0.38	2.17	0.44	2.61
0.85	-7.50	1.22	0.20	1.42	0.27	1.69	0.31	2.00	0.37	2.37
0.80	-10.00	1.21	0.16	1.37	0.22	1.59	0.25	1.84	0.30	2.13
0.75	-12.50	1.20	0.12	1.32	0.16	1.48	0.19	1.67	0.22	1.89
0.70	-15.00	1.19	0.08	1.27	0.11	1.38	0.13	1.50	0.15	1.65
0.65	-17.50	1.18	0.04	1.22	0.05	1.27	0.06	1.33	0.07	1.41
0.60	-20.00	1.16	0.00	1.16	0.00	1.16	0.00	1.16	0.00	1.16
0.55	-22.50	1.15		1.15		1.15		1.15		1.15
0.50	-25.00	1.13		1.13		1.13		1.13		1.13
0.45	-27.50	1.12		1.12		1.12		1.12		1.12
0.40	-30.00	1.10		1.10		1.10		1.10		1.10
0.35	-32.50	1.08		1.08		1.08		1.08		1.08
0.30	-35.00	1.05		1.05		1.05		1.05		1.05
0.25	-37.50	1.03		1.03		1.03		1.03		1.03
0.20	-40.00	0.99		0.99		0.99		0.99		0.99
0.15	-42.50	0.95		0.95		0.95		0.95		0.95
0.10	-45.00	0.90		0.90		0.90		0.90		0.90
0.05	-47.50	0.81		0.81		0.81		0.81		0.81
0.00125	-49.94	0.48		0.48		0.48		0.48		0.48
0.00	-50.00	0.00		0.00		0.00		0.00		0.00

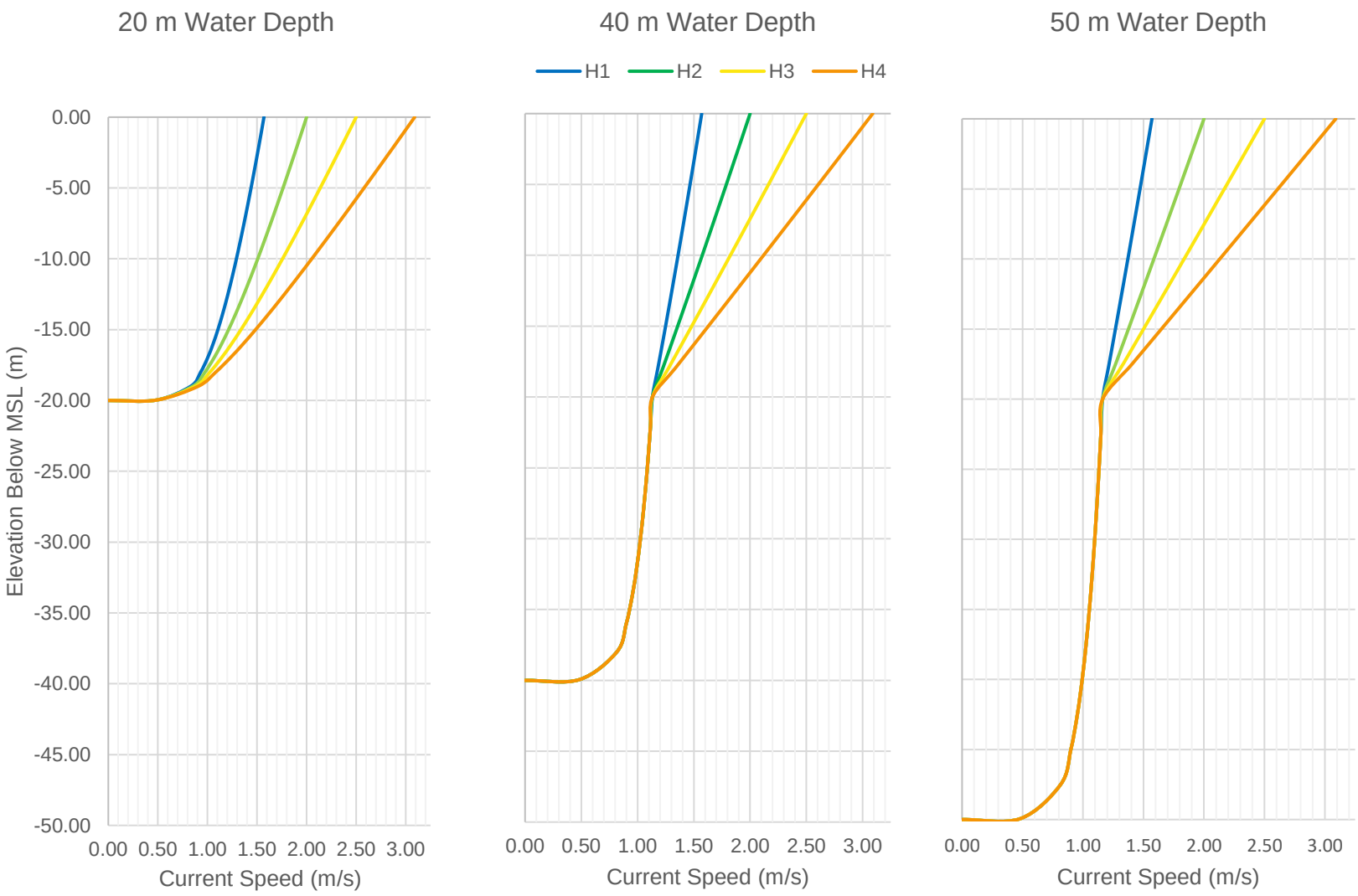

Figure A5- 1: Total Current Velocity Profile for 20, 40 and 50 Meter Water Depth

APPENDIX A6 – SURFICIAL SEDIMENTS AT WEAS

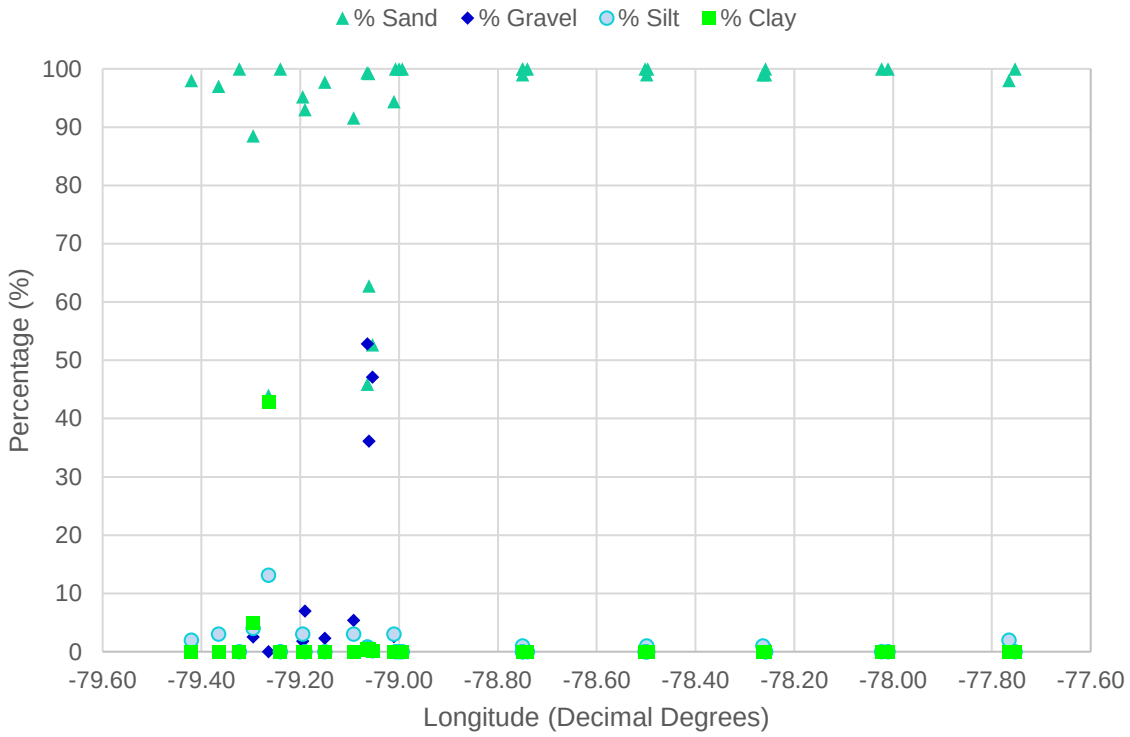

Figure A6- 1: Surficial Sediments in Long Bay, SC WEAs

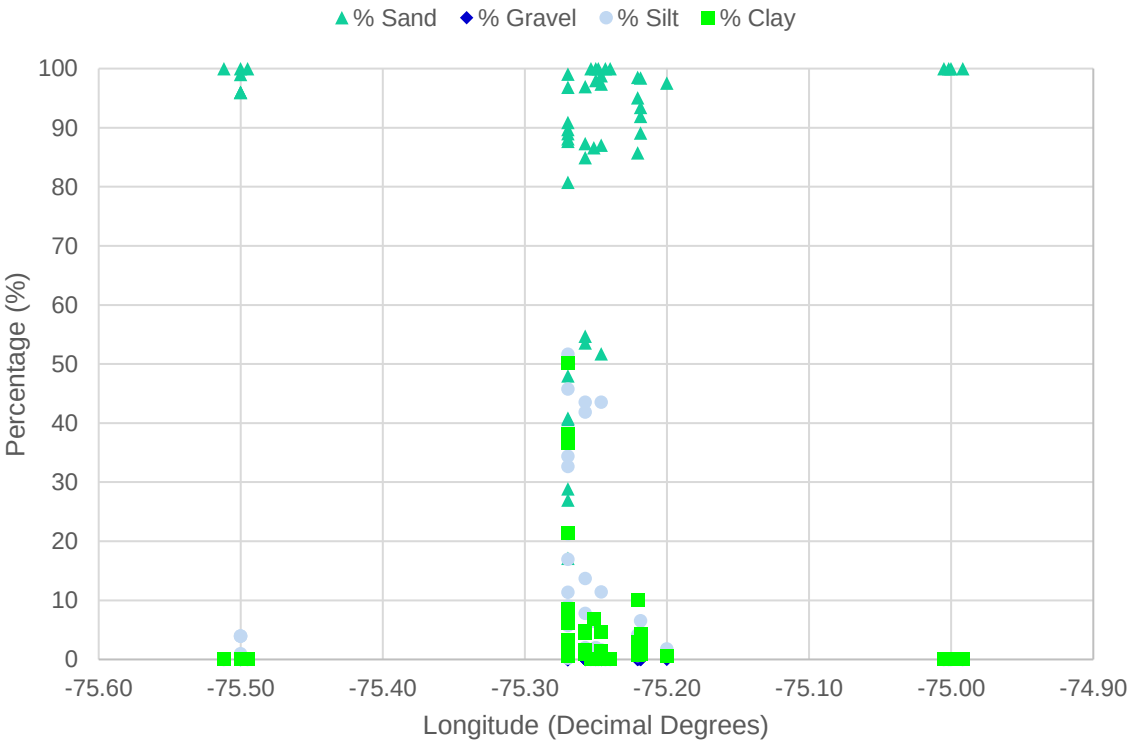

Figure A6- 2: Surficial Sediments in Chesapeake Bay WEAs

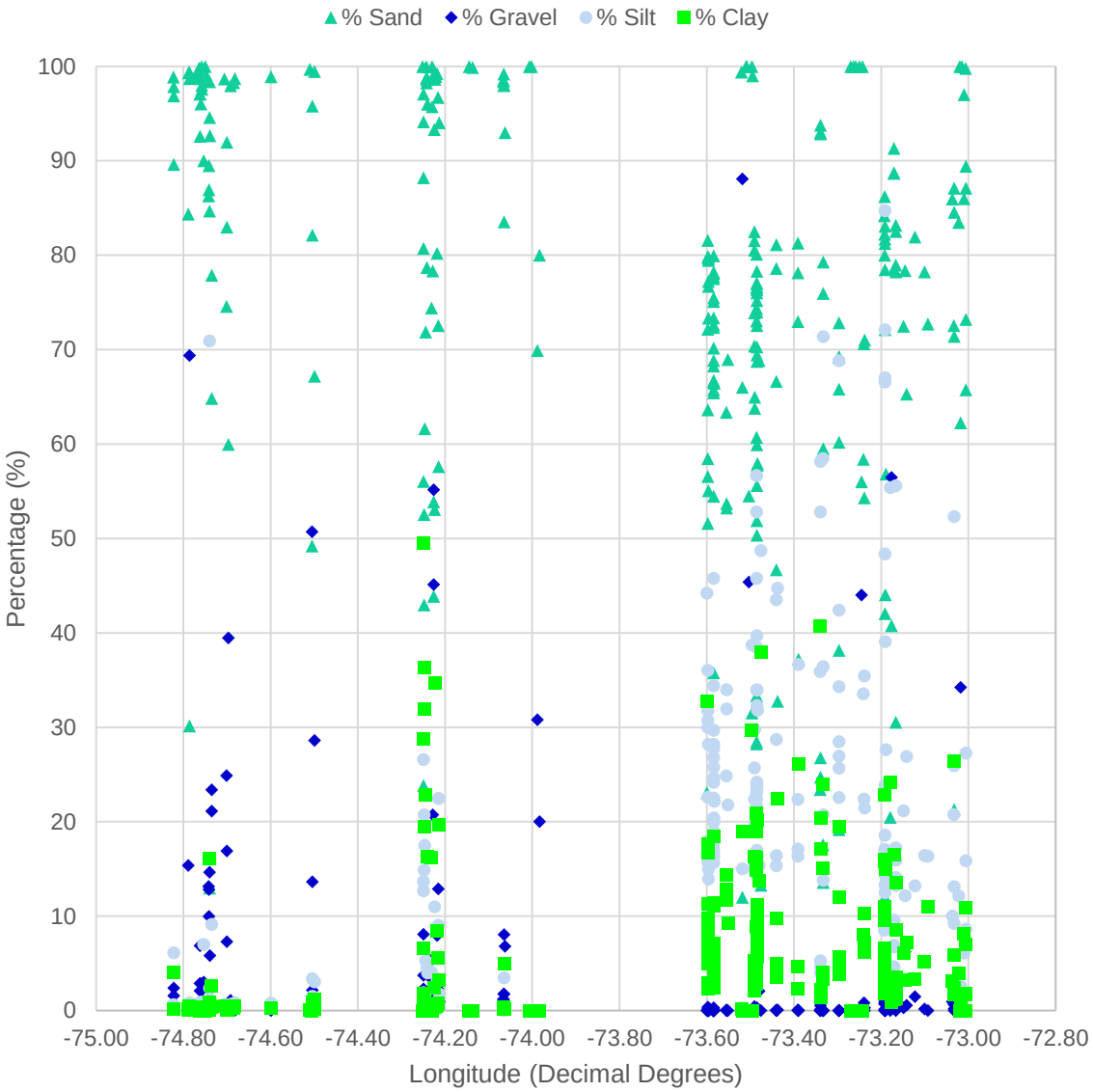

Figure A6- 3: Surficial Sediments in Delaware Bay WEAs

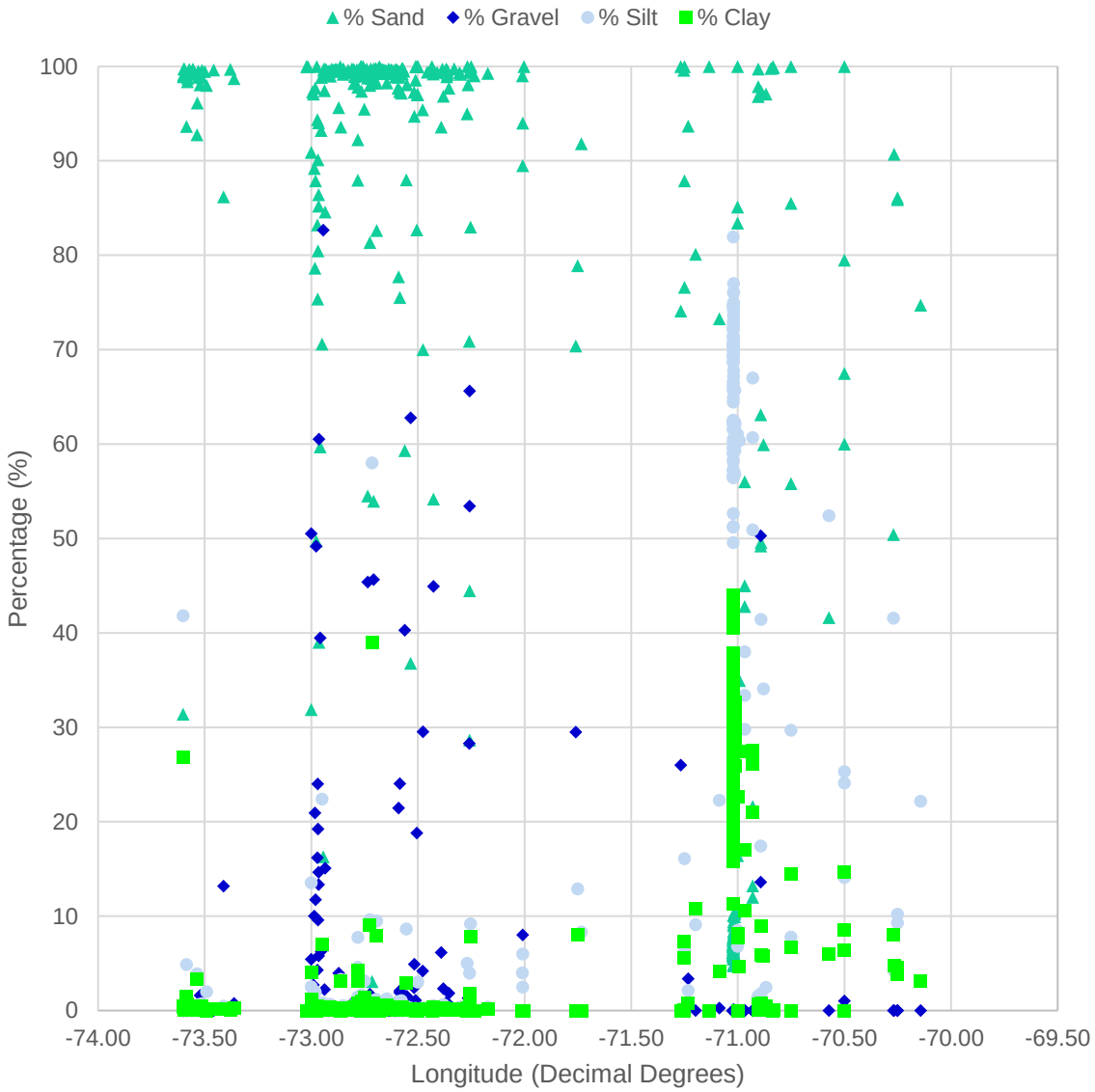

Figure A6- 4: Surficial Sediments in Southern New England WEAs

APPENDIX A7 – DESIGN LOAD CASE LIST

Table A7- 1: Design Load Case List

DLC	Water Depth (m)	Turbine Size (MW)	Saffir-Simpson Category	HH El. (m)	Vhub (m/s)	Hmax (m)	Thmax (s)	Surge + Tide (m)	Surface Current Velocity (m/s)	Tower Base Fxy (kN)	Tower Base Mxy (kN-m)	Z_{INTF} (m)	OD_{INTF} (m)	OD_{MUD} (m)	$Z_{T.C.}$ (m)	Cone Length (m)	W.T. (mm)
06_20_H1	20	6	H1	105	41.50	13.80	11.07	2.70	1.57	1,300	89,000	23	6	8	-1.2	10	75
06_20_H2	20	6	H2	105	55.70	15.60	15.04	3.30	2.00	2,300	161,000	23	6	8	-1.2	10	75
06_20_H3	20	6	H3	105	64.80	15.60	16.89	4.25	2.50	3,100	217,000	23	6	8	-1.2	10	75
06_20_H4	20	6	H4	105	76.50	15.60	17.07	5.50	3.09	4,300	302,000	23	6	8	-1.2	10	75
06_40_H1	40	6	H1	105	41.50	23.40	14.39	2.7	1.57	1,300	89,000	23	6	8	-1.2	20	80
06_40_H2	40	6	H2	105	55.70	31.20	17.20	3.3	2.00	2,300	161,000	23	6	8	-1.2	20	80
06_40_H3	40	6	H3	105	64.80	31.20	20.15	4.25	2.50	3,100	217,000	23	6	8	-1.2	20	80
06_40_H4	40	6	H4	105	76.50	31.20	20.68	5.5	3.09	4,300	302,000	23	6	8	-1.2	20	80
08_20_H1	20	8	H1	115	41.90	13.80	11.07	2.70	1.57	1,900	146,000	24	6.5	9	-2.5	15	70
08_20_H2	20	8	H2	115	56.30	15.60	15.04	3.30	2.00	3,500	263,000	24	6.5	9	-2.5	15	70
08_20_H3	20	8	H3	115	65.50	15.60	16.89	4.25	2.50	4,700	356,000	24	6.5	9	-2.5	15	70
08_20_H4	20	8	H4	115	77.20	15.60	17.07	5.50	3.09	6,500	494,000	24	6.5	9	-2.5	15	70
08_40_H1	40	8	H1	115	41.90	23.40	14.39	2.7	1.57	1,900	146,000	24	6.5	9.5	-2.5	20	75
08_40_H2	40	8	H2	115	56.30	31.20	17.20	3.3	2.00	3,500	263,000	24	6.5	9.5	-2.5	20	75
08_40_H3	40	8	H3	115	65.50	31.20	20.15	4.25	2.50	4,700	356,000	24	6.5	9.5	-2.5	20	75
08_40_H4	40	8	H4	115	77.20	31.20	20.68	5.5	3.09	6,500	494,000	24	6.5	9.5	-2.5	20	75
08_50_H1	50	8	H1	115	41.90	26.50	15.31	2.7	1.57	1,900	146,000	24	6.5	9.5	-2.5	25	80
08_50_H2	50	8	H2	115	56.30	33.48	19.37	3.3	2.00	3,500	263,000	24	6.5	9.5	-2.5	25	80
08_50_H3	50	8	H3	115	65.50	39.00	23.15	4.25	2.50	4,700	356,000	24	6.5	9.5	-2.5	25	80
08_50_H4	50	8	H4	115	77.20	39.00	24.16	5.5	3.09	6,500	494,000	24	6.5	9.5	-2.5	25	80
10_20_H1	20	10	H1	125	42.30	13.80	11.07	2.70	1.57	2,800	272,000	24	7	10	-3	25	80
10_20_H2	20	10	H2	125	56.80	15.60	15.04	3.30	2.00	5,000	490,000	24	7	10	-3	25	80
10_20_H3	20	10	H3	125	66.10	15.60	16.89	4.25	2.50	6,700	663,000	24	7	10	-3	25	80
10_20_H4	20	10	H4	125	77.90	15.60	17.07	5.50	3.09	9,300	920,000	24	7	10	-3	25	80
10_40_H1	40	10	H1	125	42.30	23.40	14.39	2.7	1.57	2,800	272,000	24	7	10	-3	25	80
10_40_H2	40	10	H2	125	56.80	31.20	17.20	3.3	2.00	5,000	490,000	24	7	10	-3	25	80
10_40_H3	40	10	H3	125	66.10	31.20	20.15	4.25	2.50	6,700	663,000	24	7	10	-3	25	80
10_40_H4	40	10	H4	125	77.90	31.20	20.68	5.5	3.09	9,300	920,000	24	7	10	-3	25	80
10_50_H1	50	10	H1	125	42.30	26.50	15.31	2.7	1.57	2,800	272,000	24	7	10.5	-3	25	85
10_50_H2	50	10	H2	125	56.80	33.48	19.37	3.3	2.00	5,000	490,000	24	7	10.5	-3	25	85
10_50_H3	50	10	H3	125	66.10	39.00	23.15	4.25	2.50	6,700	663,000	24	7	10.5	-3	25	85
10_50_H4	50	10	H4	125	77.90	39.00	24.16	5.5	3.09	9,300	920,000	24	7	10.5	-3	25	85
12_20_H1	20	12	H1	135	42.70	13.80	11.07	2.70	1.57	3,800	368,000	24	8	10	-3	15	75
12_20_H2	20	12	H2	135	57.30	15.60	15.04	3.30	2.00	6,900	662,000	24	8	10	-3	15	75
12_20_H3	20	12	H3	135	66.60	15.60	16.89	4.25	2.50	9,300	895,000	24	8	10	-3	15	75
12_20_H4	20	12	H4	135	78.60	15.60	17.07	5.50	3.09	12,900	1,246,000	24	8	10	-3	15	75
12_40_H1	40	12	H1	135	42.70	23.40	14.39	2.7	1.57	3,800	368,000	24	8	11.5	-1.2	20	85
12_40_H2	40	12	H2	135	57.30	31.20	17.20	3.3	2.00	6,900	662,000	24	8	11.5	-1.2	20	85
12_40_H3	40	12	H3	135	66.60	31.20	20.15	4.25	2.50	9,300	895,000	24	8	11.5	-1.2	20	85
12_40_H4	40	12	H4	135	78.60	31.20	20.68	5.5	3.09	12,900	1,246,000	24	8	11.5	-1.2	20	85
12_50_H1	50	12	H1	135	42.70	26.50	15.31	2.7	1.57	3,800	368,000	24	8	12	-1.2	25	95
12_50_H2	50	12	H2	135	57.30	33.48	19.37	3.3	2.00	6,900	662,000	24	8	12	-1.2	25	95
12_50_H3	50	12	H3	135	66.60	39.00	23.14	4.25	2.50	9,300	895,000	24	8	12	-1.2	25	95
12_50_H4	50	12	H4	135	78.60	39.00	24.15	5.5	3.09	12,900	1,246,000	24	8	12	-1.2	25	95

APPENDIX A8 – MUDLINE LOADS

Table A8- 1: Mudline Loads

Water Depth = 20 m

	H1				H2				H3				H4			
	6	**8**	**10**	**12**	**6**	**8**	**10**	**12**	**6**	**8**	**10**	**12**	**6**	**8**	**10**	**12**
Fxy (MN)	6	7	8	10	8	10	13	16	10	12	15	19	11	14	18	23
Mxy (MN-m)	231	325	502	664	385	556	866	1,153	487	715	1,128	1,508	631	939	1,505	2,022

Water Depth = 40 m

	H1				H2				H3				H4			
	6	**8**	**10**	**12**	**6**	**8**	**10**	**12**	**6**	**8**	**10**	**12**	**6**	**8**	**10**	**12**
Fxy (MN)	11	13	14	18	18	21	24	31	20	25	28	37	21	27	31	41
Mxy (MN-m)	502	640	854	1,111	931	1,202	1,586	2,045	1,073	1,429	1,934	2,537	1,217	1,680	2,353	3,112

Water Depth = 50 m

	H1			H2			H3			H4		
	8	**10**	**12**	**8**	**10**	**12**	**8**	**10**	**12**	**8**	**10**	**12**
Fxy (MN)	14	17	22	24	28	36	30	35	44	32	38	48
Mxy (MN-m)	813	1,060	1,295	1,445	1,878	2,418	1,796	2,368	3,065	2,065	2,815	3,676

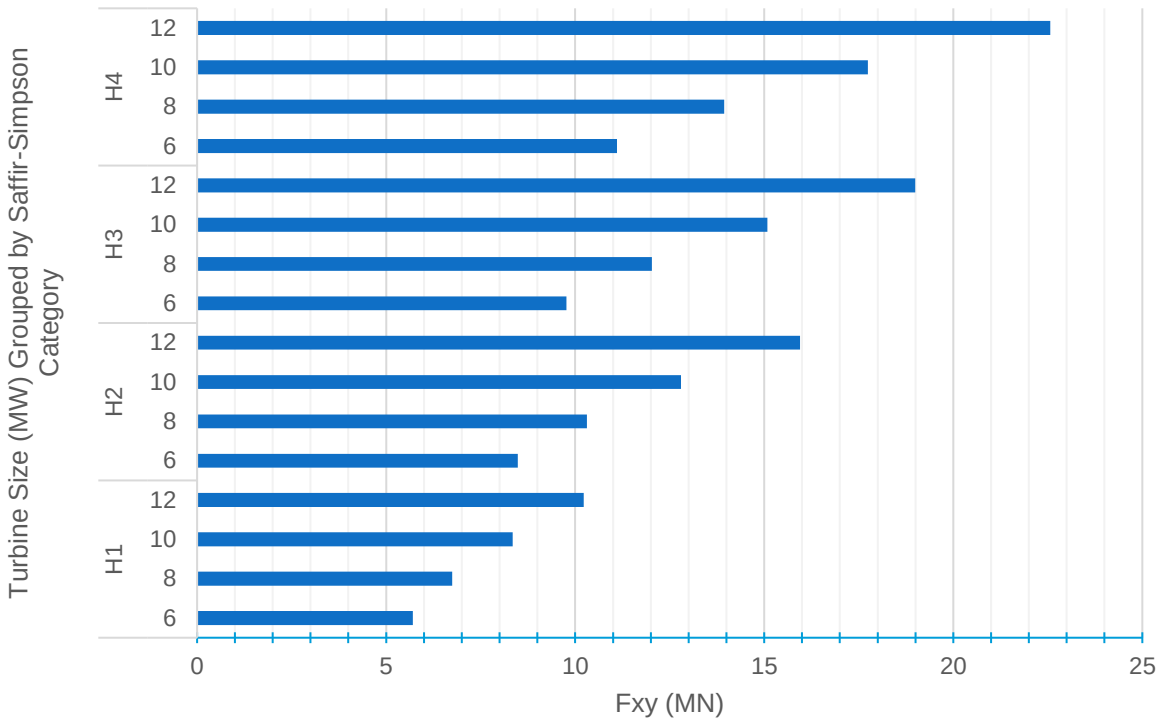

Figure A8- 1: Mudline Base Shear for Monopile in 20 meter Water Depth

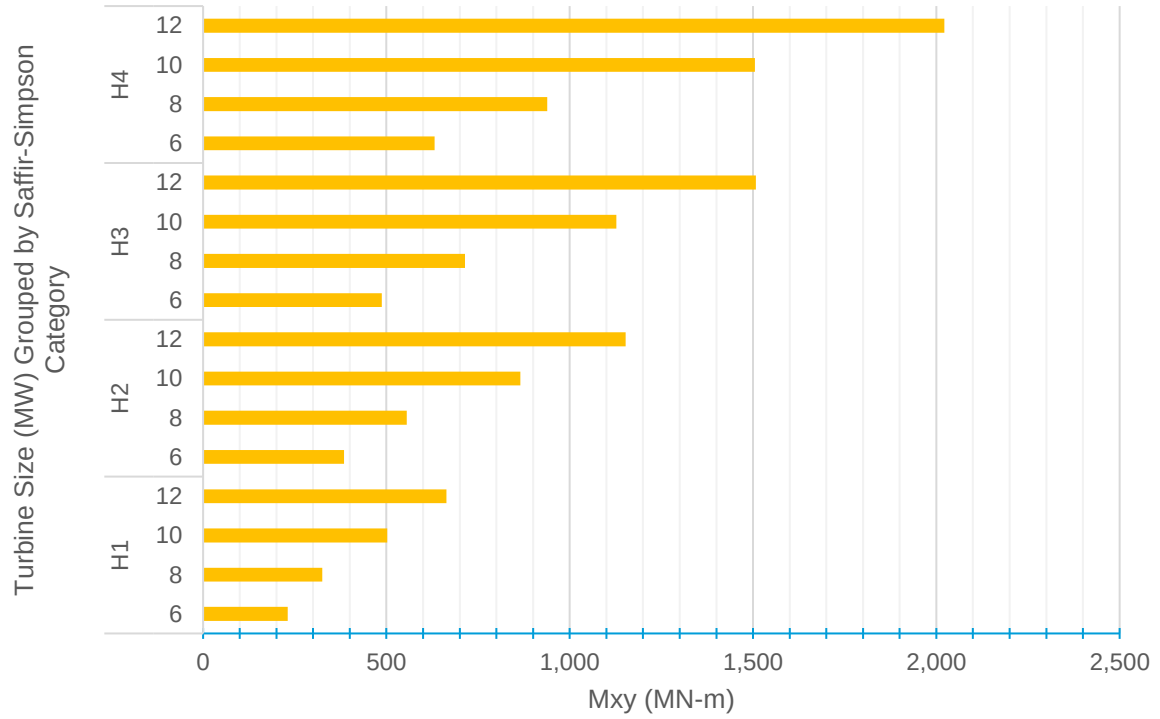

Figure A8- 2: Mudline OTM for Monopile in 20 meter Water Depth

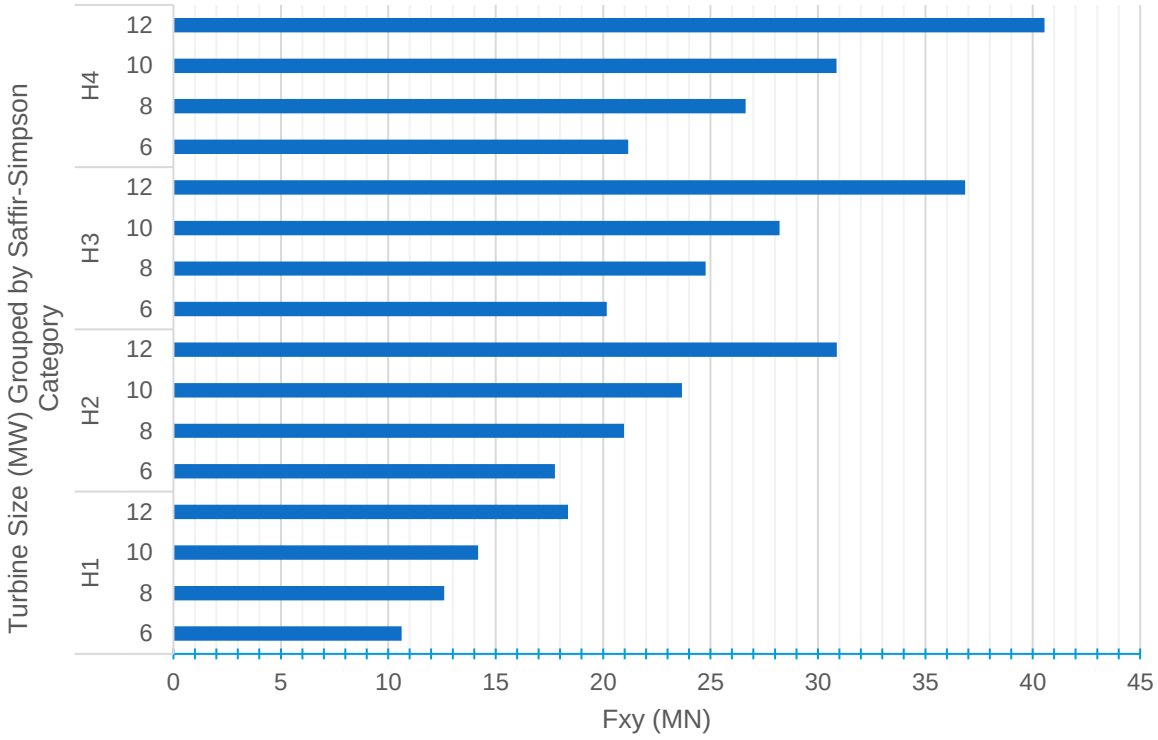

Figure A8- 3: Mudline Base Shear for Monopile in 40 meter Water Depth

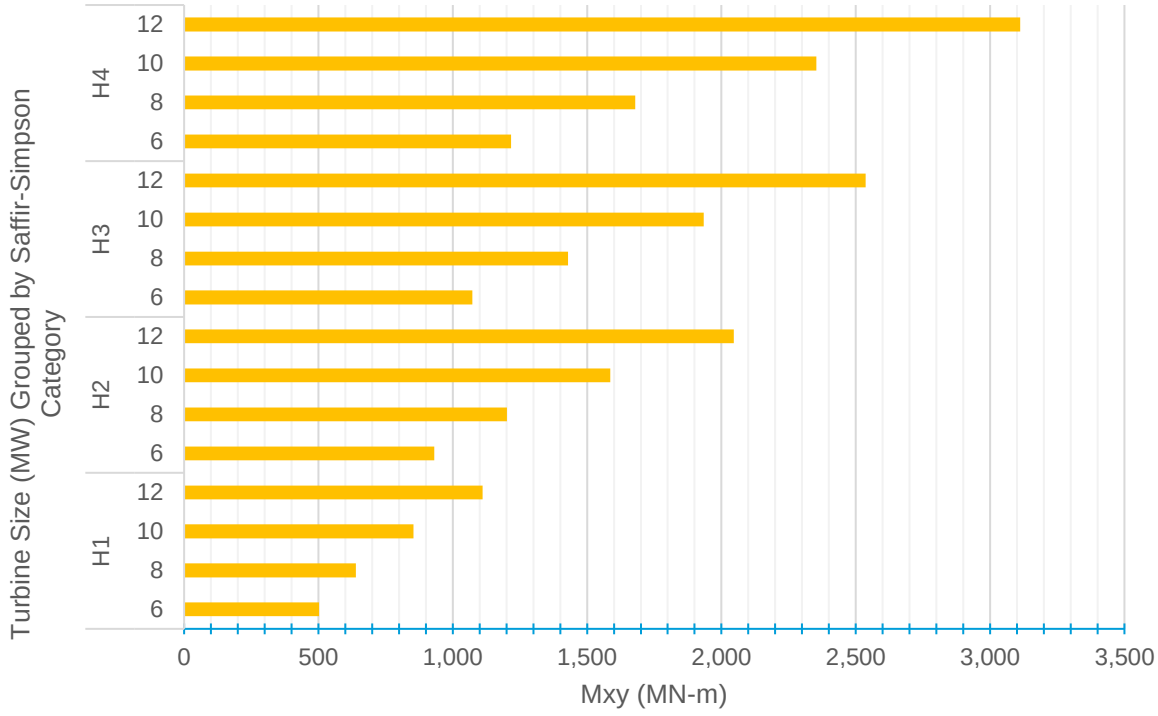

Figure A8- 4: Mudline OTM for Monopile in 40 meter Water Depth

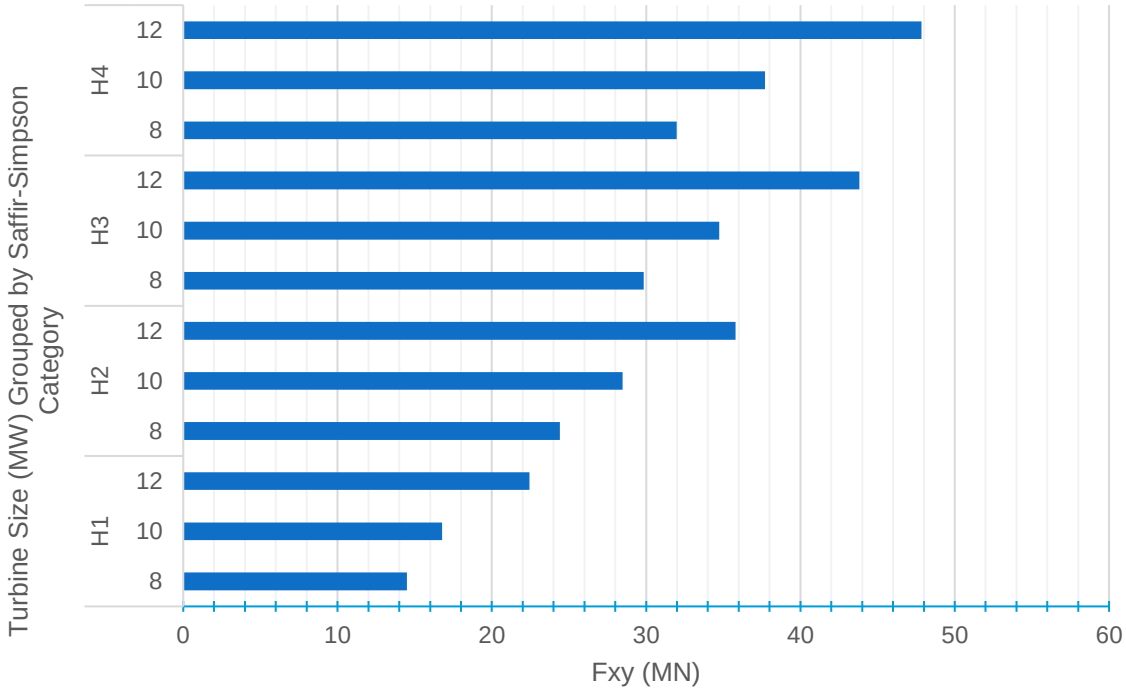

Figure A8- 5: Mudline Base Shear for Monopile in 50 meter Water Depth

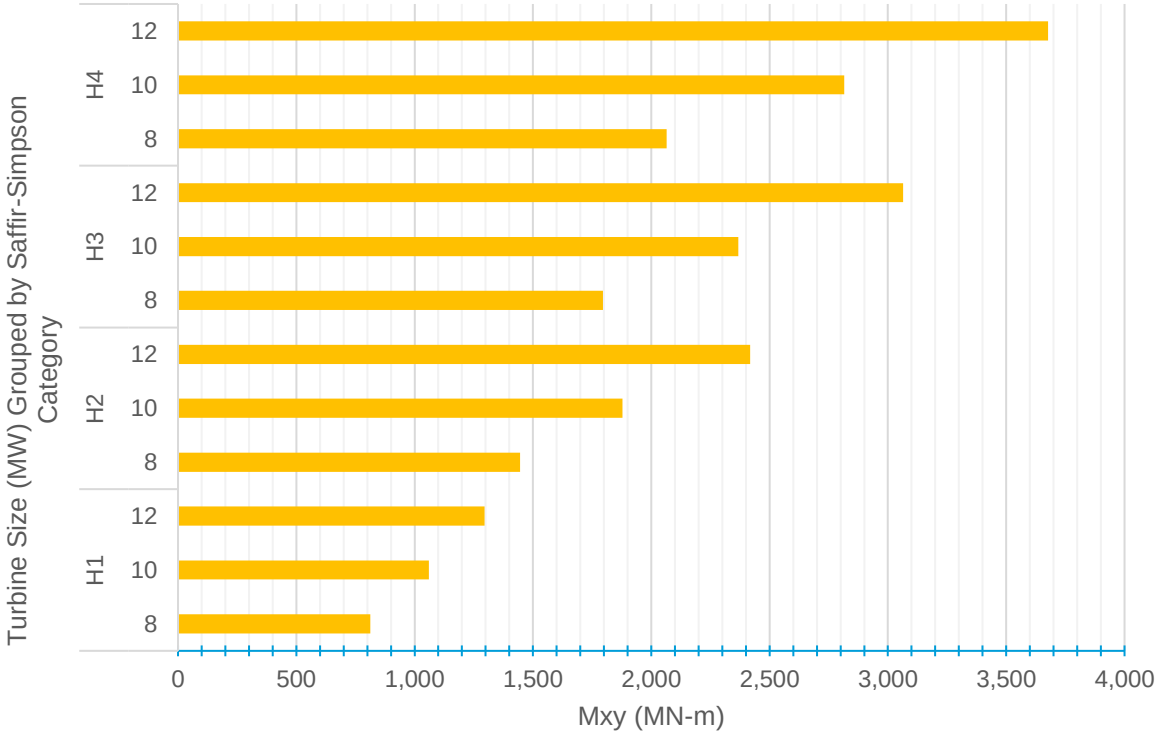

Figure A8- 6: Mudline OTM for Monopile in 50 meter Water Depth

APPENDIX A9 – DATABASE OF MONOPILE MUDLINE ROTATIONS

Table A9- 1: Database of Mudline Deflections and Rotations for All DLCs

LC	HH El. (m)	Vhub (m/s)	Hmax (m)	Twr Base Fxy (kN)	Twr Base Mxy (kN-m)	Mudline Fxy (kN)	Mudline Mxy (kN-m)	Z_{INTF} (m)	Pile Embedment, L (m)	OD_{INTF} (m)	OD_{MUD} (m)	$Z_{T.C.}$ (m)	Cone Length (m)	W.T. (mm)	L/D	Mudline Rotation, Θ (deg)	Pile Toe Deflection (mm)	Mudline Deflection, Δ (mm)
06_20_H1	105	41.50	13.80	1,300	89,000	5,704	231,116	23	29	6	8	-1.2	10	75	3.63	0.1891	24	71
06_20_H2	105	55.70	15.60	2,300	161,000	8,479	384,597	23	29	6	8	-1.2	10	75	3.63	0.3524	44	134
06_20_H3	105	64.80	15.60	3,100	217,000	9,766	487,147	23	29	6	8	-1.2	10	75	3.63	0.4711	59	180
06_20_H4	105	76.50	15.60	4,300	302,000	11,106	631,133	23	29	6	8	-1.2	10	75	3.63	0.6531	82	249
06_40_H1	105	41.50	23.40	1,300	89,000	10,620	502,084	23	39	6	8	-1.2	20	80	4.88	0.1979	26	109
06_40_H2	105	55.70	31.20	2,300	161,000	17,751	930,764	23	39	6	8	-1.2	20	80	4.88	0.4282	57	235
06_40_H3	105	64.80	31.20	3,100	217,000	20,172	1,073,256	23	39	6	8	-1.2	20	80	4.88	0.5187	69	284
06_40_H4	105	76.50	31.20	4,300	302,000	21,171	1,217,302	23	39	6	8	-1.2	20	80	4.88	0.5878	79	321
08_20_H1	115	41.90	13.80	1,900	146,000	6,749	325,462	24	30	6.5	9	-2.5	15	70	3.33	0.2008	26	79
08_20_H2	115	56.30	15.60	3,500	263,000	10,311	555,890	24	30	6.5	9	-2.5	15	70	3.33	0.3876	50	153
08_20_H3	115	65.50	15.60	4,700	356,000	12,031	714,765	24	30	6.5	9	-2.5	15	70	3.33	0.5296	70	208
08_20_H4	115	77.20	15.60	6,500	494,000	13,944	938,996	24	30	6.5	9	-2.5	15	70	3.33	0.7510	99	295
08_40_H1	115	41.90	23.40	1,900	146,000	12,605	639,765	24	40	6.5	9.5	-2.5	20	75	4.21	0.1978	28	110
08_40_H2	115	56.30	31.20	3,500	263,000	20,970	1,201,759	24	40	6.5	9.5	-2.5	20	75	4.21	0.4244	60	236
08_40_H3	115	65.50	31.20	4,700	356,000	24,774	1,429,252	24	40	6.5	9.5	-2.5	20	75	4.21	0.5407	78	299
08_40_H4	115	77.20	31.20	6,500	494,000	26,630	1,679,537	24	40	6.5	9.5	-2.5	20	75	4.21	0.6192	90	342
08_50_H1	115	41.90	26.50	1,900	146,000	14,490	813,309	24	43	6.5	9.5	-2.5	25	80	4.53	0.1966	28	120
08_50_H2	115	56.30	33.48	3,500	263,000	24,401	1,444,894	24	43	6.5	9.5	-2.5	25	80	4.53	0.4446	65	269
08_50_H3	115	65.50	39.00	4,700	356,000	29,846	1,795,835	24	43	6.5	9.5	-2.5	25	80	4.53	0.5903	87	356
08_50_H4	115	77.20	39.00	6,500	494,000	31,979	2,065,322	24	43	6.5	9.5	-2.5	25	80	4.53	0.7015	103	423
10_20_H1	125	42.30	13.80	2,800	272,000	8,348	502,489	24	35	7	10	-3	25	80	3.50	0.1966	29	91
10_20_H2	125	56.80	15.60	5,000	490,000	12,800	865,521	24	35	7	10	-3	25	80	3.50	0.3841	57	178
10_20_H3	125	66.10	15.60	6,700	663,000	15,082	1,127,554	24	35	7	10	-3	25	80	3.50	0.5281	78	245
10_20_H4	125	77.90	15.60	9,300	920,000	17,745	1,505,395	24	35	7	10	-3	25	80	3.50	0.7679	114	355
10_40_H1	125	42.30	23.40	2,800	272,000	14,177	853,947	24	43	7	10	-3	25	80	4.30	0.2059	31	123
10_40_H2	125	56.80	31.20	5,000	490,000	23,678	1,585,824	24	43	7	10	-3	25	80	4.30	0.4382	67	262
10_40_H3	125	66.10	31.20	6,700	663,000	28,217	1,934,347	24	43	7	10	-3	25	80	4.30	0.5683	87	340
10_40_H4	125	77.90	31.20	9,300	920,000	30,860	2,353,484	24	43	7	10	-3	25	80	4.30	0.7092	110	422
10_50_H1	125	42.30	26.50	2,800	272,000	16,782	1,059,682	24	46	7	10.5	-3	25	85	4.38	0.2033	31	133
10_50_H2	125	56.80	33.48	5,000	490,000	28,469	1,878,190	24	46	7	10.5	-3	25	85	4.38	0.4252	67	274
10_50_H3	125	66.10	39.00	6,700	663,000	34,736	2,367,947	24	46	7	10.5	-3	25	85	4.38	0.5713	90	368
10_50_H4	125	77.90	39.00	9,300	920,000	37,709	2,814,825	24	46	7	10.5	-3	25	85	4.38	0.6910	109	446
12_20_H1	135	42.70	13.80	3,800	368,000	10,223	663,838	24	38	8	10	-3	15	75	3.80	0.2005	30	103
12_20_H2	135	57.30	15.60	6,900	662,000	15,949	1,152,642	24	38	8	10	-3	15	75	3.80	0.4000	59	206
12_20_H3	135	66.60	15.60	9,300	895,000	18,992	1,507,561	24	38	8	10	-3	15	75	3.80	0.5513	82	284
12_20_H4	135	78.60	15.60	12,900	1,246,000	22,565	2,021,825	24	38	8	10	-3	15	75	3.80	0.7977	120	409
12_40_H1	135	42.70	23.40	3,800	368,000	18,362	1,111,390	24	45	8	11.5	-1.2	20	85	3.91	0.2054	33	128
12_40_H2	135	57.30	31.20	6,900	662,000	30,882	2,045,402	24	45	8	11.5	-1.2	20	85	3.91	0.4253	69	265
12_40_H3	135	66.60	31.20	9,300	895,000	36,855	2,536,712	24	45	8	11.5	-1.2	20	85	3.91	0.5635	91	352
12_40_H4	135	78.60	31.20	12,900	1,246,000	40,554	3,112,032	24	45	8	11.5	-1.2	20	85	3.91	0.7204	118	448
12_50_H1	135	42.70	26.50	3,800	368,000	22,448	1,294,954	24	47	8	12	-1.2	25	95	3.92	0.2053	35	134
12_50_H2	135	57.30	33.48	6,900	662,000	35,791	2,418,318	24	47	8	12	-1.2	25	95	3.92	0.4482	77	291
12_50_H3	135	66.60	39.00	9,300	895,000	43,829	3,064,533	24	47	8	12	-1.2	25	95	3.92	0.6089	105	395
12_50_H4	135	78.60	39.00	12,900	1,246,000	47,833	3,676,287	24	47	8	12	-1.2	25	95	3.92	0.7463	128	484

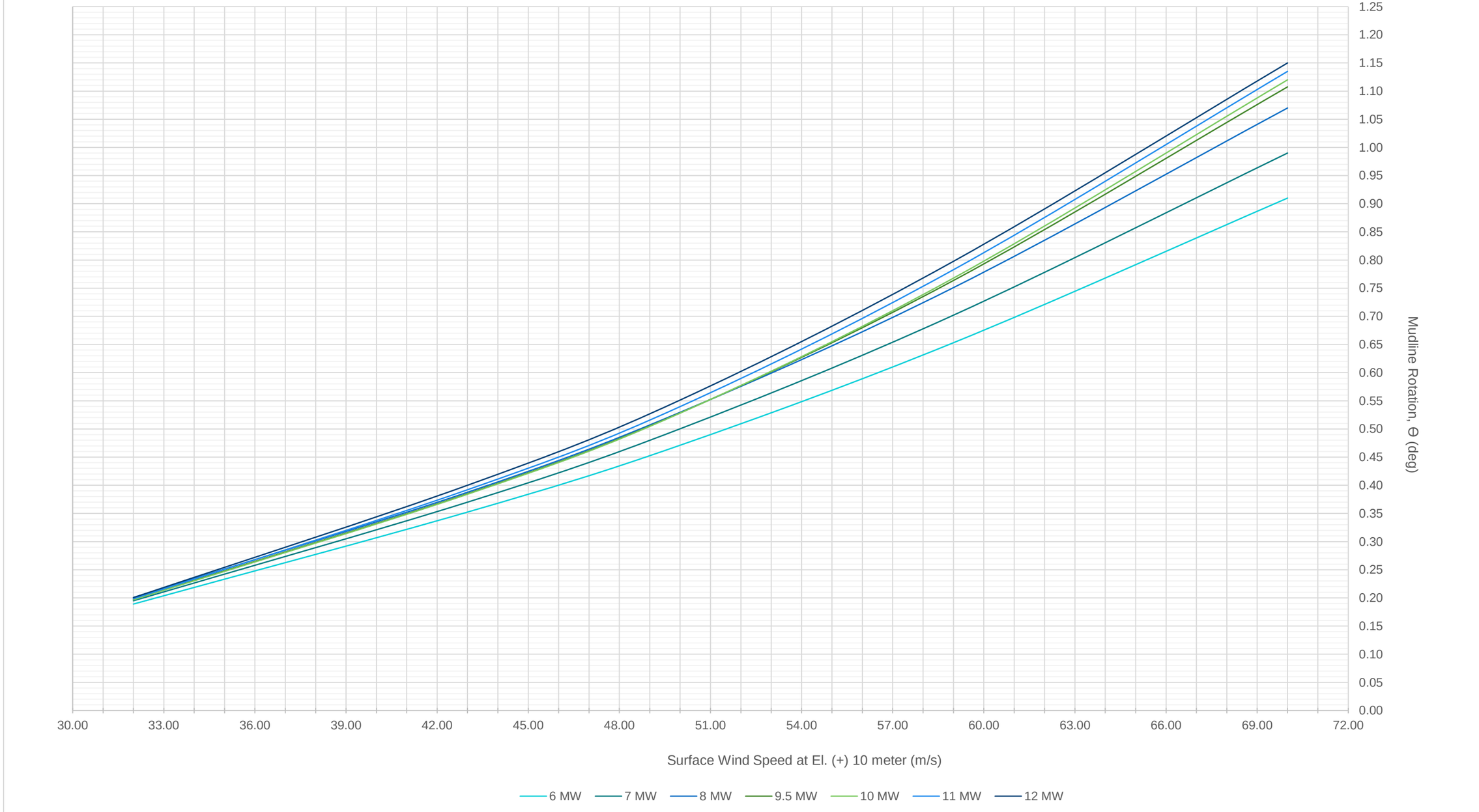

Figure A9- 1: 20 meter Water Depth Mudline Rotations

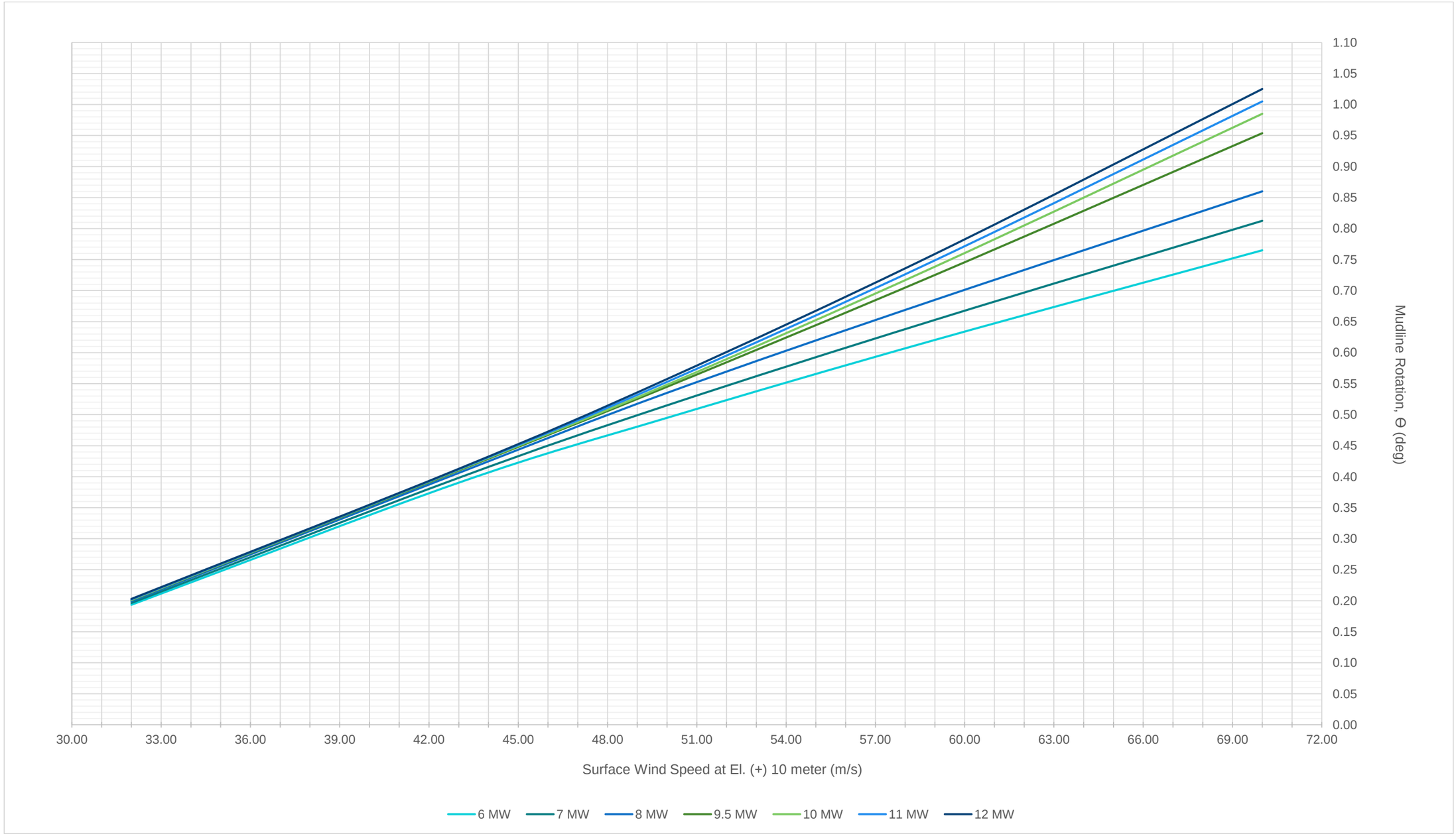

Figure A9- 2:30 meter Water Depth Mudline Rotations

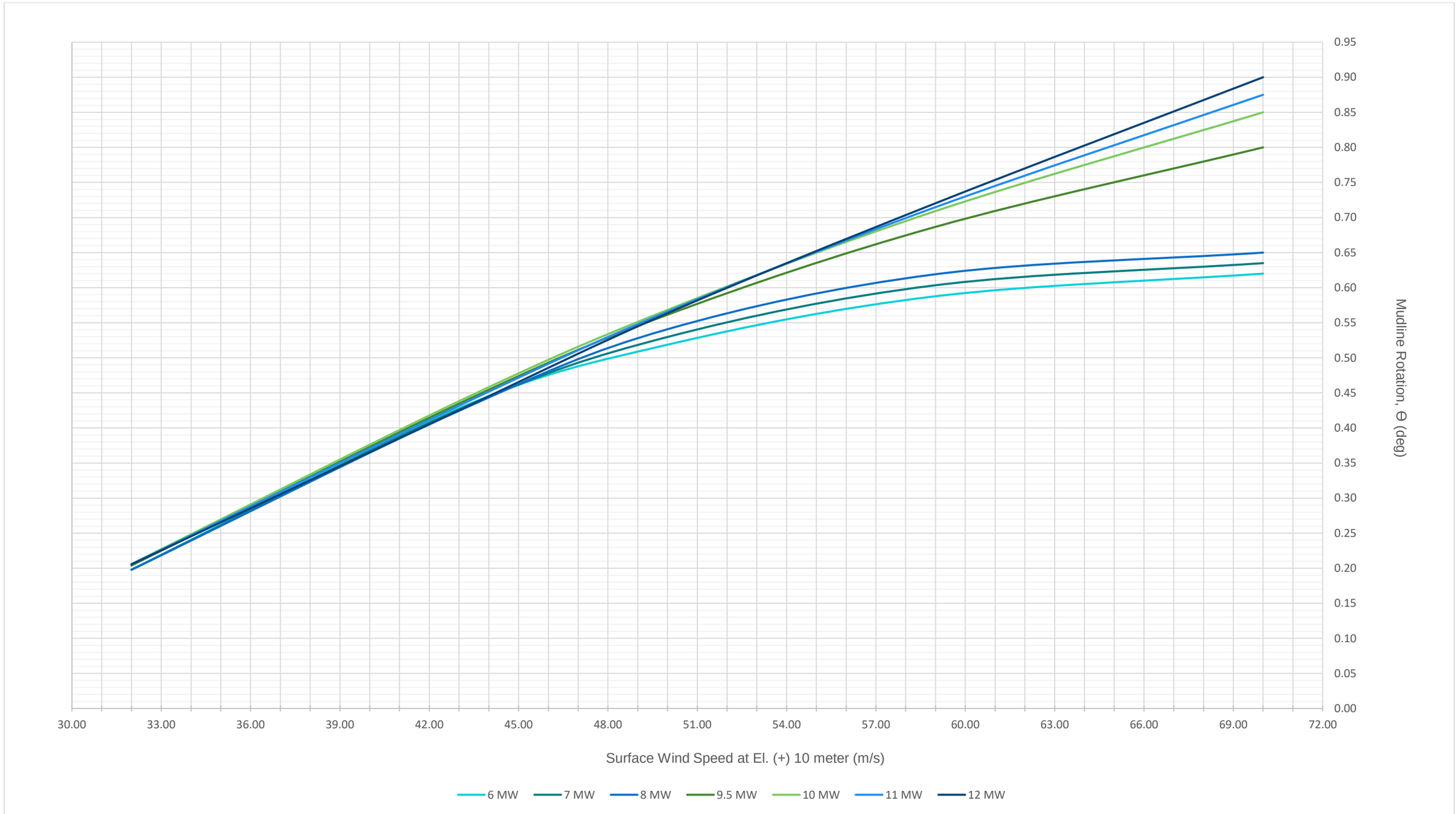

Figure A9- 3: 40 meter Water Depth Mudline Rotations

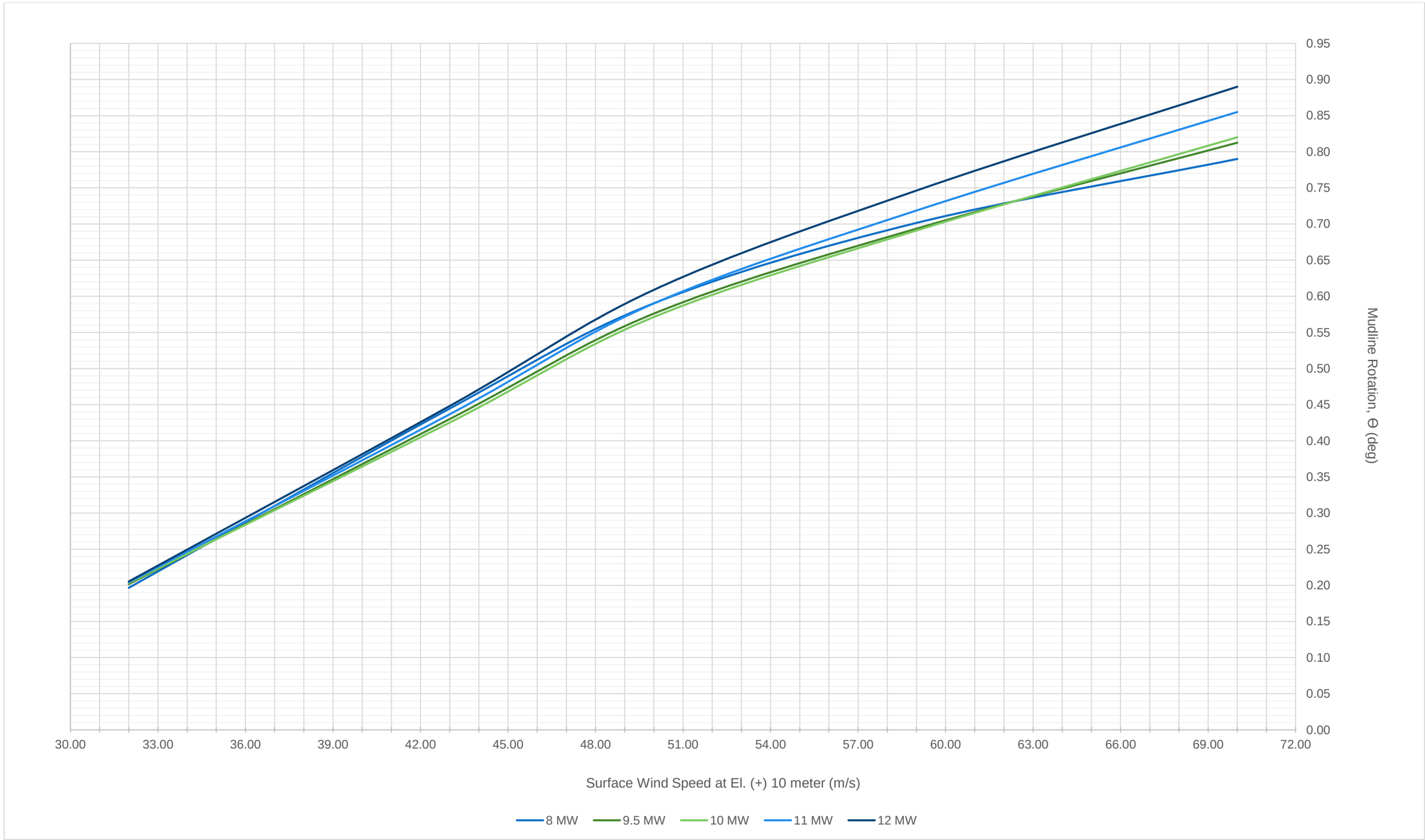

Figure A9- 4: 50 meter Water Depth Mudline Rotations

Table A9- 2: 20 meter Water Depth Mudline Rotations

	Saffir-Simpson Category				
Rotation (deg)	**H1**	**H2**	**H3**	**H4**	**H5**
6 MW	0.1891	0.3524	0.4711	0.6531	0.9100
7 MW	0.1949	0.3700	0.5003	0.7021	0.9900
8 MW	0.2008	0.3876	0.5296	0.7510	1.0700
9.5 MW	0.1977	0.3850	0.5285	0.7637	1.1075
10 MW	0.1966	0.3841	0.5281	0.7679	1.1200
11 MW	0.1985	0.3921	0.5397	0.7828	1.1350
12 MW	0.2005	0.4000	0.5513	0.7977	1.1500

Table A9- 3: 30 meter Water Depth Mudline Rotations

	Saffir-Simpson Category				
Rotation (deg)	**H1**	**H2**	**H3**	**H4**	**H5**
6 MW	0.1935	0.3903	0.4949	0.6205	0.7650
7 MW	0.1964	0.3982	0.5150	0.6528	0.8125
8 MW	0.1993	0.4060	0.5351	0.6851	0.8600
9.5 MW	0.2008	0.4099	0.5449	0.7252	0.9538
10 MW	0.2013	0.4111	0.5482	0.7386	0.9850
11 MW	0.2021	0.4119	0.5528	0.7488	1.0050
12 MW	0.2030	0.4127	0.5574	0.7590	1.0250

Table A9- 4: 40 meter Water Depth Mudline Rotations

	Saffir-Simpson Category				
Rotation (deg)	**H1**	**H2**	**H3**	**H4**	**H5**
6 MW	0.1979	0.4282	0.5187	0.5878	0.6200
7 MW	0.1978	0.4263	0.5297	0.6035	0.6350
8 MW	0.1978	0.4244	0.5407	0.6192	0.6500
9.5 MW	0.2039	0.4347	0.5614	0.6867	0.8000
10 MW	0.2059	0.4382	0.5683	0.7092	0.8500
11 MW	0.2057	0.4317	0.5659	0.7148	0.8750
12 MW	0.2054	0.4253	0.5635	0.7204	0.9000

Table A9- 5: 50 meter Water Depth Mudline Rotations

	Saffir-Simpson Category				
Rotation (deg)	**H1**	**H2**	**H3**	**H4**	**H5**
6 MW					
7 MW					
8 MW	0.1966	0.4446	0.5903	0.7015	0.7900
9.5 MW	0.2016	0.4301	0.5760	0.6936	0.8125
10 MW	0.2033	0.4252	0.5713	0.6910	0.8200
11 MW	0.2043	0.4367	0.5901	0.7186	0.8550
12 MW	0.2053	0.4482	0.6089	0.7463	0.8900

APPENDIX A10 –MONOPILE MUDLINE ROTATIONS FOR U.S. ATLANTIC COAST WEAS

Table A10- 1: Southern New England Robustness Case Mudline Rotations

Sub-Region:	Southern New England			**Unit**
Latitude:	40.93	**Longitude:**	-70.60	**(DD)**
500-YR Surface Wind Speed at El. (+) 10 m:			60	**(m/s)**
W.D. (m)	**20**	**30**	**40**	**50**
Turbine	**Rotation (deg)**			
6 MW	0.6765	0.6336	0.5907	
7 MW	0.7282	0.6673	0.6063	
8 MW	0.7800	0.7010	0.6220	0.7096
9.5 MW	0.7949	0.7460	0.6970	0.7044
10 MW	0.7999	0.7610	0.7220	0.7027
11 MW	0.8148	0.7721	0.7294	0.7310
12 MW	0.8297	0.7832	0.7367	0.7593

Table A10- 2: Delaware Bay Robustness Case Mudline Rotations

Sub-Region:	Delaware Bay			**Unit**
Latitude:	38.81	**Longitude:**	-74.23	**(DD)**
500-YR Surface Wind Speed at El. (+) 10 m:			55	**(m/s)**
W.D. (m)	**20**	**30**	**40**	**50**
Turbine	**Rotation (deg)**			
6 MW	0.5722	0.5646	0.5570	
7 MW	0.6124	0.5915	0.5707	
8 MW	0.6526	0.6184	0.5843	0.6521
9.5 MW	0.6591	0.6451	0.6310	0.6414
10 MW	0.6613	0.6540	0.6466	0.6378
11 MW	0.6748	0.6617	0.6486	0.6615
12 MW	0.6882	0.6694	0.6507	0.6852

Table A10- 3: Chesapeake Bay Robustness Case Mudline Rotations

Sub-Region:	Chesapeake Bay			**Unit**
Latitude:	36.63	**Longitude:**	-75.16	**(DD)**
500-YR Surface Wind Speed at El. (+) 10 m:			60	**(m/s)**
W.D. (m)	**20**	**30**	**40**	**50**
Turbine	**Rotation (deg)**			
6 MW	0.6765	0.6336	0.5907	
7 MW	0.7282	0.6673	0.6063	
8 MW	0.7800	0.7010	0.6220	0.7096
9.5 MW	0.7949	0.7460	0.6970	0.7044
10 MW	0.7999	0.7610	0.7220	0.7027
11 MW	0.8148	0.7721	0.7294	0.7310
12 MW	0.8297	0.7832	0.7367	0.7593

Table A10- 4: Long Bay Robustness Case Mudline Rotations

Sub-Region:	Long Bay			**Unit**
Latitude:	33.29	**Longitude:**	-78.47	**(DD)**
500-YR Surface Wind Speed at El. (+) 10 m:			64	**(m/s)**
W.D. (m)	**20**	**30**	**40**	**50**
Turbine	**Rotation (deg)**			
6 MW	0.7699	0.6862	0.6024	
7 MW	0.8329	0.7254	0.6178	
8 MW	0.8960	0.7646	0.6332	0.7417
9.5 MW	0.9200	0.8291	0.7382	0.7477
10 MW	0.9279	0.8506	0.7732	0.7496
11 MW	0.9429	0.8653	0.7876	0.7806
12 MW	0.9578	0.8799	0.8020	0.8116

APPENDIX A11 – NUMERICAL ANALYSIS INPUT PARAMETERS

Table A11- 1: Plaxis Analysis Input Parameters

LC	Water Depth (m)	Turbine Size (MW)	Saffir Simpson Category	Mudline Base Fxy (kN)	Eccentricity, e (m)	Mudline Base Mxy (kN-m)	Pile Penetration, L (m)	OD_{MUD} (m)	W.T. (mm)	L/D	Soil Volume Lateral Width (m)	Soil Volume Height (m)	Tskin,start[1] (kN)	Tskin,end[1] (kN)	Fmax[2] (kN)
06_20_H1	20	6	H1	5,704	40.52	231,116	29	8	75	3.63	96	46	2036	2036	251327
06_20_H2	20	6	H2	8,479	45.36	384,597	29	8	75	3.63	96	46	2036	2036	251327
06_20_H3	20	6	H3	9,766	49.88	487,147	29	8	75	3.63	96	46	2036	2036	251327
06_20_H4	20	6	H4	11,106	56.83	631,133	29	8	75	3.63	96	46	2036	2036	251327
06_40_H1	40	6	H1	10,620	47.28	502,084	39	8	80	4.88	96	62	2036	2036	251327
06_40_H2	40	6	H2	17,751	52.44	930,764	39	8	80	4.88	96	62	2036	2036	251327
06_40_H3	40	6	H3	20,172	53.20	1,073,256	39	8	80	4.88	96	62	2036	2036	251327
06_40_H4	40	6	H4	21,171	57.50	1,217,302	39	8	80	4.88	96	62	2036	2036	251327
08_20_H1	20	8	H1	6,749	48.22	325,462	30	9	70	3.33	108	48	2290	2290	318086
08_20_H2	20	8	H2	10,311	53.91	555,890	30	9	70	3.33	108	48	2290	2290	318086
08_20_H3	20	8	H3	12,031	59.41	714,765	30	9	70	3.33	108	48	2290	2290	318086
08_20_H4	20	8	H4	13,944	67.34	938,996	30	9	70	3.33	108	48	2290	2290	318086
08_40_H1	40	8	H1	12,605	50.76	639,765	40	9.5	75	4.21	114	64	2417	2417	354411
08_40_H2	40	8	H2	20,970	57.31	1,201,759	40	9.5	75	4.21	114	64	2417	2417	354411
08_40_H3	40	8	H3	24,774	57.69	1,429,252	40	9.5	75	4.21	114	64	2417	2417	354411
08_40_H4	40	8	H4	26,630	63.07	1,679,537	40	9.5	75	4.21	114	64	2417	2417	354411
08_50_H1	50	8	H1	14,490	56.13	813,309	43	9.5	80	4.53	114	69	2417	2417	354411
08_50_H2	50	8	H2	24,401	59.22	1,444,894	43	9.5	80	4.53	114	69	2417	2417	354411
08_50_H3	50	8	H3	29,846	60.17	1,795,835	43	9.5	80	4.53	114	69	2417	2417	354411
08_50_H4	50	8	H4	31,979	64.58	2,065,322	43	9.5	80	4.53	114	69	2417	2417	354411
10_20_H1	20	10	H1	8,348	60.20	502,489	35	10	80	3.50	120	56	2545	2545	392699
10_20_H2	20	10	H2	12,800	67.62	865,521	35	10	80	3.50	120	56	2545	2545	392699
10_20_H3	20	10	H3	15,082	74.76	1,127,554	35	10	80	3.50	120	56	2545	2545	392699
10_20_H4	20	10	H4	17,745	84.83	1,505,395	35	10	80	3.50	120	56	2545	2545	392699
10_40_H1	40	10	H1	14,177	60.24	853,947	43	10	80	4.30	120	69	2545	2545	392699
10_40_H2	40	10	H2	23,678	66.97	1,585,824	43	10	80	4.30	120	69	2545	2545	392699
10_40_H3	40	10	H3	28,217	68.55	1,934,347	43	10	80	4.30	120	69	2545	2545	392699
10_40_H4	40	10	H4	30,860	76.26	2,353,484	43	10	80	4.30	120	69	2545	2545	392699
10_50_H1	50	10	H1	16,782	63.14	1,059,682	46	10.5	85	4.38	126	74	2672	2672	432951
10_50_H2	50	10	H2	28,469	65.97	1,878,190	46	10.5	85	4.38	126	74	2672	2672	432951
10_50_H3	50	10	H3	34,736	68.17	2,367,947	46	10.5	85	4.38	126	74	2672	2672	432951
10_50_H4	50	10	H4	37,709	74.65	2,814,825	46	10.5	85	4.38	126	74	2672	2672	432951
12_20_H1	20	12	H1	10,223	64.93	663,838	38	10	75	3.80	120	61	2545	2545	392699
12_20_H2	20	12	H2	15,949	72.27	1,152,642	38	10	75	3.80	120	61	2545	2545	392699
12_20_H3	20	12	H3	18,992	79.38	1,507,561	38	10	75	3.80	120	61	2545	2545	392699
12_20_H4	20	12	H4	22,565	89.60	2,021,825	38	10	75	3.80	120	61	2545	2545	392699
12_40_H1	40	12	H1	18,362	60.53	1,111,390	45	11.5	85	3.91	138	72	2926	2926	519345
12_40_H2	40	12	H2	30,882	66.23	2,045,402	45	11.5	85	3.91	138	72	2926	2926	519345
12_40_H3	40	12	H3	36,855	68.83	2,536,712	45	11.5	85	3.91	138	72	2926	2926	519345
12_40_H4	40	12	H4	40,554	76.74	3,112,032	45	11.5	85	3.91	138	72	2926	2926	519345
12_50_H1	50	12	H1	22,448	57.69	1,294,954	47	12	95	3.92	144	75	3054	3054	565487
12_50_H2	50	12	H2	35,791	67.57	2,418,318	47	12	95	3.92	144	75	3054	3054	565487
12_50_H3	50	12	H3	43,829	69.92	3,064,533	47	12	95	3.92	144	75	3054	3054	565487
12_50_H4	50	12	H4	47,833	76.86	3,676,287	47	12	95	3.92	144	75	3054	3054	565487

[1] Limiting shaft friction value from Table 1 in [35]
[2] Limiting unit end bearing value from Table 1 in [35]

VITA

Laura Emily Hulliger was born and raised in New Orleans, Louisiana. She received her Bachelor's Degree in Civil and Environmental Engineering from the University of New Orleans in 2013. She received an internship in 2011 with Keystone Engineering Inc., in Metairie, LA and continued her career with Keystone for the next 8 years working in structural analysis and design of offshore wind and oil and gas structures. During her time there, she was lucky enough to work as one of two primary steel jacket foundation design engineers for the first offshore wind farm in the United States. Namely, the Block Island Wind Farm. Her passion for offshore wind began here and continues to this day. She currently works for Orsted, helping to design, build and operate the next wave of offshore wind farms in the United States.